Low Frequency North Atlantic SST Variability: Weather Noise Forcing and Coupled Response

A dissertation submitted in partial fulfillment of the requirements for the degree of Doctor of Philosophy at George Mason University

By

Meizhu Fan
Master of Science
University of Northern Virginia, 2003
Master of Science
Chinese Academy of Meteorological Science, 1992

Director: Dr. Edwin K. Schneider, Professor
Department of Atmospheric, Oceanic and Earth Sciences

Fall Semester 2008
George Mason University
Fairfax, VA

ACKNOWLEDGEMENTS

I would like to express my gratitude to my dissertation committee. I would especially like to thank my advisor, Dr. Ed Schneider, for giving me guidance and counsel. He always encouraged me to develop independent thinking and research skills. He always read and responded to the drafts of each chapter of my work more quickly than I could have hoped. His comments are always extremely perceptive, helpful and appropriate. I thank him for always being willing to meet me whenever I asked. I would also like to specifically thank Dr. Ben Kirtman. His encouragement and help on my experiments setting-up and his comments and suggestions on my research have been invaluable. I would also like to thank the rest of my dissertation committee, Dr. Bohua Huang and Dr. Paul Schopf, for their invaluable advice and support during my doctoral work.

I would also like to thank the scientists and staff at the Center for Ocean-Land-Atmosphere Studies (COLA), Dr. Zhaohua Wu, Dr. Zeng-zhen Hu, Dr. D. Straus, and Jennifer Adams, for their suggestions and technical support.

I extend many thanks to many of my fellow students, especially Kathy Pegion, Daeho Jin, Xiaohua Pan, and Deepthi Achuthavarier, for their help, suggestion, and friendship.

Finally, I would like to thank my family, my husband and my daughter, for supporting and encouraging me during my doctoral work.

TABLE OF CONTENTS

LIST OF TABLES

LIST OF FIGURES

ABSTRACT

LOW FREQUENCY NORTH ATLANTIC SST VARIABILITY: WEATHER NOISE FORCING AND COUPLED RESPONSE

Meizhu Fan, PhD

George Mason University, 2008

Dissertation Director: Dr. Edwin K. Schneider

A method to diagnose the causes of low frequency SST variability is developed, tested and applied in an ideal case and real climate. In the ideal case, a free simulation of the COLA CGCM is taken as synthetic observations. For real climate, we take NCEP reanalysis atmospheric data and Reynolds SST as observations. Both the synthetic and actual observation data show that weather noise is the main component of atmospheric variability at subtropics and high-latitude.

Diagnoses of results from the ideal case suggest that most of the synthetic observed SST variability can be reproduced by the weather noise surface fluxes forcing. This includes the "observed" low frequency SST patterns in the North Atlantic and their corresponding time evolution. Among all the noise surface fluxes, heat flux plays a major role.

The results from simulations using actual observations also suggest that the observed SST variability is mostly atmospheric weather noise forced. The regional

atmospheric noise forcing, especially the heat flux noise forcing, is the major source of the low frequency SST variability in the North Atlantic.

The observed SST tripole mode has about a 12 year period and it can be reasonably reproduced by the weather noise forcing in terms of its period, spatial pattern and variance. Based on our diagnosis, it is argued that the SST tripole is mainly forced by local atmospheric heat flux noise. The gyre circulation plays a secondary role: the anomalous gyre circulation advects mean thermal features across the inter-gyre boundary, and the mean gyre advection carries SST anomalies along the inter-gyre boundary. The diagnosis is compared with a delayed oscillator theory. We find that the delayed oscillator theory is not supported and that the SST tripole mode is forced by weather noise heat flux noise. However, the result may be model dependent.

Chapter 1 Introduction

1.1 Observational studies in the North Atlantic climate variability

The dominant mode of the atmospheric variability in the North Atlantic sector is the NAO (North Atlantic Oscillation). The NAO is a large-scale oscillation of atmospheric mass between the subtropical high and the polar low, and is the strongest in winter. To describe the NAO, a number of different NAO indices have been introduced based on the SLP (sea level pressure) difference between two stations, e.g. the stations of Lisbon and Iceland (Hurrell 1995), the stations of Azores and Iceland (Rogers 1984), or the stations of Gibraltar and Iceland (Jones et al. 1997). An alternative NAO index is also introduced based on the leading principal component of pressure anomalies such as CPC NAO index has been induced by Barnston and Livezey (1987). No matter which NAO index is applied, it not only varies from year to year and has a broadband spectrum (noise-like), but also exhibits a tendency to remain in one phase for intervals lasting several years to decade, particularly since about 1950 (Fig. 1.1, which is taken from Hurrell's website http://www.cgd.ucar.edu/cas/jhurrell/nao.stat.winter.html; Hurrell 1995). A positive NAO index phase shows a stronger than normal subtropical high and an anomalously deeper Icelandic low. The corresponding midlatitude surface westerlies are strong and locate more north than usual, and there is a strong storm track that trends from the U.S. coast toward the Europe/North-Europe, resulting in warm/wet winters in

Europe and the eastern United States, and cold/dry winters in south Europe and Greenland. A negative NAO index phase shows that both the subtropical high and the Iceland low are weaker than normal, the westerlies are weaker, and storms tend to move from the United States into the Labrador Sea region while those that do make it across the Atlantic move into southern Europe and the Mediterranean, bring warm/moist air into the Mediterranean and Greenland, and dry/cold air to northern Europe and the east coast of the United States. With the evolution of the NAO, the underlying ocean has corresponding changes.

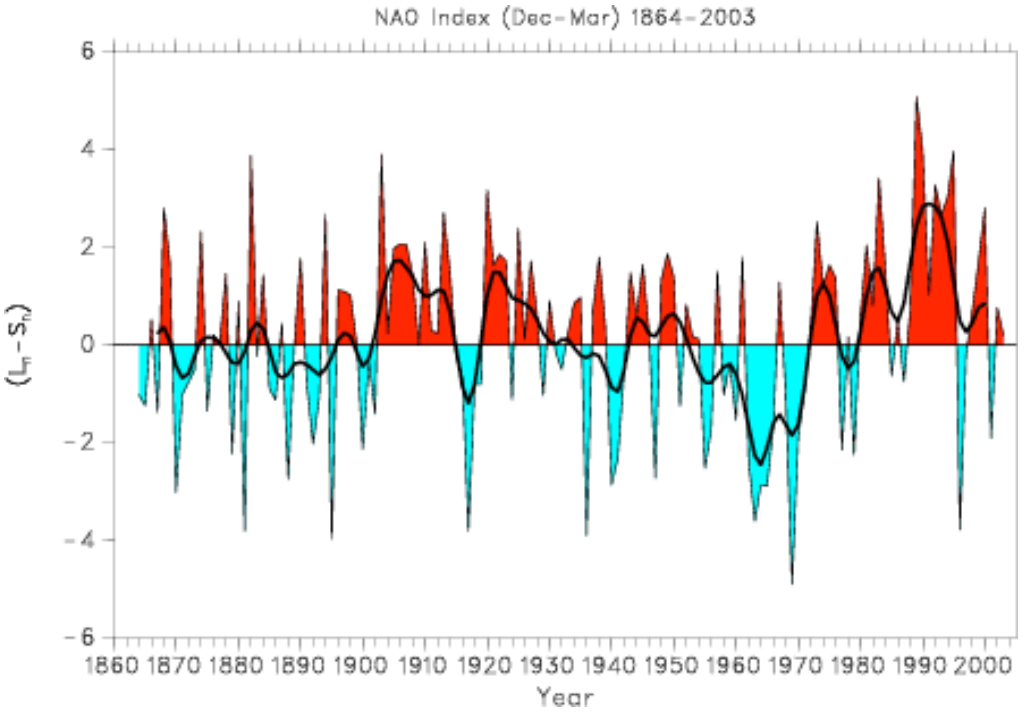

Figure 1.1: Winter (DJFM) index of the NAO based on the difference of normalized sea level pressure (SLP) between Lisbon, Portugal and Stykkisholmur/Reykjavik, Iceland since 1864 (color). The SLP anomalies at each station were normalized by division of each seasonal mean pressure by the long-term mean (1864-1983) standard deviation. Black line is the low frequency part of NAO (taken from Hurrell's website http://www.cgd.ucar.edu/cas/jhurrell/nao.stat.winter.html).

Using composite analysis based on monthly NAO index, Cayan (1992a) has studied the wintertime (October-April) anomalies in the atmospheric circulation, and its relationship with the anomalies in the ocean-to-atmosphere heat flux over the North Atlantic using the COADS (Comprehensive Ocean-Atmosphere Data Set, Woodruff et al. 1987) dataset, and found that the NAO is responsible for generating systematic patterns of large amplitude anomalies of wind speed, and latent and sensible heat flux. Cayan identified a dominant North Atlantic circulation pattern and determined its effect on ocean-atmosphere heat exchange. In his following paper (Cayan 1992b), Cayan showed that during winter, about 10-40% of the monthly change in the SST anomaly is estimated to be due to the local anomalies of ocean-atmosphere heat flux: Anomalous ocean-to-atmosphere heat fluxes above cold water (negative SST), and vice versa, which is indicative of the atmosphere forcing the ocean.

Also using the COADS data and applying EOF analysis, Deser and Blackmon (1993) found an anomaly dipole spatial pattern (same as tripole pattern in some literature if the domain is extended further south (e. g. Wu and Liu 2005) with biennial and decadal timescales, and a monopole spatial pattern with an interdecadal timescale. From Deser and Blackmon (1993) , the dipole pattern has centers east of Newfoundland and near the southeast coast of the US (their Fig. 1c). The nearly decadal period of these oscillations is somewhat irregular with a period of approximately 9 years from 1900-1945 and approximately 12 years from 1945-1989 (their Fig. 1d). Corresponding wind fluctuations occur locally over the regions of large surface temperature anomalies, with stronger westerly (easterly) anomalies overlying negative (positive) SST anomalies (their Fig. 4a).

The pattern of negative SST anomalies east of Newfoundland and positive SST anomalies southeast of the US corresponds to a positive NAO pattern (their Fig. 4b). This suggests that the SST anomalies are maintained by the circulation anomalies: the surface wind anomalies that alter the fluxes of latent and sensible heat at the ocean surface and vertical mixing processes in the ocean, forcing the formation of SST anomalies.

The monopole spatial distribution from Deser and Blackmon (1993) has the biggest SST anomaly along the Gulf Stream (their Fig. 1a, referred to as the Gulf Stream pattern) and is associated with a warming trend that occurred during the 1920s and 1930s (their Fig. 1b). Relatively cold temperatures dominated from 1900-1929, followed by relatively warm temperatures from 1939-1968. Different from the dipole pattern, the corresponding wind changes occur downstream of the largest SST anomalies: anomalous cyclonic (anticyclonic) circulation occurs downstream of the largest positive (negative) SST anomaly (their Fig. 7). Deser and Blackmon (1993) argued that the strongest SST anomaly along the Gulf Stream, occurring remotely from the anomalies of wind and SLP, might have been a result of altered oceanic advection rather than local wind forcing.

Kushnir (1994) applied composite analysis and used the same COADS data, found similar patterns as Deser and Blackmon (1993) for both the dipole and monopole patterns. Kushnir (1994) argued that the monopole SST anomaly variability is governed by a basinwide dynamic interaction that involves changes in the large-scale oceanic circulation, including the thermohaline circulation (THC). The corresponding atmospheric anomalies act to attenuate local interdecadal SST variability.

Wu and Liu (2005) used the SST from Hadley Centre Global Sea Ice and Sea Surface Temperature dataset (Rayner et al. 2003) and 500hPa geopotential height from NCAR/NCEP reanalysis dataset (Kalnay et al. 1996), applied EOF analysis, and found similar patterns of SST anomalies. The atmospheric pattern corresponding to the SST dipole pattern is similar to that of Deser and Blackmon (1993) and Kushnir (1994). For the monopole pattern, a warm (cold) SST anomaly corresponds to a downstream ridge (trough). In contrast to Kushnir's conclusions, Wu and Liu claim that this reflects the predominant forcing of the atmosphere on the ocean.

Levitus et al. (1994) investigated the North Atlantic (between $20^0 N$ and $70^0 N$) ocean subsurface temperature data at a depth of 125 m, which is only available from 1947 through 1990. They found variability with similar spatial distributions as those of SST (Deser and Blackmon 1993, Kishnir 1994).

Using 1966-1995 ocean surface and subsurface (down to 400 m) observed temperature data, Molinari et al. (1997) related subsurface temperature variability in the western middle-latitude Atlantic to decadal fluctuations in the NAO index. They found that for the decadal timescale variability, changes in the western middle-latitude Atlantic surface-subsurface temperature anomaly coincide with the NAO index changes: Periods of positive temperature anomaly appear with periods of positive NAO index, and vice versa.

1.2 Mechanisms of low frequency climate variability

Low frequency climate variability (including interannual, decadal and interdecadal variability) can be caused by fluctuations in external forcing. This kind of

external forcing includes the natural variations in incoming solar radiation (e.g. Lean et al. 1995) and volcanoes (e.g. Robock and Mao 1992), as well as the anthropogenic greenhouse gases (e.g. Shindell et al. 1999). Low frequency climate variability can also occur with no variability in external forcing. These fluctuations are due to the internal dynamics of climate system. Internal dynamics include the interactions between, as well as the changes internal to, the different climate subsystems.

If there are no fluctuations in external forcing, the SST low frequency variability can be thought of as induced mainly by atmospheric and oceanic internal variability and by coupled feedbacks between the atmosphere and ocean, and can be expressed as following 4 scenarios: (1) The simplest view is that the ocean may just passively respond to the atmospheric weather noise and has no feedback to the atmosphere (Hasselmann 1976, Saravanan and McWilliams 1998). This is the "no feedback" case. (2) If there is feedback, the ocean not only responses to the atmospheric weather noise, but also modulates the atmospheric variability. The SST variability is zero when the weather noise forcing is eliminated, this is the "stable coupled" case (Frankignoul et al. 1997, Barsugli and Battisti 1998, Bhatt et al. 1998, Saravann and McWilliams 1998, Bretherton and Battisti 2001, Czaja and Marshall, Wu et al. 2004, Yeh and Kirtman 2004). (3) Another case is that the low frequency variability of SST can exist in the absence of weather noise both from the atmosphere and the ocean. In this case, the low frequency variability of SST is sustained by unstable coupled feedbacks between the ocean and the atmosphere (Latif and Barnett 1994, Latif and Barnett 1996, Gu and Philander 1997,

Grötzner et al. 1998). (4) The oceanic internal fluctuations, referred as oceanic "noise", can also have an influence (Wu et al. 2004).

In the no feedback case of (1), the interaction between ocean and atmosphere is "one way". The ocean passively responds to the atmospheric weather noise (assumed stochastic) locally (Hasselmann 1976). The ocean mixed layer selectively amplifies the lower frequencies compared to the higher frequencies, therefore reddening the white spectrum of the atmospheric weather noise forcing. Because of the linearity of the model, the structure of the response is determined by the structure of the forcing and local properties of the ocean (mixed layer depth). Saravanan and McWilliams (1998) suggest that the ocean passively responds to atmospheric variability at a preferred resonant decadal time scale, set by a typical oceanic advective velocity and a length scale determined by dominant atmospheric variability pattern.

In the stable coupled feedback case of (2), the low frequency variability of SST is also forced by the atmospheric weather noise. Different from the "no feedback" case, the weather noise induced ocean variability can modulate the atmospheric variability. The interaction between ocean and atmosphere is "two way". The coupling is stable and acts to reduce the damping, enhancing the persistence and variance (Barsugli and Battisti 1998, Bhatt et al. 1998, Saravann and McWilliams 1998, Bretherton and Battisti 2001). In addition to the coupling, the other reddening processes can involve the mixed layer re-emergence (Alexander and Deser 1995, Bhatt et al. 1998), mean flow advection by ocean currents (Saravann and McWilliams 1998), propagation of Rossby waves (Frankignoul et

al. 1997), and the thermohaline circulation (Delworth 1993). The relative importance of these reddening processes depends on timesacle of the variability.

By analyzing the integration of GFDL coupled model, Delworth et al. (1993) identified an interdecadal SST variability with a broad spectral period of 50 yr. A meridional overturning index describing the strength of the model's THC shows a similar peak in its spectrum. The spatial structure of the SST anomaly agrees with observations of monopole mode (Deser et al. 1993, Kushnir 1994, Wu and Liu 2005). The causes of the mode involve both the Meridional Overturning Circulation (MOC) and horizontal gyre circulation. The gyre circulation transports the anomalies of upper-ocean heat and salt from the south into the northern sinking region of THC. Salinity-related density anomalies in the sinking region drive anomalies in the strength of the THC, and then cause the SST anomaly. The gyre circulation, however, is not in phase with the MOC, and the authors argue that it is this phase difference that is important to the interdecadal oscillation of the THC. The role of the atmosphere is not clear.

The weather noise is internal to the atmosphere. The atmospheric stochastic forcing is automatically included in the integration of coupled GCM of Delworth et al. (1993), but is not distinguished from the responses. So, it is not possible to analyze its effect on THC. Using a simple model (four-box model) with stochastic heat forcing, Griffies and Tziperman (1995) showed the resemblances as in Delworth et al. (1993), including the anomalous regression patterns of salinity and THC, temperature and THC, as well as the phase relationship of these two regression patterns. They also show that unlike the analysis of Delworth et al. (1993), in which the anomalous gyre transport plays

a critical role in driving the THC anomaly, the existence of the interdecadal THC oscillation could be explained without the gyre effect. Thus, they attribute the interdecadal variability of the THC to atmospheric stochastic forcing.

In the unstable coupled feedback case of (3), the low frequency variability can exist in the absence of the weather noise. A critical condition for one type of unstable coupled perturbation to oscillate is the delayed response of the ocean to the atmosphere disturbance (Suarez and Schopf 1998). Different oceanic processes may provide this delay, such as shoaling/deeping of equatorial thermocline due to Rossby wave propagation (Zebiak and Cane 1987), advection by the wind-driven subtropical gyre (Latif and Barnett 1994, Latif and Barnett 1996, Grötzner et al. 1998, Latif 1998), or subduction due to shallow meridional circulations (Gu and Philander 1997).

The mechanism of delayed oscillator was first suggested by Suarez and Schopf (1988) to explain the oscillatory nature and interannual timescale of ENSO phenomenon. The interaction between SST and wind-stress reinforce each other, so that perturbations can become large. The memory of the coupled system, which resides in the ocean thermocline, provides delayed negative feedbacks, which enable continuous oscillations. The period of the oscillation is longer than the twice the sum of the information travel time to the western boundary (free Rossby wave) and then back to the disturbed region (free Kelvin wave) (Cane and Sarachik 1977, Schneider et al. 1995).

Latif and Barnett (1994, 1996) applied the delayed oscillator explanation to the SST low frequency oscillation in Northern Pacific found in their coupled GCM. They connect low frequency SST variability with changing heat transports of the wind-driven

ocean gyre and its interaction with the Aleutian low in the atmosphere (their atmospheric response to this SST anomaly is an anomalous high at Aleutian region). To see how this works, first suppose the subtropical ocean gyre is anomalously strong. Anomalous warm water transported northward by the Kuroshio leads to positive SST anomalies in the North Pacific weakening the Aleutian low in the atmosphere. The weakened Aleutian low is accompanied by reduced westerlies and increased net surface heat flux into the ocean, which tends to reinforce the SST anomaly. So that coupled ocean and atmosphere act as a positive feedback system. The anomalous easterly winds in the midlatitudes imply a positive wind-stress curl anomaly in the subtropical gyre region. Because of the inertia of the ocean, the response of the subtropical gyre to the wind-stress curl has a time delay, which is determined by the time for the Rossby waves to cross the basin. So, some time later, the anomalous positive wind-stress curl will reduce the subtropical gyre and, thus, reduce heat transport in the western boundary current (Kuroshio). The net effect is to cause the previously reinforced SST anomaly to change sign. The process then repeats with opposite sign. This causes the North Pacific climate system to oscillate on a decadal timescale. The same mechanism is proposed to explain oscillation in the North Atlantic climate system (Latif 1998, Grötzner et al. 1998) obtained using the same coupled GCM. For both regions the period of the oscillation is approximately the time a large scale free baroclinic Rossby wave needs to cross the North Pacific or North Atlantic basin.

Another delayed oscillator theory proposed by Marshall et al. (2001) and Czaja and Marshall (2001) is in accord with above scenario's unstable delayed oscillator, both emphasize the coupled behaviors. Different from unstable coupled ocean-atmosphere

oscillation, Czaja and Marshall (2001) emphasize that the oscillation is heavily damped (belongs to case 2).

In the damped decadal oscillation theory interpreting the observed North Atlantic SST tripole, two factors are important: The major one is played by the wind-driven anomalous ocean circulation, the intergyre gyre (IGG, a gyre anomaly "stradding the climatological subtropical and subpolar gyres", Marshall et al. 2001). The IGG response to the surface windstress forcing has to act as a delayed negative feedback in order to reproduce the low frequency decrease of power seen in the observed SST tripole. The heat transport across the separated Gulf Stream axis by IGG can compensate the thermal impact of the NAO at the surface at longer time scales. Another is the positive feedback of SST tripole on the atmospheric circulation. Once a feedback between SST and wind-stress is allowed, the system behaves as a delayed oscillator, with the delay set by the propagation of first mode of baroclinic Rossby waves. The ocean-atmosphere coupling introduces enhanced power in the surface temperature spectrum around the delay time-scale, determining a major deviation from the essentially red noise spectrum displayed by Frankignoul and Hasselmann (1977) model.

For example, suppose the North Atlantic SST tripole is positive at subpole and tropics and negative at subtropics. The atmospheric circulation response to this SST anomaly is negative NAO like anomaly (positive feedback): reduced surface westerlies across the middle latitudes, combined with weaker than average trade winds in the tropics, determine a cyclonic (positive) wind stress curl anomaly over the subtropics, while an anticyclonic surface circulation anomaly develops over the subpolar. The

vorticity source associated with the NAO anomaly drives a Sverdrup response of the barotropic wind driven circulation some time later, leading to a negative IGG. This negative IGG determines an reduced meridional heat transport across the subtropical/subpolar gyre boundary, which in turn leads to the cooling (warming) of the subpolar (subtropical) basin. The IGG acts to reduce, with some delay, the anomalous SST gradient across the climatological gyre boundary. The consequent sign reversal in the North Atlantic SST tripole, forces the NAO to enter into a positive phase, through a positive NAO/SST feedback. Once the NAO has stepped into a positive phase, the previously described stages of the oscillation repeat with reversed sign, and the oscillation completes its cycle. Our study will adopt Marshall et al. (2001) and Czaja and Marshall (2001) theoretical model to quantitatively analyze the results from our simulation to investigate the roles of stochastic forcing, ocean circulation, and coupled behavior.

Gu and Philander (1997) related the extratropical and tropical oceanic anomalies based on subduction processes in a shallow meridional circulation. In the North Pacific ocean, the atmospherically forced thermal anomaly (suppose positive) at some latitude can reach the equatorial thermocline by moving equatorward through certain pathways along isopycnal surfaces. These pathways are mainly located in the central and eastern Pacific. Because of equatorial upwelling, when the extratropical positive SST anomaly reaches the equatorial thermocline, it causes a positive SST anomaly and initiates unstable coupling between SSTs and wind-stress in the tropics. The atmospheric responses to the SST anomaly are similar to those observed during El Nino situations,

that is, westerly wind anomalies over the western equatorial Pacific and in midlatitudes. The anomalous westerlies cause surface ocean cooling in the North Pacific, mainly by enhanced heat loss from the ocean to the atmosphere. The cold SST anomaly will be subducted and move sourthward along the isopycnal surface. It will be upwelled to the surface when it reached the equatorial region, and then reduces/reverses the previous positive SST anomaly. Then, the processes repeat, forming the oscillation. The period of the oscillation is determined mainly by the time it takes parcels to travel from the midlatitude to the equator. Thus, the combination of a slow "oceanic bridge" from the midlatitudes to the tropics and a fast " atmospheric bridge" from the tropics to the midlatitudes can lead to self-sustained decadal oscillations.

The processes involved in the unstable coupled feedbacks can be considered to operate even if the coupled system is stable. In this case, they can act as a positive feedback to noise forcing, and also influence the structure and timescale of the coupled response.

In case of (4), the low frequency variability of SST is internally generated by the ocean. Wu et al. (2004) studied the North Atlantic SST low frequency variability and by comparing two experiments, one applies the interactive ensemble coupled GCM (Kirtman and Shukla 2002), another uses ocean-only GCM. Both show a center of variability of compariable magnitude in the same region off the coast of Newfoundland. An ocean only simulation confirmed that this variability is produced by processes internal to the ocean.

Chapter 2 Background: Weather Noise Forcing of Surface Climate Variability[1]

2.1 Introduction

As described in chapter 1 section 1.2, one of the mechanisms for explaining low frequency SST variability is that the ocean is forced stochastically by fluxes representing weather noise (Hasselmann 1976). Weather noise is the part of the atmospheric variability that is not the direct response to the boundary or external forcing. In Hasselmann's one point slab ocean linear model, the weather noise forcing is taken to be random noise independent of the climate state, and therefore to have a white (frequency independent) power spectrum. In the absence of the weather noise forcing there is no SST variability. The heat capacity of the ocean acts as an integrator, leading to reddening of the power spectrum of the SST response, with the response to low frequencies in the forcing enhanced relative to high frequencies. Damping towards the mean climate causes the response to flatten near zero frequency. The model thus provides a simple explanation for the red shape of the spectrum of observed SST variability. In this case, variability at all frequencies is present in the stochastic forcing, and the low frequency response is selectively amplified. Hasselmann's model suggests the null hypothesis: that all surface temperature climate variability is the response to weather noise forcing. We will adopt this as our null hypothesis in this study.

[1] Material in this section has been taken and modified from Schneider and Fan (2007).

When Hasselmann's theory is applied to understanding the behavior of coupled atmosphere-ocean models, it is instructive to explicitly include the feedback between the atmosphere and the SST variability forced by the noise. This was done by Barsugli and Battisti (1998; BB98 in the following), using an extension of Hasselmann's model that includes a coupled linear thermodynamic atmosphere (Schopf 1985). The BB98 model will be used in later sections of this chapter as first step to test our method. The air-sea coupling in BB98 is proportional to the air-sea temperature difference. The atmospheric temperature is forced by specified "noise", leading to a heat flux which causes an SST response. The atmospheric temperature adjusts in response to the new SST, and so on. The total atmospheric evolution consists of a response to the noise plus the response to the SST, while the ocean responds to the noise (indirectly through the atmosphere) and to the feedback from the atmospheric response to the SST. Figure 2.1a is a schematic diagram showing these elements and how they interact to determine the SST evolution in the BB98 model. The result of this (stable) coupled feedback is reduced damping of the low frequency SST anomalies, and hence increased persistence of SST anomalies. The BB98 extension of Hasselmann's theory can be used to aid in the interpretation of observations and results from more complex coupled models (Kirtman et al., 2005).

The BB98 model provides a framework for interpretation of uncoupled GCM experiments in which the atmosphere responds to a specified evolution of SST (Bretherton and Battisti 2001). An SST solution of the BB98 coupled model (representing the observed evolution) is produced by forcing the model with a specific realization of the noise. This will be referred to as the "control" case. Next, an ensemble

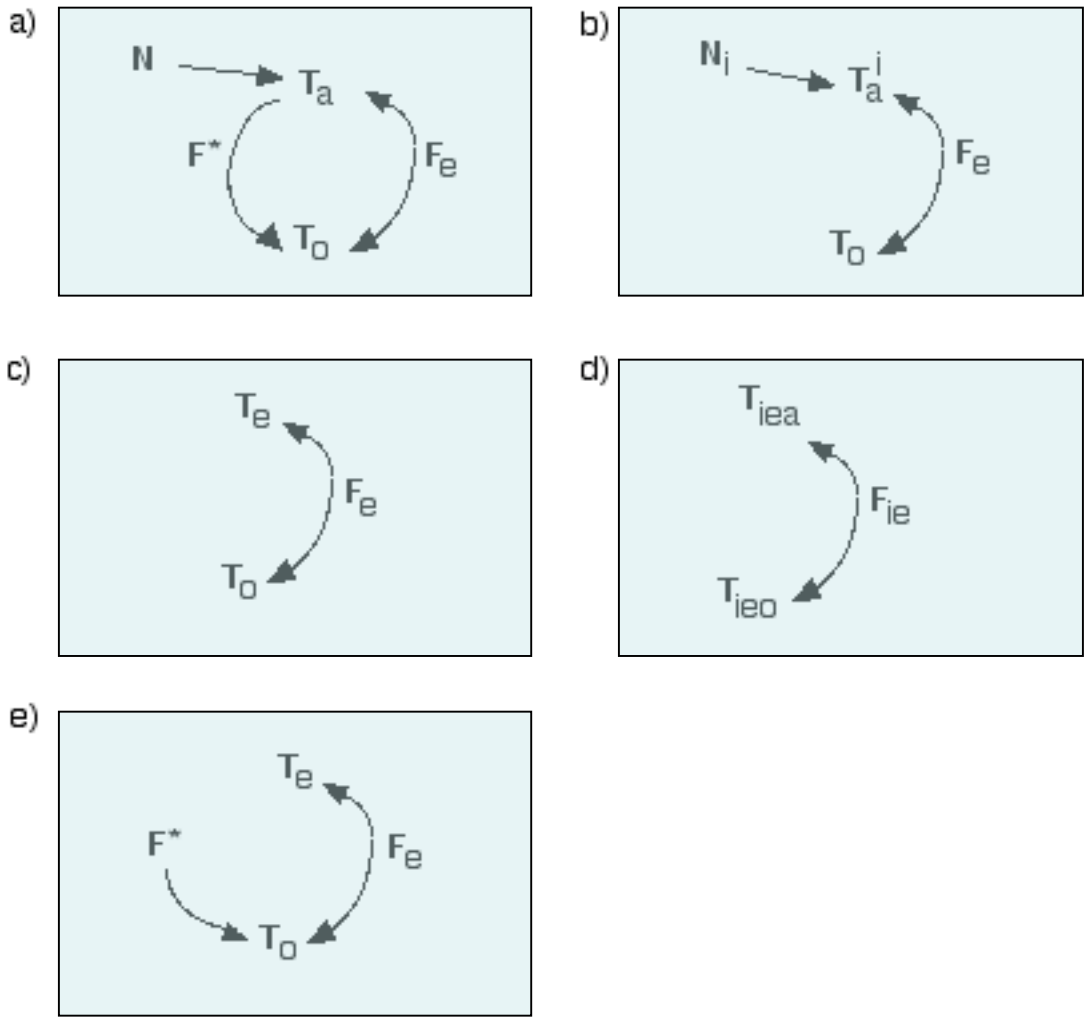

Figure 2.1 Schmeatic diagram shows elements and how they interact to determine the surface temperature T_o (SST) evolution and how the atmosphere response to this T_o evolution in: a) regular BB98 model with specific atmospheric noise N (Eqs. (1) and (2)); b) T_o forced BB98 atmospheric model with atmospheric noise N_i (Eq. (3); c) ensemble mean of BB98 atmospheric model realizations that forced by surface temperature T_o, but with different atmospheric noise – this determines the forced response given infinite realizations in the ensemble (Eq. (4)); d) interactive ensemble BB98 model (Eqs. (5) and (6) with F=0); e) interactive ensemble BB98 model with noise heat flux forcing (Eqs. (5) and (6) with $F=F^*$).

Note that notations here are the same as in Equations (section 2.2). T_a includes two parts: one comes from the specific noise N; the other is the feedback from T_o, which is T_e. F^* is the noise heat flux corresponding to special noise N and F_e is feedback flux. With noise heat flux forcing F^*, surface temperature T_o is reproduced. See text for details.

of atmospheric simulations is made with each member forced by this SST, but by a different realization of the noise. The SST forced ensemble corresponds to the situation of forcing an ensemble of AGCM simulations with the same specified observed SST evolution (e.g. Lau 1985, Gates 1992, and many others). The different instances of the specified noise conceptually represent the different chaotic weather evolution of the atmosphere resulting from starting from different initial conditions. The result of forcing a member of the atmospheric ensemble with this SST is the response to the stochastic weather noise (different for each member) plus the response forced by the specified SST (the same for each member). Figure 2.1b shows a schematic diagram of how the atmosphere responses to the SST evolution in the BB98 atmospheric model. The ensemble mean of a large number of such realizations using different specifications of the noise gives the forced response, since the ensemble mean response to the noise is zero in this linear model. Fig. 2.1c is its schematic diagram showing how atmosphere response to the SST evolution. In the Bretherton and Battisti example, the SST forced response is only about 40% of the total atmospheric variability of the control case, and is coherent with the control evolution. The result commonly found in SST forced atmospheric ensembles, that the ensemble mean atmospheric response to the SST resembles the observed evolution but explains only order half of the observed amplitude, is then consistent with the SST being forced by the atmospheric noise. The part of the control case atmospheric variability not explained as the response to the SST is the atmospheric response to the stochastic forcing. The SST forced response of the atmosphere is then more correctly interpreted as the feedback of the atmosphere to the noise-forced SST

variability. It is important to note that *there is only one noise evolution that is consistent with the SST evolution*, the one specified for the control simulation.

The ideas in BB98 and Bretherton and Battisti (2000) suggest a dynamically consistent method 1) to isolate weather noise forcing from atmospheric response to SST and 2) to test the null hypothesis in a special coupled model framework. This method uses a generalization of the "interactive ensemble" coupling strategy (Kirtman and Shukla, 2002; Chapter 3 section 3.1.4 Fig 3.1). In the interactive ensemble, an ensemble of atmospheric models is forced by the same SST. Each atmospheric model is started with different initial conditions, so that the weather noise can be viewed as random noise uncorrelated between members. These conditions are as in the standard SST forced ensemble. However the SST, rather than being specified, is predicted from an oceanic model forced by the ensemble mean surface flux(es) averaged over all atmospheric realizations. In the limit of an infinite number of the atmospheric realizations in the ensemble, the surface fluxes provided to the ocean are noise free and are exactly the model's atmospheric feedback/response to the time evolving SST. Figure 2.1d is a schematic diagram showing the elements and how they interact to determine the SST evolution in the interactive ensemble BB98 model. This contrasts with the traditional coupled model (one atmosphere coupled to one ocean, Fig. 2.1a), in which addition of a specified noise of reasonable amplitude to the surface fluxes would not be expected a priori to produce reproducible effects in independent coupled model realizations.

2.2 Interactive ensemble in the context of the simple model

This section demonstrates the method in the context of the BB98 model. A single realization of the model's response to a specified stochastic forcing provides the control surface temperature evolution and total surface heat flux, as in Bretherton and Battisti. The ensemble mean surface heat flux from an ensemble of atmospheric models forced by the control surface temperature evolution defines the feedback atmospheric surface heat flux. Removing this feedback heat flux from the total of the control simulation defines the noise surface heat flux. The interactive ensemble version of the coupled model is then forced by this surface heat flux noise, and it is shown that the control surface temperature evolution is recovered. Figure 2.1e is a schematic diagram showing the elements and how they interact to determine the SST evolution in the interactive ensemble BB98 model forced by surface heat flux noise.

The BB98 model, using the formulation of Bretherton and Battisti (2000), is

$$dT_a/dt = -aT_a + bT_o + N(t) \tag{2.1}$$

$$\beta\, dT_o/dt = cT_a - hT_o \tag{2.2}$$

where Eq. (2.1) is the atmospheric model and (2.2) is the ocean model. The ocean is a motionless slab mixed layer forced by surface fluxes. T_a is the atmospheric temperature and T_o is the ocean temperature. The atmosphere is forced by random noise $N(t)$, which parameterizes the chaotic weather noise resulting from nonlinear internal atmospheric dynamics. Nondimensional parameters are time t; the ratio of the heat capacity of the ocean to that of the atmosphere β; and a, b, c, and h, positive constants which result from

simple parameterizations of turbulent and radiative heat fluxes. The values used in Barsugli and Battisti (1998) are a=1.12, b=0.5, c=1, h=1.08, and β=20 (50m mixed layer ocean), with time nondimensionalized by 4.84 days. With these parameter choices, the effective turbulent heat flux damping coefficient for low frequency variability, estimated by assuming the atmosphere is in equilibrium with the ocean, is $15 Wm^{-2}K^{-1}$.

The control simulation, which will be referred to as the "observations," is the solution to (2.1) and (2.2) for T_a and T_o forced by a specific instance of $N(t)$ (Fig. 2.1a; Figure 2.1 is a schematic diagram showing the elements and how they interact to determine the SST evolution corresponding to each equation). The BB98 model satisfies the null hypothesis. The symbols T_a, T_o, and N are reserved for the observations in the following. The SST forced ensemble is produced by doing a number of atmospheric simulations, each forced with the observed ocean temperature T_o but with different realization of the random noise $N_i(t)$. This procedure represents forcing a number of simulations of a dynamical atmospheric model by the observed SST. The different noise forcings represent the effects of each simulation starting from a different atmospheric initial condition. The evolution for the atmospheric temperature of the i^{th} member of the ensemble, T_a^i, is found from

$$dT_a^i/dt = -aT_a^i + bT_o + N_i(t) \qquad (2.3).$$

The equation governing the ensemble mean atmospheric temperature T_a is found by taking ensemble mean of (2.3) for an infinite number of realizations of the random noise

forcing $N_i(t)$, Since the noise averages to zero and the coefficients are constant in this case,

$$dT_e/dt = -aT_e + bT_o \qquad (2.4).$$

For the simple model, the analog of the interactive ensemble is to couple the atmospheric ensemble (2.4) to the ocean (2.2), replacing T_a in (2) by T_e. The equations governing the interactive ensemble atmospheric temperature, T_{iea}, and ocean temperature, T_{ieo} , are

$$dT_{iea}/dt = -aT_{iea} + bT_{ieo} \qquad (2.5)$$

$$\beta\, dT_{ieo}/dt = cT_{iea} - hT_{ieo} + F(t) \qquad (2.6),$$

where an externally specified forcing of the ocean *F(t)* is included. Note that the inclusion of external forcing of the ocean is not part of the original interactive ensemble method.

As there is now no explicit forcing of the atmosphere by noise, the atmospheric solution is the forced response of the atmosphere to the ocean temperature. However, if the noise forcing of the atmosphere is eliminated, the original interactive ensemble version of the simple model ($F(t) = 0$) will not produce any variability. In order to produce SST variability in the interactive ensemble, forcing applied to the ocean, representing specified fluxes, is included.

The special case considered here is to choose the forcing of the ocean $F = F^*$ so that the solution to the interactive ensemble reproduces the observed SST variability.

Setting $T_{ieo} = T_o$ in (2.5) and comparing to (2.4), it is seen that $T_{iea} = T_e$, plus a decaying transient accounting for initial conditions which will be neglected. Substituting in (2.6) and subtracting (2.2),

$$F^* = c(T_a - T_e) \tag{2.7}$$

From (2.2), the total surface flux forcing the ocean, F_{tot}, is

$$F_{tot} = cT_a - hT_o \tag{2.8a}$$

In the forced ensemble (2.4), the fluxes due to the atmospheric feedback, F_e, evaluated from (2.2), are

$$F_e = cT_e - hT_o \tag{2.8b}$$

Then

$$F^* = F_{tot} - F_e \tag{2.8c}$$

Equation (2.8c) states that the specified flux which will reproduce the observed ocean temperature evolution when forcing the interactive ensemble is the total surface (heat) flux forcing the ocean minus the SST forced flux. The total flux is in principle observable, while the SST forced flux must be calculated by a model (the possibility that this can be extracted using statistical tools without a model will not be examined here). While the interactive ensemble ocean temperature evolution is the same as the observations for this forcing, the ensemble mean atmosphere differs substantially from the observed atmosphere, since the noise which forced the observed atmosphere (and SST) is filtered out.

The necessary assumption concerning the noise forcing for this demonstration to be valid is that the ensemble mean of the different noise realizations N_j is zero (for an infinite ensemble). Otherwise, there is no requirement concerning the spectral distribution of the forcing in time, although it might be useful to consider stochastic forcing for conceptual purposes.

There is nothing in the simple model or the reconstruction of surface temperature variability using the interactive ensemble version that precludes their application to surface types other than ocean. The same models, although with different specifications of the heat capacity parameter β can be applied to other surface types, such as land or sea ice. In the case of land or sea ice, the values of β will usually be much less than for ocean.

2.3 Procedure of weather noise forcing using the IE simple model

In order to illustrate the procedure, the application of the interactive ensemble to testing the null hypothesis is illustrated using the simple model derived in the previous section. Two data sets of monthly mean surface heat flux and surface temperature are used to represent the observations: the NCEP (National Center for Environmental Prediction) reanalysis for 1951-2000 (Kalney et al. 1996), and a CGCM control simulation (see section 2.2 for model description).

First, T_e for each month for the reanalysis period is found by solving Eq. (2.4), with T_o specified as the monthly evolution of surface temperature anomalies from the respective "observation" (means as a function of month over the reanalysis period removed). T_e represents the forced atmospheric temperature, defined as the mean from an

ensemble of atmospheric simulations forced by the observed surface skin temperature. A time step of 5 days is used, with the monthly forcing data interpolated to the appropriate time, and the month length taken as 30 days. The surface heat flux from the atmospheric feedback to the observed surface temperature is then evaluated using (2.8b). The atmospheric heat flux feedback is removed from the observed net surface flux anomalies (net solar plus net longwave minus sensible minus latent, monthly means removed) using (2.8c). The resulting flux time series F^* is used to force the interactive ensemble, Eqs. (2.5) and (2.6). This procedure is carried out at each grid point, whether ocean, land, or sea ice. However, the different heat capacities of the active layer of land, sea ice, and ocean need to be taken into account. For simplicity, an energy balance approximation is made over land and sea ice, with the left hand side of (2.6) set to zero, to approximate the small heat capacity of land or sea ice compared to that of the ocean or atmosphere.

Following the above procedure, the interactive ensemble produces a time series of monthly mean surface temperature for the NCEP data and the CGCM control simulation data. The results are shown in the next section.

2.4 Results

Fig. 2.2 shows the correlation of the interactive ensemble surface temperature with the analyzed surface temperature (Fig. 2.2a) and the ratio of the SSTA variance produced by the simple model to the observed variance (Fig. 2.2b) for the NCEP monthly mean data. These can be viewed as estimating the importance of weather noise heat flux forcing in producing the surface temperature variability observed in the latter half of the

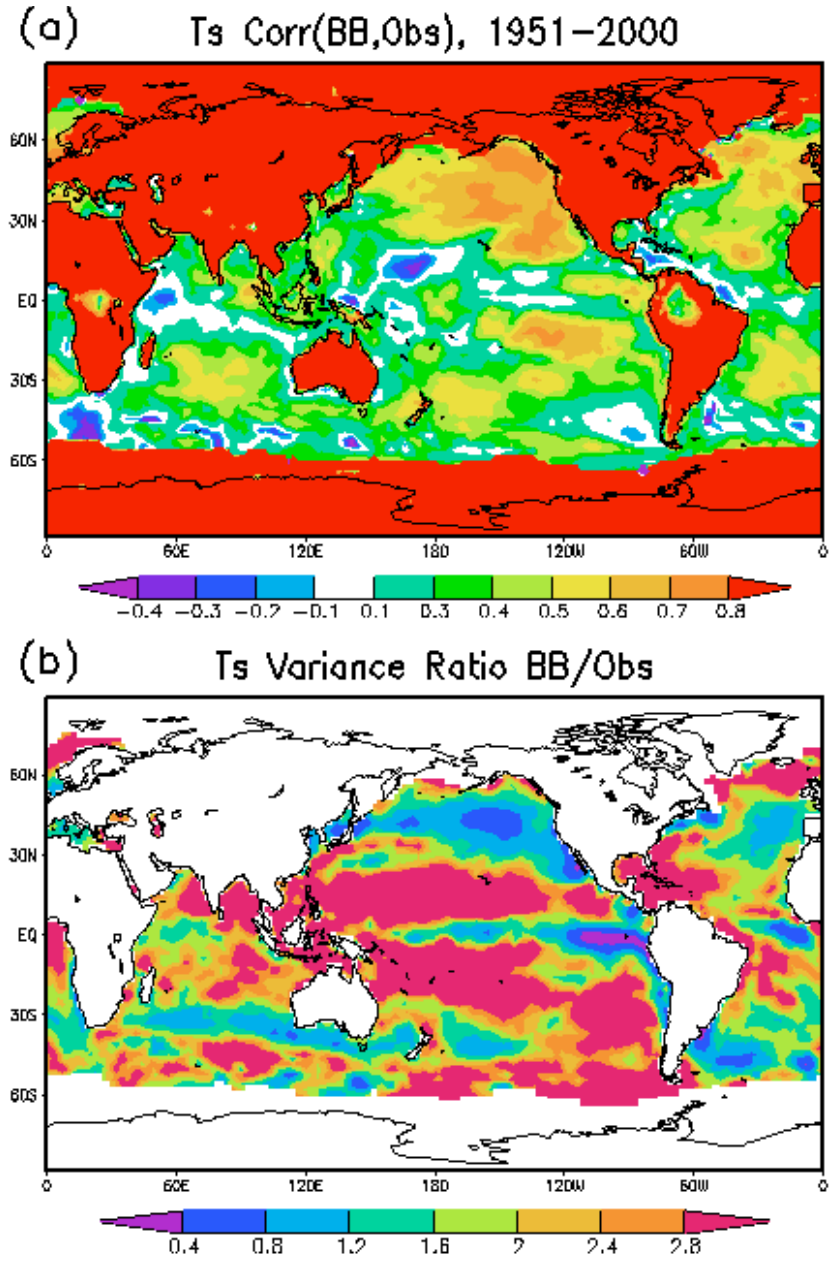

Figure 2.2 (a) Point correlation of monthly mean surface temperature from weather noise forced simple coupled model simulation and from observation (NCEP reanalysis 1951-2000). The weather noise is derived from the total surface fluxes of the NCEP reanalysis using Ts forced simple

twentieth century. In regions where the correlations are close to one and the variance ratio is not small or too big, the surface temperature variability is produced by weather noise heat flux forcing and the null hypothesis is satisfied, while in regions where correlations are not high, other processes are important. Regions where the variability is noise forced then include almost all land and sea ice, and much of the extratropical north Pacific and north Atlantic. There is also a large region in the tropical eastern Pacific where correlations are high. Other regions, such as the equatorial oceans do not have large correlations.

However, the inference that the regions of high correlation are noise forced and that those where correlations are not high are not noise forced is both model dependent and data dependent. In order to interpret the results of Fig. 2.2, the effects of the assumptions and inaccuracies of both the simple model and the reanalysis procedure must be taken into account and evaluated. Some of these are enumerated below:

1) The reanalysis surface heat fluxes are derived quantities (forecast or model generated), constrained by the assimilated data. As such, errors can be introduced by poor data coverage as well as biases and inadequate parameterizations in the reanalysis models.

2) The BB98 atmospheric model is far from perfect: its physical parameterizations are broad caricatures of the actual physical processes and it lacks dynamics. This affects both the estimate of the weather noise surface fluxes and the interactive ensemble response to those fluxes. In estimating the noise, the forced response removed using the simple model is only the local thermodynamic feedback of the

atmosphere to the observed surface temperature anomalies. The atmospheric model physical parameterizations are not realistic, and the local feedbacks therefore contain errors. The neglect of atmospheric dynamics means that the simple model does not correctly represent the scale dependence and propagation characteristics of the atmospheric response to the SST and the associated feedbacks. The feedbacks from surface temperature anomalies in other locations (both nearby and remote) are neglected and are therefore aliased as "noise" by our definition. In order to more correctly calculate the feedbacks, it is necessary to use an atmospheric model which includes dynamics, such as an atmospheric GCM. For example, ENSO teleconnections present in the reanalysis surface fluxes from the physical system are not included in the simple model and are then included erroneously as part of the local weather noise. Then the remotely forced part of the response (for an estimate see Lau and Nath, 1996) is not correctly removed, and errors are introduced into the derived noise. Calculating the atmospheric feedbacks using a model with more realistic physical parameterizations and dynamics, and using these feedbacks to define the weather noise heat flux, would produce a more realistic estimate of the noise than using the simple model. A more realistic atmospheric model would also improve the physical significance of the interactive ensemble diagnosis.

3) The BB98 ocean model does not include ocean dynamics. Therefore, heat fluxes due to oceanic motions are neglected. Notice, for example, the Gulf Stream region in Fig. 2.2a, where correlations are low. One explanation for those low correlations could be oceanic advection of the noise forced SST anomalies away from the forcing region (Frankignoul and Reynolds, 1983; Saravanan and McWilliams, 1998). In fact, the

locations of many of the major ocean surface currents, such as the Kuroshio, and Antarctic Circumpolar Current (ACC) among others, show up as regions of low correlation in Fig. 2.2a. Therefore, the interpretation of some of the regions of low correlation as not being weather noise forced could change if a more realistic dynamical ocean model is used in the interactive ensemble diagnosis and the definition of weather noise forcing is generalized to include the surface momentum and freshwater fluxes.

Throughout the tropical oceans, the correlations are small. This is probably a consequence of the neglect of the heat flux divergences due to ocean dynamics (e.g. forced by surface wind stress). We might expect that the SST variability in this region is caused by the heat flux divergence due to motions in the oceans forced by the surface wind stress, and that the atmospheric heat fluxes exist primarily to damp this variability (i.e. are forced by the SST). If this is the case, the low correlations are due to the neglect of ocean dynamics. In addition, a systematic underestimation of the SST forced atmospheric heat flux in the BB98 atmospheric model could lead to the negative correlations in low latitude, for example if the noise forced heat flux was small compared to the feedback heat flux.

4) The ocean heat storage is not correctly represented. A single constant value is used for the depth of the ocean mixed layer in the simple model, whereas the mixed layer depth in reality varies in space and time. The variance ratios in Figs. 2.2b are much larger than one in extensive regions. This could be due in part to choosing a mixed layer depth that is too shallow in these areas. The regions where the simple model overestimates the SST variance are also regions of generally reduced correlation. Errors in the mixed layer

depth specification could lead to errors in the correlations, as the mixed layer depth affects the phase of the response relative to the forcing (Schneider 1997). The reanalysis fluxes seem to contain useful phase information about the future in extratropical regions where the variance ratio is not much larger than one, which could be evidence that the mixed layer depth and the reanalysis fluxes are reasonably accurate for these regions.

5) Over land and sea ice, the reanalysis surface temperature used is the skin temperature, which is a forecast quantity forced locally by the reanalysis surface heat fluxes. Additionally, the net heat flux over these regions should be close to zero averaged over a sufficient time, as the heat capacity is small. In this situation, the low frequency forced response surface heat flux found from (2.4) and the noise flux found from (2.2) will be equal and opposite, and a surface energy balance heat budget will reproduce the reanalysis surface temperature. Therefore, the diagnosis over land and sea ice is expected to be degenerate: the land and sea ice surface temperatures estimated from energy balance using reanalysis surface fluxes will agree with the reanalysis surface temperatures, and correlations will be high. This is the case in most regions over land and sea ice, except some regions, such as near the equator in the Amazon, Indonesia, and Africa (Fig. 2.2). In the Amazon low correlation region, examination of the total NCEP surface heat flux shows that the condition of zero net heat flux does not hold, so that the argument given above fails. Large discontinuities in the flux in August-September 1984 (to relative negative anomalies) and in January-February 1994 (back to pre-1984 levels) can be seen, although the surface temperature behaves smoothly. The simple model

diagnosis then highlights land areas where there are potentially serious problems with the NCEP reanalysis.

6) External forcing (due for example to changes in atmospheric gaseous composition, particle distribution, and incoming solar flux) is not included in the diagnostic calculations. In the simple model, changes in atmospheric composition might be represented by specifying time dependent coefficients in the longwave radiative parameterization coefficients. Changes in incoming solar flux or effects of volcanic eruptions might be represented by specifying the time/space history of the external forcing $G(t)$ on the right hand side of Eq. (2.3) and in the specified surface temperature atmospheric ensemble (2.4):

$$dT_a/dt = -aT_a + bT_o + N(t) + G(t) \qquad (2.3a)$$

$$dT_e/dt = -aT_e + bT_o + G(t) \qquad (2.4a).$$

If external forcing is not included in the interactive ensemble, but is included in the observations/control model (e.g. by having $G \neq 0$ in (2.3a) but $G = 0$ in (2.4a)), then the atmospheric model ensemble diagnosis will interpret the external forcing contribution to the surface fluxes as "noise" external forcing, and the interactive ensemble forced with this estimate of the noise will reproduce the surface temperature evolution. In order to correctly diagnose the role of external forcing, it must be included in both the observed/control surface fluxes and the diagnostic atmospheric model.

External forcing is not included in the NCEP reanalysis model. The simple model diagnosis using the reanalysis fluxes then can be misleading in that external forcing is not

fully represented in the surface heat flux, although its effects are present in the surface temperature, and in that external forcing is not included in the diagnostic atmospheric model.

2.5 Summary

In the framework of a theoretical ocean-atmosphere coupled model of BB98, we have shown that the observed ocean temperature evolution can be reproduced when the interactive ensemble is forced by the noise surface (heat). A necessary assumption concerning the noise forcing is that the ensemble mean of the different noise realizations is zero (for an infinite ensemble).

The simple model diagnosis reproduces the observed surface temperature reasonably well in some regions, but fails in other regions. This behavior is explained as probably resulting from of the inadequacies of the coupled model, which includes no atmospheric dynamics, no ocean dynamics, and no external forcing, as well as the inadequacies of the analysis, which potentially include quality and quantity of surface temperature data assimilated and incomplete specification of external forcing. These inadequacies can decrease the quality of the reproduction in some regions (tropical oceans, regions of strong ocean currents) and inflate it in other regions (especially land/sea ice areas). However, the faithfulness of the reproduction in some regions (western North Pacific, western North Atlantic) probably indicates that local thermodynamic processes dominate and that the analysis data is reasonably reliable.

The method is applied in later chapters to a more realistic coupled GCM and the procedure is to force the interactive ensemble version of a coupled GCM with the observed noise in the surface fluxes, including heat, momentum, and freshwater.

Chapter 3 Models and Experimental Design

3.1 Models

The coupled GCM (CGCM) used in this study is the anomaly coupled GCM (Kirtman et al. 1997, Kirtman et al. 2002) which combines the Center for Ocean-Land-Atmosphere Studies (COLA) atmospheric GCM version 2 (AGCM) and the Geophysical Fluid Dynamics Laboratory (GFDL) Modular Ocean Model version 3 (MOM3, OGCM). The interactive ensemble coupling technique (Kirtman and Shukla 2002) is applied to the CGCM to reduce the atmospheric internal variability. Here, some of the description of the model is taken from Schneider et al. (2006).

3.1.1 Atmospheric model AGCM

The atmospheric model is the COLA version 2 AGCM. The model physics is described in Schneider (2002). The dynamical core is from the National Center for Atmospheric Research (NCAR) Community Climate Model version 3 (CCM3) described in Kiehl et al. (1998). The horizontal discretization is spectral with triangular truncation at zonal wavenumber 42. The vertical coordinate is sigma with 18 unevenly levels. The parameterization of the solar radiation is after Briegleb (1992) and terrestrial radiation follows Harshvardhan et al. (1987), and includes a realistic evolution of the Earth's orbital parameters (Marx 2001). The deep convection is an implementation of the relaxed Arakawa–Schubert scheme of Moorthi and Suarez (1992) described by DeWitt (1996).

The convective cloud fraction follows the scheme used by the NCAR CCM (Kiehl et al. 1994; DeWitt and Schneider 1996). There is a turbulent closure scheme for the subgrid-scale exchange of heat, momentum, and moisture as in Miyakoda and Sirutis (1977) and Mellor and Yamada (1982, level 2.0). The Simple Biosphere (SiB) model (Xue et al., 1991) is used for the land surface processes.

3.1.2 Oceanic model OGCM

The ocean model is the Geophysical Fluid Dynamics Laboratory (GFDL) Modular Ocean Model version 3 (MOM3) (Pacanowski and Griffies, 1998), a finite-difference treatment of the primitive equations of motion using the Boussinesq and hydrostatic approximations in spherical coordinates. The zonal resolution of the MOM3 is always1.5°, and the meridional resolution is 0.5° between 10°S and 10°N, gradually increasing to 1.5° at 30°N and 30°S and fixed at 1.5° in the extratropics. The model domain is that of the world ocean between 74°S and 65°N. The model has 25 levels in the vertical with 17 levels in the upper 450 m. The coastline and bottom topography in the model are realistic except that ocean depths less than 100 m are set to 100 m and the maximum depth is set to 6000 m. The meridional boundaries are taken as impermeable and insulating. The vertical mixing scheme is the non-local K-profile parameterization of Large et al. (1994). The horizontal mixing of tracers and momentum is Laplacian. The momentum mixing uses the space-time dependent scheme of Smagorinsky (1963) and the tracer mixing uses Redi (1982) diffusion along with Gent and McWilliams (1990) quasi-adiabatic stirring. Climatological sea ice distribution is assumed. There is no sea-ice feedback in this model.

3.1.3 Anomaly coupling model CGCM

The CGCM used in this study is the anomaly coupling version (Kirtman et al. , 1997 and Kirtman et al., 2002). This anomaly coupling strategy applies fluxes adjustiment method. In this strategy, only information about anomalies is transmitted between the atmosphere and ocean components of the coupled model at air-sea interface. The anomalies are computed relative to the model climatologies of each component, while the climatologies upon which the anomalies are superimposed are specified from observations—observed climatologies. The model climatologies are defined by separate uncoupled extended simulations of the oceanic and atmospheric models. In the case of the atmosphere, the model climatology is computed from a 30-yr (1961–90) integration with observed specified SST. This SST is also used to define the observed SST climatology. The observed SST dataset is described in Smith et al. (1996). In the case of the ocean model SST climatology, an extended uncoupled ocean model simulation is made using 30 yr of 1000-mb NCEP–NCAR reanalysis winds. The NCEP–NCAR winds are converted to a wind stress following Trenberth et al. (1990). As with the SST, this observed wind stress product is used to define the observed momentum flux climatology. The heat flux and the freshwater flux in this ocean-only simulation is parameterized using damping of SST and sea surface salinity to observed conditions with a 100-day timescale. The heat and freshwater flux ‘‘observed’’ climatologies are then calculated from the results of the extended ocean-only simulation. The ocean and atmosphere model exchange daily mean fluxes and SST anomalies once a day using utilities supplied with MOM3. There were some problems in the COLA implementation of these utilities. There

is no surface temperature anomaly transmitted to the atmosphere in some grid boxes that contain mixed surface type (land/water, land/sea ice, water/sea ice, or land/water/sea ice). The surface temperature seen by the AGCM in these regions is a climatological surface temperature (Schneider and Fan 2007).

3.1.4 The CGCM interactive ensemble technique

The interactive ensemble technique was developed by Kirtman and Shukla (2002). A schematic diagram of this technique is shown in Figure 3.1. In interactive ensemble air-sea coupled model frame, multiple realizations of the atmospheric component are coupled to a single realization of the oceanic component. Each atmospheric realization is forced by the same SST from the ocean component but started with different initial states. Due to the chaotic nature of atmospheric dynamics the "weather" in each atmospheric model will behave very differently and have no correlation among the members, but will have approximately the same statistics. An approximation is to view the weather as random noise. In the limit of an infinite number of atmospheric models in the ensemble, the ensemble mean of the atmospheric surface fluxes (heat, momentum, and freshwater) is the noise free atmospheric response to the SST forcing, just as in the AMIP ensemble (named after the Atmospheric Model Intercomparison Project; Gates et al. 1998). However, in contrast to the AMIP ensemble, in which the SST forcing is specified, in the interactive ensemble coupling strategy, the SST is predicted from the oceanic component that itself is forced by the noise free/reduced (for a finite ensemble size) ensemble mean atmospheric surface fluxes. This interactive ensemble strategy can be used in simple models as well as in coupled GCMs.

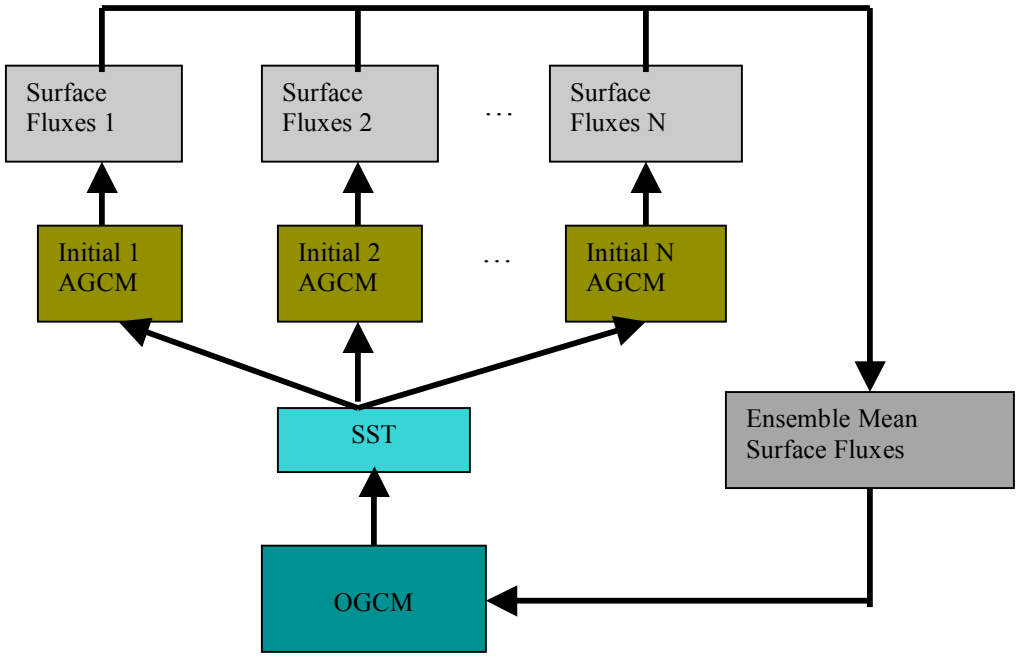

Figure 3.1 Schematic diagram of interactive ensemble approach (AGCM and OGCM can be any atmospheric model and oceanic model, respectively).

In this study, the interactive ensemble CGCM (IE-CGCM) uses six copies of AGCM coupled to a single OGCM. Each AGCM is started with slightly different initial states and forced by the same SST from the OGCM. The OGCM receives the ensemble mean fluxes of heat, momentum, and freshwater over all the six AGCM realizations. Once a day, the AGCM and OGCM exchange fluxes and SSTs. Again, in regions that grid boxes contain mixed surface type, the AGCM sees no surface temperature anomaly, but climatological surface temperature.

3.2 Experimental design

3.2.1 Goals

The potential role of weather noise forcing on SST variability was introduced by Hasselmann (1976). Hasselmann's model suggests the null hypothesis: that all SST climate variability is the response to weather noise forcing (see chapter 2 section 2.1). Previous studies (discussed in chapter 2), which are theoretical and based on simple model, are very successful in fixing concepts and in delineating potential mechanisms of low frequency variability of the coupled system, especially by producing a clear distinction between the roles of noise forcing and other processes. Simple models have the virtue of specifying and controlling the noise, but are not realistic. On the other hand, traditional coupled general circulation models are more realistic, but have no control on weather noise due to the chaotic nature of atmospheric internal variability.

The interactive ensemble coupling strategy (Kirtman and Shukla 2002) reduces the amplitude of atmospheric weather noise in the surface forcing of the ocean to, in principle, an arbitrarily small magnitude. This makes it possible to extend those theoretical simple model studies to a model closely related to a state of the art fully coupled GCM, in which the weather noise forcing can in principle be specified and controlled. Additionally, the interactive ensemble suggests a self-consistent definition of weather noise (Schneider and Fan 2007; chapter 2). Using these tools, two questions are addressed.

1) The first is whether the null hypothesis is satisfied by the CGCM. The null hypothesis test uses data generated by a specific CGCM simulation. The weather noise surface fluxes are found by removing the AGCM feedback to the SST from this

simulation. The weather noise surface fluxes are then used to force the CGCM interactive ensemble. If the weather noise surface flux forcing of the interactive ensemble CGCM reproduces the original CGCM surface temperature variability, and in addition the interactive ensemble is sensitive to the noise forcing, the null hypothesis is satisfied.

2) The second is to diagnose the relative roles of weather noise forcing, coupled feedbacks, and ocean dynamics on the observed low frequency SST variability in the North Atlantic, and especially to explore possible mechanisms of the two major modes of North Atlantic SST variability. The investigation of the North Atlantic uses similar procedure as in the null hypothesis test, but the weather noise forcing is restricted to the North Atlantic in the interactive ensemble, and the relative effects of the heat flux, momentum flux, and freshwater flux weather noise are considered. The model properties are investigated using data generated by the CGCM simulation. The investigation of real climate system use reanalysis surface fluxes and SST.

3.2.2 "Observational" data sets

In this study, two types of "observation" data sets are used. One is the "perfect observation" (CTL in Table 3.1). It is a 50 year segment taken from a multi-century "current climate" run of the CGCM conducted with constant external forcing. The other is "reanalysis observation" (OBS in Table 3.1), in which the atmosphere data is from NCEP/NCAR reanalysis (Kalnay et al. 1996) and SST from Reynolds (Smith et al. 1996).

Table 3.1: Observation data sets: CTL (perfect observation) and OBS (reanalysis observation).

Data set name	Description
CTL (perfect observation)	50 year segment from a multi-century "current climate" run conducted with external forcing held constant, a control simulation.
OBS (reanalysis observation)	Atmosphere data is from NCEP/NCAR reanalysis (Kalnay et al. 1996) and SST is from Reynolds (Smith et al. 1996).

3.2.3 Experimental procedure

Our experimental procedure is first to determine the evolution of the noise in surface fluxes. Then, the noise is used to force the interactive ensemble CGCM (IE-CGCM). Using perfect observations CTL and reanalysis observations OBS, two groups of experiments are carried out following the same experimental procedure.

As described in chapter 2, the atmospheric variability is composed of weather noise, as well as the feedbacks from SST (forced response). The surface flux noise can be determined by removing the feedbacks of surface fluxes from the total "observations" (Figure 3.2). To define the feedbacks of surface fluxes, 10 AGCM simulations are forced by the same "observed" SST but started with slightly different initial conditions. The ensemble mean surface fluxes of heat, momentum, and freshwater are taken as the feedbacks of surface fluxes. This approach avoids the problems of incorrect feedbacks noted by Frankignoul (1999), which are associated with using an analogous approach, but with a statistical atmosphere derived from the observed atmosphere-ocean simultaneous

co-variability, because the lagged correlations are properly taken into account by the AGCM ensemble mean response to the evolution of SST.

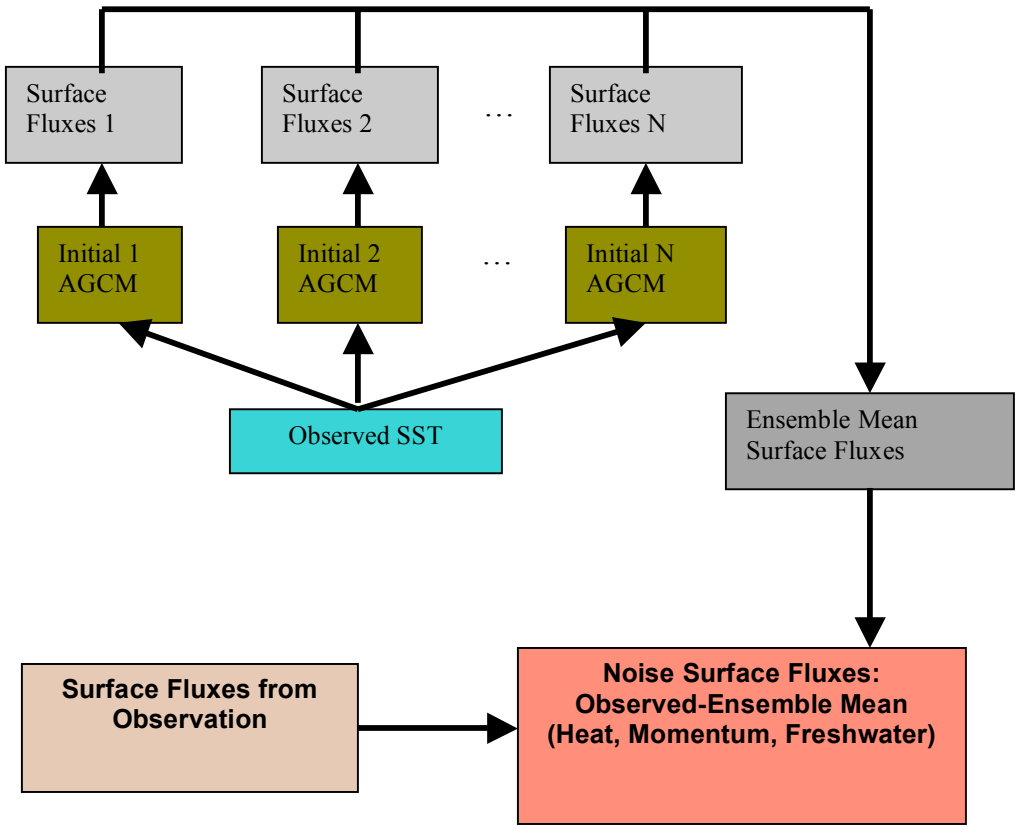

Figure 3.2 Schematic diagram of determination of noise surface fluxes (AGCM can be any atmospheric model).

The weather noise surface fluxes can then be specified as external forcing to the IE-CGCM. The schematic diagram of weather noise forcing of interactive ensemble is shown in Figure 3.3.

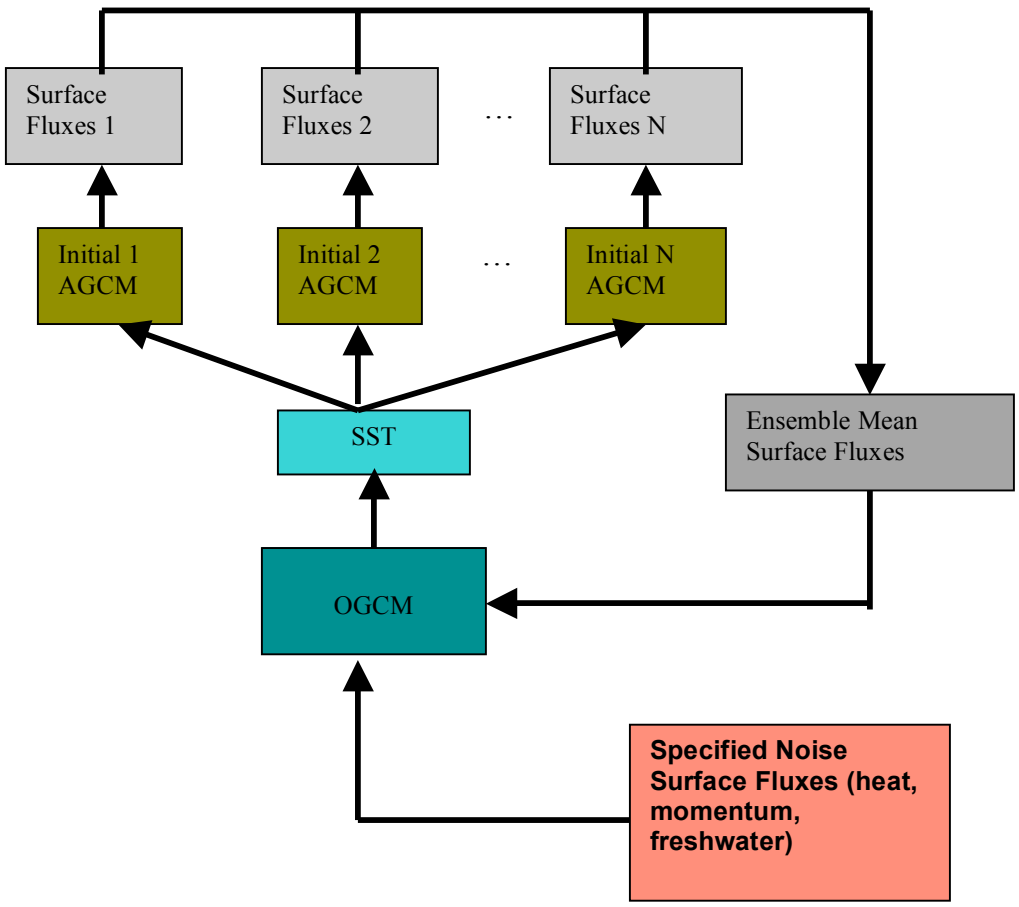

Figure 3.3 Schematic diagram of noise forcing of interactive ensemble (AGCM and OGCM can be any atmospheric model and oceanic model, respectively).

3.2.3.1 Experiments with perfect observation/perfect model

In this group, the CTL (Table 3.1) is used as observations and thus the model and data can be taken as perfect. In the real climate case, the accuracy of the noise estimate of the "reanalysis observation" depends on the realism of the feedbacks calculated by our model and the accuracy of the reanalysis, which in turn depends to some extent on the realism of the NCEP atmospheric GCM as well as the accuracy and time-space coverage

of the observations. The atmospheric model response to the observed SST forcing (the feedbacks), which includes an implicit response to the external forcing, is model dependent. The results from the free evolution of a coupled GCM are known perfectly and it is also known that there is no external forcing. With error-free and external-forcing-free "perfect observation" and a "perfect model", we are in the best position to evaluate the noise accurately and to test the null hypothesis.

a. Determination of the noise

To estimate the weather noise of the surface fluxes in the atmospheric synthetic observations, we subtract the fluxes due to the coupled feedbacks from the observations. The feedback surface fluxes are determined as the time-dependent ensemble mean of 10 AGCM simulations (P_10AGCM in Table 3.2). These 10 AGCM simulations are forced by the same SST that comes from CTL (monthly mean, Table 3.1) over OGCM's ocean domain 74°S-65°N, but start from slightly different initial conditions. Since the same AGCM model is used in both "observation run" (CTL in Table 3.1) and "forcing run" (P_10AGCM in Table 3.2), the forced fluxes are the same in the observations, and in the results of each member of P_10 AGCM, although the noise differs in each case. In P_10AGCM of Table 3.2, each member of the ensemble produces a solution that consists of the forced solution (same for each member) plus weather noise (unique but with similar statistics for each member), and ensemble averaging reduces the noise in the surface fluxes (to zero if in the limit of infinite number of AGCM simulations). The variance of random noise would be expected to be reduced to V/N in the mean of an N member ensemble if the typical variance of random noise in a single simulation is V.

Schneider et al. (2003) have found that an ensemble over 10 simulations is sufficient to give reasonably stable results for the trend of the forced signal over the North Atlantic with the COLA AGCM (removing about 90% of the noise variance). This procedure is exactly equivalent to finding the surface fluxes in the interactive ensemble with the appropriate number of atmospheres, but where the SST evolution is specified instead of determined interactively.

Table 3.2 Experiments forced by the "observed" SST

Experiment	Description	Purpose
P_10AGCM	10 member ensemble of AGCM forced by the same evolution of SST from CTL (Table 3.1) over OGCM's ocean domain 74^0S-65^0N, with slightly different initial conditions. Same AGCM is used in P_10AGCM and in CTL.	The ensemble mean surface flux of the 10 members is taken as the feedback surface flux. Then the noise surface flux is determined by removing the feedback from the total.
R_10AGCM	10 member ensemble of AGCM forced by the same evolution of SST from OBS (Table 3.1) over 40^0S-65^0N, with slightly different initial conditions.	The ensemble mean surface flux of the 10 members is taken as the feedback surface flux. Then the noise surface flux is determined by removing the feedback from the total.

The effect of the error in determining the noise from using a 10 member ensemble as compared to a large ensemble is a matter for further investigation. Also, land surface/sea ice surface conditions are not specified in the calculation of the atmospheric

feedback. Because of this, the weather noise defined by removing the feedback from the total erroneously contains the land/sea ice surface feedbacks.

b. Weather noise forcing experiments

After the weather noise surface fluxes are determined, they are used to force the interactive ensemble CGCM (IE-CGCM). No weather noise forcing is applied over land/sea ice. Three noise forcing experiments are carried out and are shown in Table 3.3. The ocean initial condition in each noise forcing experiment is the same as that of the ocean in the control simulation CTL (Table 3.1). Since the CTL is used as the observations, the external forcing and the errors that come from model and data are eliminated.

Table 3.3: Noise forcing experiments using IE-CGCM with perfect observation/perfect model (CTL in Table 3.1).

Experiment	Forcing noise	Forcing region
P_Gctl	All types of noise surface fluxes (heat, momentum, and freshwater)	Global ocean
P_NActl	All types of noise surface fluxes (heat, momentum, and freshwater)	North Atlantic between 15°N and 65°N
P_NAh	Noise heat flux	North Atlantic between 15°N and 65°N

To illustrate our method and test the null hypothesis, experiment P_Gctl is carried out. In the experiment of P_Gctl, all types of weather noise surface fluxes (heat, momentum and fresh water) are used to force the IE-CGCM globally. There are essentially two possible outcomes from this experiment, both of which might occur

simultaneously in time but in different regions. First, P_Gctl will reproduce the observed SST in places and times where the observed low frequency SST variability is locally forced by the weather noise. The SST response to non-local noise forcing (through atmospheric teleconnections) will also be reproduced. However, in regions where the coupled low frequency variability is due to unstable coupled processes, such as ENSO (Zebiak 1989) or the Latif and Barnett (1994) mechanism, or ocean-only variability (e.g. tropical instability waves induced SST, Hayes et al. 1989) the simulated low frequency SST may not agree with the observed. In this case, the SST variability will be different between P_Gctl and CTL. Differences also can occur due to the errors from various approximations made in applying the method. Potential sources of error include the finite model ensemble sizes, the use of monthly mean rather than instantaneous forcing in calculating the atmospheric feedbacks to the control SST and the response to the weather noise, and incomplete implementation of the procedure over land and sea ice. Differences due to intrinsic coupled variability of the interactive ensemble cause the null hypothesis to be violated.

Experiment P_NActl is designed to illustrate the effect of the local noise forcing on the North Atlantic SST variability. In P_NActl, all types of weather noise (heat, fresh water, and momentum fluxes) are used to force the IE-CGCM 15°N - 65°N in the North Atlantic Ocean. The noise forcing is restricted to the North Atlantic. Outside of that region, the weather noise forcing is taken to be zero. The low frequency variability of North Atlantic SST will then be due to processes local to that region and teleconnection from remote forcing due to a) unstable coupled variability in other regions; b) feedbacks

from the remote response to variability in other parts of the North Atlantic. The contribution of non-local noise forcing on North Atlantic low frequency SST variability will be evaluated by comparing the simulated North Atlantic SST in P_NActl to that from the P_Gctl.

The experiment P_NAh is similar to P_NActl, with the forcing region restricted to 15°N - 65°N in the North Atlantic Ocean, but the forcing weather noise includes the heat flux only. The role of local heat flux noise on SST variability will be investigated. The effects of weather noise momentum and freshwater on the ocean currents are eliminated.

By comparing the results from P_Gctl, P_NActl, P_NAh, and CTL, the roles of noise forcing of remote versus local, as well as heat flux versus momentum and freshwater on North Atlantic SST variability and the major modes of low frequency variability from simulation CTL can be diagnosised.

3.2.3.2 Experiments with Reanalysis observation

Compared to the perfect synthetic observation case, the real climate system is more complicated. The reanalysis data set OBS (Table 3.1) is used in this group of experiments and can be taken as the unique realization of the real climate system. The real climate variability includes the responses of ocean-atmosphere system to the external forcing such as changes in atmospheric composition or solar forcing, as well as the internally generated variability.

a. Determination of the noise

As before, we subtract the forced fluxes from the observed total fluxes to get the noise. The forced fluxes are determined as the time-dependent ensemble mean of 10

AGCM simulations (R_10AGCM in Table 3.2), which are forced by the 1951-2000 reanalysis SST evolution between 40°S to 65°N, but started at slightly different initial conditions. Land and sea-ice again are free to vary. The implementation of the noise calculation is incomplete, and the diagnosed noise will have errors due to this.

Table 3.4: Noise forcing experiments using IE-CGCM with reanalysis observation (OBS in Table 3.1).

Experiment	Forcing noise	Forcing region
R_Gctl	All types of noise surface fluxes (heat, momentum, and freshwater)	Global ocean
R_NActl	All types of noise surface fluxes (heat, momentum, and freshwater)	North Atlantic between 15°N and 65°N
R_NAh	Noise heat flux	North Atlantic between 15°N and 65°N
R_NAm	Noise momentum flux	North Atlantic between 15°N and 65°N

b. Weather noise forcing experiments

Following similar procedures as in perfect observation/perfect model experiments, after the weather noises surface fluxes are determined, they are used to force the IE-CGCM. Four noise forcing experiments are carried out and are shown in Table 3.4. Here, the ocean initial conditions in the noise forcing experiments are the same as those in the perfect observation/perfect model noise forcing experiments, but differ from the reanalysis. Also, there are many potential sources of error in the noise estimate based on the "reanalysis observation", as pointed out previously in section 3.2.3.1, as well as the neglect of feedback from 40°S south SST. This is different from the "perfect-

observation" case, in which the inaccuracy of the noise only comes from the finite number of ensemble members in "forcing run" and the neglect of feedbacks from land and sea ice.

There are 4 noise forcing experiments using the OBS observations: R_Gctl, R_NActl, R_NAh, and R_NAm. The first three follow the same procedures as that of using the CTL observations: P_Gctl, P_NActl, and P_NAh. The last one, R_NAm, is added to investigate Czaja and Marshall's (2001) "intergyre gyre" mechanism of the North Atlantic SST tripole mode. In this experiment, noise forcing includes only the momentum flux noise. As in the perfect observation/perfect model case, the roles of remote versus local, and heat/momentum/freshwater forcing on the North Atlantic SST variability can be diagnosised. The possible mechanisms of the two major observed North Atlantic SST modes – tripole and monopole, which may involve the wind-driven gyre circulation and the meridional overturning circulation (MOC), will be investigated.

Fig. 3.4 is a schematic diagram showing a simplified view of the elements and how they interact to determine the SST evolution in the North Atlantic region. This diagram will be explained more fully in later chapters.

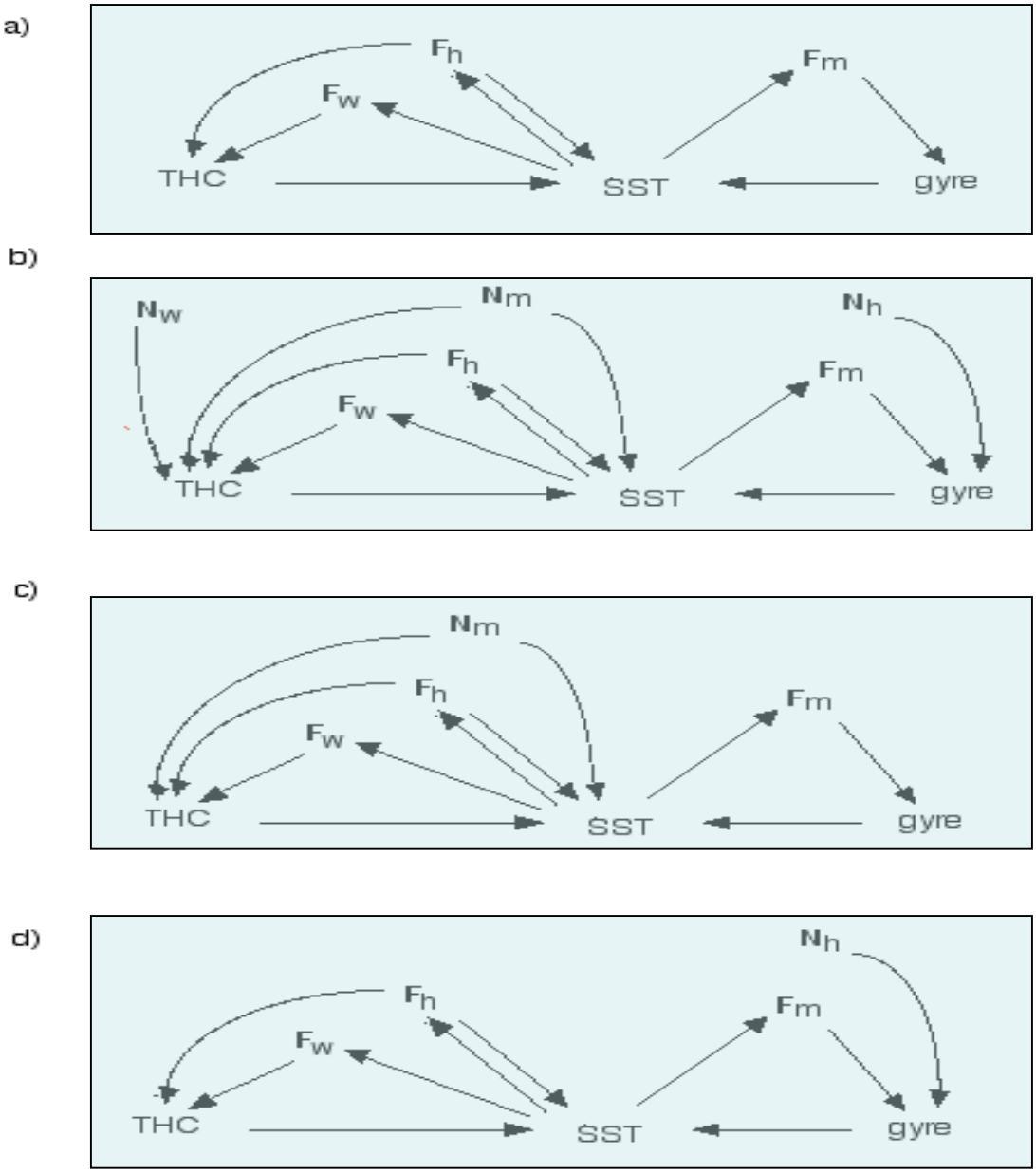

Figure 3.4 Schematic diagram showing elements and how they interact to determine the SST evolution in the North Atlantic in: a) IE-CGCM with no forcing; b) IE-CGCM with all types of noise (freshwater, heat, and momentum) forcing; c) IE-CGCM with heat flux noise forcing; d) IE-CGCM with momentum flux noise forcing. N_w, N_h, N_m are the noise of freshwater, heat, and momentum flux. F_w, F_h, F_m are the feedback of freshwater, heat, and momentum flux.

Chapter 4 Results from the Weather Noise Forcing of IE-CGCM with Perfect Observation/Perfect Model

To test our method and the null hypothesis, results from experiments based on the perfect observation/perfect model experiment are investigated. In the perfect observation/perfect model configuration, the perfect "observation", CTL, is a 50-yr segment from a CGCM multicentury "current Climate" run conducted with constant external forcing (Table 3.1). An AGCM ensemble (P_10AGCM, see Table 3.2) is then forced by the evolution of the CTL monthly SST, and its ensemble mean surface fluxes are defined as feedback surface fluxes. The weather noise surface fluxes are determined by removing the feedback fluxes from the CTL total fluxes. The weather noise surface fluxes are then used to force the CGCM interactive ensemble (IE-CGCM). In all simulations mentioned above, the model components are the same as in CTL simulation. Land surface/sea ice surface conditions are not specified in the calculation of the atmospheric feedback, and no weather noise forcing is applied over land or sea ice in the interactive ensemble.

Many of the results described in this chapter can be inferred from the statistics of a long simulation of the interactive ensemble CGCM with no externally specified weather noise forcing (Wu et al. 2004, Kirtman and Shukla 2002, Kirtman et al. 2005). However, the event-by-event comparison made possible by the inclusion of the noise forcing allows

a more complete understanding of the mechanisms for the evolution of the modes of variability in CTL and the inherent predictability of the model, as well as providing necessary guidance for the evaluation of the results found using reanalysis data.

Three weather noise forcing experiments are carried out: P_Gctl, P_NActl, and P_NAh (see Table 3.3 for details). In each experiment, the ocean initial condition is exactly the same as that of ocean in the CTL.

P_Gctl then serves as a test as to whether the model's climate variability satisfies the null hypothesis that surface temperature climate variability is the response to weather noise forcing. Differences between CTL evolution and the interactive ensemble reconstruction of P_Gctl can occur for two reasons: 1) error from various approximations made in applying the method, and 2) intrinsic variability of the interactive ensemble not due to the weather noise forcing. Potential sources of error include the finite model ensemble sizes, the use of monthly mean rather than instantaneous SST in calculating the atmospheric response to the CTL SST, and incomplete implementation of the procedure over land and sea ice.

Comparing results from P_Gctl and P_NActl will tell us the sensitivity of the CGCM interactive ensemble to weather noise forcing and test the null hypothesis further. The role of noise heat flux relative to those of the momentum and fresh water fluxes on the low frequency SST variability in the North Atlantic can be investigated by comparing the results from P_NActl and P_NAh.

4.1 CTL properties

Our goals in this study are to test our null hypothesis and prove our method, and then apply it to real climate to diagnose the relative roles of weather noise forcing, coupled feedbacks, and ocean dynamics on the low frequency SST variability in the North Atlantic, and especially to explore possible mechanisms of the two major modes of North Atlantic SST variability. Therefore, in this section, the North Atlantic Oscillation (NAO) and North Atlantic SST variability will be investigated closely in our perfect "observation" CTL and verified against the variability in nature.

4.1.1 NAO and North Atlantic SST variability from observation

In the atmosphere, the North Atlantic Oscillation is the primary mode of variability in the North Atlantic sector and its spatial pattern can be defined as the leading EOF of sea level pressure (SLP) anomaly in the North Atlantic region (Hurrell et al. 2003), with largest variability during the boreal winter months. Figure 4.1 is the first EOF of winter (JFM) SLP anomaly from observation. It accounts 53.2% of the total variance and is dominated by a dipole structure, with a positive center of action straddling the subtropical Atlantic, and a negative lobe approximately centered over the Arctic, which is consistent with the observed winter NAO from Hurrell et al. (2003).

In the ocean, observational studies show that the North Atlantic SST anomalies are characterized by two distinctive patterns: a tripole and a monopole (e.g., Deser and Blackmon 1993; Wu and Liu 2005). Figures 4.2a and 4.2b are the leading two EOFs of the North Atlantic winter (JFM) SST anomalies (linearly detrended) from observation. The first EOF (Fig. 4.2a), which accounts for 31.3% of the total variance, shows a tripole

pattern, with anomalies extending from the southeast coast of the United States into the central basin, surrounded by anomalies with opposite polarities in the subpolar south of Greenland and the Tropics south of 30°N. The second EOF (Fig. 4.2b), which accounts for 25.4% of the total variance, shows a monopole with uniform polarity over the North Atlantic.

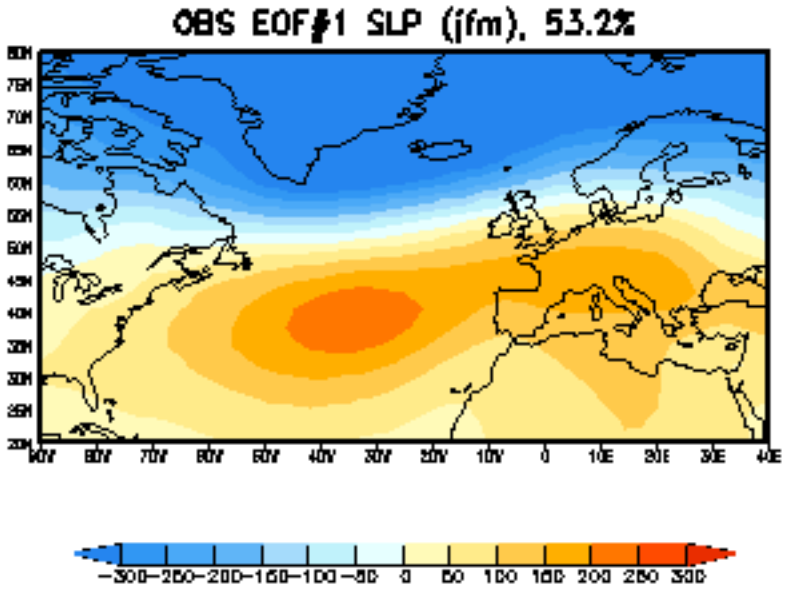

Figure 4.1 Leading EOF of the North Atlantic winter (JFM) sea level pressure (SLP) anomaly from observation, accounts for 53.2% of total variance. Unit is Pa per standard deviation of the corresponding PC.

Both observations and modeling studies suggest that the tripole SST anomaly might be forced by intrinsic atmospheric variability, the NAO, in conjunction with heat transport by ocean, such as the mean flow advection or intrinsic Rossby wave dynamics in the ocean (Frankignoul et al. 1997; Saravanan and McWilliams 1998), as well as

anomalous advection of the mean temperature gradient (e.g., Grotzner et al. 1998; Marshall et al. 2001, Czaja and Marshall 2001). Our analyses show that the tripole pattern of Fig. 4.2a corresponds to the opposite sign of the NAO pattern of Fig. 4.1. On the other hand, the monopole SST anomaly might be associated with the fluctuations in the thermohaline-driven meridional overturning cell (MOC) of the North Atlantic Ocean (e.g., Kushnir 1994; Delworth et al. 1993).

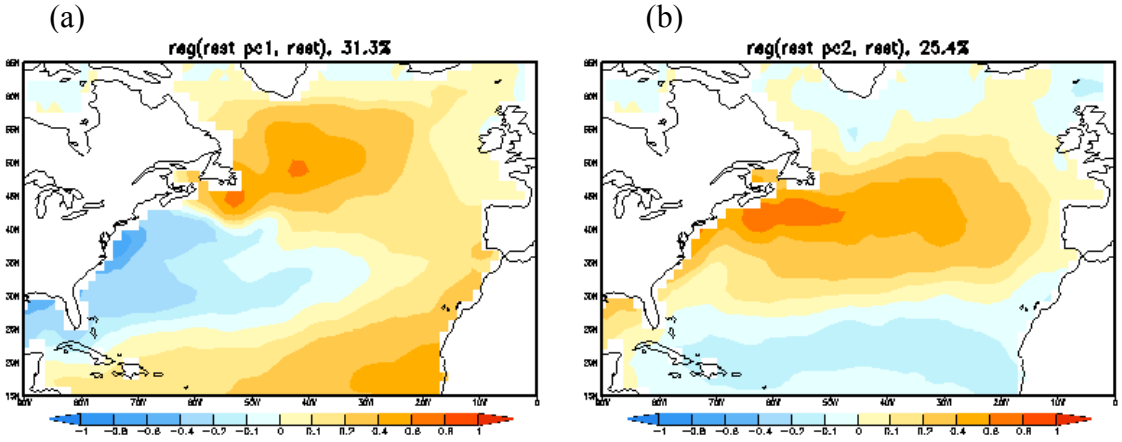

Figure 4.2 Leading EOFs of the North Atlantic winter (JFM) SST anomalies (linear detrended) from observation: (a) SST first EOF (tripole mode), accounts for 31.3% of total variance. (b) SST second EOF (monopole mode), accounts for 25.4% of total variance. Unit is K per standard deviation of the corresponding PC.

4.1.2 NAO and North Atlantic SST variability from CTL

The leading EOF of the North Atlantic JFM surface pressure anomaly from CTL is shown in Figures 4.3. It accounts for 71.6% of total variance and exhibits a north-south dipole structure, with a resemblance to the NAO-like pattern, although centers are located too far north-east compared to the observed (Fig. 4.1).

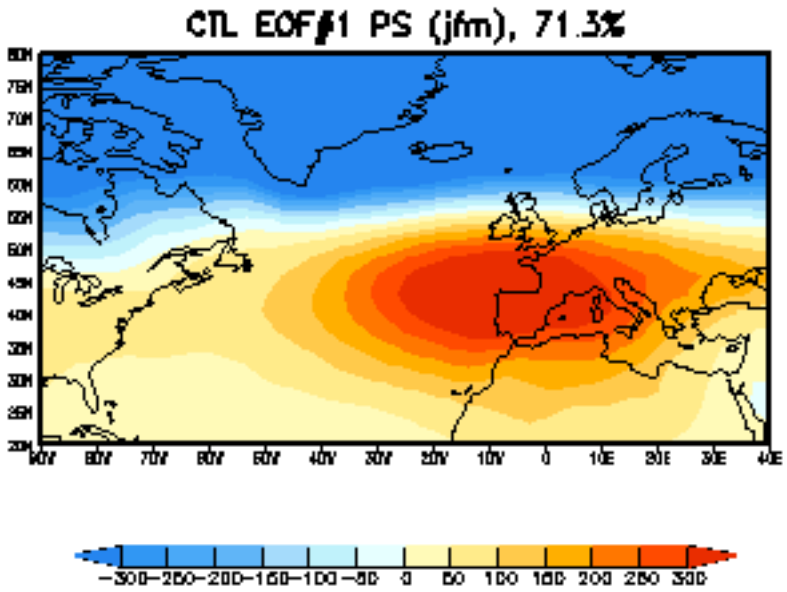

Figure 4.3 Leading EOF of the North Atlantic winter (JFM) surface pressure anomaly from CTL, accounts for 71.3% of total variance. Unit is Pa per standard deviation of the corresponding PC.

The leading two EOFs of the North Atlantic winter (JFM) SST anomalies (linearly detrended) from CTL are shown in Figures 4.4a and 4.4b. They exhibit two distinctive patterns. The first EOF (Fig. 4.4a), which accounts for 27.3% of the total variance, shows a monopole-like pattern with close-to-uniform polarity over the main North Atlantic basin, although the center shows an eastward shift compared with the observed one (Fig. 4.4a versus Fig. 4.2b). The second EOF (Fig. 4.4b), which accounts for 20.7% of the total variance, has a tripole-like pattern with anomalous warming in the subpolar, cooling in the Gulf stream region and extending from the southeast coast of the United States to the southwest coast of Europe, and warming in the Tropics south of 30°N. Compared with the observation, the amplitude of subpolar center of the CTL

tripole is weaker. Also, the subtropical center extends/shifts much farther east: from basin-center to southeast coast of Europe, which is not seen in the observation (Fig. 4.4b versus Fig. 4.2a), and might be related with the eastward shift of NAO in CTL (Fig. 4.3 and below). Overall, the CTL tripole and monopole resemble the observed patterns (Fig 4.4b versus Fig. 4.2a and Fig. 4.4a versus Fig. 4.2b), in spite of the shifting of the EOF orders as well as some other notable deficiencies.

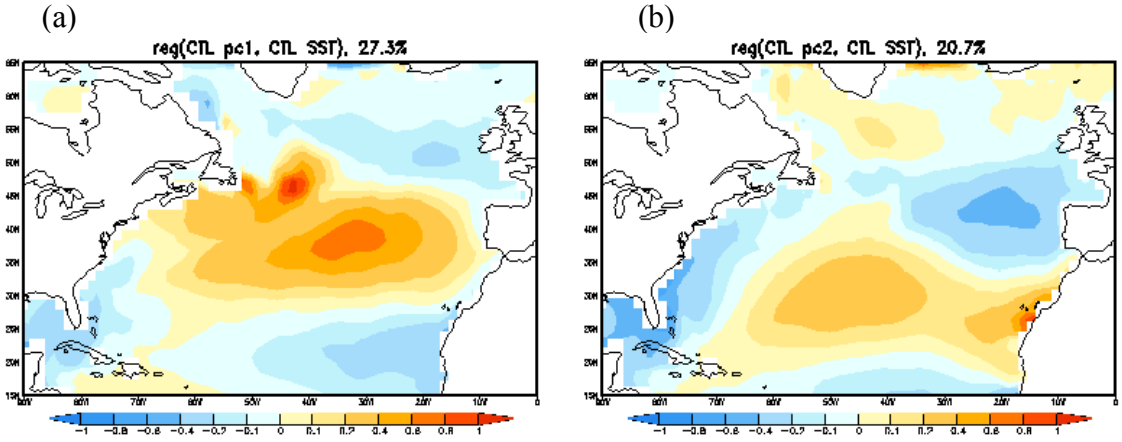

Figure 4.4 Same as Fig. 4.2, but SST anomalies come from CTL: (a) SST first EOF ("monopole" mode), accounts for 27.3% of total variance. (b) SST second EOF ("tripole" mode), accounts for 20.7% of total variance. Unit is K per standard deviation of the corresponding PC.

Associated with the SST tripole-like mode, the CTL atmosphere reveals a coherent NAO-like pattern. We take the JFM surface pressure from CTL and regress it onto the second EOF's (Fig. 4.4b) corresponding principle component (normalized), and the result is shown in Figure 4.5. From Fig. 4.5, corresponding to tripole-like SST pattern, the atmosphere exhibits a north-south dipole in the surface pressure, resembling

the CTL negative phase of NAO-like pattern (Fig. 4.3, opposite sign). A negative NAO anomaly, i.e. a positive polar and negative subtropical surface pressure anomaly, is associated with cooling in the subtropics, and warming in the subpolar lobe and Tropics south of 30°N. The possible importance of ocean role on this tripole-like mode will be discussed in a later section.

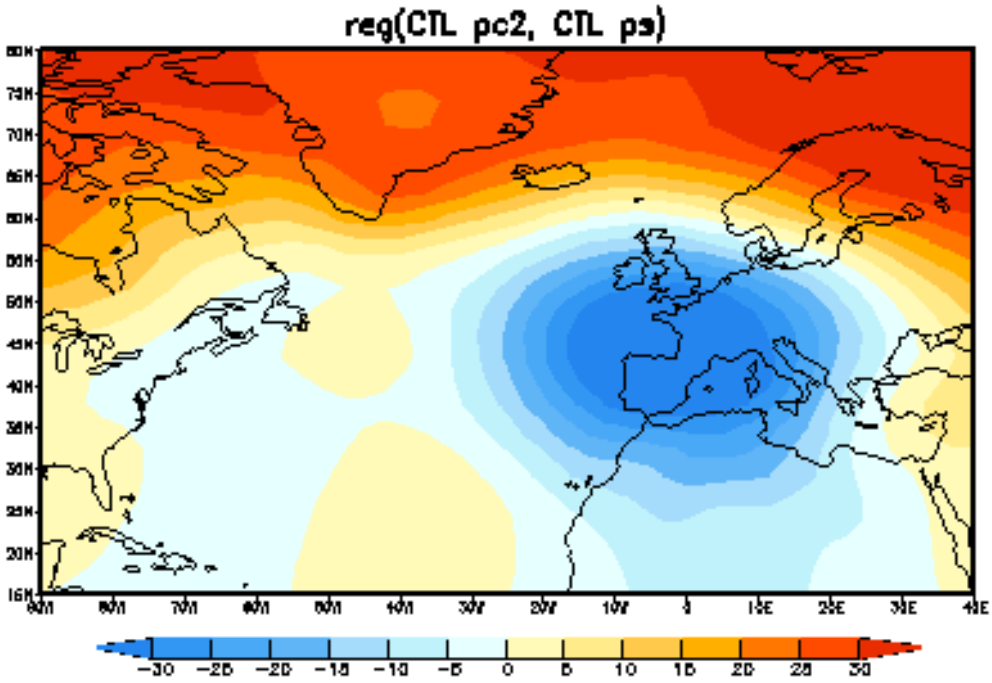

Figure 4.5 Regression of CTL surface pressure onto the principle component (PC) of second EOF of CTL SST ("tripole" mode, Fig. 4.2b). Unit is Pa per standard deviation of the corresponding SST PC.

(a)

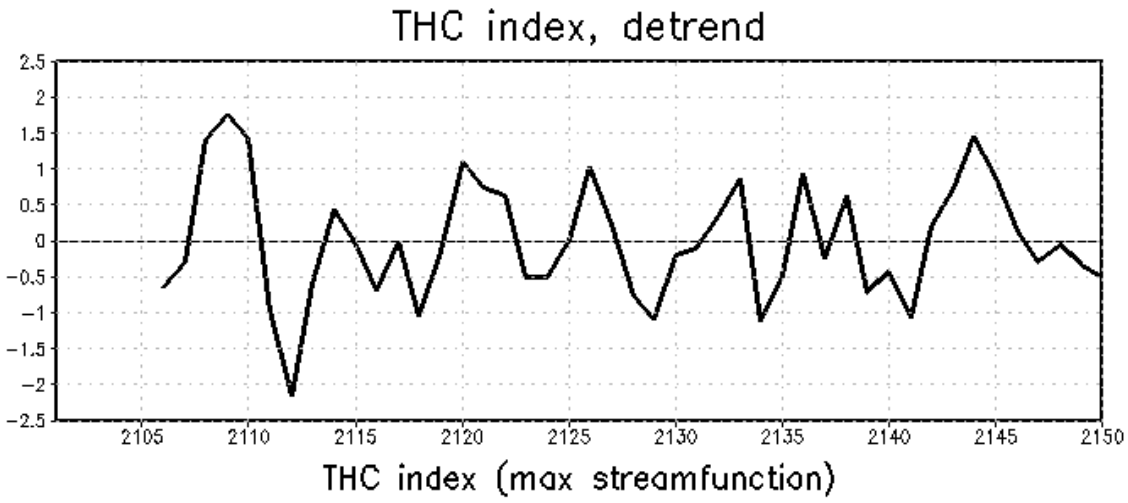

(b)

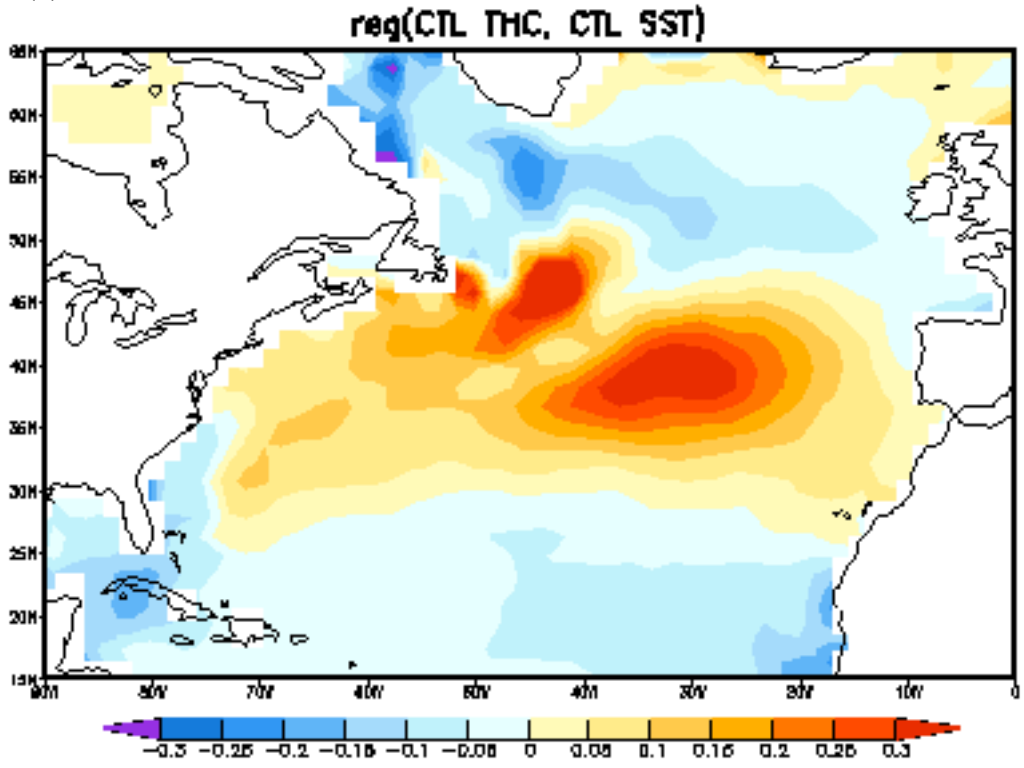

Figure 4.6 (a) Time evolution of the CTL North Atlantic THC index, which is the maximum annual mean stream function. (b) The regression of CTL SST onto the CTL THC. Unit is K per standard deviation of the THC.

The monopole SST anomaly is suspected to be associated with the fluctuations in the thermohaline circulation (THC) (e.g., Kushnir 1994; Delworth et al. 1993). The intensity of the THC in the North Atlantic is defined each year as the maximum streamfunction representing the annual-mean meridional circulation, found from the zonal average of the meridional velocity across the basin. A time series of this index from CTL, which represents the fluctuations in the intensity of the annual-mean THC, is shown in Figure 4.6a. From Fig. 4.6a, the decadal feature in this index is obvious. The spatial pattern of the CTL SST anomalies associated with fluctuations in the intensity of the THC (the regression of CTL JFM SST with THC index) is shown in Figure 4.6b. The pattern of SST change bears a strong resemblance to the SST monopole-like pattern (Fig 4.4a), supporting the suspected association, although the mechanism of THC is not clear here and will be discussed in a later section.

In summary, CTL produces some similarities to the observed North Atlantic SST variability, although with some distortion. The relationships between tripole mode and atmospheric NAO, as well as monopole mode and THC appear to be similar in CTL to previous studies.

4.2 Characteristics of weather noise

Before evaluating the role of weather noise forcing in surface climate variability, the definition of weather noise is discussed and its properties are displayed. The total atmospheric variability is composed of weather noise and signal (feedback from SST). Thus the residual atmospheric variability between total and feedback can be defined as the noise. Now the question is how the feedback is defined. One technique is to construct

statistical models of the atmospheric response to SST by simultaneous regressions of the atmospheric fluxes against the SST. For example, Kleeman and Moore (1997) use this approach to estimate the stochastic component of the surface wind stress as a residual. Similar procedures are applied by Blanke et al. (1997) and Kirtman and Schopf (1998) among others. As pointed out by Frankignoul (1999), this procedure can confuse the noise that forces the SST with the atmospheric response to the SST, due to the ocean's finite heat capacity. In particular, if the SST variability is forced thermodynamically by noise, the regression approach will produce a heat flux that would tend to amplify the SST anomalies, while the feedback (the correct forced response) must damp the SST anomalies. This confusion of forcing and response can produce totally misleading conclusions, for example about predictability of the SST anomalies. Similar considerations apply to time filtering of data and identifying stochastic noise with shorter time scales (Boer 2004). In order to separate the atmospheric response component from the noise, the lagged correlations must also be considered. We define the feedback as the time-dependent ensemble mean of AGCM simulations forced by observed SST, but started from slightly different initial conditions. The SST forcing of the atmosphere at all (resolved) time and space lags is taken into account in this GCM based approach. The concept that weather noise is determined by subtracting this feedback from the total is defensible. A verification of this procedure is that it recovers the known specified noise forcing in simple models (chapter 2). Next, we will investigate the characteristics of weather noise defined in this way in perfect model/perfect observation configuration. While the purpose here is to use the weather noise to force the IE-CGCM and to make

inferences about the mechanisms for modes of low frequency SST variability, this is a new procedure to determine weather noise, and the resulting properties of the weather noise are of intrinsic interest by themselves.

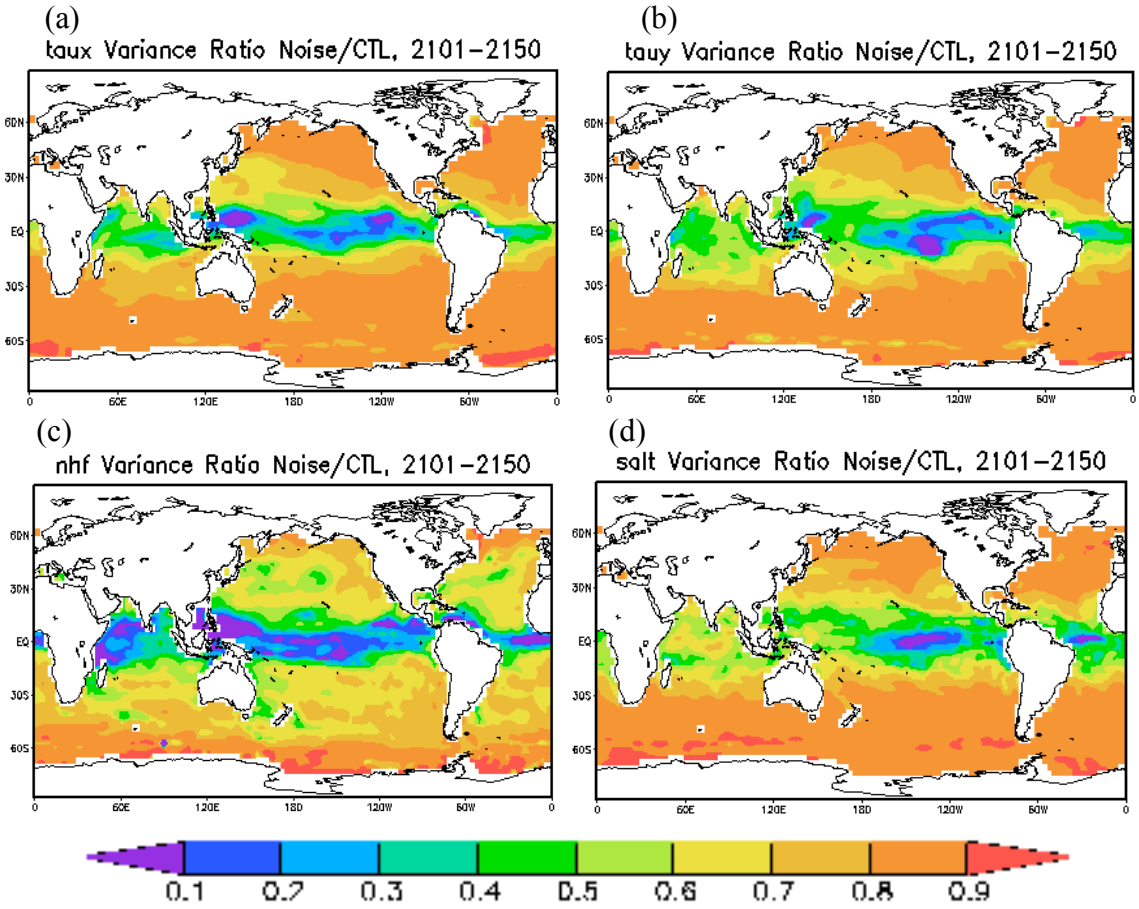

Figure 4.7 Variance ratio (noise to total) of monthly mean zonal windstress (a), meridonal windstress (b), heat (c), and salinity flux (d). Total surface fluxes are from CTL. Noise surface fluxes are defined by subtracting feedback surface fluxes from the total. Feedback surface fluxes are the ensemble mean of surface fluxes of P_10AGCM.

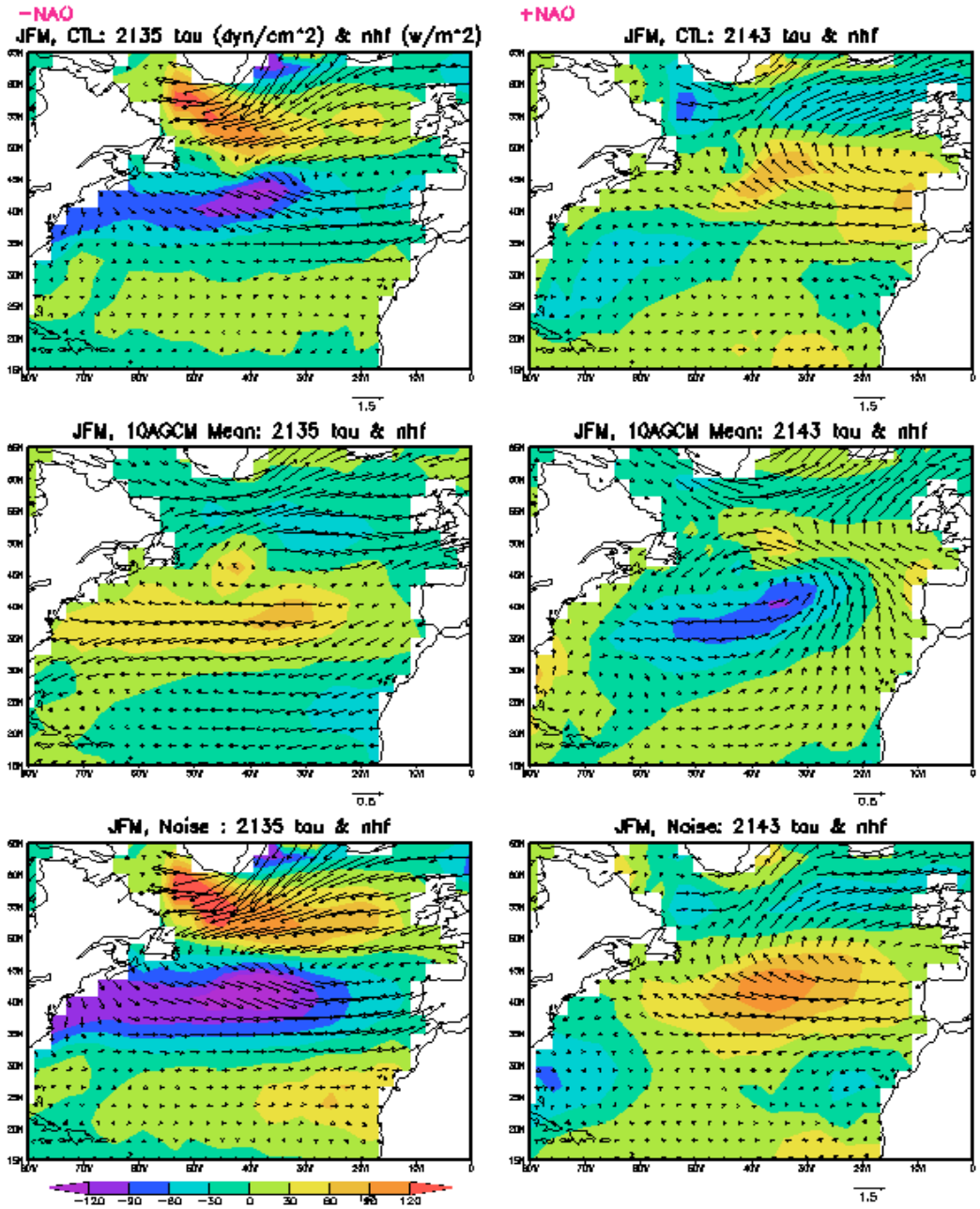

Figure 4.8 The wintertime (JFM) spatial structure of heat flux (downward positive, shaded) and windstress (vector) for 2135 (strong negative NAO index, left panel) and 2143 (strong positive NAO index, right panel). The top panels are from the synthetic observation CTL; the middle panels are the ensemble mean of P_10AGCM; the bottom panels are the noise, total (top) minus feedback (middle). NAO index is defined as the principal component of the first EOF of surface pressure from CTL. Units for heat flux and windstress are W/m^2 and N/m^2, respectively. The windstress vector length is 0.5 units in the middle panel compared to 1.5 units in the corresponding top and bottom panel.

The weather noise in CTL was evaluated using the above procedure. The feedbacks were evaluated from the AGCM ensemble P_10AGCM, and these were subtracted from the CTL fields. Figure 4.7 is the variance ratio of noise to total for zonal windstress (a), meridional windstress (b), heat flux (c), and salinity flux (d) from monthly mean data. In general, the variance of the noise dominates over that of the feedbacks in the extra-tropics. In the case of the momentum and fresh water fluxes, the noise explains 60% ~ 90% of total surface fluxes variance. The noise heat flux explains 40% ~ 80% of the total and has a structure that seems to be related to major ocean currents such as western boundary currents. The noise explains less than 40% of the total heat flux over the tropics and further reduces to 20% near the equator. Over some equatorial regions, e.g. western equatorial Pacific, noise explains less than 10% of the total. These features seen in the surface fluxes are also seen in other atmospheric variables, such as precipitation and surface pressure (figures are not shown). It must be pointed out that although the variance of noise fluxes near the equator is small, less than 30% over most of the equatorial Pacific, its role on SST variability is important. The equatorial Pacific SST variability cannot be produced without these noise surface fluxes. This result will be shown in detail in the following (section 4.3).

To see the characteristics of noise surface fluxes related to North Atlantic climate variability, two typical years with extreme wintertime (JFM) atmospheric states are selected. One is the simulation year "2135", during which the NAO is extremely weak (large negative NAO index. NAO index is defined as the principle component of the first EOF of surface pressure from CTL with sign convention to agree with commonly used

NAO indices, see Fig. 4.3). Another is the year "2143", during which the NAO is extremely strong (large positive NAO index). To emphasize the role of noise surface fluxes in forcing the North Atlantic surface climate variability, we show the fluxes of these two years over North Atlantic basin (15-65°N), including the total fluxes (top panels of Figure 4.8), which is the observation (from CTL); the forced fluxes (middle panels of Fig. 4.8), which comes from the ensemble mean of P_10AGCM; and the observed noise (bottom panels of Fig. 4.8), which is the difference between the total and the forced fluxes.

From the top-left panel of Fig. 4.8, the observed total anomaly of heat flux has a tripole pattern, with negative anomalies (heat flux downward to the ocean is positive) extending from the southeast coast of the United States into the central basin to the west coast of southern Europe, and positive anomalies in the high-midlatitudes south of Greenland and in the Tropics. The corresponding anomaly of windstress is westward north of 35°N, eastward south of 35°N, a typical negative NAO circulation pattern. In 2143 (top-right panel of Fig. 4.8), the total heat flux and windstress anomalies are both opposite to those in 2135.

The heat flux and windstress of ensemble mean of P_10AGCM, which is a 10 member AGCM ensemble forced by the CTL SST, are the feedbacks or "forced response." For both the years 2135 and 2143, the magnitudes of both the heat flux and windstress are small compared to the observed total (Fig. 4.8 middle. Note that windstress vector length is 0.5 units compared to 1.5 units in the corresponding top and bottom panels). The difference between the observations and the forced responses are

taken as weather noise (bottom panels of Fig. 4.8). The noise heat flux and noise momentum flux have similar patterns as the observed total for both 2135 and 2143 with larger amplitudes compared to the feedbacks. The sign between the noise and the feedback is opposite both for heat flux and windstress flux, for example, the feedback heat flux in year 2135 (middle-left) is positive in subtropics, negative in the high-midlatitudes south of Greenland and in the Tropics, opposite to the noise heat flux (bottom-left). The feedback windstress flux is positive NAO circulation: An anticyclonic circulation at subtropics and a cyclonic circulation at high latitude. The atmospheric response to SST is negative feedback both for heat flux and windstress flux.

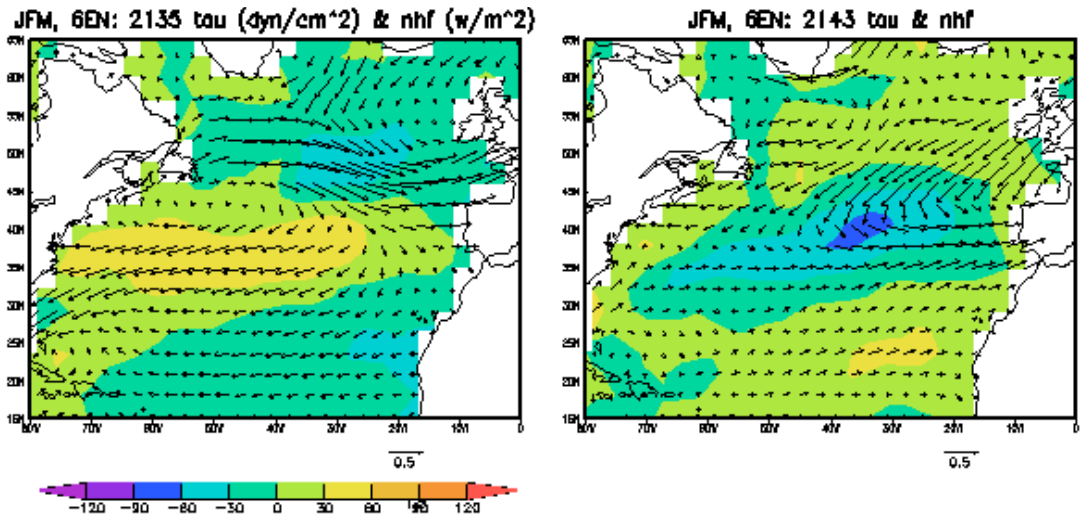

Figure 4.9 Same as the middle panel of Fig. 4.8, but the heat flux and windstress are the ensemble mean of 6 members AGCM from global noise forced simulation P_Gctl. Units for heat flux and windstress are W/m^2 and N/m^2, respectively.

The heat flux and windstress of ensemble mean of the global noise forced simulation P_Gctl (6 members AGCM) for year 2135 and 2143 are shown in Figure 4.9. The patterns in Fig. 4.9 are similar as that in the middle panel of Fig. 4.8, especially for the heat flux. This is because that the CTL SSTs in year 2135 and 2143 are well reproduced. The differences between Fig. 4.9 and the middle panel of Fig. 4.8 are partially due to the different size of AGCM ensemble (6 members versus 10 members).

4.3 Weather noise forcing in reproducing the "observed" surface temperature anomaly

The response of the interactive ensemble to forcing from the weather noise as defined above is considered next. The map of point-to-point correlation coefficient and the corresponding variance ratio of surface temperature anomaly from the global noise forced simulation P_Gctl with that from the "observation" CTL is shown in Figure 4.10. These results can be viewed as estimates of the importance of weather noise flux forcing over ocean in producing the surface temperature variability seen in the CTL. The regions of highest correlation in Fig. 4.10a are in the northern and southern subtropical oceans. Errors are introduced into the definition of the noise by the finite size of the AGCM ensemble (10 members) and into the interactive ensemble diagnosis by the finite AGCM ensemble (6 members). If these errors are uncorrelated with CTL and with each other, an estimate of the highest correlation expected from the interactive ensemble is 0.89 ($\approx 1/\sqrt{1+1/10+1/6}$ assuming random uncorrelated errors). The regions of highest correlation approach this maximum. Over the rest of the oceans, even over most of the tropical oceans, the correlations are generally high, >0.7. There are several regions of

lower correlations, especially in the Southern Ocean south of 45°S and in the western equatorial Pacific. However, aside from these regions, it appears that the SST variability is either predominantly weather noise forced or is caused by some type of variability that is insensitive to the weather noise forcing. Identification of the mechanisms for the regions of high and low correlations will be discussed further below.

Over land and sea ice, correlations in Fig. 4.10a are much lower than over the oceans. Significant correlations are found over most land areas equatorward of 30° latitude, with largest correlations near the equator. The results over land can be viewed as an estimate of the "predictability" of land surface temperature anomalies, given that the SST is known, and is expected to be smaller than the correlations from the SST forced AGCM ensemble P_10AGCM.

Correlations of the SST are relatively large in the eastern and central equatorial Pacific, where the anomalies are larger, compared to those in the western equatorial Pacific, where the anomalies are smaller. To see this more clearly, a time-longitude diagram of monthly mean SSTA along the equator in the Pacific Ocean is shown in Figure 4.11. We can see that the succession and general structure of ENSO-like warm and cold events seen in CTL is well simulated in P_Gctl after some disagreement in the first several years.

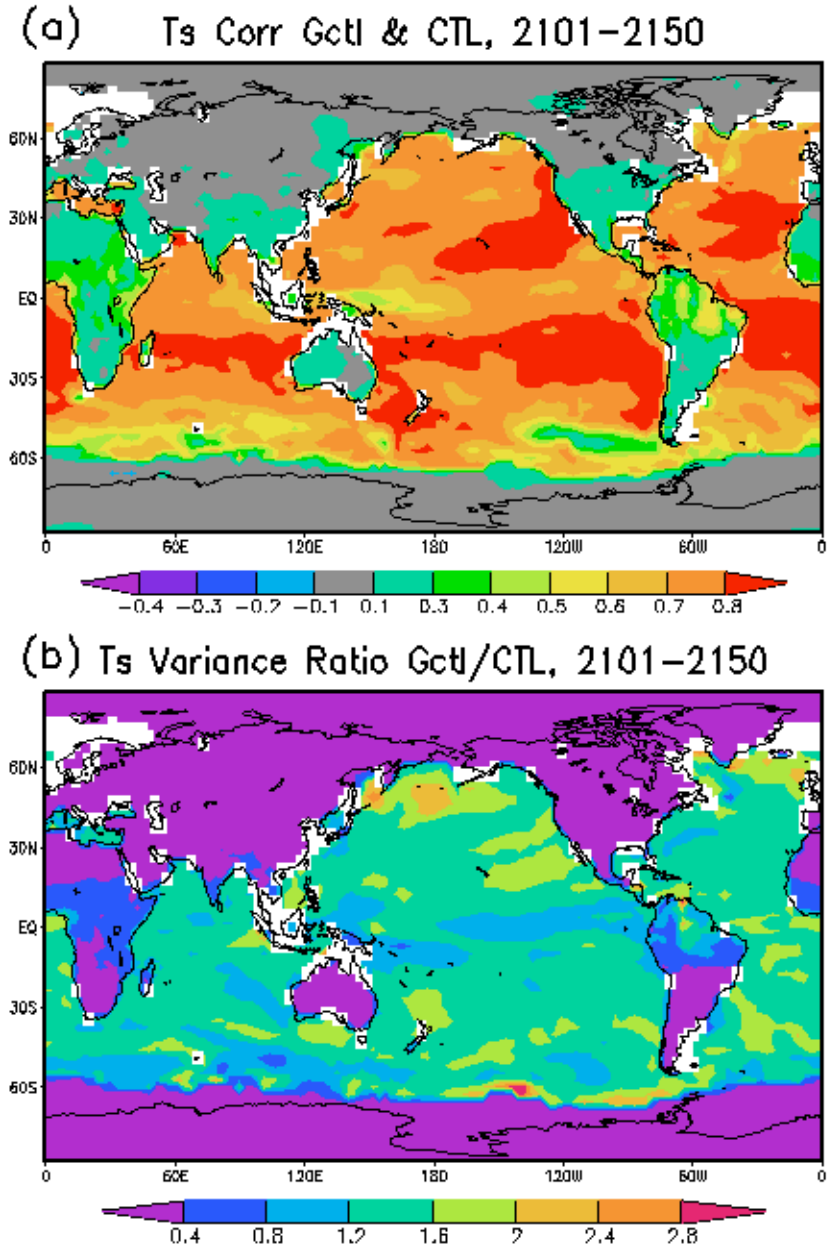

Figure 4.10 (a) Point correlation coefficient of monthly mean surface temperature anomaly from global weather noise forced interactive ensemble simulation P_Gctl (Table 3.3) with that from synthetic observation CTL (Table 2.1). Correlations in non-gray shaded regions are significantly different from zero with 95% confidence assuming 600 degrees of freedom. Surface temperature anomalies supplied to the atmosphere are identically zero in the white regions in the coupled GCM due to coupling issues (see text for detail). (b) Ratio of surface temperature variance from P_Gctl to that from CTL.

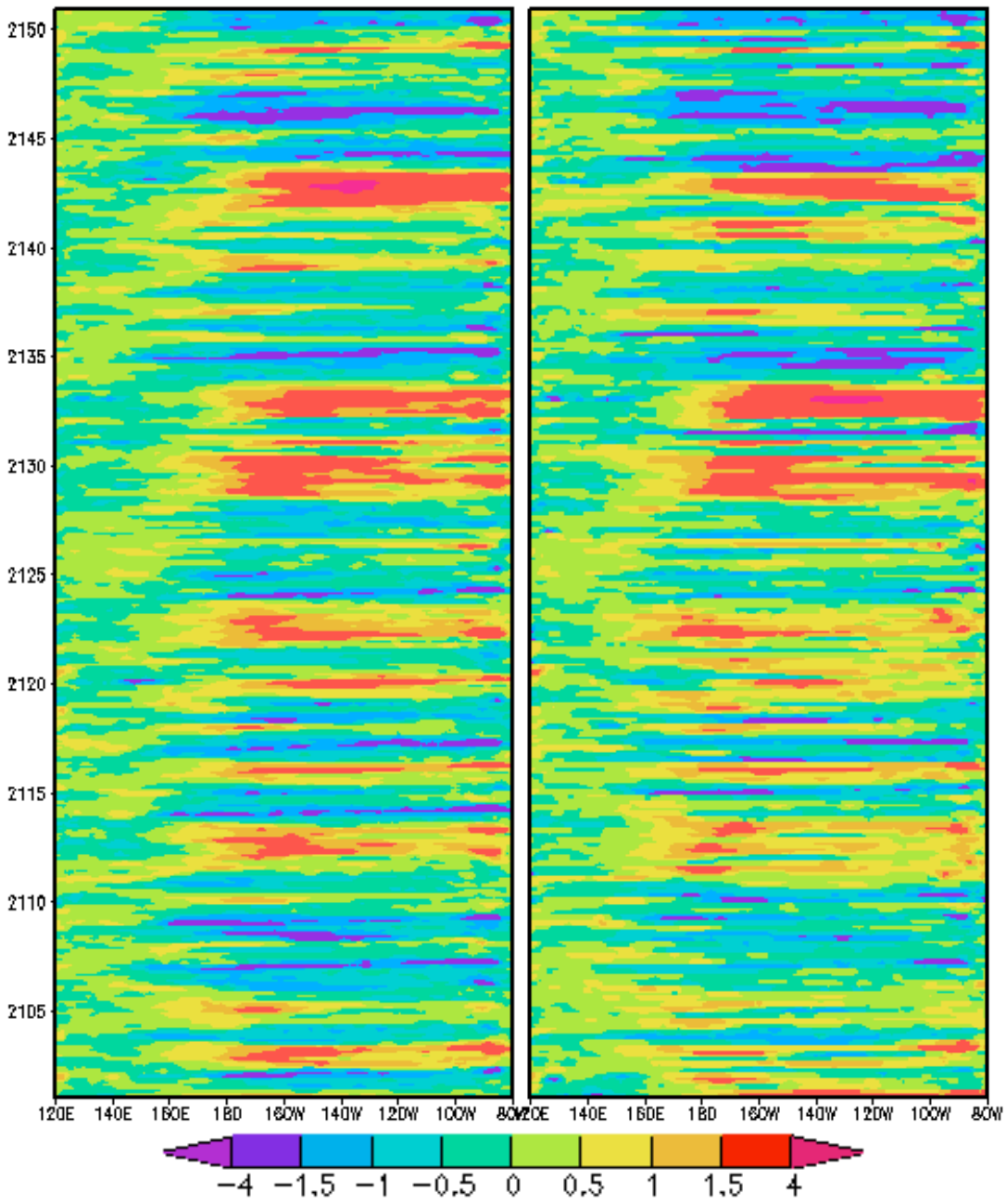

Figure 4.11 Time-longitude diagram of monthly mean SST anomaly (K) along the Equator in the Pacific Ocean. Left panel: SSTA is from CTL and Right panel: SSTA is from P_Gctl.

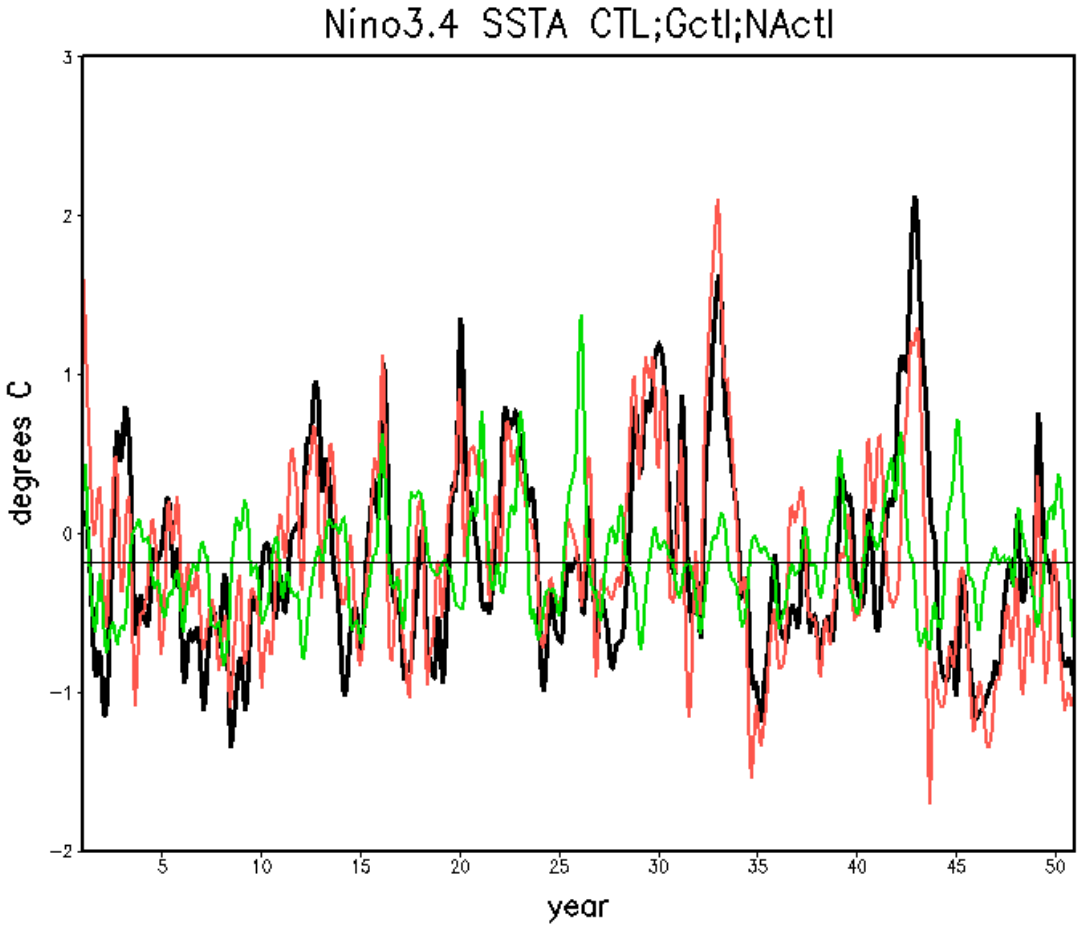

Figure 4.12 Time series of Nino-3.4 SSTA index: CTL (black), global weather-noise-forced interactive ensemble P_Gctl (red), and North Atlantic weather-noise-forced interactive ensemble P_NActl (green).

Thus, these high correlations of warm and cold events in the eastern and central equatorial Pacific are a consequence of similar ENSO-like variability. Figure 4.12 is the time evolution of monthly Nino3.4 (190°E-240°E, 5°S-5°N) SSTA, in which the black curve is from CTL, the red curve is from P_Gctl, and green curve is from P_NActl. The largest difference between the CTL "observation" and the P_Gctl global noise forced interactive ensemble indices occurs in the first month of the simulation, possibly

indicating a cold start issue in the SST forced AGCM ensemble. Since the error in the ocean initial state is zero through the experimental design, the likely cause for this issue is then initial error in the noise, which could come from the influence of the cold start of the feedback calculation, P_10AGCM. After the first few months, the two simulations agree well: The correlation between the indices for CTL and P_GCTL is 0.77 over the full period and both indices have variance $0.52\,^{\circ}\mathrm{K}^{2}$.

There is more than one potential explanation for the agreement in the Nino3.4 variability between CTL and P_Gctl. One possibility is that it is noise forced. Another is that the CGCM's internal coupled equatorial Pacific variability is insensitive to the weather noise (Zebiak 1989 describes this kind of behavior). In the latter case P_Gctl would reproduce the CTL since both have the same ocean initial conditions. The fact that the global noise forced interactive ensemble P_Gctl and CTL Nino3.4 indices have a large difference in the first month of simulation, despite starting from identical ocean initial states, argues against this noise-independent interpretation, since once small differences develop, solutions to a chaotic system will continue to diverge thereafter.

Results from North Atlantic noise forced simulation P_NActl are also relevant this issue. Figure 4.13 is the map of point-to-point correlation coefficient of P_NActl and CTL, and the corresponding variance ratio of surface temperature anomaly. The 50-yr monthly surface temperature correlation between the CTL and the P_NActl is high only in the region where the noise forcing is applied. Additionally, the variance outside the forcing region is much reduced, except in some isolated regions which will be discussed below. This is additional evidence that the Nino3.4 variability (as well as the surface

temperature variability in most other regions) is weather noise forced in the CTL "observations". Also, the P_NActl Nino3.4 SSTA, expressed by the purple curve in Fig. 4.12, is of substantially smaller amplitude than and uncorrelated with the CTL Nino3.4 SSTA (correlation 0.057, variance $0.14\,^{\circ}\mathrm{K}^{2}$).

The ratio of the SSTA variance of P_Gctl to CTL (Fig. 4.10b) is much closer to one (0.8~1.6) for most of the ice-free ocean than found with the simple model of Chap. 2 . The variance ratio is order 0.5 for land equatorward of 30°latitude, and small for land and sea ice poleward of 30°latitude. The regions of higher variance over land correspond the regions of higher correlation. Looking in more detail over the oceans, the ratio still has substantial variability. The reasons that this ratio is not one over the oceans and correspondingly the reasons for its variability remain to be explored. However, one hypothesis is that this behavior arises because the local mixed layer depth in the interactive ensemble CGCM of P_Gctl differs from that in CTL, which could be due to the reduction in ocean stirring from using monthly mean rather than instantaneous weather noise forcing. If so, this issue could be addressed in interactive ensemble CGCMs by informing the ocean about the mean strength of the instantaneous weather noise stirring of the atmospheric ensemble members.

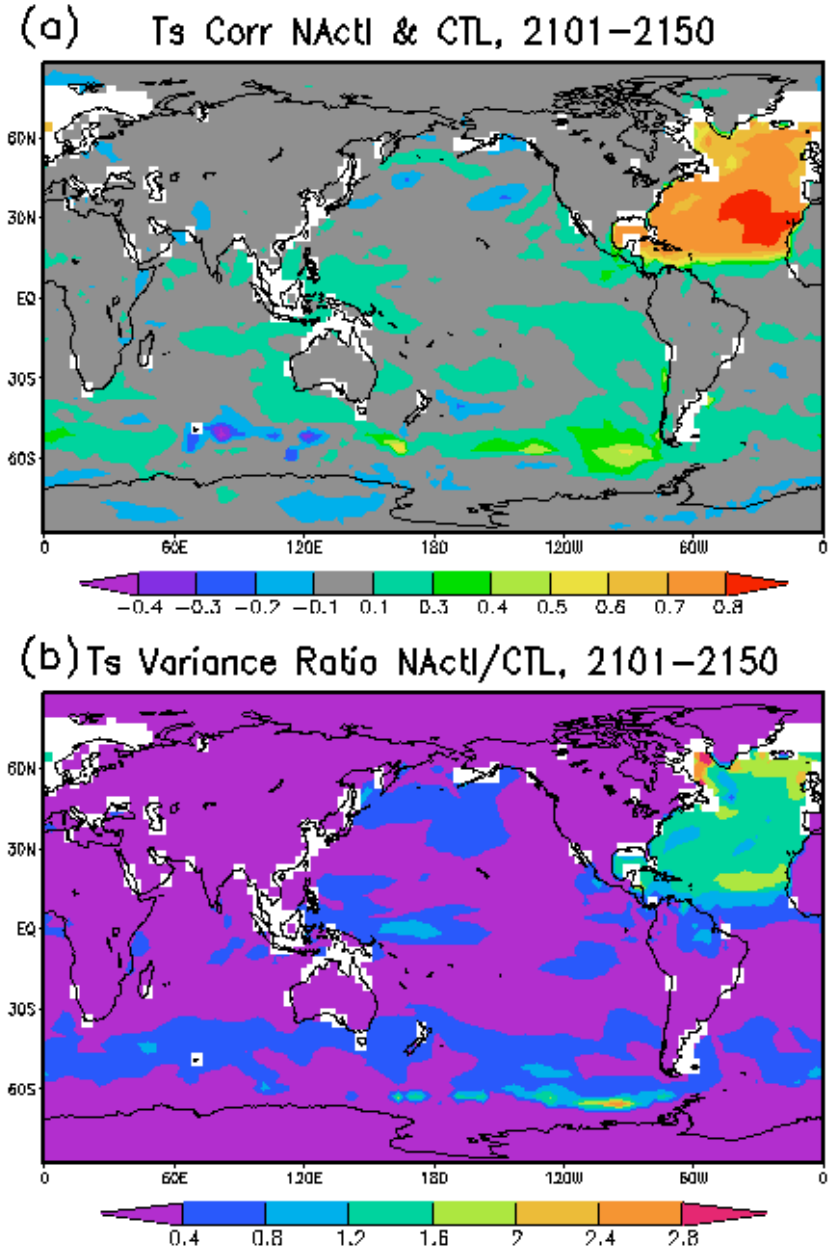

Figure 4.13 (a) Point correlation coefficient of monthly mean surface temperature anomalies from simulation P_NActl (Table 3.3) with that from CTL (Table 2.1). Correlations in shaded regions are significantly different from zero with 95% confidence assuming 600 degrees of freedom. (b) Ratio of surface temperature variance from P_NActl to that from CTL. Simulation P_NActl is the same as P_Gctl, but weather noise forcing is restricted to the North Atlantic between 15° and 65°N.

4.4 SST variability that cannot be explained by the weather noise forcing

4.4.1 Internal atmosphere-ocean coupled variability

There is a region of enhanced SST variability in the western equatorial Pacific in North Atlantic noise forced simulation P_NActl in Fig. 4.13b. This is evidence of the equatorial Pacific internal coupled variability identified in the unforced interactive ensemble by Kirtman and Shukla (2002) and Kirtman et al. (2005). The region of this internal coupled variability corresponds to a region of relatively low correlation in Fig. 4.10a. A western Pacific index of SST defined as the average over 160°E-180°E, 5°S-5°N has correlation 0.61 between the CTL and P_Gctl. That is, the agreement between the global noise forced interactive ensemble P_Gctl and the "observation" CTL are reduced in the region where there is self-sustained internal coupled variability. On the other hand, the western Pacific index is uncorrelated between P_NActl and either the CTL or global noise forced simulation P_Gctl. Therefore, the SST variability in this area is influenced by both the noise forcing and the internal coupled variability.

4.4.2 Oceanic internal variability

The correlation coefficients in Fig. 4.10a contain substantial spatial structure. Correlation coefficients over oceans are higher in the eastern subtropical and midlatitude North Atlantic and North Pacific than in surrounding regions. There is a tropical band of lower correlation, and another band of lower correlation in the Southern Ocean. At least part of the explanation for this structure is the ocean model's own internally generated "weather noise". The effect of the ocean model's internal variability on SST is estimated from a multidecade ocean-only simulation in which the OGCM surface fluxes were

prescribed to be the observed climatological wind stress and a parameterized damping heat flux (Wu et al. 2004). The OGCM's internally generated SST variability is shown in Figure 4.14, which is standard deviation of monthly SST anomalies from 46 years of an OGCM-only simulation forced by climatological wind stress. There is a general correspondence between the regions of relative large internally generated SST variability in Fig. 4.14 and extratropical regions of relative low correlation coefficients in Fig. 4.10a. However, there is no tropical signal apparent in the ocean weather noise, consistent with the interpretation of the enhanced SST variance in the western equatorial Pacific in Fig. 4.13b as intrinsic coupled variability. The large ocean internal variability seen in eastern equatorial Pacific and western Indian Ocean in Jochum and Murtugudde's (2004 and 2005) high resolution primitive equation ocean model are not obvious in our model partially due to the monthly averaging largely removed the tropical instable waves (TIWs) (B. Kirtman 2008, personal communication). Fig. 4.14 suggests that the weather noise in the null hypothesis should include variability intrinsic to the ocean, and that a generalized interactive ensemble, with the SST determined by the ensemble mean of several OGCMs (Kirtman et al. 2006), could be used to help quantify the role of oceanic internal variability.

Results from the North Atlantic heat flux noise forced simulation P_NAh have very similar features to those from P_NActl discussed above (figures are not shown). This implies that compared to momentum and freshwater flux noise, heat flux noise is more important in North Atlantic SST variability. This will be discussed below.

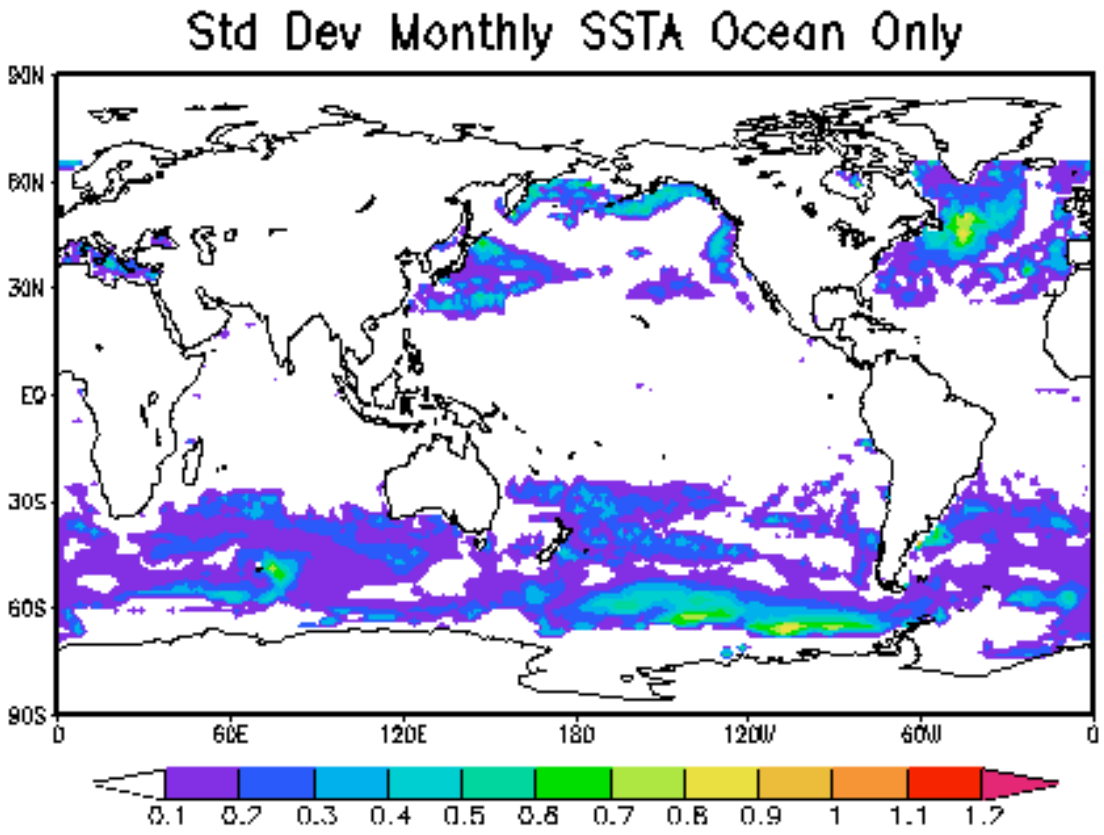

Figure 4.14 A measure of "weather noise" internal to the ocean GCM: standard deviation of monthly SST anomalies from 46 years of an OGCM-only simulation forced by climatological wind stress.

4.5 SST variability in the North Atlantic with atmosphere weather noise forcing

In section 4.3, it is shown that atmosphere weather noise forcing can reasonably reproduce the CTL SST variability. In this section, we will examine this result more closely, with focus on the North Atlantic.

4.5.1 Reproducing winter North Atlantic SST variability

Over the North Atlantic sector, the most prominent atmospheric circulation variability is the NAO. The NAO has its largest variability during boreal winter season and is suspected of playing an important role in North Atlantic SST variability. Thus our analysis begins with North Atlantic JFM SST variability.

(a) Case study: Comparison of simulation year "2135" and "2143"

To examine the agreement of North Atlantic SST variability between the weather noise forced simulation P_Gctl and the "observational" simulation CTL, two typical years with extreme wintertime (JFM) atmospheric states are selected based on NAO index (section 4.2). One is the year "2135", during which the NAO is extremely weak (strong negative NAO index according to the NAO pattern shown in Fig. 4.3). Another is the year "2143", during which the NAO is extremely strong (strong positive NAO index according to the NAO pattern shown in Fig. 4.3).

Figure 4.15 is the JFM anomalies of the SST from CTL (top panels) and P_Gctl (bottom panels) in year "2135" (left panels) and "2143" (right panels). The CTL JFM SST shows negative anomalies extending from the southeast coast of the United States to the west coast of southern Europe with a center at east-central basin in year "2135" (top-left panel). The CTL SST in year "2143" shows a positive anomaly center at east-central basin (top-right panel), opposite to that in "2135". The negative SST anomaly corresponds to the negative heat flux (heat flux from the ocean to the atmosphere) and eastward momentum flux noise, positive SST anomaly corresponds to the positive heat flux (heat flux from the atmosphere to the ocean) and westward momentum flux noise

(Fig. 4.15 versus Fig. 4.8's bottom panels). This reflects the predominant weather noise forcing on the ocean. The North Atlantic SST anomalies in CTL are well reproduced in the global-noise-forcing simulation P_Gctl for both years of "2135" (bottom-left panel of Fig. 4.15) and "2143" (bottom-right panel of Fig. 4.15), except for the reduced amplitude in "2143". This further confirms that at least for these two extreme years, the SST low variability over North Atlantic basin is mainly forced by the weather noise.

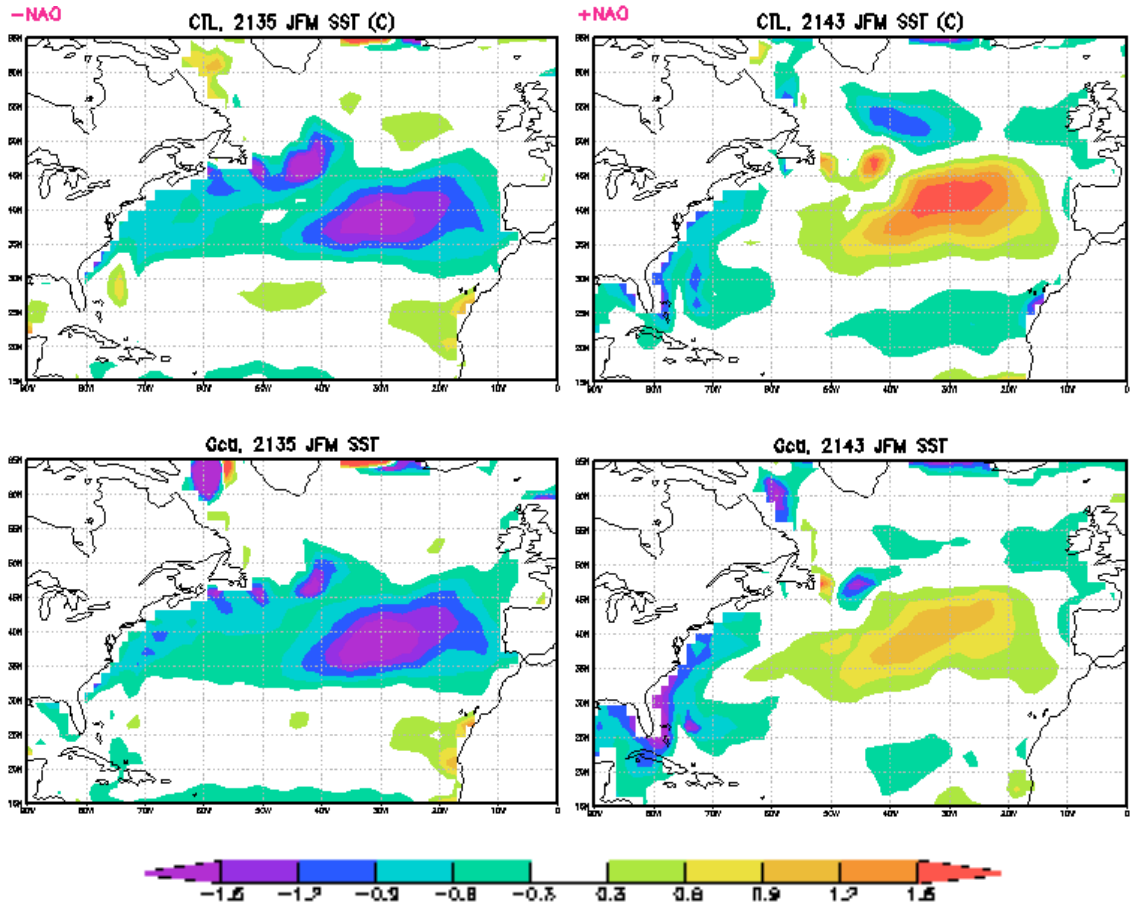

Figure 4.15 The wintertime (JFM) spatial structure of SST anomaly (K) for year 2135 (strong negative NAO index, left panels) and year 2143 (strong positive NAO index, right panels). The top panels are from CTL; the bottom panels are from P_Gctl. NAO index is defined as the principle component of the first EOF of surface pressure from CTL.

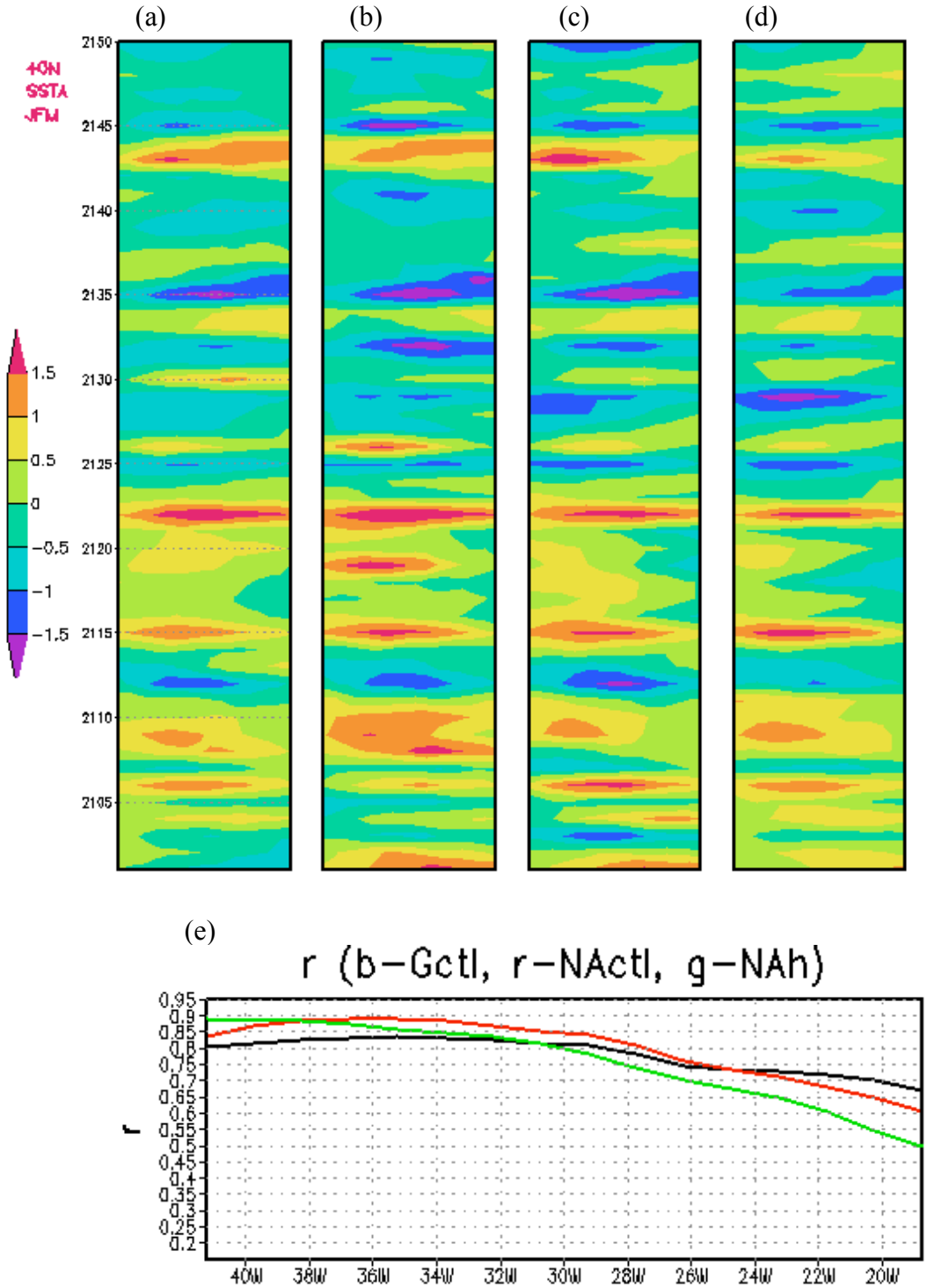

Figure 4.16 Time-longitude diagram of JFM SST anomaly (K) along 40°N between 40°W and 20°W. (a), (b), (c), and (d) are for SSTA from CTL, P_Gctl, P_NActl, and P_NAh, respectively. (e) is the corresponding SSTA correlation coefficient along 40°N between CTL and P_Gctl (black curve), P_NActl (red curve), and P_NAh (green curve).

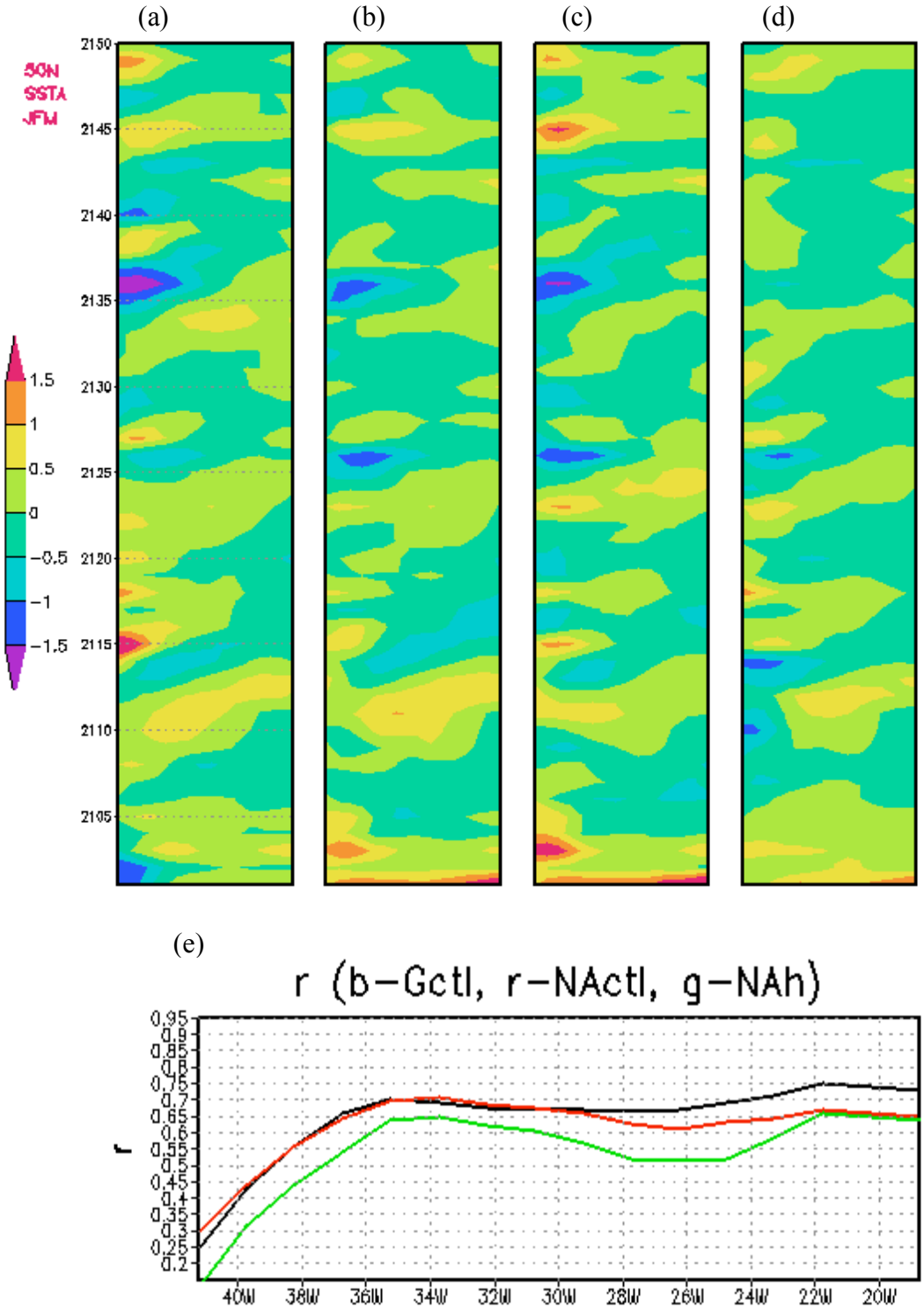

Figure 4.17 Same as Fig. 4.16, but SSTA along 50°N.

(b) Longitude-time section

From Fig. 4.15, we have seen that the JFM SST anomaly center of the two special years is around 40°W--20°W, 40°N. To see the event-by-event time evolution of SST anomaly there, diagrams of longitude-time section are plotted in top panels of Figure 4.16. The JFM temporal variability of SSTA along 40°N between 40°W and 20°W between CTL (Fig. 4.16a) and P_Gctl (Fig. 4.16b) have similar event-by-event evolutions except in the first couple of years. The bottom panel of Fig. 4.16 (Fig. 4.16e) is the corresponding SSTA correlation coefficient (r) between CTL and noise forcing simulations along 40°N. We can see that r between CTL and P_Gctl (black curve) is generally larger than 0.7 (much larger than 0.35, which is the critical value of student-t test at 5% significant level given 33 degrees of freedom). The event-by-event CTL SST variability is well reproduced in P_Gctl at this region. Comparing to Fig. 4.16b (P_Gctl), Fig. 4.16c (P_NActl) is more similar to Fig. 4.16a (CTL), and generally has higher correlation (red curve versus black curve, Fig. 4.16e). The simulation P_NAh (Fig. 4.16d) also has a similar SST evolution to CTL. These suggest that the SST variability in the North Atlantic is locally noise forced and mostly comes from the heat flux noise forcing. The effect of remote noise forcing (by atmosphere bridge) on North Atlantic SST variability can be found by comparing P_Gctl, P_NActl, and CTL. We will not discuss this here.

Figure 4.17 is a similar longitude-time section but along 50°N. It also shows similar features between CTL and the noise forced simulations, although with reduced correlation comparing to Fig. 4.16, but still generally larger than 0.35.

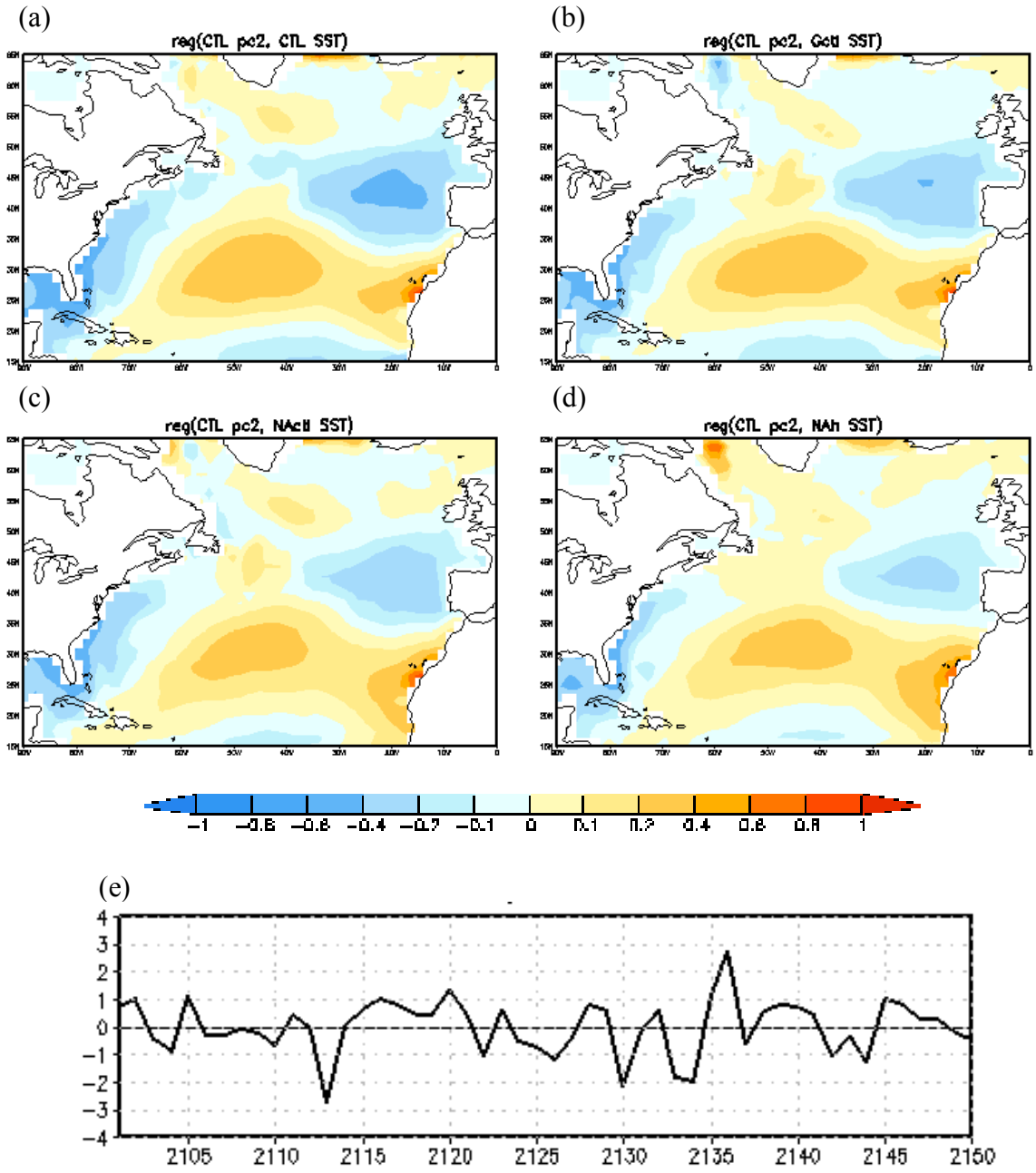

Figure 4.18 Second mode (tripole) of North Atlantic JFM SST anomaly: (a) CTL (b) P_Gctl (c) P_NActl, and (d) P_NAh, which are the regression of SST's from each simulation onto the CTL SST second PC (principle component of second EOF, (e), normalized). Units for (a), (b), (c), (d) are K per standard deviation of the corresponding PC.

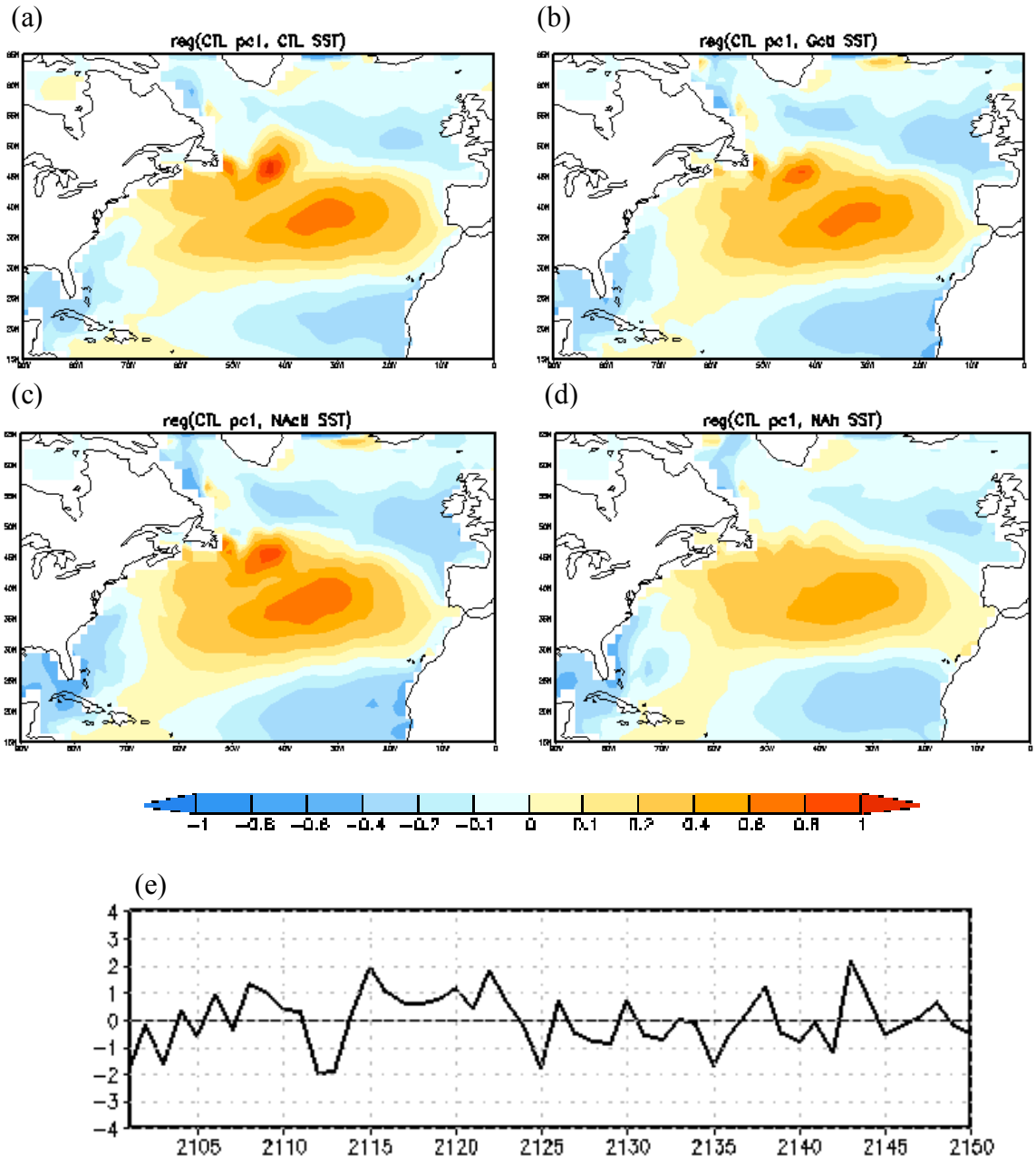

Figure 4.19 First mode (monopole) of North Atlantic JFM SST anomaly: (a) CTL (b) P_Gctl (c) P_NActl, and (d) P_NAh, which are the regression of SST's from each simulation onto the normalized CTL SST first PC (principle component of first EOF, (e)). Units for (a), (b), (c), (d) are K per standard deviation of the corresponding PC.

(c) Tripole-like mode

Figure 4.18 is the tripole pattern from CTL and noise forcing simulations. We define the second EOF of the CTL SST as the CTL tripole pattern (Fig. 4.18a, as Fig. 4.4b in section 4.1.2) and its corresponding principle component as the tripole mode index (Fig. 4.18e). Then the P_Gctl tripole pattern (Fig. 4.18b) is determined by projecting P_Gctl SST onto the CTL tripole index. The P_NActl tripole pattern (Fig. 4.18c) and P_NAh tripole pattern (Fig. 4.18d) are obtained in the same way. Figure 4.18a and Fig. 4.18b have very similar patterns, although the amplitude of the negative anomaly is slightly reduced in Fig. 4.18b near the west coast of southern Europe, and there is a weak positive anomaly in Gulf Stream extension area which is not seen in CTL tripole pattern. Note that the Gulf Stream extension area is the place where oceanic weather noise plays a role in SST variability in this model (section 4.4.2, and Wu et al. 2004). Since the CTL tripole index is used in the regression, the similarity between Fig. 4.18a and Fig. 4.18b suggests that the time evolution of CTL tripole-mode as well as its spatial pattern are reasonably reproduced in P_Gctl. Fig. 4.18c and Fig. 4.18d are very similar to Fig. 4.18b. These suggest that the CTL SST tripole-like mode in the North Atlantic is locally noise forced, and mostly forced by the heat flux noise.

(d) Monopole-like mode

We define the first EOF of CTL SST as the CTL monopole-like pattern (section 4.1.2 Fig. 4.4a) and its corresponding principle component as the monopole mode index. Then we obtain P_Gctl, P_NActl, and P_NAh monopole patterns by projecting their SST onto the CTL monopole index. The CTL monopole index is shown in Figure 4.19e. The

monopole patterns from each simulation CTL, P_Gctl, P_NActl, and P_NAh are shown in Figure 4.19a, 4.19b, 4.19c, and 4.19d, respectively. They show similar spatial structures, and amplitudes are similar, except Fig. 4.19d, which has relatively small amplitude. These confirm that the time evolution of CTL monopole mode as well as its spatial pattern are well reproduced in P_Gctl, P_NActl, and P_NAh, although the last one with reduced amplitude. Thus the North Atlantic regional weather noise forcing plays an important role on the CTL monopole-like mode and, from the similarity of panels b and c, the role of weather noise forcing outside of North Atlantic region is very limited. Although the heat flux noise seems play the most important role on the CTL monopole mode, the effect of momentum flux and freshwater flux noise cannot be neglected, since without them, the intensity of monopole mode is reduced.

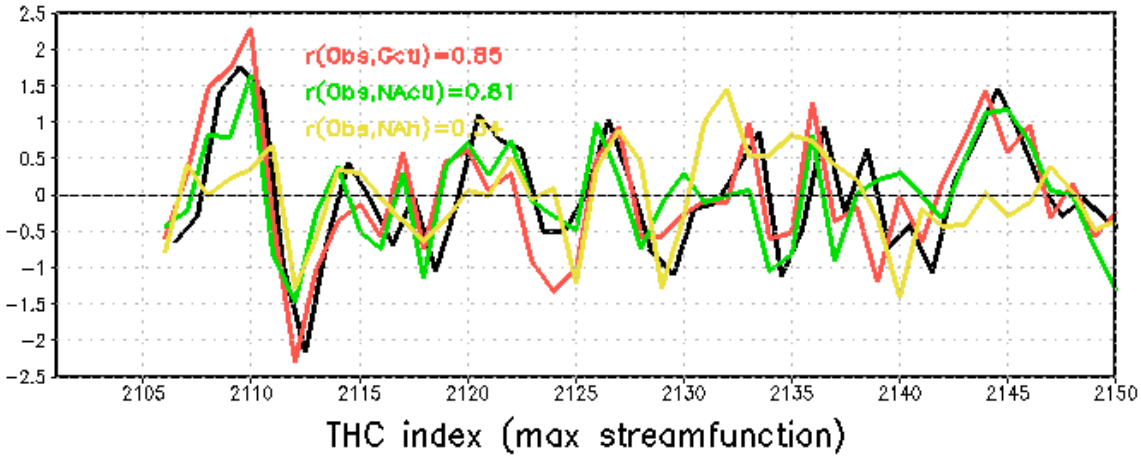

Figure 4.20 Time evolution of the North Atlantic THC index, which is the maximum annual mean stream function: CTL (black), P_Gctl (red), P_NActl (green), and P_NAh (yellow).

The monopole SST mode is suspected to be associated with the fluctuations in the THC (e.g., Kushnir 1994; Delworth et al. 1993). Figure 4.20 is the time evolution of the Atlantic THC index, which is the maximum of the annual mean stream function of the zonal mean overturning. The black curve is from CTL (as Fig. 4.6a), red from P_Gctl, green from P_NActl, and yellow from P_NAh. We can see that the black curve and red curve agree very well. The correlation between them is 0.85, which suggest that the CTL THC variability is well reproduced in P_Gctl. The correlation between the black curve and green one is 0.81, and between black and yellow is 0.34, which is highly reduced.

4.5.2 Seasonality

The maps of SSTA point-to-point correlation coefficient between the CTL and P_Gctl are shown in Figure 4.21a (JFM) and Figure 4.21b (JJA). We can see that in some regions, Fig. 4.21a has smaller correlation than that of Fig. 4.21b and seems correlated with ocean current/windstress. This might imply that weather noise plays a more important role on the North Atlantic low frequency SST variability in JJA than that in JFM. In JJA, the ocean mixed layer is generally shallower than in JFM, and the effect of oceanic dynamics on SST possibly is weaker than that of JFM.

Similar features exist in the longitude-time section. Figures 4.22a, 4.22b, 4.22c, 4.22d are the time evolution of JJA SSTA along 40°N between 40°W and 20°W from CTL and noise forcing simulations P_Gctl, P_NActl, P_NAh, respectively, and Fig. 4.22e is the corresponding correlation between CTL and noise forcing simulations. We can see that CTL, P_Gctl, and P_NActl have very similar event-by-event evolution, and the correlation between P_Gctl, P_NActl and CTL are both larger than 0.8, and between

P_NAh and CTL is larger than 0.75. The corresponding noise forced simulations reproduce more CTL -like features during JJA than that during JFM (Fig. 4.22 versus Fig. 4.16).

A similar conclusion is reached from the longitude-time section along 50°N: The noise forced simulations reproduce CTL SST anomalies better during JJA (Figure 4.22) than during JFM (Fig. 4.16).

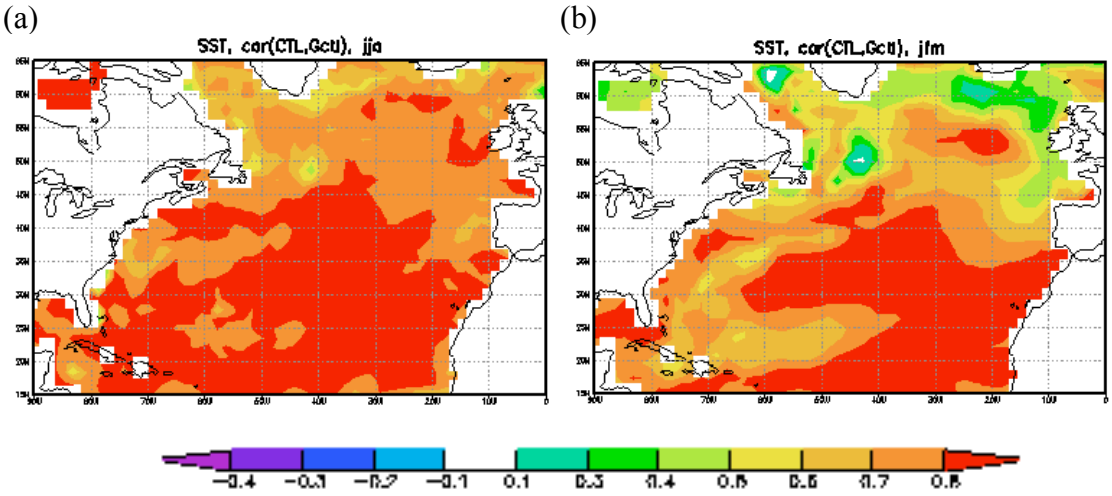

Figure 4.21 Point correlation coefficient of SSTA from P_Gctl with that from "observation" CTL during (a) JFM and (b) JJA.

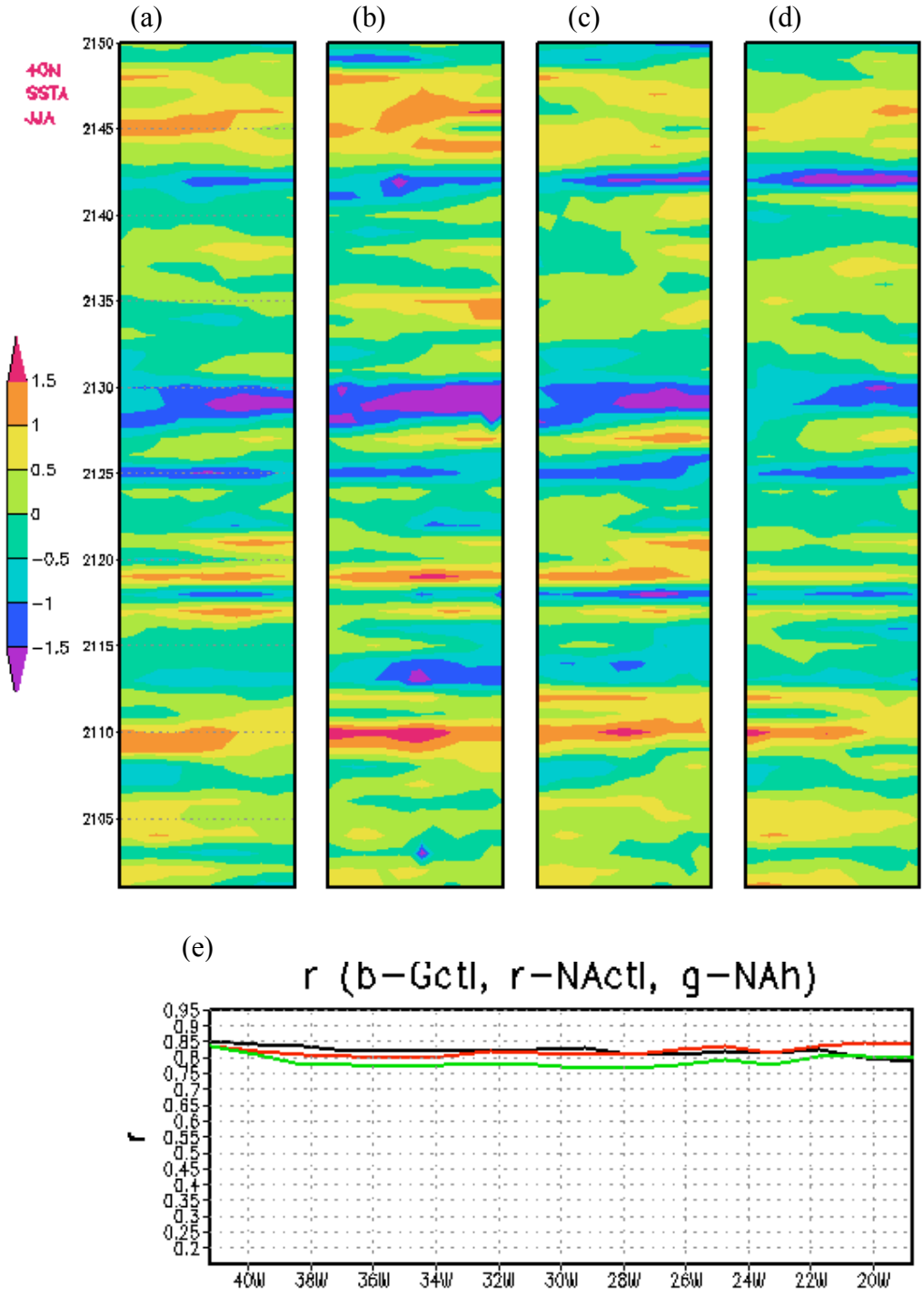

Figure 4.22 As Fig. 4.16 but for JJA: Time-longitude diagram of JJA SST anomaly (K) along 40°N between 40°W and 20°W. (a), (b), (c), and (d) are for SSTA from CTL, P_Gctl, P_NActl, and P_NAh, respectively. (e) is the corresponding SSTA correlation coefficient along 40°N between CTL and P_Gctl (black curve), P_NActl (red curve), and P_NAh (green curve).

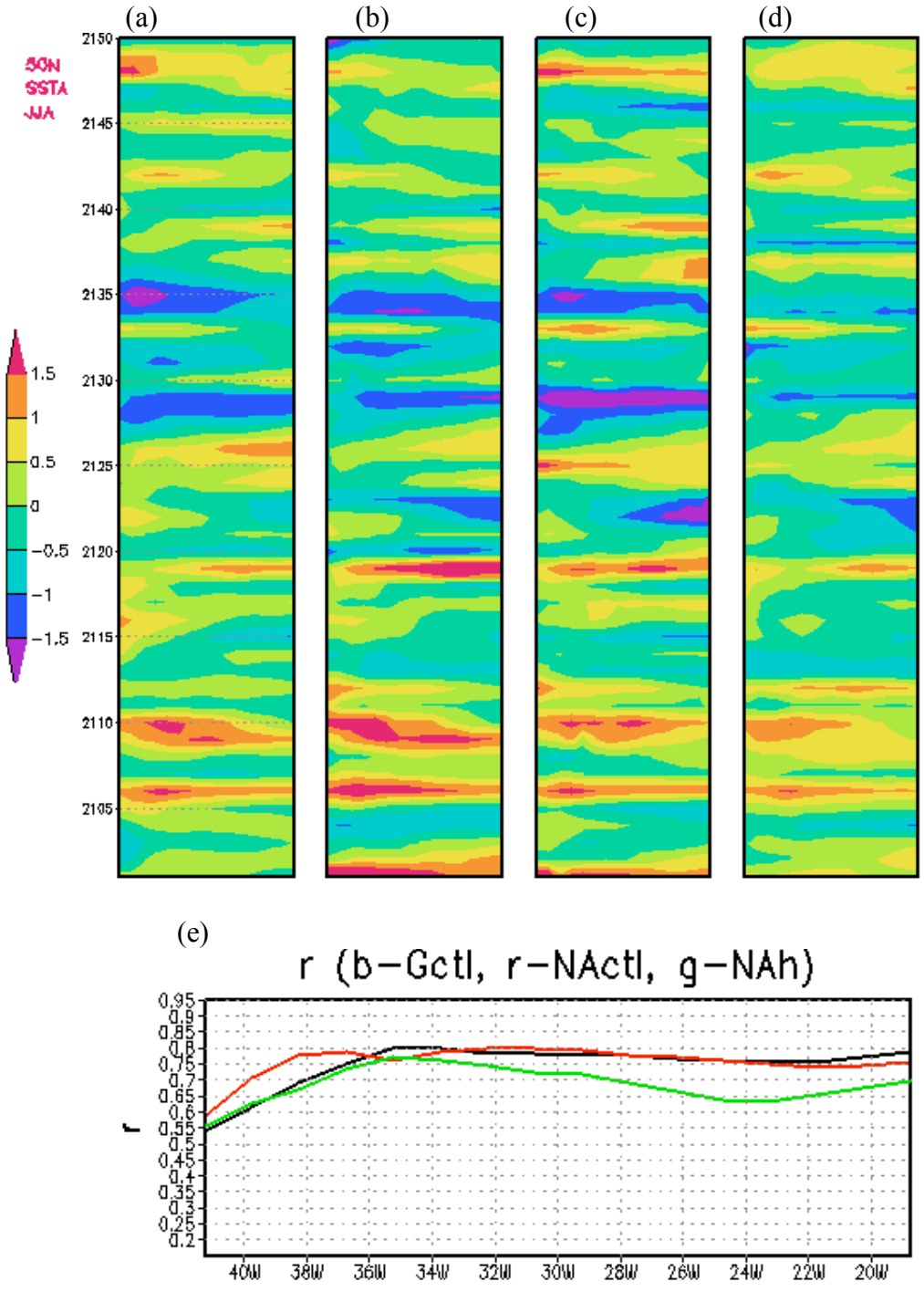

Figure 4.23 As Fig. 4.22 but along 50°N.

4.5.3 Coupled feedbacks

Figure 4.24 shows the relationship between the CTL tripole index (corresponding to the tripole pattern of Fig. 4.3b) and features of the CTL simulation. The top-left panel of Fig. 4.24 is the correlation coefficient between the CTL surface air temperature (TS) and the CTL SST tripole index. Over ocean, TS is the same as SST except for the sea-ice covered region. We can see the tripole pattern of SST variability over the North Atlantic and a possible weak association of the positive phase of the North Atlantic pattern with cold ENSO. The correlation coefficient between the CTL surface pressure with the tripole index (top-right panel) shows that the atmosphere exhibits a north-south dipole in surface pressure, with a resemblance to the negative NAO pattern: A positive polar anomaly (weaker-than-normal Icelandic low) and a negative subtropical anomaly (weaker-than-normal subtropical high) are associated with cooling in the subtropics and warming in the subpolar (very weak) and eastern subtropical Atlantic, and vice versa. It appears that in the North Atlantic, the surface pressure is not explicable by the thermal response (Kushnir et al. 2002). The correlation coefficient between the observed precipitation (P) and the tripole index (bottom-left panel) shows that P in the North Atlantic basin has negative correlation coefficient with the SSTA: over warm SSTA, there is less precipitation, and vice versa. It appears that the precipitation is not driven by the SST but is related to the surface pressure. In the Central-Eastern Tropical Pacific, cold SST corresponds to the less precipitation. The 300mb geopotential height (H300) pattern is similar to the surface pressure over North Atlantic (bottom-right panel), showing a barotropic structure.

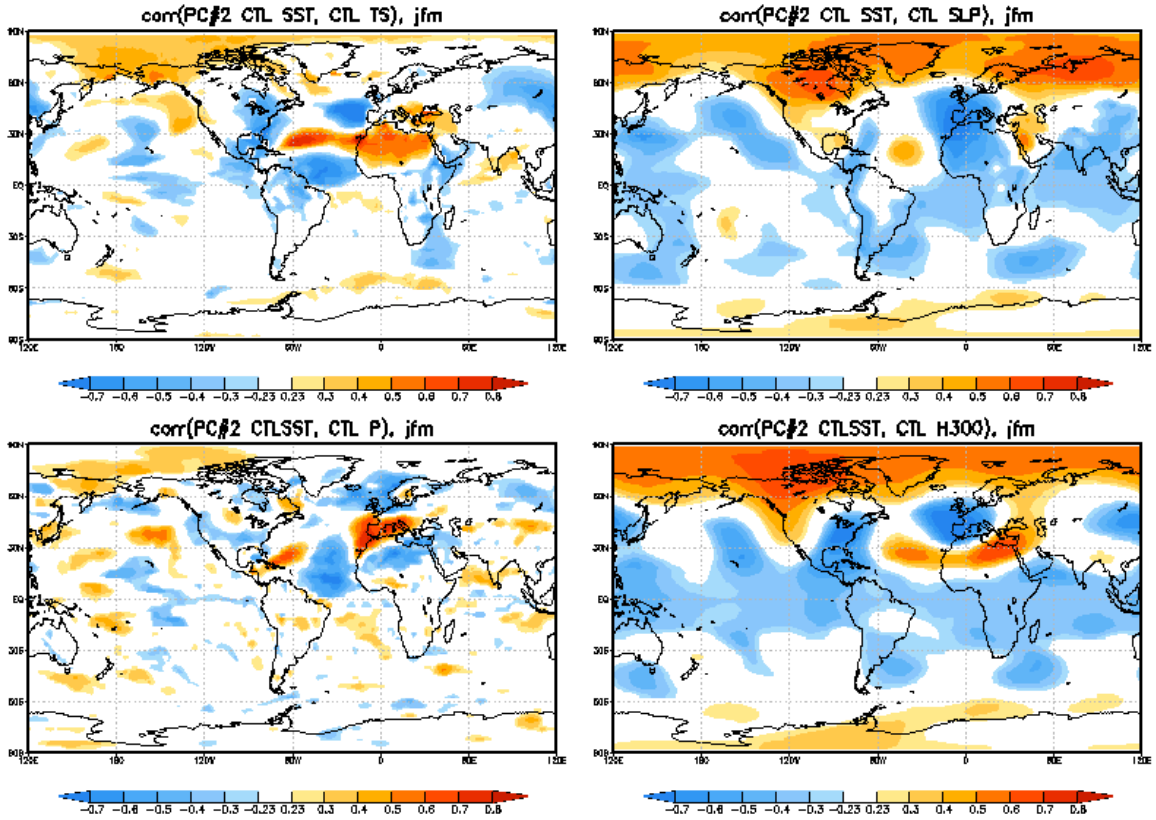

Figure 4.24 The JFM correlation coefficient between the CTL tripole index (principle component of second EOF of CTL SST) and the anomaly of CTL surface temperature (TS, left-top panel), surface pressure (PS, right-top panel), precipitation (P, left-bottom panel), and 300mb geopotential height (H500, right-bottom panel).

Figure 4.25 is the same as Fig. 4.24, but with atmospheric variables from the ensemble mean of 10 members of P_10AGCM (reduced noise). This is the forced SST response of the model. We can see the same tripole pattern of TS over the North Atlantic basin as Fig. 4.24, although with reduced strength. The surface pressure and precipitation appear to be surface thermally driven in North Atlantic and Tropical Pacific: high surface pressure and negative precipitation over the cold TS, and vice visa. The

correlation at surface pressure and H300 over North Atlantic are weak and it is hard to say whether there is positive or negative feedback. The differences between Fig. 4.25 and Fig. 4.24 for surface temperature, surface pressure, precipitation, 300mb geopotential height (e.g. the strength of the polar/subpolar center is reduced or in opposite sign) are caused by the reduced noise. Much of the structure in the observation is that of the noise.

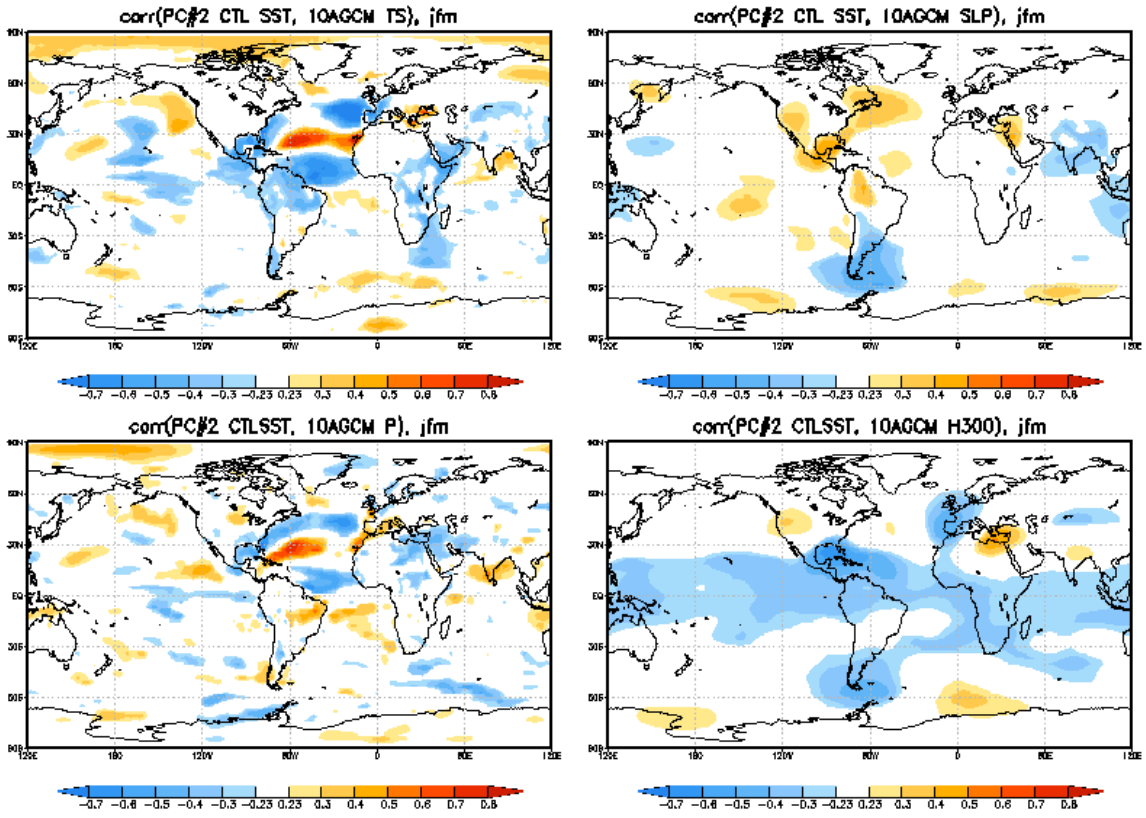

Figure 4.25 Same as Fig. 4.24 but the TS, PS, TS, P, and H300 from P_10AGCM.

Figure 4.26 is the same as Fig. 4.25, but with atmosphere variables from the ensemble mean of 6 members of AGCM of P_Gctl. We can see the similar tripole TS

pattern over North Atlantic basin as Fig. 4.25 with a slightly reduced strength of center. For the North Atlantic region, as in Fig. 4.25, the surface pressure and precipitation appear to be surface thermally driven (Kushnir et al. 2002) with positive surface pressure and negative precipitation anomalies over cold SST, although the signals are really weak.

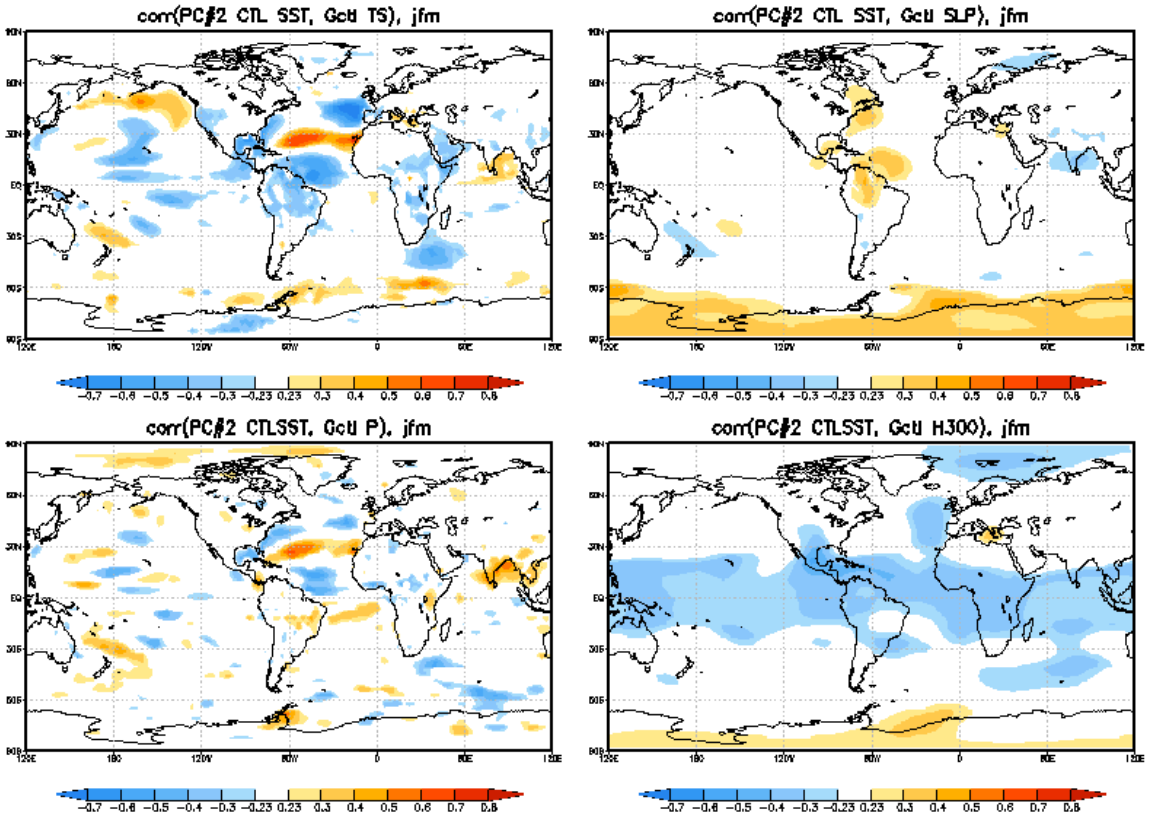

Figure 4.26 Same as Fig. 4.24 but with TS, PS, P, and H300 from P_Gctl.

From above analysis, the simulation of P_Gctl reproduces large part of "observed" CTL JFM low frequency North Atlantic SST variability both in temporal and spatial structures, although with some noticeable exceptions.

4.6 Summary and discussion

CTL has major features similar to the real climate in the North Atlantic, although with northeast shifted atmospheric NAO and SST tripole patterns. Weather noise is the main component of atmospheric variability at mid and high latitudes. In the tropics, the main component of atmospheric variability comes from the atmosphere response to the underlying SST.

The results from the statistics and the event-by-event comparison of CTL and the noise forced simulations suggest that the CTL SST variability is mostly atmospheric weather noise forced. Differences between CTL evolution and the global-noise-forcing simulation P_Gctl can occur for two possible reasons: 1) error from various approximations made in applying the method, and 2) intrinsic variability of the interactive ensemble not due to the weather noise forcing, including intrinsic atmosphere-ocean coupled variability and oceanic internal chaotic variability, the oceanic weather noise. Potential sources of error from various approximations include the finite model ensemble sizes, the use of monthly mean rather than instantaneous forcing in calculating the atmospheric feedbacks to the control SST and the response to the weather noise, and incomplete implementation of the procedure over land and sea ice. Although the quantitative importance of these extensions on the determination of the weather noise over the oceans and the subsequent interactive ensemble SST reconstruction is not

known, the land-induced feedbacks on the ocean could be expected to be comparable in magnitude to the ocean-induced feedbacks on land, which were shown in Fig. 4.10.

The regional atmospheric weather noise forcing, especially the heat flux noise forcing, is the main source of the low frequency SST variability in the North Atlantic, but not the complete story. Local oceanic processes such as gyre and THC circulations may modulate the low frequency SST variability, especially in winter. More CTL-like SST variability is reproduced in JJA than in JFM with noise forcing, although weaker atmospheric noise is observed in JJA than in JFM. The role of the ocean circulation, as well as the role of different flux noise (e.g. heat flux and momentum flux) forces, in the low frequency SST variability will be looked at in more detail in Chapter 5, where actual observation data is used. The North Atlantic low frequency SST variability may also be influenced by the local SST response to the remote SST variability because of 1) unstable coupling such as western equatorial Pacific SST variability, 2) feedbacks from the remote response to North Atlantic variability through the atmosphere bridge which causes the North Atlantic low frequency SST variability difference between P_Gctl and P_Nactl, or 3) feedbacks from noise forced SST variability in other regions.

Chapter 5 Results from the Weather Noise Forcing of IE-CGCM with Reanalysis Observation

To explore the real climate of the later 20th century, results from experiments based on reanalysis are investigated. In this experimental configuration, the reanalysis data is used as observation (OBS in Table 3.1). The atmospheric data is from the NCEP/NCAR reanalysis (Kalnay et al. 1996) and SST is from Reynolds (Smith et al. 1996). An AGCM ensemble (R_10AGCM, see Table 3.2) is then forced by the time evolution of 1951-2000 Reynolds SST between 40°S to 65°N, and its ensemble mean of the 10 members' surface fluxes are defined as feedback surface fluxes. The weather noise surface fluxes are determined by removing the feedback fluxes from the NCEP total fluxes. The weather noise surface fluxes are then used to force the interactive ensemble CGCM (IE-CGCM). In all simulations mentioned above, the model components are same. Land surface/sea ice surface conditions are not specified in the calculation of the atmospheric feedback, and no weather noise forcing is applied over land or sea ice in the interactive ensemble.

Four weather noise forcing experiments are carried out: R_Gctl, R_NActl, R_NAh, and R_NAm (see Table 3.4 for details). The ocean initial conditions are the same in each experiment and come from the CTL (Chapter 4).

Among the four noise forcing experiments R_Gctl, R_NActl, R_NAh, and R_NAm, the first three correspond to simulations made using CTL observations: P_Gctl, P_NActl, and P_NAh. The last one, R_NAm, is added to investigate Czaja and Marshall's (2001) "intergyre gyre" mechanism of the North Atlantic SST tripole mode. In this experiment, noise forcing includes only the momentum flux noise. As in the perfect observation/perfect model case, the roles of remote versus local, and heat/momentum/freshwater forcing on the North Atlantic SST variability can be diagnosised. The possible mechanisms of the two major observed North Atlantic SST modes – tripole and monopole, which may involve the wind-driven gyre circulation and the thermohaline circulation (THC) induced meridional overturning circulation (MOC), will be investigated.

5.1 Characteristics of weather noise

As in the perfect observation/perfect model case, before evaluating the role of weather noise forcing in surface climate variability, the properties of weather noise are investigated. We define the feedback as the time-dependent ensemble mean of R_10AGCM and assume that the total atmospheric variability is composed of weather noise and feedback from SST. The residual between total and feedback atmospheric variability is defined as the noise. There are many potential sources of error in the noise estimate based on reanalysis: the accuracy of the noise estimate depends on the realism of the feedbacks calculated by our model and the accuracy of the reanalysis, which in turn depends to some extent on the realism of the NCEP atmospheric GCM as well as the accuracy and time-space coverage of the observations; The atmospheric model response

to the observed SST forcing (the feedbacks), which includes an implicit response to the external forcing, is model dependent; Our SST forcing in R_10AGCM is limited to be between 40°S and 65°N. This is different from the perfect observation/perfect model case, in which the inaccuracy of the noise only comes from the finite number of ensemble members in the SST forced AGCM ensemble and the neglect of feedbacks from land and sea ice.

Figure 5.1 is the variance ratio of noise to total for zonal windstress (a), meridional windstress (b), heat flux (c), and salinity flux (d) from monthly mean data. In general, the variance of the noise dominates over that of the feedbacks in the extra-tropics. In the case of the momentum and salinity fluxes, the noise explains more than 60% of the total surface fluxes variance in the extratropics. The noise heat flux explains more than 40% of total, with relatively small noise ratio over extension regions of western boundary currents. The noise explains less than 40% of the total over the tropics and further reduces to 20% near the equator. Close to land boundaries over equatorial regions, e.g. western/Eastern equatorial India, Pacific, and Atlantic, noise explains less than 10% of the total. Over high latitudes, especially in the Southern Hemisphere, the ratio of noise to total is higher than 90%, which is larger than that of the perfect observation/perfect model case. This might be due to the neglect of feedbacks from ocean south of 40°S and north of 65°N, since in R_10AGCM, the AGCM is the forced by climatological SST in these regions. Another possibility is unrealistic feedbacks calculated by the COLA AGCM. Again, as in the perfect observation/perfect model case, the neglect of possible remote feedbacks from land/sea ice might also play a role. The

relative roles of noise and feedbacks seen in the surface fluxes are also seen in other atmospheric variables, such as precipitation and surface pressure (figures not shown).

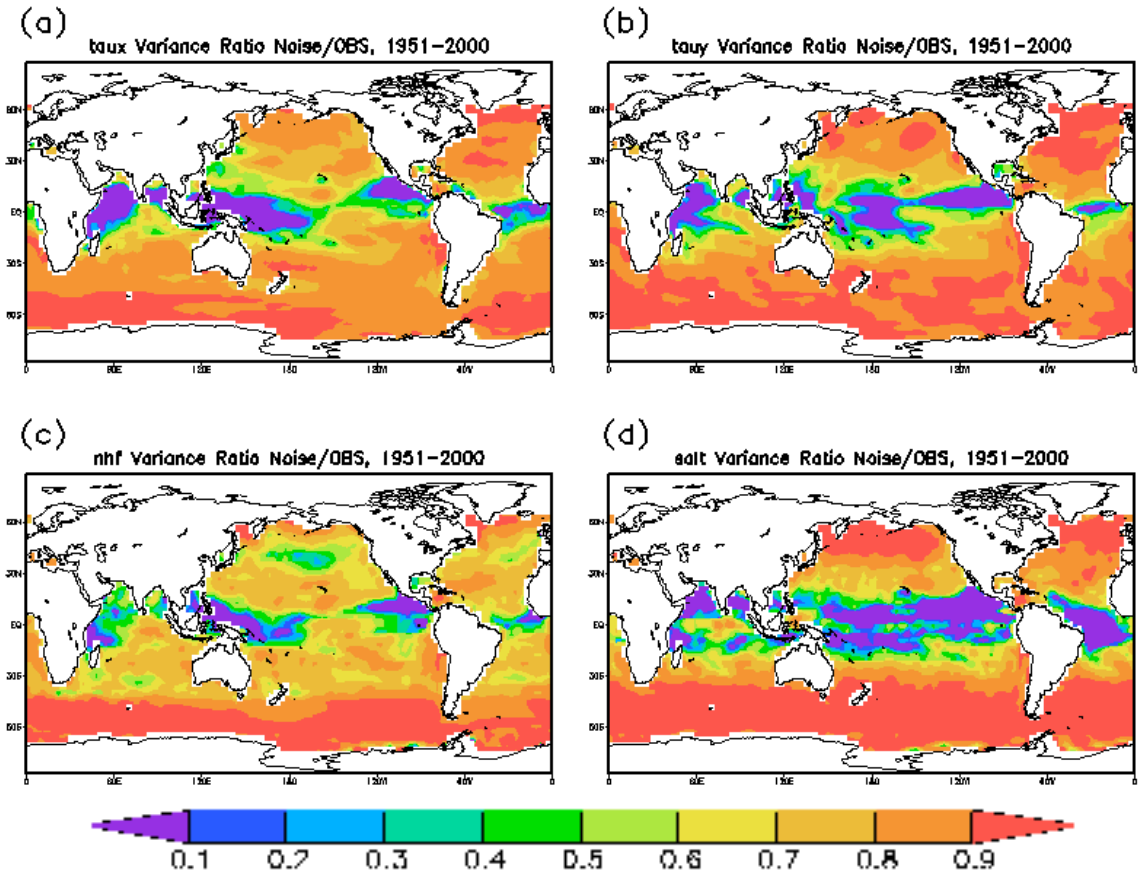

Figure 5.1 Variance ratio (noise to total) of monthly mean zonal windstress (a), meridonal windstress (b), heat flux (c), and salinity flux (d). Total surface fluxes are from NCEP reanalysis. Noise surface fluxes are defined by subtracting feedback surface fluxes from the total. Feedback surface fluxes are the ensemble mean of surface fluxes of R_10AGCM.

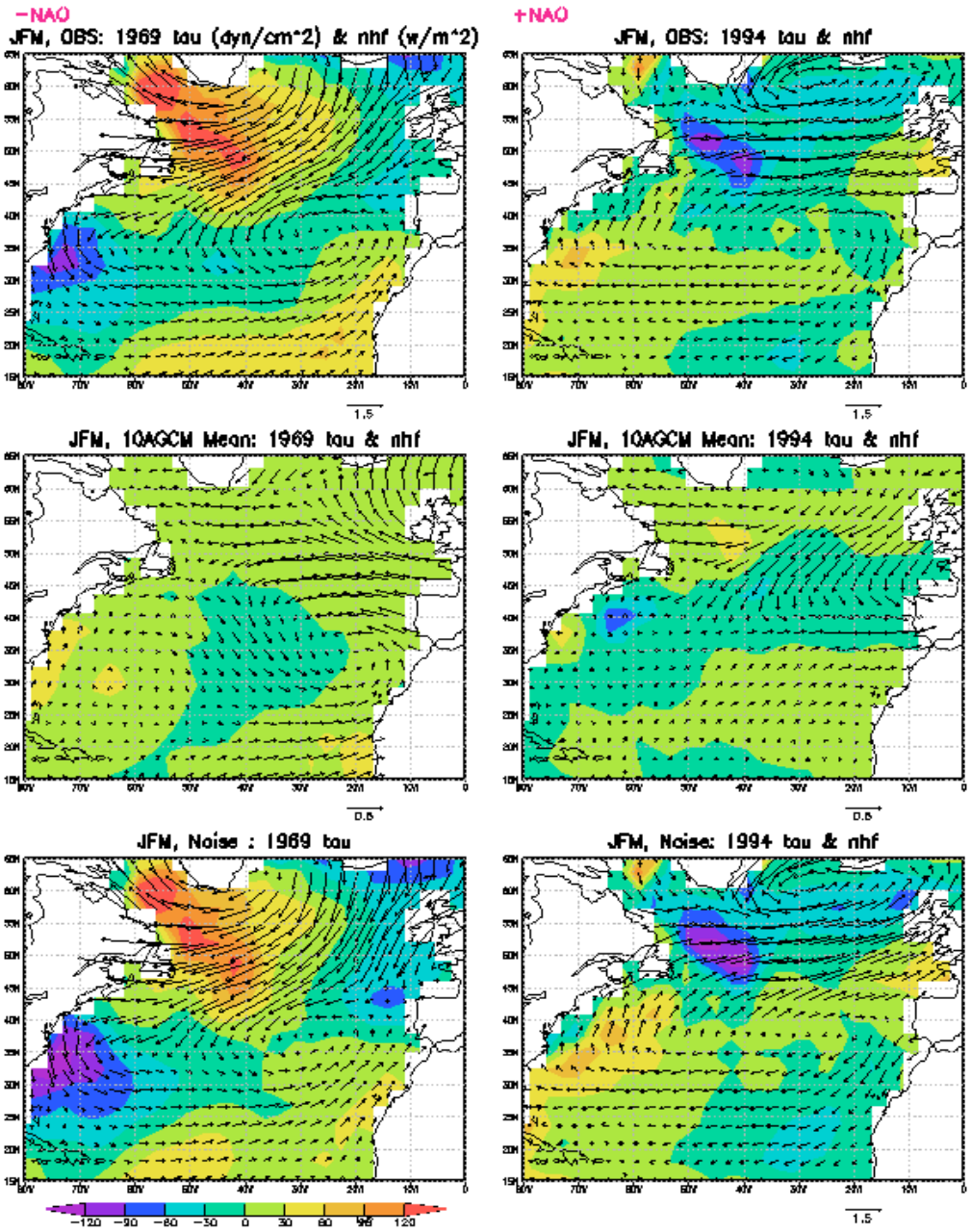

Figure 5.2 The wintertime (JFM) spatial structure of heat flux (downward positive, shaded) and momentum flux (vector) for 1969 (strong negative NAO index, left panel) and 1994 (strong positive NAO index, right panel). The top panels are from the NCEP reanalysis; the middle panels are the ensemble mean of R_10AGCM; the bottom panels are the noise, total (top) minus feedback (middle). NAO index is defined as the principal component of the first EOF of sea level pressure from the NCEP reanalysis. Units for heat flux and windstress are W/m^2 and N/m^2, respectively. The windstress vector length is 0.5 units in the middle panel compared to 1.5 units in the corresponding top and bottom panel.

To see the characteristics of noise surface fluxes related to North Atlantic climate variability, two typical years with extreme wintertime (JFM) atmospheric states are selected based on the observed NAO index (defined as the principal component of the first EOF of SLP from the NCEP reanalysis). One is 1969, during which the NAO is extremely weak (large negative NAO index). Another is 1994, during which the NAO is extremely strong (large positive NAO index). To determine the role of noise surface fluxes in forcing the surface climate variability, first, we check the fluxes of these two years over North Atlantic basin (15° - 65°N), including the total fluxes (top panels of Figure 5.2), which is the observation (from NCEP reanalysis); the forced fluxes (middle panels of Fig. 5.2), which come from the ensemble mean of R_10AGCM; and the estimated noise (bottom panels of Fig. 5.2), which is the difference between the total and the forced fluxes.

From the top-left panel of Fig. 5.2, the observed total anomaly of heat flux has a tripole pattern, with negative anomalies (heat flux downward to the ocean is positive) extending from the southeast coast of the United States into the central basin to the west coast of Europe, and positive anomalies in the high-midlatitudes south of Greenland and in the Tropics. The corresponding anomaly of windstress is westward north of 35°N, eastward south of 35°N. In 1994 (top-right panel of Fig. 5.2), the total heat flux and windstress anomalies are both opposite to those in 1969.

The heat flux and windstress of the ensemble mean of R_10AGCM, which is a 10 member AGCM ensemble forced by the Reynolds SST, are the feedbacks or "forced response". For both 1969 and 1994, the magnitudes of both the heat flux and windstress

are small compared to the observed total (Fig. 5.2 middle. Note that windstress vector length is 0.5 units compared to 1.5 units in the corresponding top and bottom panels). The difference between the reanalysis and the forced responses are taken as weather noise (bottom panels of Fig. 5.2). The noise heat flux and noise momentum flux have similar patterns as the observed total for both 1969 and 1994 with larger amplitudes. Clearly, the feedback surface fluxes in the North Atlantic are small compared to the weather noise in these cases.

5.2 Weather noise forcing in reproducing the observed surface temperature anomaly

The interactive ensemble CGCM is now forced with the diagnosed weather noise. Figure 5.3 is the map of point-to-point correlation coefficient and the corresponding variance ratio of SST anomaly from the global noise forced simulation R_Gctl with that from the observation, the Reynolds SST. The regions of relatively high correlation are in the northern and southern subtropical oceans, and have variance ratio not too far from one. Over the tropics, correlations are much lower, with larger variance ratio than over the subtropics. The correlations are reduced everywhere compared to the ideal case, especially over the tropics. But over most of the subtropics to the extratropics, the correlations are mostly still larger than .4.

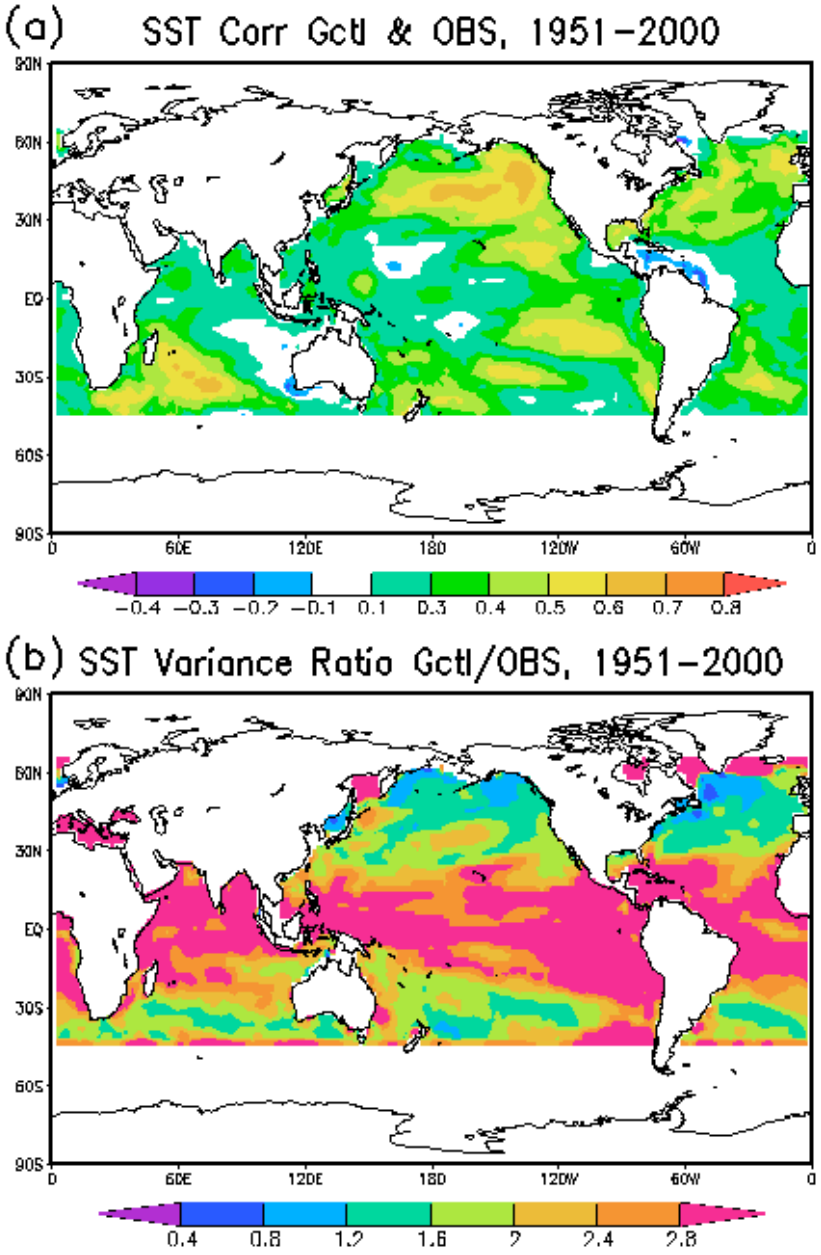

Figure 5.3 (a) Point correlation coefficient of monthly mean SST anomaly from global weather noise forced interactive ensemble simulation R_Gctl with that from observation. Correlations in shaded regions are significantly different from zero with 95% confidence assuming 600 degrees of freedom. (b) Ratio of surface temperature variance from R_Gctl to that from observation.

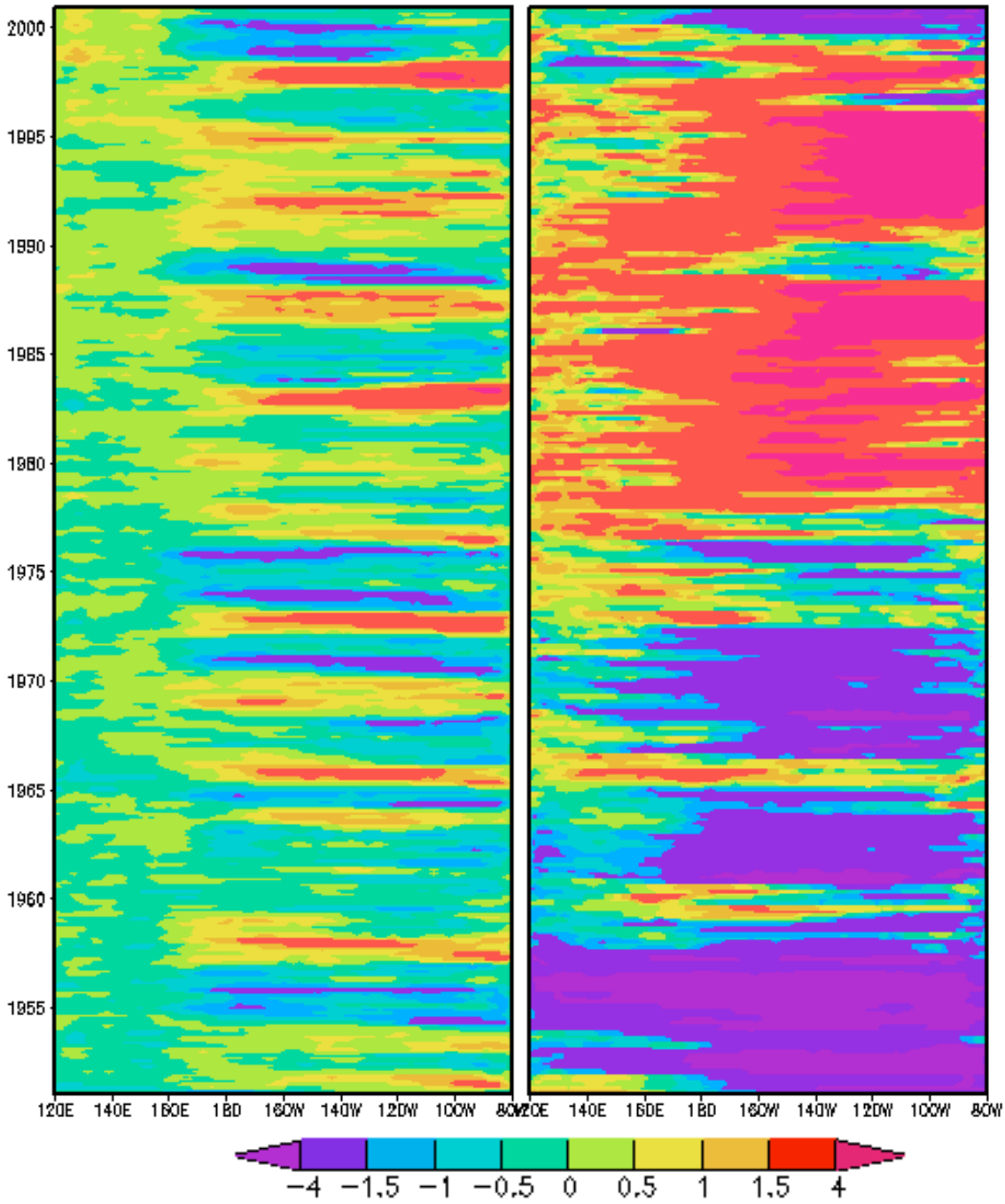

Figure 5.4 Time-longitude diagram of monthly mean SST anomaly (K) along the Equator in the Pacific Ocean. Left panel: SSTA is from observation and Right panel: SSTA is from R_Gctl.

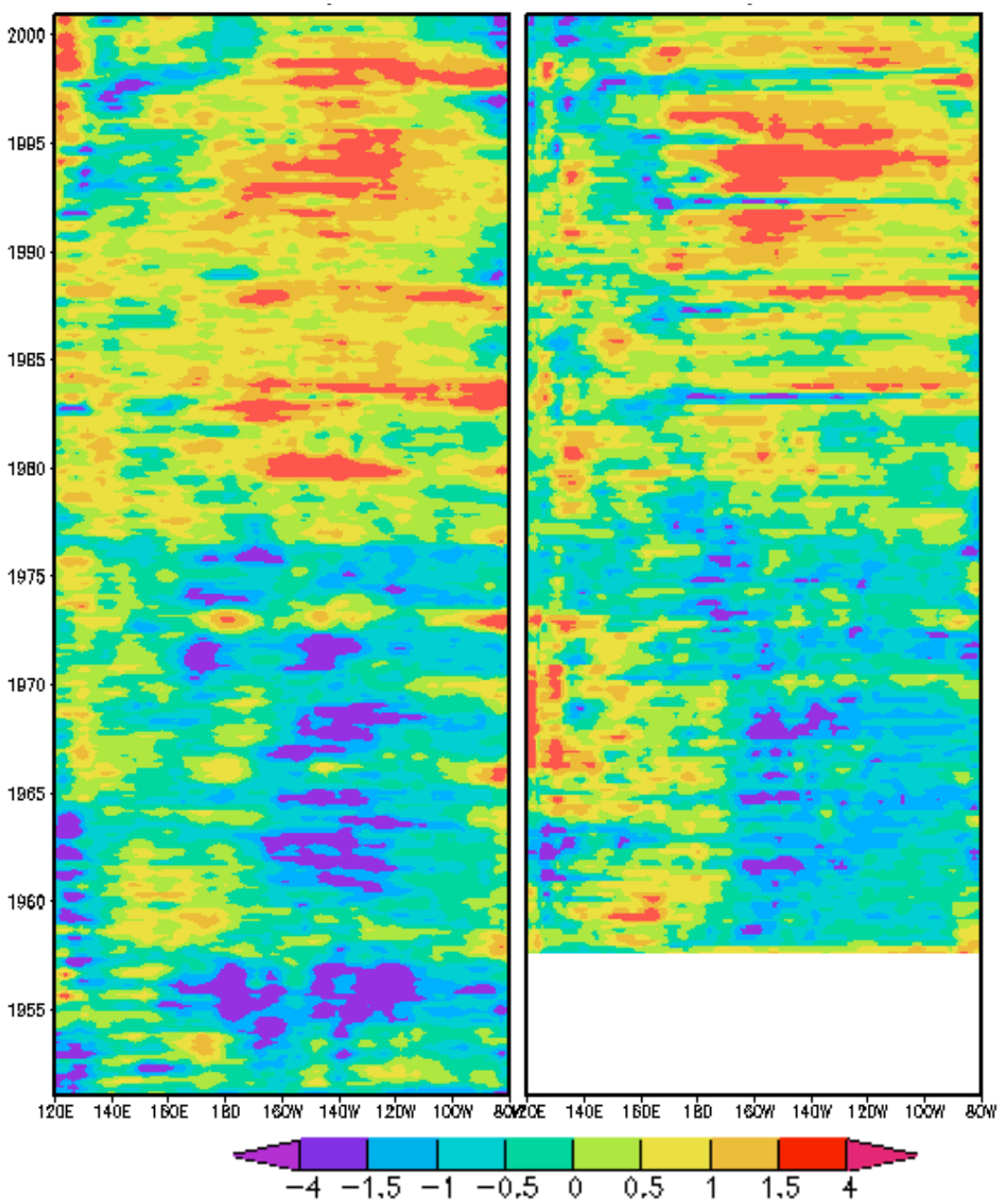

Figure 5.5 Time-longitude diagram of monthly mean SST anomaly (K) along Equator in Pacific Ocean from interactive ensemble BB98 model (Chap. 2) simulation. Left panel: use NCEP heat flux and Right panel: use ERA40 heat flux.

To further examine the SST variability in the tropics, a time-longitude diagram of monthly mean SSTA in the Pacific Ocean along the equator is shown in Figure 5.4. We can see that the SST from R_Gctl (right panel) is very different from the observations (left panel). Low frequency (decadal and longer time scale) variability dominates in R_Gctl but not in the observations. There appears to be a large jump around 1976 in R_Gctl but not in the observations. We suspect that the problems in R_Gctl might come from NCEP reanalysis data. To diagnose this, we use the heat flux both from NCEP and ERA40 to force a simple model (BB98), which is introduced in chapter 2 and Schneider and Fan (2007). The results are shown in Figure 5.5. Fig. 5.5 is the same time-longitude diagram of monthly mean SSTA along the equator as Fig 5.4, but from the simple model of BB98. The left panel is the result of using the NCEP heat flux and the right panel is the result of using the ERA40 heat flux. BB98 forced by the NCEP heat flux behaves similarly to R_Gctl, with sharp warming near 1976. Using the ERA40 heat flux in BB98 gives a warming trend, but less severe. It seems that the ERA40 heat flux produces more realistic SST variability compared to the NCEP heat flux. There are several possible sources of problems in the NCEP reanalysis data, such as: (1) data discontinuity due to the addition of satellite observations (also in ERA40) and (2) NCEP reanalysis model does not include external forcing (e.g. green house gas). The tropical SST anomalies will spread the signal to other regions by atmospheric teleconnections, and the unrealistic sharp warming starting around 1976 will have effects on other regions' SST anomalies.

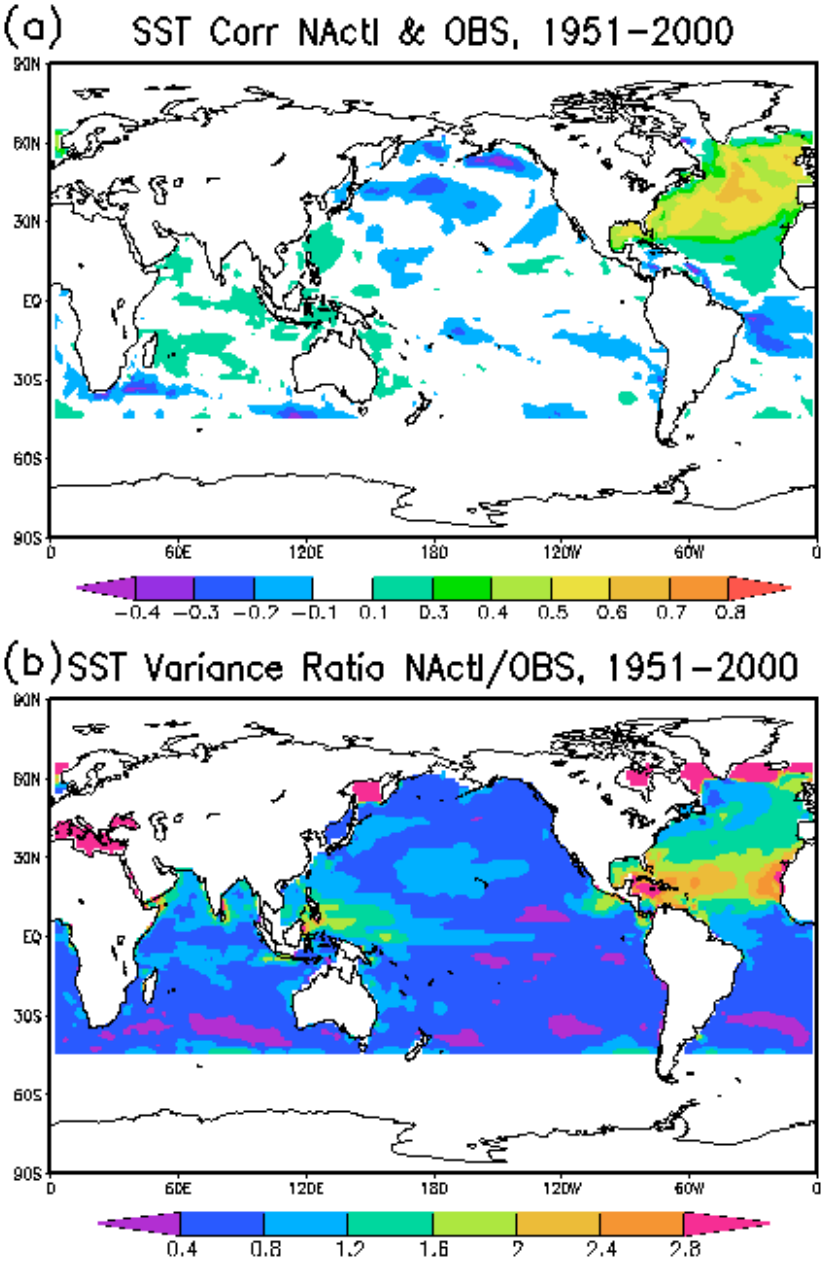

Figure 5.6 (a) Point correlation coefficient of monthly mean surface temperature anomalies from simulation R_NActl (Table 3.4) and reanalysis SST. Correlations in shaded regions are significantly different from zero with 95% confidence assuming 600 degrees of freedom. (b) Ratio of surface temperature variance from R_NActl to that from observation. Simulation R_NActl is the same as R_Gctl, but weather noise forcing is restricted to the North Atlantic between 15° and 65°N.

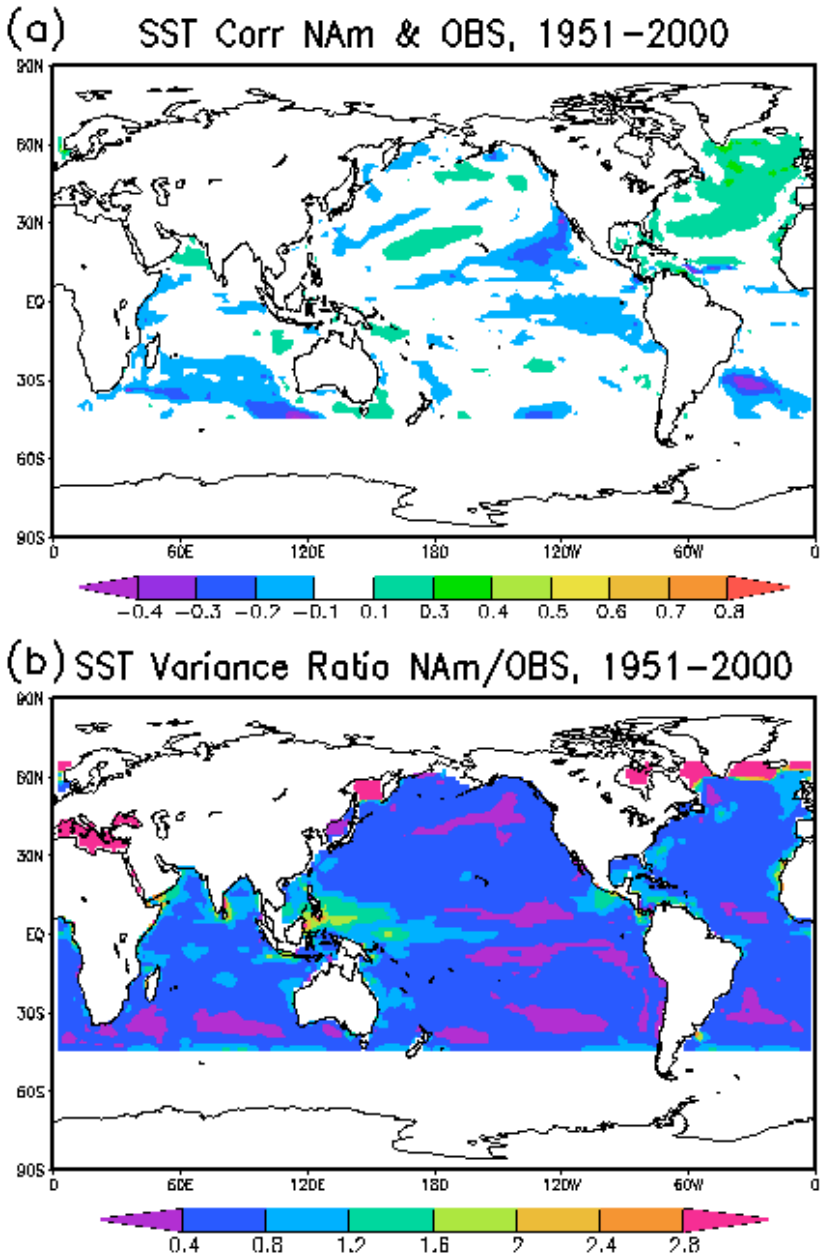

Figure 5.7 (a) Point correlation coefficient of monthly mean surface temperature anomalies from simulation R_NAm (Table 3.4) and reanalysis SST. Correlations in shaded regions are significantly different from zero with 95% confidence assuming 600 degrees of freedom. (b) Ratio of surface temperature variance from R_NAm to that from observation. Simulation R_NAm is the same as R_Gctl, but weather noise forcing is restricted to the North Atlantic between 15° and 65°N and weather noise includes windstress flux only.

Figure 5.6 is the map of point-to-point correlation coefficient (Fig. 5.6a) and the corresponding variance ratio (Fig. 5.6b) of SST between R_NActl and observations. The 50-yr monthly surface temperature correlation is relatively high only in the region where the noise forcing is applied, mostly higher than .5, and with reasonably realistic variance ratio of 0.8~1.6. The variance outside the forcing region is highly reduced, except in some isolated regions, such as the Pacific warm pool, the tropical North Atlantic (near the boundary of the forcing region). This is evidence that the SST variability is weather noise forced.

Without weather noise forcing, the tropical SST variability is highly reduced, although the noise forcing cannot reproduce the observed SST variability. Over the North Atlantic, the correlation in R_NActl (Fig. 5.6a) is a little higher than in R_Gctl (Fig. 5.3a) (mostly 0.5~0.6 versus 0.4~0.5), and the SST variance ratio in R_NActl (Fig. 5.6b) is close to one (0.8~1.6) as in R_Gctl (Fig. 5.3b). This might imply that the North Atlantic SST variability is reasonably reproduced by weather noise forcing and that the regional noise forcing plays the major role. Feedback from the erroneous tropical SST causes the degradation of the results in R_Gctl. Similar results are found in the North Atlantic heat flux noise only forcing experiment R_NAh (figure is not shown).

Results from the North Atlantic momentum flux only forcing experiment R_NAm are shown in Figure 5.7. We see that in the North Atlantic forcing region, both the correlation and variance ratios are highly reduced. The variance ratio near the southern boundary of the forcing region in the tropical North Atlantic is also reduced. The variance ratio in the Pacific warm pool is still high. These results indicate that a large

proportion of Pacific warm pool SST variability is not related to the weather noise forcing, but the North Atlantic SST variability is mostly weather noise forced and regional heat flux noise plays the major role.

5.3 SST variability in the North Atlantic with atmosphere weather noise forcing

In previous section, it is shown that atmosphere weather noise forcing can reasonably reproduce the observed North Atlantic monthly SST anomalies. In this section, we will check it more closely, with focus on the North Atlantic low frequency SST variability.

5.3.1 Reproducing winter North Atlantic SST variability

Over North Atlantic sector, the most prominent atmospheric circulation variability is the NAO. The NAO has its largest variability during boreal winter season and is suspected playing an important role in North Atlantic SST variability. so our analysis begins with North Atlantic JFM SST variability.

(a) Case study: Comparison of year 1969 and 1994

To examine the agreement of North Atlantic SST variability between the weather noise forced simulation R_NActl and the observations, two typical years with extreme wintertime (JFM) atmospheric states are selected based on NAO index. One is the year 1969, during which the NAO is extremely weak. Another is the year 1994, during which the NAO is extremely strong. Figure 5.8 is the JFM anomalies of the SST from the observations (top panels) and R_NActl (bottom panels) in year 1969 (left panels) and 1994 (right panels). The observed JFM SST anomalies show the tripole pattern with opposite sign in 1969 (top-left panel) and 1994 (top-right panel), with negative anomaly

corresponding to the negative noise heat flux (heat flux from the ocean to the atmosphere) and eastward momentum flux noise, positive anomaly corresponding to the positive heat flux (heat flux from the atmosphere to the ocean) and westward momentum flux noise (Fig. 5.8 versus Fig. 5.2 bottom panel). This reflects the predominant weather noise forcing on the ocean. The North Atlantic SST anomalies in observations are reasonably reproduced in the North Atlantic-noise-forcing simulation R_NActl for both 1969 (bottom-left panel of Fig. 5.8) and 1994 (bottom-right panel of Fig. 5.8), especially for 1969. This further reflects that at least for these two typical years, the SST low variability over North Atlantic basin is mainly forced by the local weather noise.

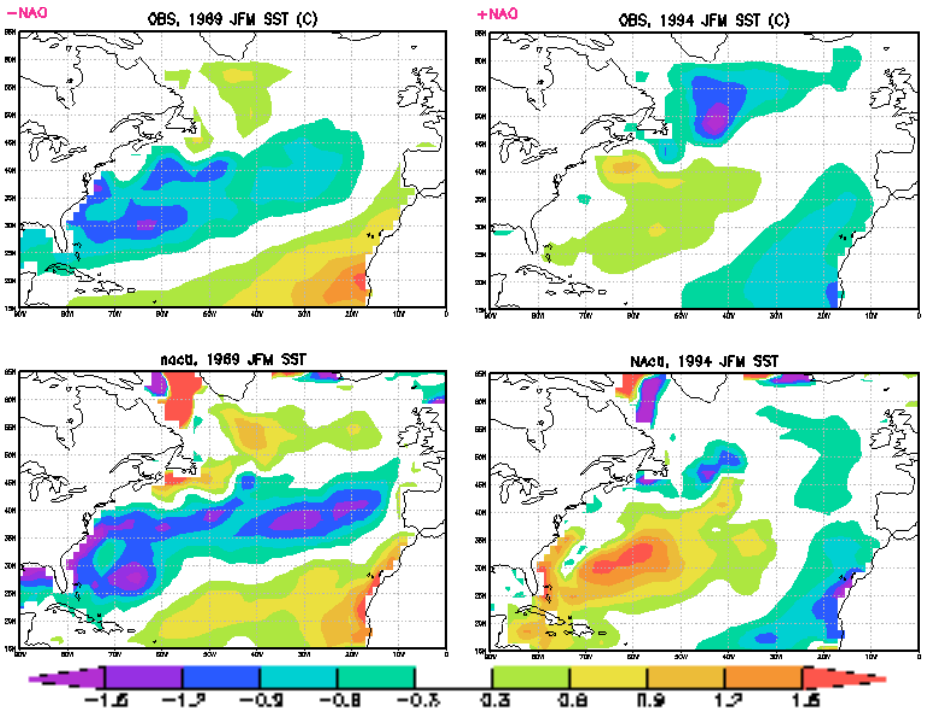

Figure 5.8 The wintertime (JFM) spatial structure of SST anomaly (K) for 1969 (strong negative NAO index, left panels) and 1994 (strong positive NAO index, right panels). The top panels are from observation and the bottom panels are from R_NActl. NAO index is defined as the principle component of the first EOF of NCEP reanalysis surface pressure.

(b) Longitude-time section

As in the perfect observation/perfect model case, we choose a special section (40°W--20°W, 40°N) to see the event-by-event time evolution of SST anomaly. Figure 5.9 shows longitude-time sections and corresponding correlations between observations and different noise forcing simulations. Comparison of the JFM temporal variability of SSTA along 40°N between 40°W and 20°W between observations (Fig. 5.9a) and R_Gctl (Fig. 5.9b) shows some similarities. The bottom panel (Fig. 5.9e) is the corresponding SSTA correlation coefficient between observations and the noise forced simulations along 40°N. We can see that the correlation between observations and R_Gctl (black curve) is generally larger than 0.35, which is the critical value for the student-t test at the 5% significance level for 33 degrees of freedom. Compared to R_Gctl (Fig. 5.9b), R_NActl (Fig. 5.9c) has a more similar time evolution to the observations (Fig. 5.9a), and generally has a higher correlation (red curve versus black curve, Fig. 4.15e), larger than .65. The simulation R_NAh (Fig. 5.9d) also has a similar SST evolution to the observations, with correlations generally larger than .65. These results suggest that the SST variability in the North Atlantic is locally noise forced and mostly comes from the heat flux noise forcing. The effect of feedbacks from SST anomalies forced by remote noise forcing and transmitted to the North Atlantic through the atmospheric bridge, found by comparing R_Gctl, R_NActl, and observations, seems to be a degradation of the agreement, probably due to the large tropical biases in R_Gctl.

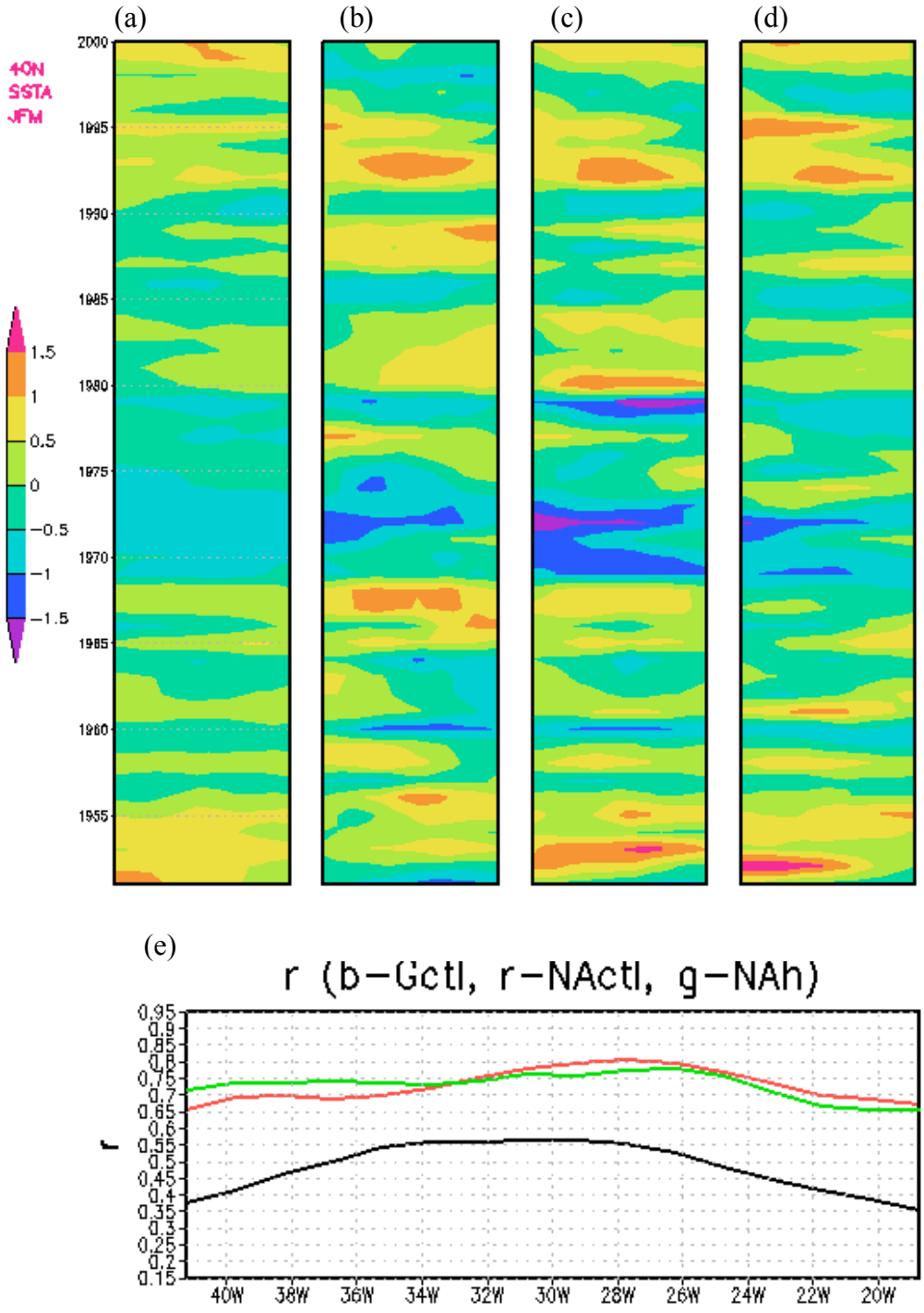

Figure 5.9 Time-longitude diagram of JFM SST anomaly (K) along 40°N between 40°W and 20°W. (a), (b), (c), and (d) are for SSTA from observation, R_Gctl, R_NActl, and R_NAh, respectively. (e) is the corresponding SSTA correlation coefficient along 40°N between observation and R_Gctl (black curve), R_NActl (red curve), and R_NAh (green curve).

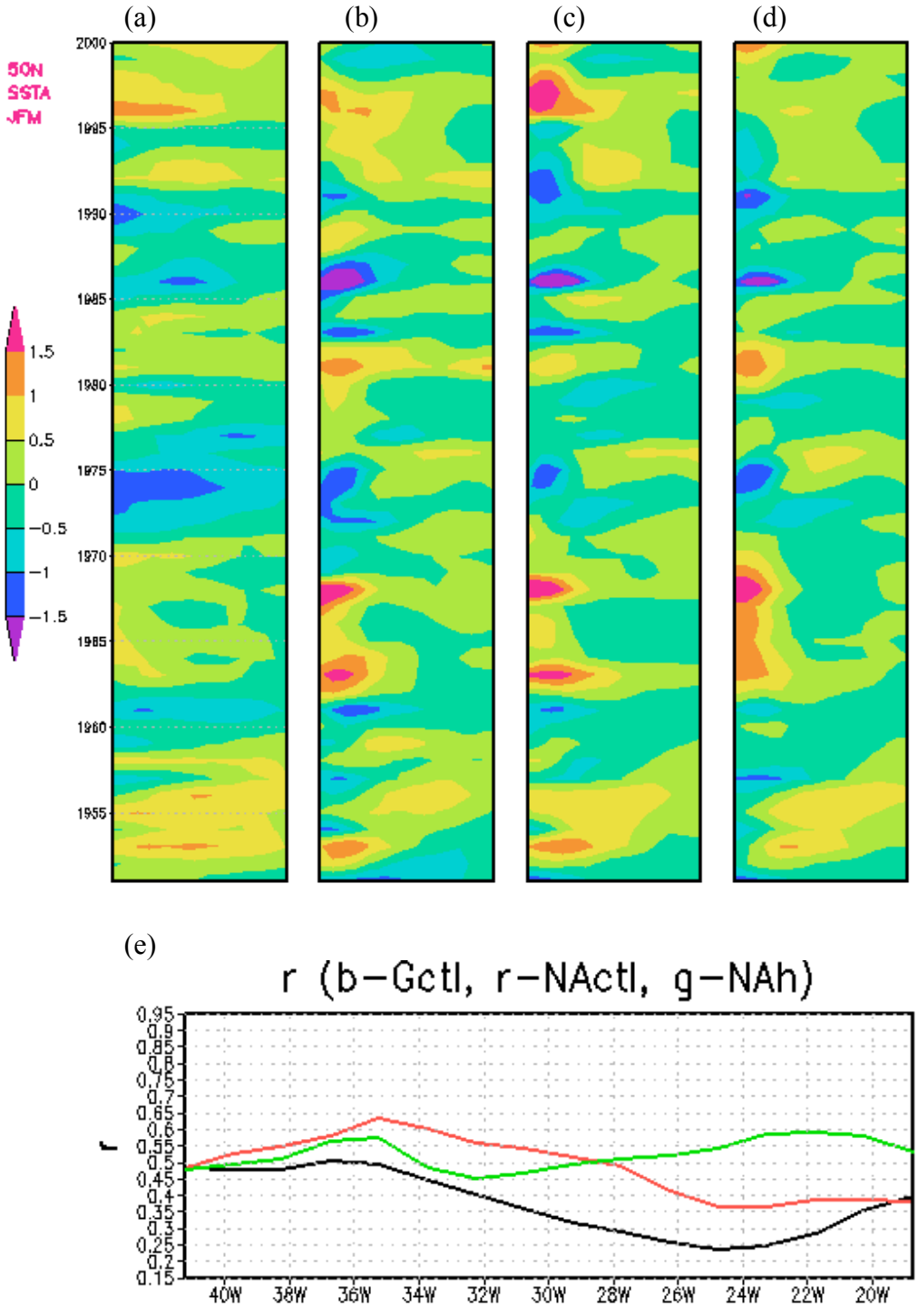

Figure 5.10: Same as Fig. 5.9, but SSTA along 50°N.

Figure 5.10 is the same longitude-time section but along 50°N. It also shows similar features between the observation and noise forcing simulations, although with reduced correlation comparing to Fig. 5.9, especially for R_Gctl, with which the correlation with the observation is reduced to less than 0.35 east of 30°W. In the noise forced simulations there seems to be eastward propagation of the SST anomalies, which is not seen in the observation. This might be caused by the deficiency of OGCM.

(c) Tripole mode

In perfect observation/perfect model case, we use EOFs to represent North Atlantic SST's physical modes. However, here we will use other methods. In the real world, it is well known that there are two major SST low frequency modes in the North Atlantic, the tripole and the monopole.

Czaja and Marshall (2001) constructed an index (T_{gs}) of the tripole mode, which is defined as the SST anomaly averaged over areas north and south of the separated Gulf-Stream, as indicated in Figure 5.11a (the two purple boxes), the north one minus the south one. The choose of this particular index is based on the physics as discussed in their paper:

> "(1) it is a measur of low-level baroclinicity to which cyclogenesis at the beginning of the Atlantic storm-track may be sensitive, and
>
> (2) it may respond to anomalies in ocean heat transport associated with both wind-driven gyres and thermohaline circulation."

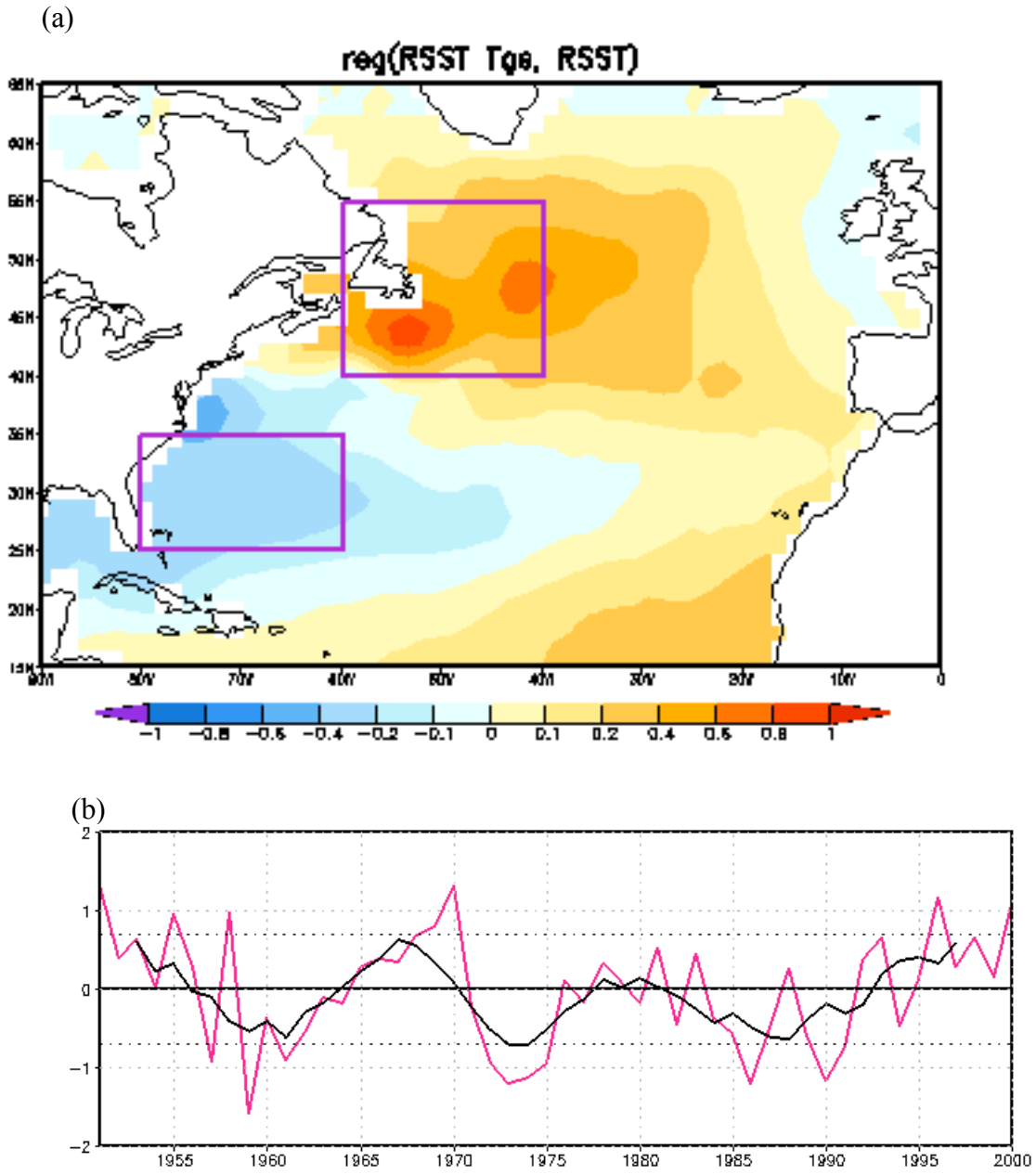

Figure 5.11 Observed JFM North Atlantic tripole pattern (a) and the corresponding index Tgs (K) (b). The red curve in (b) is the yearly JFM mean while the black curve indicates a 6-year running mean. The two purple boxes indicate the regions used to construct the SST index Tgs=TN-TS, where TN is the average SST anomaly in the northern box (40-55°N, 60-40°W) and TS the average SST anomaly in the southern box (25-35°N, 80-60°W). The shaded map is the regression of the index (normalized red line) with the time evolution of observed SST, with unit K per standard deviation of the index Tgs.

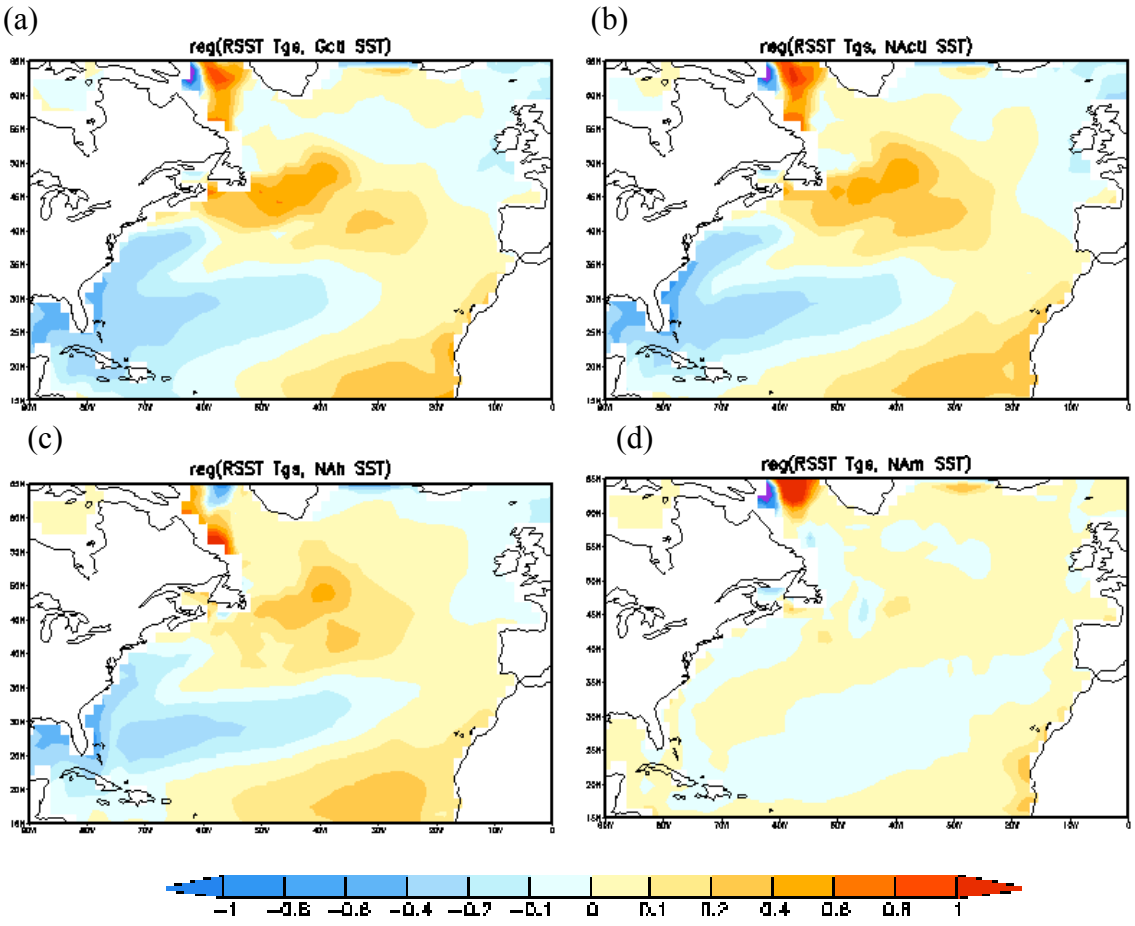

Figure 5.12 Simulated North Atlantic JFM SST tripole pattern in: (a) R_Gctl; (b) R_NActl; (c) R_NAh; (d) R_NAm. The tripole pattern in each noise forced simulation is determined by regressing the time evolution of SST from the simulation onto the observed index (normalized red line in Fig. 5.11b). Unit is K per standard deviation of the index Tgs.

Following the definition, the observed JFM tripole index T_{gs} is shown in Figure 5.11b (before the analysis, SST data is linearly detrended). The red line is the JFM mean index, and black line is a 6 year running mean. Similar results can be found in Czaja and Marshall (2001) for the time period: 1951-2000, although different SST data set is used. The map (Fig. 5.11a) is the corresponding SST tripole pattern, which is the regression of

the normalized index (normalized red line in Fig. 5.11b) with the time evolution of observed SST. It has negative anomalies extending from the southeast coast of the United States into the central basin, surrounded by positive anomalies in the midlatitudes south of Greenland and the tropical North Atlantic. This pattern is suspected to be closely related to the NAO and possible heat transport by ocean currents, such as the intergyre gyre (IGG, Marshall et al. 2001, Czaja and Marshall 2001). We will explore this in Chapter 6.

Figure 5.12 is the simulated tripole pattern from noise forced simulations. The R_Gctl tripole pattern (Fig. 5.12a) is determined by projecting R_Gctl SST onto the observed tripole index T_{gs} (normalized red curve in Fig. 5.11b). The R_NActl (Fig. 5.12b), R_NAh (Fig. 5.12c), and R_NAm tripole patterns (Fig. 5.12d) are obtained in the same way. This analysis method is used to remove SST variability associated with the large tropical biases. Figure 5.12a has a very similar pattern to Fig. 5.11a, although with some distortions: The amplitude of the subpolar positive anomaly is slightly reduced, its northern boundary shrinks southward, and its southern boundary extends southward too far, which induces a double lobe in the subtropical negative anomaly. Since the observed tripole index is used in the regression, the similarity between Fig. 5.12a and Fig. 5.11a suggests that the time evolution of the observed tripole mode as well as its spatial pattern are reasonably reproduced in R_Gctl. Figures 5.12b and Fig. 5.12c are very similar to Fig. 5.12a, but Fig. 5.12d is not. That is, although with some distortion, the pattern and its evolution are reproduced by simulations R_Gctl, R_NActl, R_NAh, but not by R_NAm.

This might imply that it is the North Atlantic regional noise heat flux that plays the major role in producing North Atlantic tripole mode.

We have seen that the tripole pattern can be reasonably reproduced by weather noise forcing. Next we will check its time evolution.

To show the typical time evolution of large-scale SST anomalies associated with index T_{gs}, again following Czaja and Marshall (2001), the observed composite maps of SST anomalies based on T_{gs} are constructed and are shown in Figure 5.13. The maps are obtained by subtracting the low-index (T_{gs}< -0.7K) composite from the high-index (T_{gs} > 0.7) composite. Numbers on the right-bottom corner of each map indicate the time lags (years) of SST anomalies relative to the high/low index, i.e. the "+1" map is obtained by subtracting the low-index + 1-year composite from the high-index + 1-year composite, and so on. The map at 0 time lag (top left panel) represents the typical amplitude of SST anomalies in the North Atlantic in JFM, with the same pattern as Fig. 5.11a, but the unit here is K. We can see the gradual time evolution of the tripole pattern with increasing time lag: The initial SST tripole pattern reduces gradually and reaches its transformation phase after 3 years. The opposite phase shows up after 4 years, increases gradually, and reaches its peak amplitude 6~7 years later. Then this opposite sign pattern weakens and transforms to the initial phase. The full cycle takes about 11 years. The tripole pattern has decadal variability. The 6 year running mean of index T_{gs} also shows the decadal features (black curve of Fig. 5.11b).

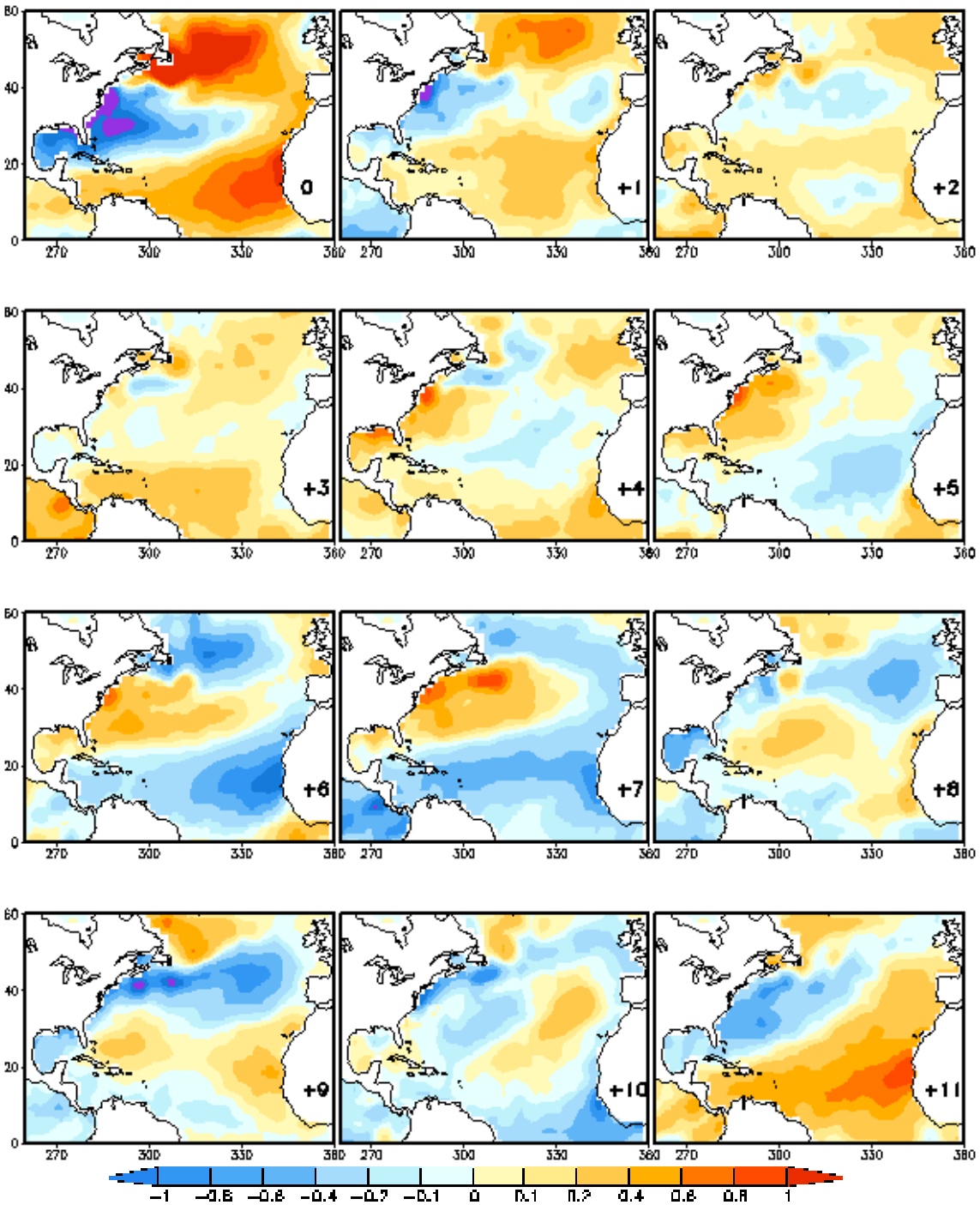

Figure 5.13 Observed composite maps of SST anomalies (K) based on years in which |Tgs| > 0.7 K (red curve in Fig. 5.11b). The map is obtained by subtracting the low-index composite from the high-index composite. Numbers on right-bottom corner indicate the time lags (years) of SST anomalies relative to the high/low index, i.e. the "+1" map is obtained by subtracting the low-index + 1-year composite from the high-index + 1-year composite.

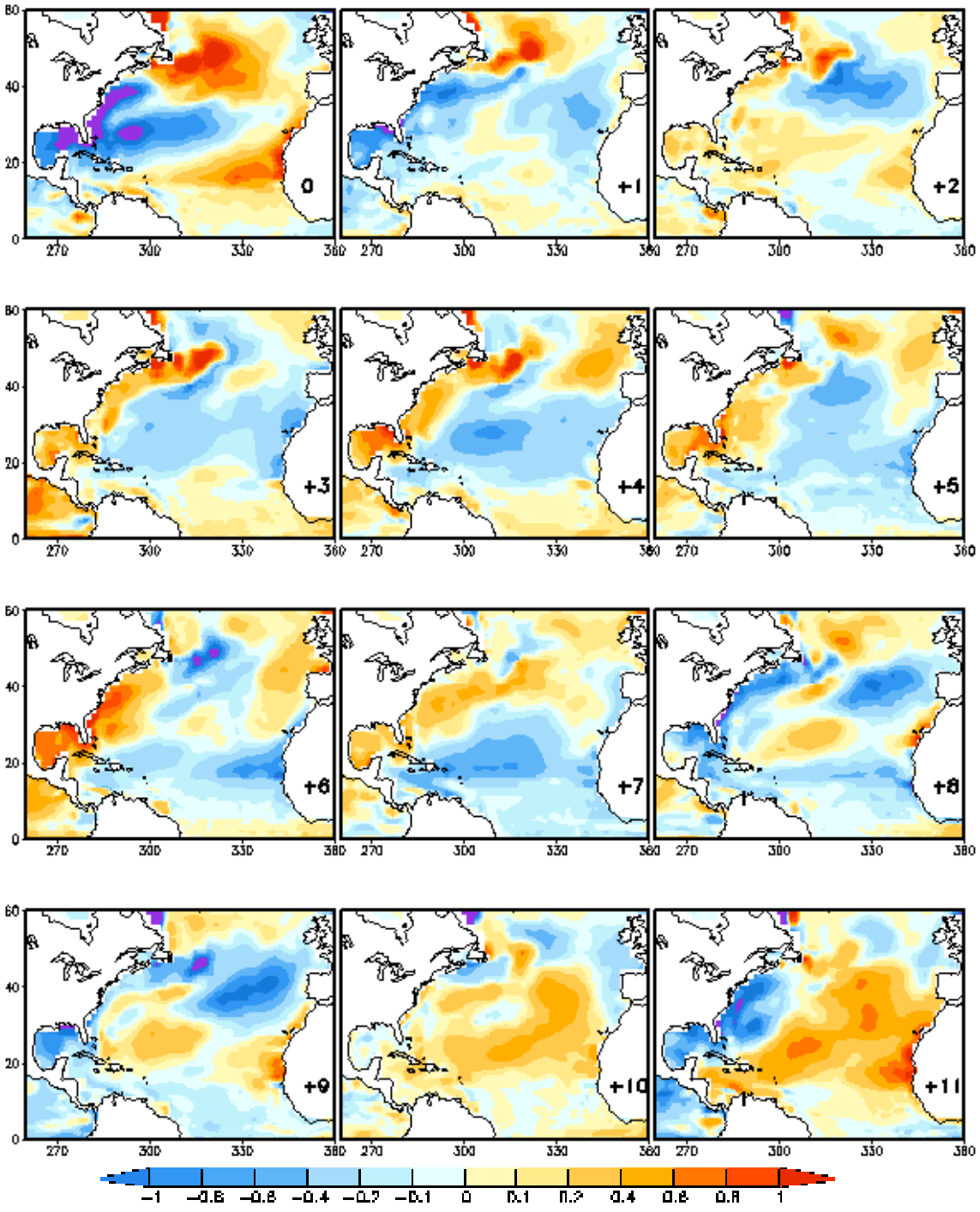

Figure 5.14 Same as Fig. 5.13, but for composite maps of R_NActl SST anomalies (K) based on observed index Tgs.

Figure 5.14 is the R_NActl time evolution of SST anomaly composite maps associated with observed index T_{gs}. It is obtained in the same way as Fig. 5.13. We find that although the anomaly pattern in R_NActl is somewhat distorted, the fundamental time evolution of the pattern is similar as in observations: The initial SST tripole pattern reduces gradually and reaches its the opposite phase 3 years later, which increases gradually and reaches its largest amplitude around 6 years later. Then this opposite phased pattern weakens and transforms to the initial phase. After 11 years the initial pattern reappears. Again, R_Gctl and R_NAh have similar features as R_NActl, but not R_NAm (figures are not shown). The time evolution of tripole pattern can be represented roughly by its index. The indices from observations and each simulation are shown in Figure 5.15, in which the top panel is for JFM mean and the bottom panel is with 6 years running mean. In both panels, the index from R_Gctl (red curve), R_NActl (green curve), and R_NAh (purple curve) match the observed one (black curve) reasonably well, with correlations 0.71, 0.72, and 0.56, respectively in JFM mean (top panel), and 0.76, 0.72, and 0.61, respectively with 6 years running mean (bottom panel). The decadal feature is obvious. The index from R_NAm is very different from the observed one, with correlation between them -0.05 in JFM mean and -0.43 with 6 years running mean.

All in all, the North Atlantic tripole mode, both its time evolution as well as its spatial pattern are reasonably simulated in R_Gctl, R_NActl, R_NAh, which might imply that it is the North Atlantic regional noise heat flux which plays the major role in producing this mode. We will explore this further in Chapter 6.

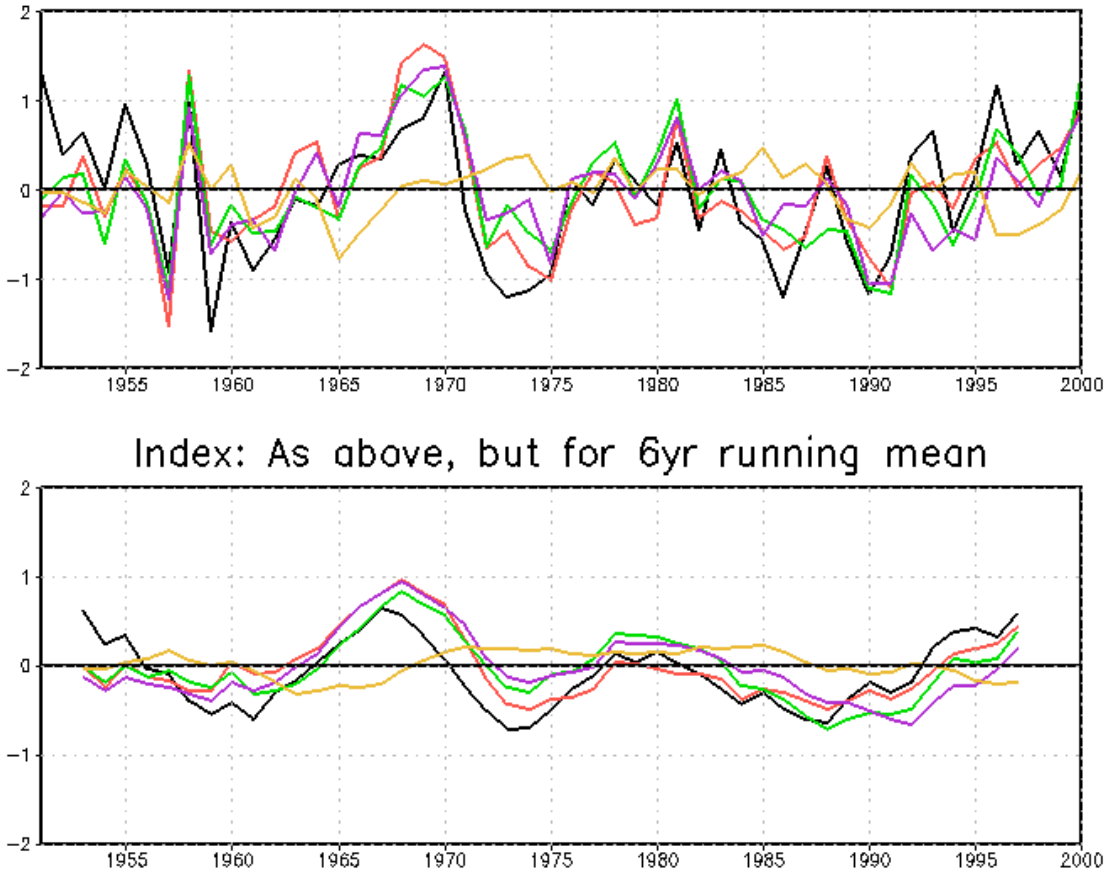

Figure 5.15 Time evolution of tripole index Tgs (linearly detrended. K) from observations (black curve, as in Fig. 5.11b), R_Gctl (red curve), R_NActl (green curve), R_NAh (purple curve), and R_NAm (yellow curve). Top panel is the JFM mean and bottom is 6 years running mean. The definition of index Tgs is as in Fig. 5.11.

(d) Monopole mode

The observed monopole mode has multidecadal variability and its index can be represented by Atlantic multidecadal Oscillation (AMO) index, which is the North Atlantic domain average SST. Figure 5.16a is the observed JFM mean AMO index (red curve) and its corresponding 21 years running (black curve). By regressing the red curve with SSTs from observation, we get the observed AMO pattern (Figure 5.16(b)). This

pattern is similar to that found by Kushnir (1994), which was analyzed by the composite method using COADS data. To see the very low frequency part of the mode, the 21 year running mean AMO index (black curve) is regressed to the observed SST and shown in Figure 5.16(c), which is very different from Fig. 5.16(b). By projecting SSTs from R_Gctl, R_NActl, R_NAh, and R_NAm onto the black curve, we obtain the results in Figure 5.17. We find that the observed spatial pattern (Fig. 5.16(c)) is approximated in R_Gctl, R_NActl, and R_NAh, although with significant errors, particularly the negative centers in the tropics. R_NAm does not capture the major centers. The similar pattern in R_NAh as in R_Gctl and R_NActl, suggests that the local noise heat flux plays the major role in producing this mode and the errors in that heat flux cause the significant errors in the tropics.

The AMO SST mode is suspected to be associated with the fluctuations in the THC: in Delworth et al. (1993), a zero lag composite analysis based on THC index shown an AMO-like SST pattern similar to the pattern found by Kushnir (1994). Figure 5.18 is the time evolution of THC index from each simulation, which is defined as the maximum annual mean stream function. We can see that there is a large change in the R_Gctl THC before and after 1976 (same year as the large SST jump seen in the equatorial Pacific in Fig. 5.4), which is not seen in other simulations. The mean THC for the first 25 years is 25.5 Sv and for the second 25 years is 22.3 Sv. For this reason, we remove the first and second 25 years mean THC separately to get the R_Gctl THC anomaly. The THC anomalies from other simulations are obtained by linearly detrending. We can see that there are similarities between the curves. The correlation based on the

results in Fig. 5.18b between R_Gctl and R_NActl is 0.79, between the R_Gctl and R_NAh is 0.66, and between R_Gctl and R_NAm is 0.27, based on THC anomaly of 1960 to 2000 (there are large differences at the first several years). Since there is no observed THC index, we use R_Gctl THC index instead of to compute the correlation to the observed SST, which is shown in Figure 5.19. Unexpectedly, the correlation pattern at 0 lag is more of a tripole-like pattern instead of an AMO-like pattern. The correlation pattern at +6 lag is an AMO-like pattern. The tripole and AMO patterns are not independent. The tripole pattern appears earlier than THC, and THC appears than AMO, possibly implies that the tripole cause THC anomaly, lead to AMO pattern. It needs further work to test it.

In summary, the diagnosis from the COLA AGCM/CGCM is that the later 20th century North Atlantic SST variability is predominantly forced by the weather noise, for both of the two major low frequency patterns of variability

- Tripole mode: it can be reproduced reasonably well both for its spatial pattern and its time evolution, and local heat flux noise plays the major role.
- AMO mode: its evolution can be simulated but with significant errors. It is caused by the local heat flux noise.

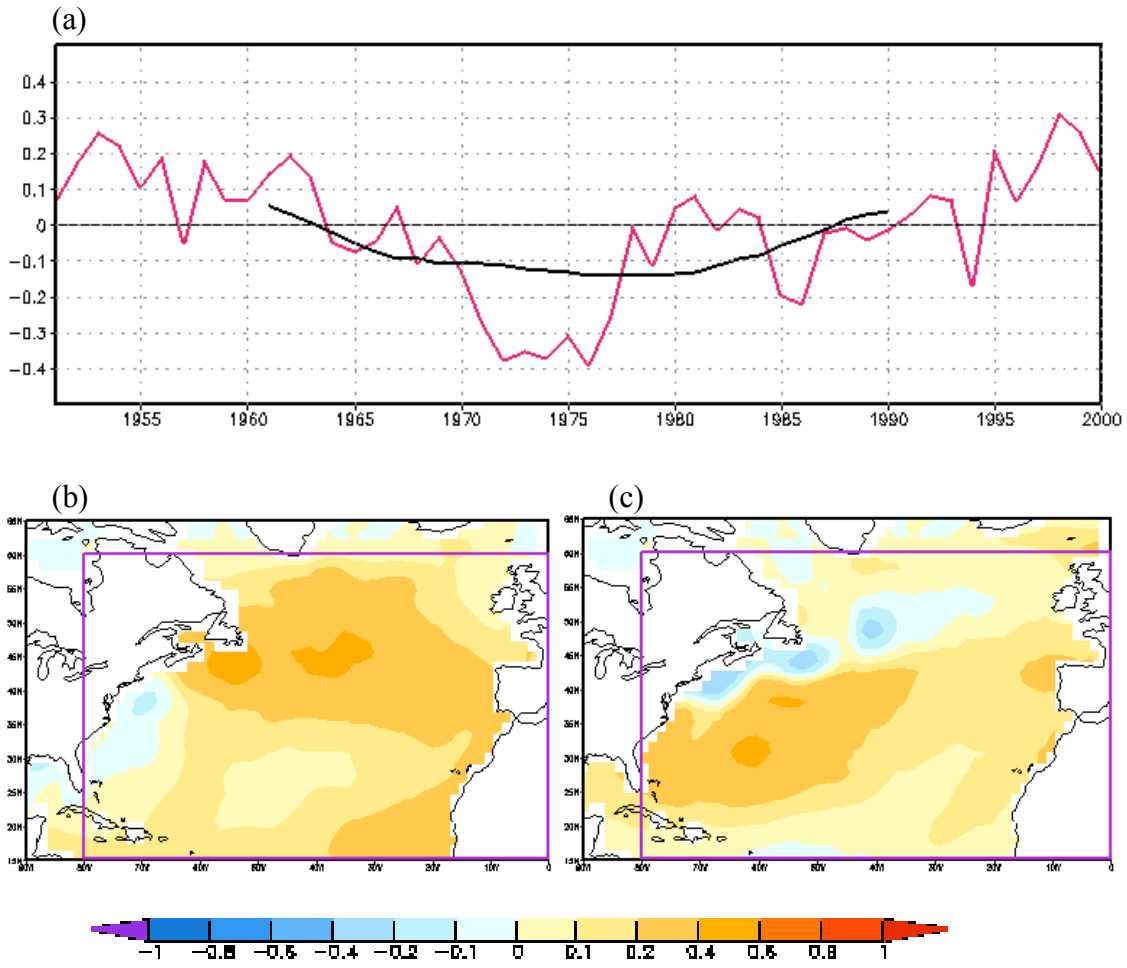

Figure 5.16 Observed JFM AMO index (K), and its corresponding spatial pattern. The red curve in (a) is the JFM mean data while the black curve indicates a 21-year running mean. The purple box indicates the region used to construct the SST index (15-60°N, 80-0°W). The shaded maps are the regressions of the time evolution of observed SST with the AMO index: (b) corresponding to red line, and (c) corresponding to black line in (a) respectively, with unit K per standard deviation of the AMO index.

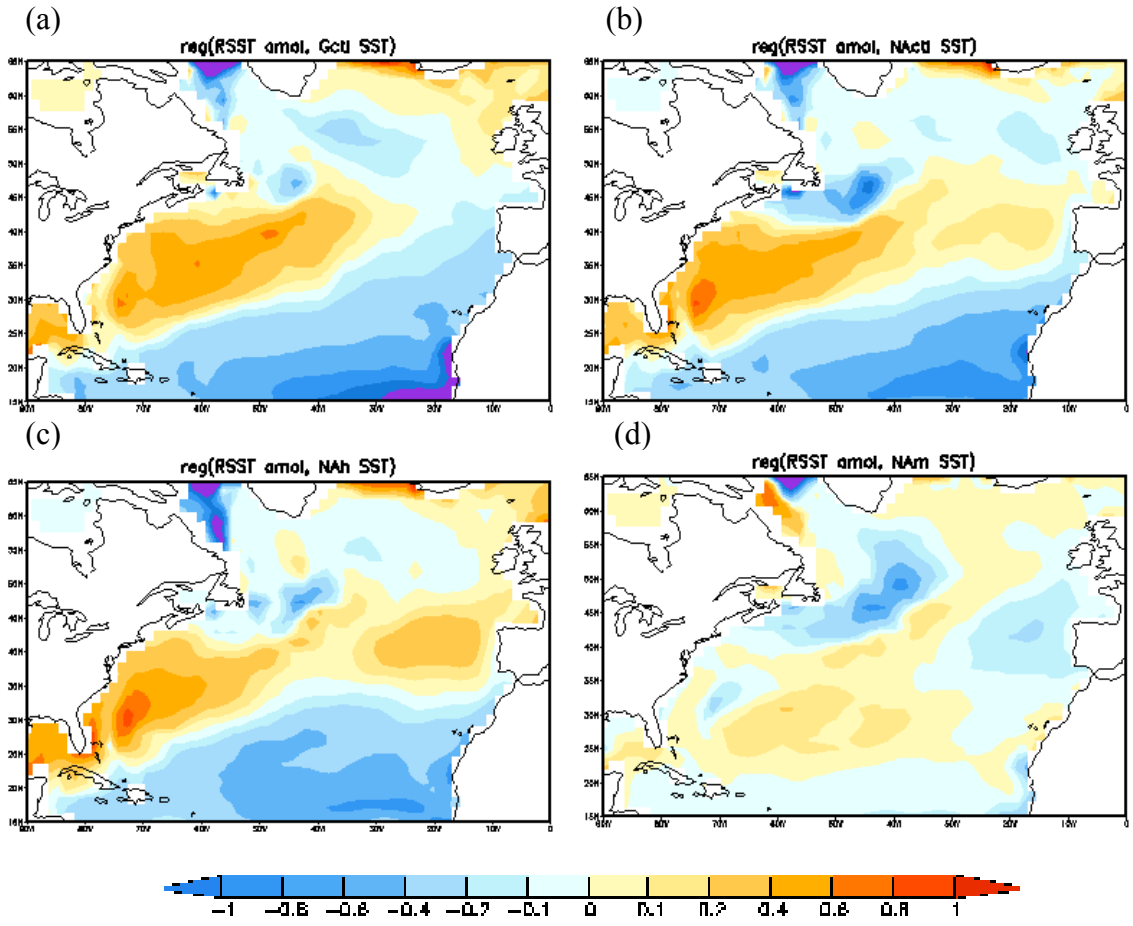

Figure 5.17 Simulated North Atlantic JFM SST monopole pattern in: (a) R_Gctl; (b) R_NActl; (c) R_NAh; (d) R_NAm. The monopole pattern in each noise forced simulation is determined by regressing the time evolution of SST from each simulation onto the observed index (normalized black line in Fig. 5.16a). Unit is K per standard deviation of the AMO index.

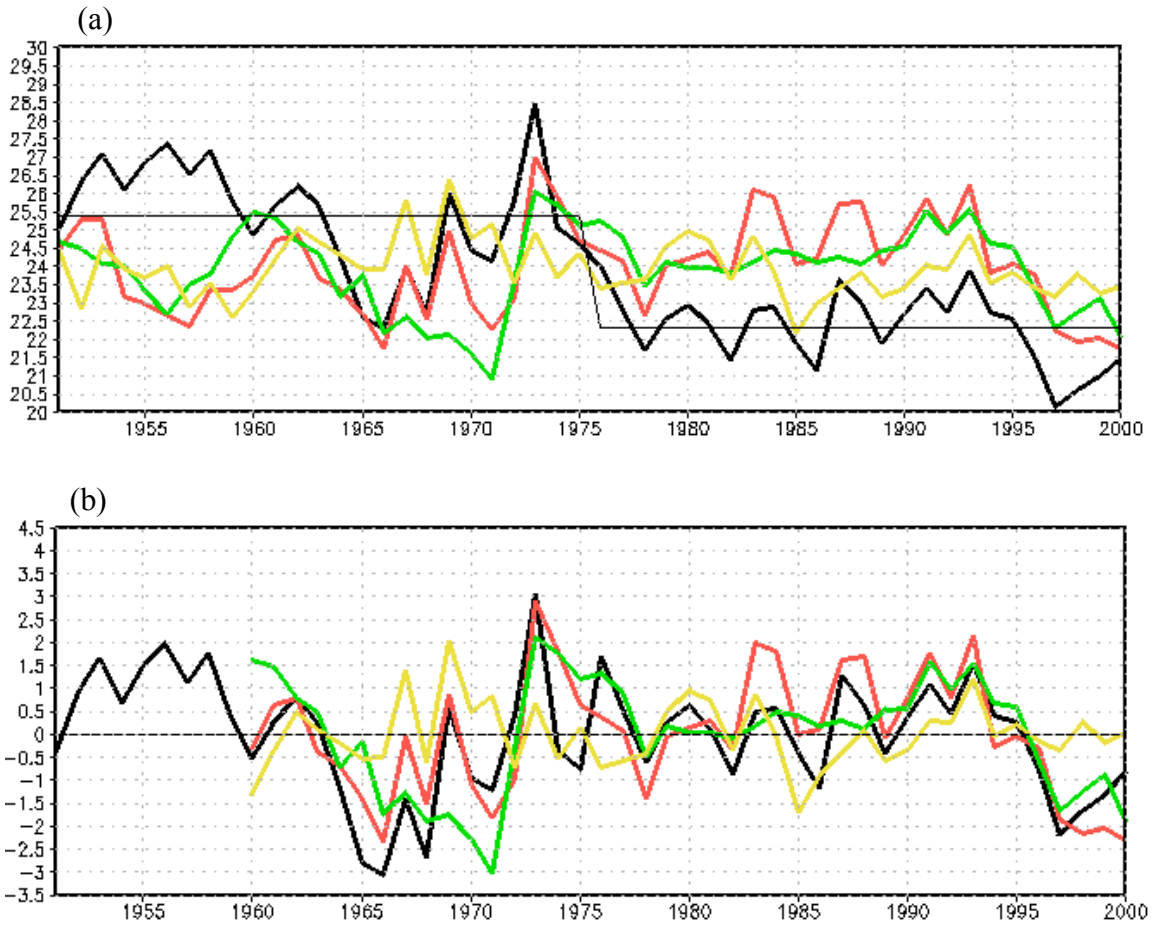

Figure 5.18 Time evolution of the North Atlantic THC index (Sv), which is defined as the maximum annual mean stream function: R_Gctl (black), R_NActl (red), R_NAh (green), and P_NAm (yellow). (a) unfiltered data, and (b) with jump in climatological mean removed (R_Gctl, first 25 yr and second 25 yr mean, the black thin line in Fig. (a), is removed separately) or linear de-trended (R_NActl, R_NAh and R_NAm).

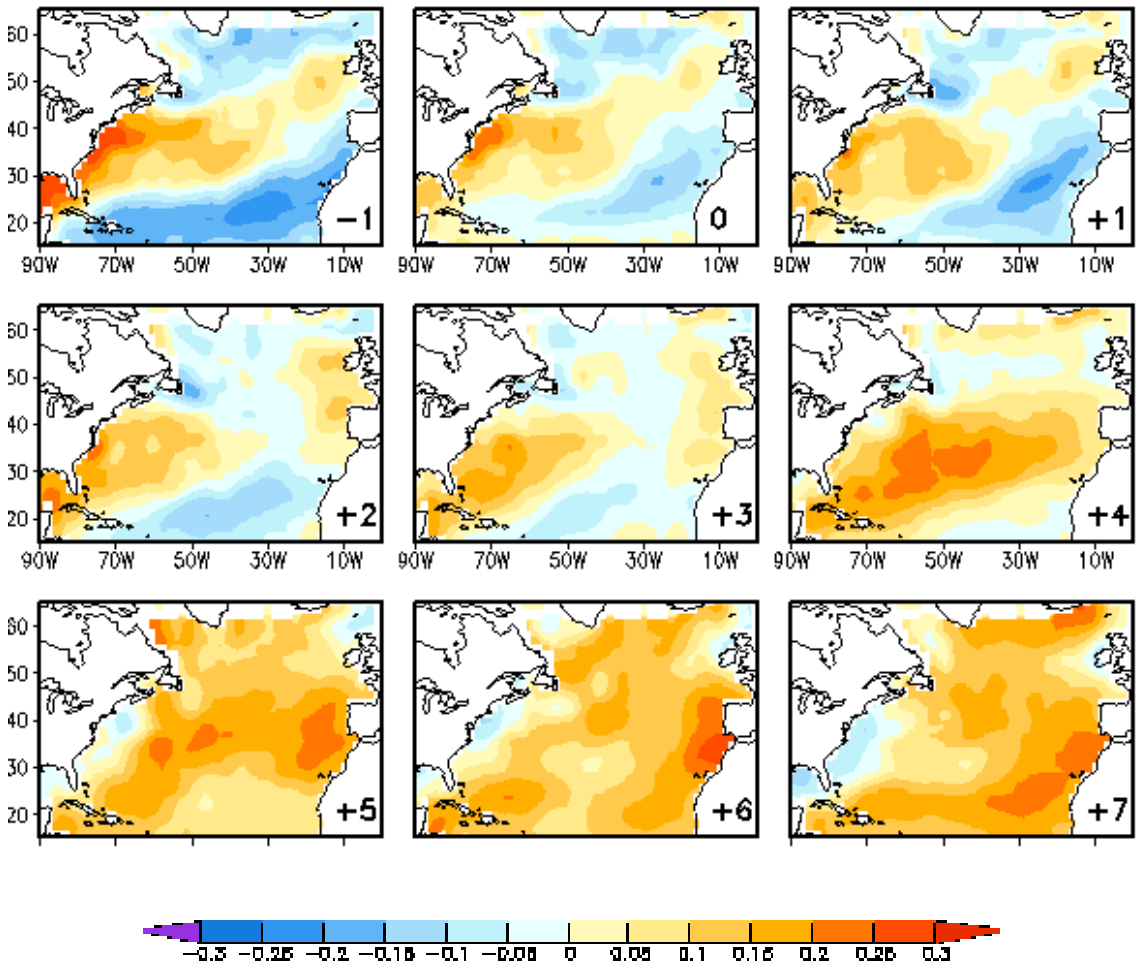

Figure 5.19 correlation of THC index from R_Gctl (black curve in Fig. 5.18b) with observed SST for several time lags (indicated in the bottom right corner of each sub-panel). The THC leads for positive lags.

5.3.2 Seasonality

The maps of SSTA point-to-point correlation coefficient between the observations and the R_Gctl are shown in Fig. 5.20a (JFM) and Fig. 5.20b (JJA). We can

see that in many regions (but with obvious exceptions), Fig. 5.20a has smaller correlation than that of Fig. 5.20b. This might imply that in these regions weather noise plays a more important role on the North Atlantic low frequency SST variability in JJA than in JFM. In JJA, the ocean mixed layer is relatively shallower than in JFM, and the effect of oceanic dynamics on SST possibly is weaker than in JFM.

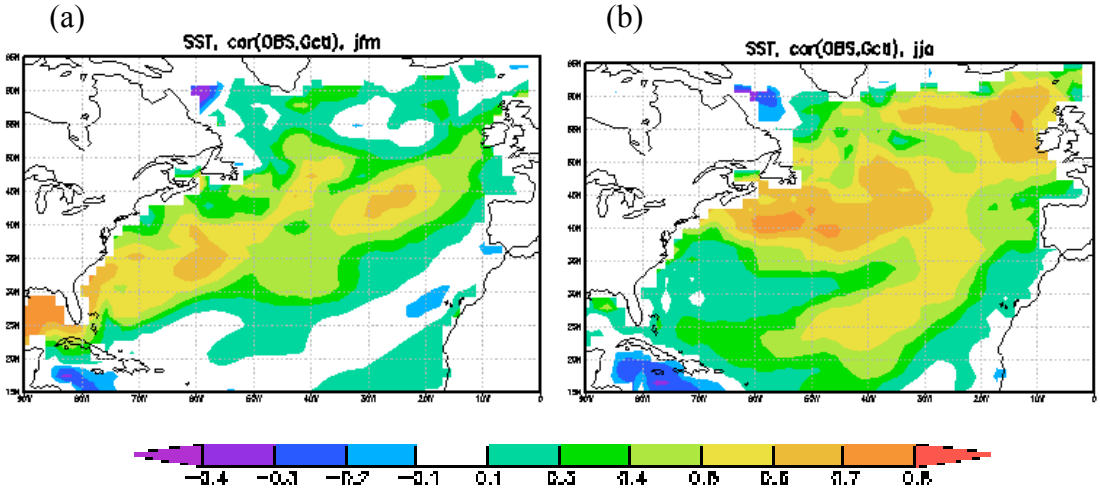

Figure 5.20 Point correlation coefficient of SSTA from R_Gctl with that from observations during (a) JFM and (b) JJA.

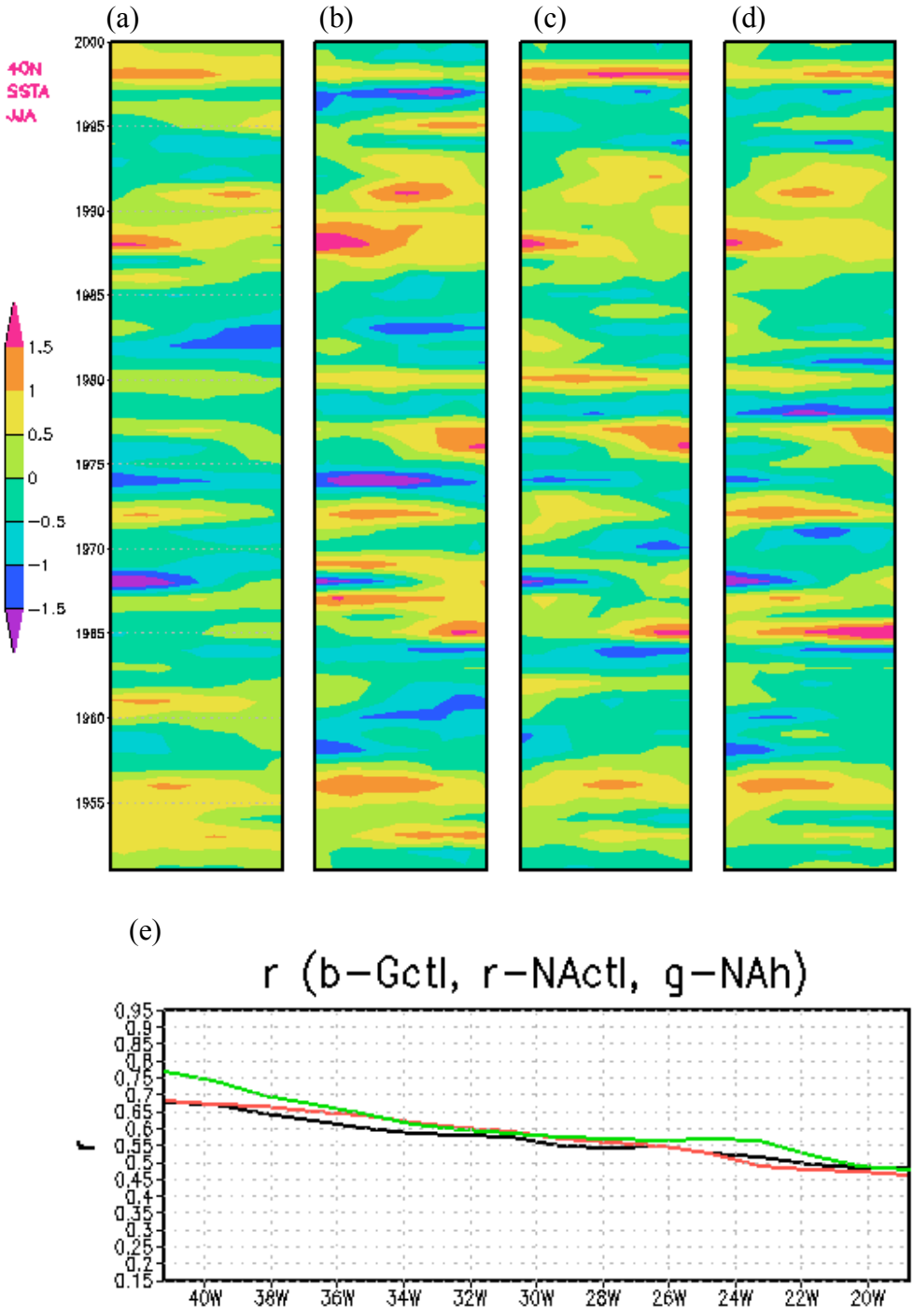

Figure 5.21 As Fig. 5.9 but for JJA: Time-longitude diagram of JJA SST anomaly (K) along 40°N between 40°W and 20°W. (a), (b), (c), and (d) are for SSTA from observation, R_Gctl, R_NActl, and R_NAh, respectively. (e) is the corresponding SSTA correlation coefficient along 40°N between observation and R_Gctl (black curve), R_NActl (red curve), and R_NAh (green curve).

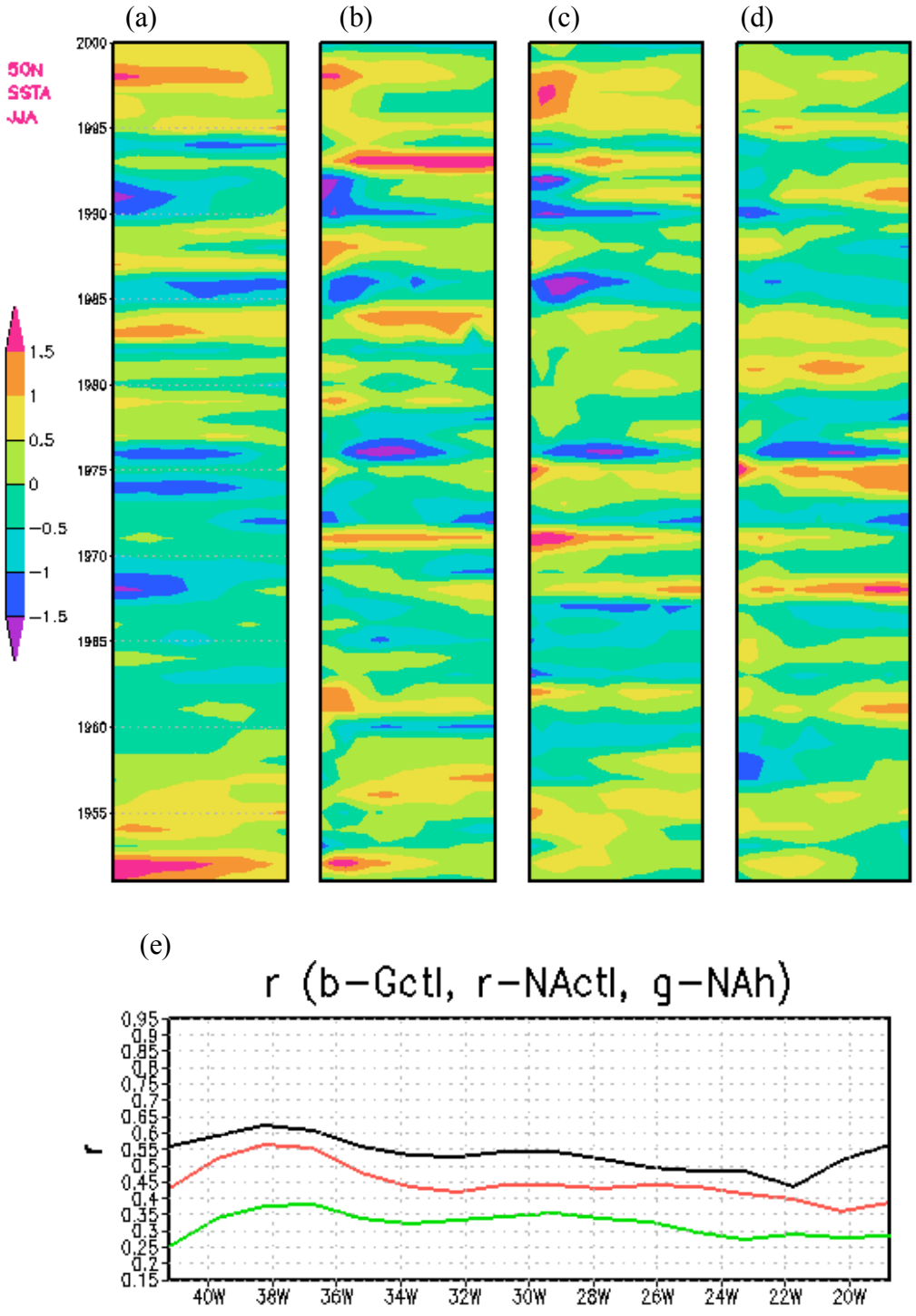

Figure 5.22 As Fig. 5.21 but along 50°N.

Similar features exist in longitude-time sections. Figures 5.21a, 5.21b, 5.21c, 5.21d are the time evolution of JJA SSTA along 40°N between 40°W and 20°W from the observation and the noise forcing simulations R_Gctl, R_NActl, R_NAh, respectively, and Fig. 5.21e is the corresponding correlation between the observation and the noise forcing simulations. We can see that R_Gctl, R_NActl, and R_NAh have very similar event-by-event evolution and all are similar to that in the observations. The correlation between the observations and the simulations are generally higher than 0.55. The corresponding noise forced simulations reproduce more observation-like features during JJA than that during JFM (Fig. 4.21 versus Fig. 5.9).

Similar conclusions can be made about the time evolution along 50°N: The global noise forced simulation R_Gctl produces much more observation-like SST anomalies during JJA (Figure 5.22) than during JFM (Fig. 5.10).

5.3.3 Coupled feedbacks

The top-left panel of Fig. 5.23 is the correlation between the observed surface air temperature (TS) and the observed SST tripole index (red curve of Fig. 5.11b). Over ocean, TS are the same as SST except in the sea-ice covered regions. We can see the tripole pattern of SST variability over the North Atlantic. There is no association of the North Atlantic pattern with cold ENSO as there was in the perfect model case in Chapter 4. The correlation coefficient between the observed sea level pressure with the tripole index (top-right panel) shows that the atmosphere exhibits a north-south dipole in surface pressure, with a resemblance to the negative NAO pattern: A positive polar anomaly (weaker-than-normal Icelandic low) and a negative subtropical anomaly (weaker-than-

normal subtropical high) are associated with cooling in the subtropics and warming in the subpolar (very weak) and eastern subtropical Atlantic, and vice versa. It appears that in the North Atlantic, the sea level pressure is not explicable by the thermal response to the SSTA (Kushnir et al. 2002). The correlation coefficient between the observed precipitation (P) and the tripole index (bottom-left panel) shows that in North Atlantic basin, P has negative correlation coefficient with the SSTA: over warm SSTA, there is less precipitation, and vice versa. It appears that the precipitation is not driven by the SST but is dynamically related to the sea level pressure. The positive phase of the tripole appears to be related to a northward shift in the ITCZ in the tropical Atlantic. The 500mb geopotential height (H500) pattern is similar to the surface pressure over North Atlantic (bottom-right panel), showing a barotropic structure, especially in higher latitudes.

Figure 5.24 is the same as Fig. 5.23, but with atmospheric variables from the ensemble mean of 10 members of R_10AGCM . This is the forced response of the model. We can see the same tripole pattern of TS over North Atlantic basin as Fig. 5.23. There is no significant correlation between surface pressure/500mb geopotential height and the tripole index. The precipitation appears to be surface thermally driven (Kushnir et al. 2002) with negative precipitation anomalies over cold SST, and vice visa. The differences between Fig. 5.24 and Fig. 5.23 for surface temperature, surface pressure/sea level pressure, precipitation, 500mb geopotential height are caused by elimination of the weather noise and are model dependent. Much of the structure in the observation is that of the noise according to the COLA AGCM.

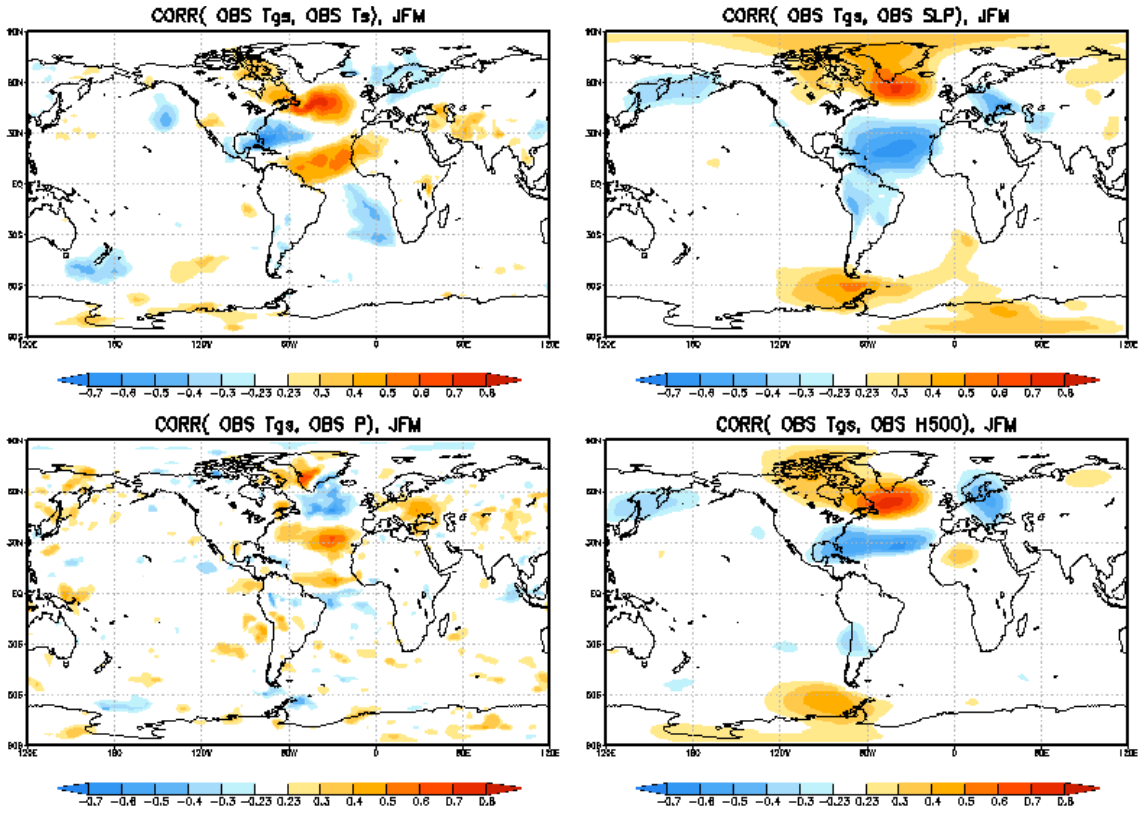

Figure 5.23 The JFM correlation coefficient between the observed tripole index Tgs (normalized red curve in Fig. 5.11b) and the anomaly of observed surface air temperature (TS, left-top panel), sea level pressure (SLP, right-top panel), precipitation (P, left-bottom panel), and 500mb geopotential height (H500, right-bottom panel).

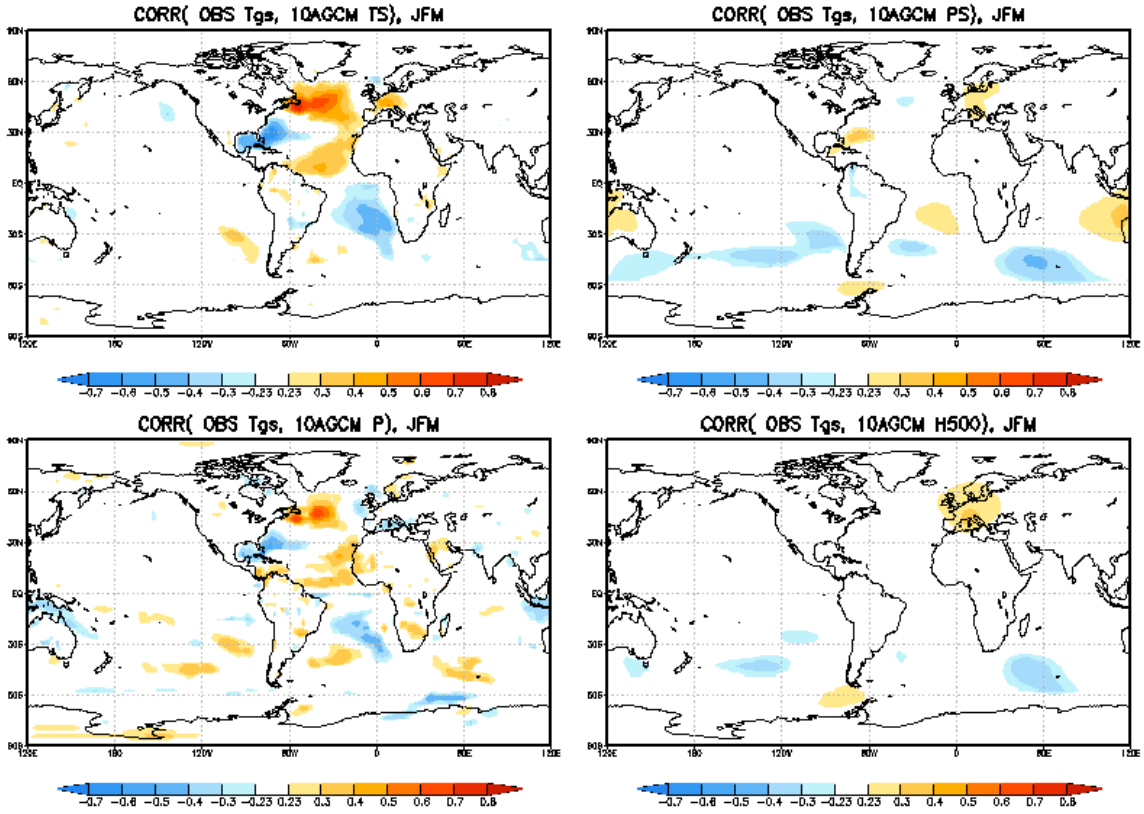

Figure 5.24 The JFM correlation coefficient between the observed tripole index Tgs (normalized red curve in Fig. 5.11b) and the anomaly of R_10AGCM surface temperature (TS, left-top panel), surface pressure (PS, right-top panel), precipitation (P, left-bottom panel), and 500mb geopotential height (H500, right-bottom panel). TS, PS, P, and H500 is the 10 members ensemble mean (represent the feedbacks from SST forcing).

5.4 Summary and discussion

The COLA model diagnosis produces the result that weather noise is the main component of atmospheric variability at midlatitude and north. In the tropics, the main component of atmospheric variability comes from the atmospheric response to the SST.

The results from the statistics and event-by-event comparisons of observations and noise forced simulations suggest that the observed SST variability is mostly atmospheric weather noise forced. JJA SST variability can be better reproduced by noise forcing than JFM's. The major features of the North Atlantic SST tripole are reproduced, including its time evolution and spatial pattern. Differences between the observed evolution and that in the global-noise-forced simulation R_Gctl can occur for many possible reasons: In addition to the two discussed with regard to the synthetic observation case, errors from various approximations made in applying the method, there are many potential sources of error in the noise estimate based on the reanalysis. The accuracy of the noise estimate depends on the realism of the feedbacks calculated by our model, the COLA AGCM, and the accuracy of the reanalysis, which in turn depends on the realism of the NCEP AGCM as well as the accuracy and time-space coverage of the observations. Our results suggest strongly that there is a spurious large jump around 1976 in the NCEP heat flux in the equatorial Pacific. The atmospheric model response to the observed SST forcing (the feedbacks), which includes an implicit response to the external forcing, is model dependent, and SST forcing in R_10AGCM is limited to be between 40°S and 65°N .

The regional atmospheric stochastic forcing, especially the heat flux noise forcing, is the main source of the low frequency SST variability in North Atlantic, but not the complete story. Local oceanic processes such as gyre and THC may modulate the low frequency SST variability. The role of gyre, as well as the role of different flux noise (e.g. heat flux and momentum flux) forces, in the low frequency SST variability will be

checked in more detail in next chapter. The North Atlantic low frequency SST variability may also be influenced by the local SST response to the remote SST variability because of 1) unstable coupling such as western equatorial Pacific SST variability, or 2) feedbacks from the remote response to North Atlantic variability through atmosphere bridge, which causes the North Atlantic low frequency SST variability difference between R_Gctl and R_NActl.

Chapter 6 Possible Mechanisms of the Observed North Atlantic SST Tripole Mode

In this study, we not only aim to prove our method to test the null hypothesis that the SST variability is forced by atmospheric weather noise, but also to apply the method to evaluate proposed mechanisms of observed North Atlantic SST low frequency variability. This will be done in this chapter.

6.1 Deficiency of COLA CGCM

In chapter 4, we have tested our method in a perfect model/perfect observation configuration, in which a free evolution of a CGCM simulation (CTL) is taken as ideal observations. From the CTL simulation, the first two North Atlantic SST EOFs from CTL show a monopole-like mode and a tripole-like mode. These two modes are well reproduced, both for their spatial pattern and time evolutions, in our special frame of interactive ensemble CGCM forced by atmospheric weather noise.

Although CTL simulated major features of the observed climate, it is far from realistic. The North Atlantic low frequency SST variability (the first two EOFs of SST) is distorted from the observed, both for the spatial patterns and the timescales. For example, the tripole-like mode has an artificial center near the east coast of Europe, not seen in observation, and possibly caused by an eastward displacement of the NAO in the AGCM (chapter 4 section 4.1). The model tripole-like mode has a 5 year oscillation compared to a 12-14 year oscillation in the observations (we will see in section 6.3). Another example

is the thermohaline circulation (THC). The THC is thought to be related to the SST AMO mode (Delworth et al. 1993). Fluctuations in the THC are caused in part by the fluctuations in the density of seawater, which involves the effects of temperature and salinity. The THC anomaly may be underestimated in our model. Since our model's ocean domain is south of 65°N (74°S - 65°N), and the THC sinking region is mainly located 60°N north (52-72°N in Delworth et al. 1993), the sinking region in our model may be shifted. Additionally, the climatological sea ice is used in our model, and the simulation period is short. All of these may make the THC in our model far from realistic. Therefore, this study will not further consider the mechanisms of the modes from (CTL), or the role of the THC in the mechanism of the observed North Atlantic low frequency SST variability.

In addition to the deficiencies of our model, deficiencies of the NCEP reanalysis data are also obvious too (chapter section 5.2, Fig. 5.4 and Fig. 5.5). These also need to be considered during diagnosis.

6.2 Observed tripole mode and corresponding atmospheric variability

Following Czaja and Marshall (2001), an index measuring the meridional SST gradient across the separated Gulf Stream is used as the index of the SST tripole mode (taken as T_{gs}). The index is defined as the SST anomaly averaged over areas north and south of the separated Gulf-Stream, as indicated as the two purple boxes in Figure 6.1a (Fig. 6.1 is the same as Fig. 5.11), the one over north minus the one over south (as in section 5.3.1(c)).

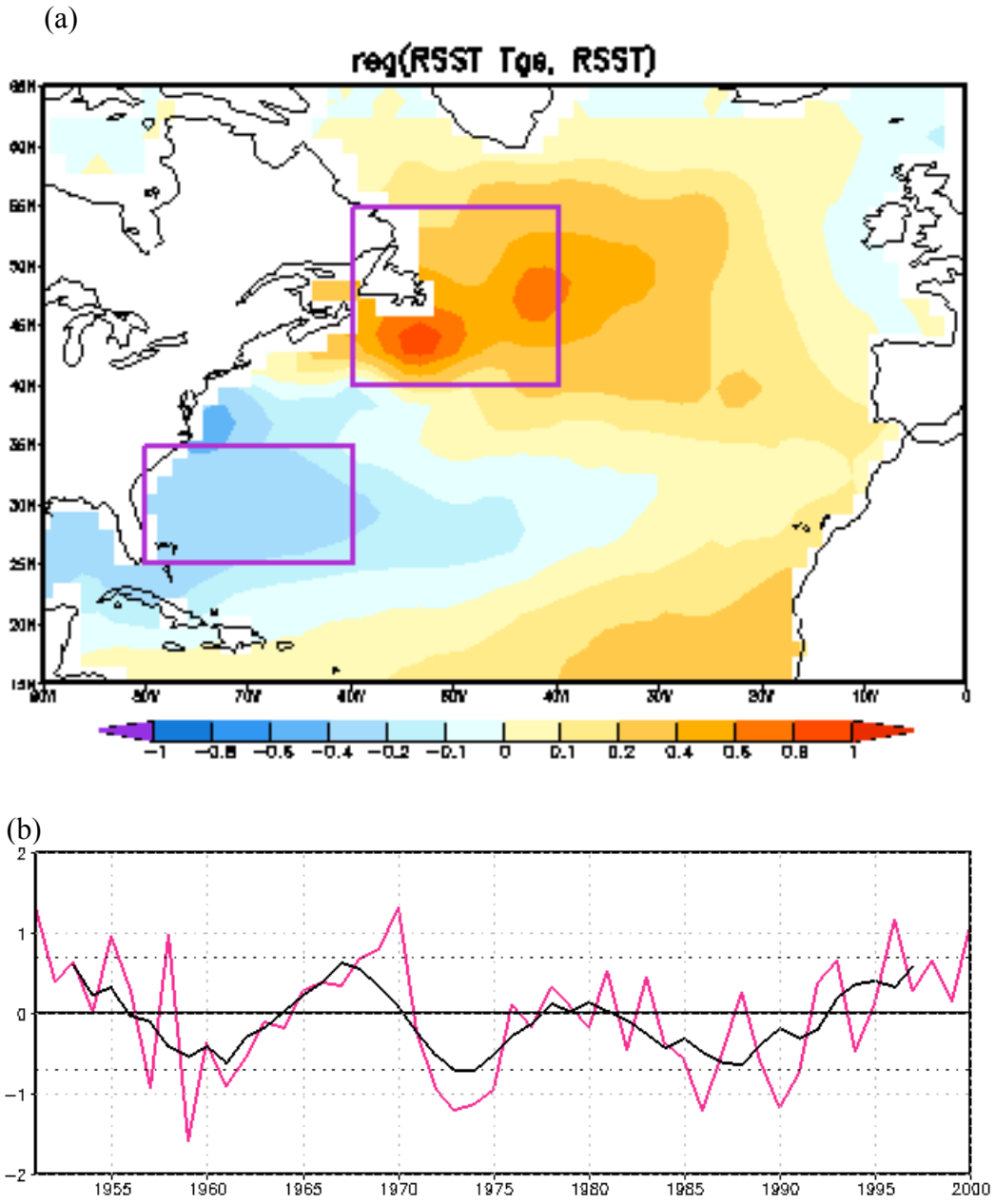

Figure 6.1 Same as Fig. 5.11: Observed JFM North Atlantic tripole pattern (a) and the corresponding index Tgs (K) (b). The red curve in Fig. 6.1b is the yearly JFM mean while the black curve indicates a 6-year running mean. The two purple boxes indicate the regions used to construct the SST index Tgs=TN-TS, where TN is the average SST anomaly in the northern box (40-55°N, 60-40°W) and TS the average SST anomaly in the southern box (25-35°N, 80-60°W). The shaded map is the regression of the index (normalized red line) with the time evolution of observed SST, with unit K per standard deviation of the index Tgs.

The observed JFM tripole index T_{gs} is shown in Figure 6.1b: The red line is the JFM mean index, and black line is the one with 6 yr running mean, which shows a decadal variability. Similar curves can be found in Czaja and Marshall (2001) for the time period: 1951-2000, although different SST data set is used. The shaded map (Fig. 6.1a) is the corresponding SST tripole pattern, which is the regression of the normalized index (normalized red line in Fig. 6.1b) with the time evolution of observed SST. It has negative anomalies extending from the southeast coast of the United States into the central basin, surrounded by positive anomalies in the midlatitudes south of Greenland and the tropical North Atlantic. The maximum amplitude anomalies reached are 0.8 and 0.4°K per standard deviation of the tripole index at the north box and south box, respectively.

Figure 6.2 is the correlation between the JFM SST tripole index and the NCEP reanalysis sea level pressure (SLP) and 500hPa geopotential height (GPH).The correlation maps show that the 0-lag free tropospheric circulation anomalies associated with a NAO anomaly event (negative NAO here) are equivalent barotropic in the extratropics, with a positive (negative) GPH anomaly corresponding to the warm SST-high pressure (cold SST-low pressure) NAO center of action. These co-varying patterns of atmospheric and oceanic variability in the reanalysis are consistent with Deser and Blackmon (1993) and Sutton and Allen (1997) and imply possible interactions between NAO and the North Atlantic SST tripole mode. We will examine this below.

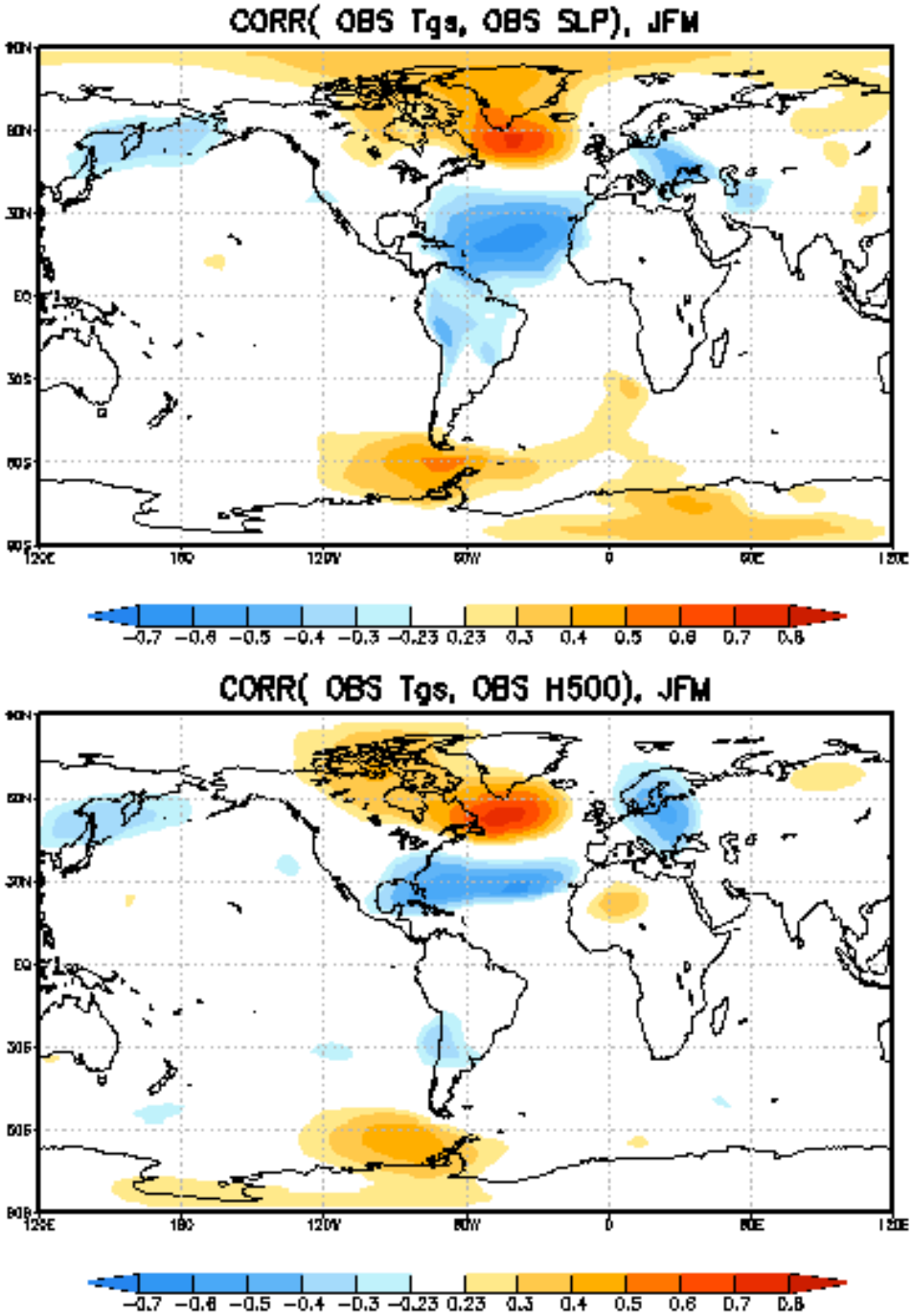

Figure 6.2 Observed patterns of JFM sea level pressure (SLP; top panel) and 500 hPa geopotential height (GPH; bottom panel) corresponding to the North Atlantic SST tripole pattern (Fig. 6.1a). They are the correlation coefficient between the tripole index Tgs (normalized red line of Fig. 6.1b) and the time evolution of NCEP reanalysis SLP and 500hPa GPH, respectively. Shaded areas are statistically significant at 95% level.

6.3 Evolution of tripole mode: lead-lag analysis

The spatial and temporal evolution associated with the North Atlantic SST tripole variability is now inspected in detail. Figure 6.3 is correlation maps of observed SST tripole index Tgs against observed JFM SST anomalies at lags from -7 to +7 years (the index leads for positive lags). The zero lag correlation map shows the well known tripole pattern (same as Fig. 6.1a, corresponding to NAO-; Tripole Pattern hereafter, its reversed pattern is Reversed Triploe Pattern hereafter). Now let us investigate the sequence of lag-lead correlation maps. At -7 lag, there is a reversed triploe pattern, it is strongest at -6 lag. This pattern decays, and disappears at -3 lag. At -2 lag the Tripole Pattern appears and is strongest at 0 lag, then decays again and disappears at +3 lag. At +4 lag the Reversed Tripole Pattern appears again and is strongest at +7 lag. Apparently, the observed North Atlantic SST tripole mode has about a 12~14 year period. Let us focus on the positive anomaly center at the southeast coast of the USA at -6 lag. Over time, this center propagates northeastward, following the path of the mean gyre. At -3 lag, there is a cross-gyre propagation: Part of the anomaly propagates to the Labrador Sea region, and another part continuously propagates around the subtropical gyre. After that, the anomaly at subpolar latitudes propagates around the subpolar gyre and the anomaly in the subtropics propagates around subtropical gyre. The cross-gyre propagation might be related with the heat transport of inter-gyre gyre (IGG) proposed by Marshall et al. (2001) and Czaja and Marshall (2001). The SST anomalies at -3 lag are very uniform over the North Atlantic basin, possibly due to the cross-gyre heat transport. The analogous lead-lag correlation maps of the observed NAO index (leading PC of SLP) against observed JFM SST

anomalies shows similar features to Fig. 6.3 (not shown). It seems that the NAO and North Atlantic SST tripole have co-varying features (simultaneity).

Figure 6.4 is correlation maps of observed SST tripole index T_{gs} against R_NActl JFM SST anomalies at lags from -7 to +7. Again, the index leads for positive lags. Apparently, it has very similar features as in Fig. 6.3: The simulated North Atlantic SST tripole mode has about a 12~14 years period; The anomaly propagates following the path of the mean gyre, except at -3 lag, at which there seems a cross-gyre propagation. It must be pointed out that the anomaly propagation around the mean gyre is slower in R_NActl than in the observations (e.g. compare -2 and -1 lags between Fig. 6.3 and Fig. 6.4), leading to the distorted tripole pattern at 0 lag (fork-shape of negative center). Figure 6.5 is the corresponding regression maps. The SST anomalies have comparable amplitude as in observations (not shown except at 0 lag in Fig. 6.1a). The similar SST tripole evolution features between observation and R_NActl, as well as the reasonable amplitude variability, make it possible to use the ocean data from simulation R_NActl to analyze the possible role of ocean circulation on the North Atlantic SST tripole mode (below).

Next we will investigate the various roles of atmospheric noise forcing and the ocean circulations.

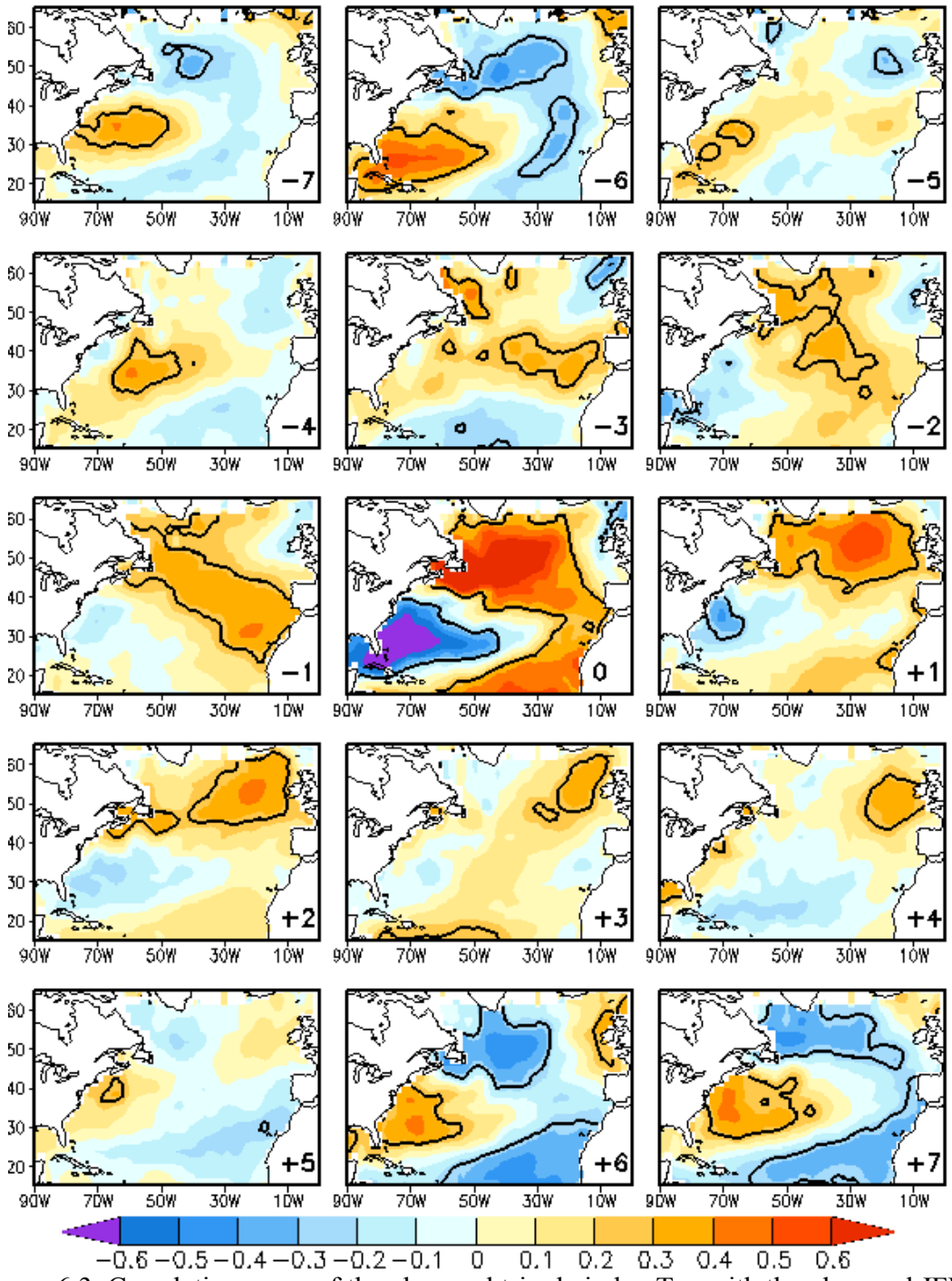

Figure 6.3 Correlation maps of the observed tripole index Tgs with the observed JFM SST for several time lags (indicated in the bottom right corner of each sub-panel). The index Tgs leads for positive lags. Correlation values are indicated with colored shading. Thick black contours encircle regions that are statically significant at the 90% level.

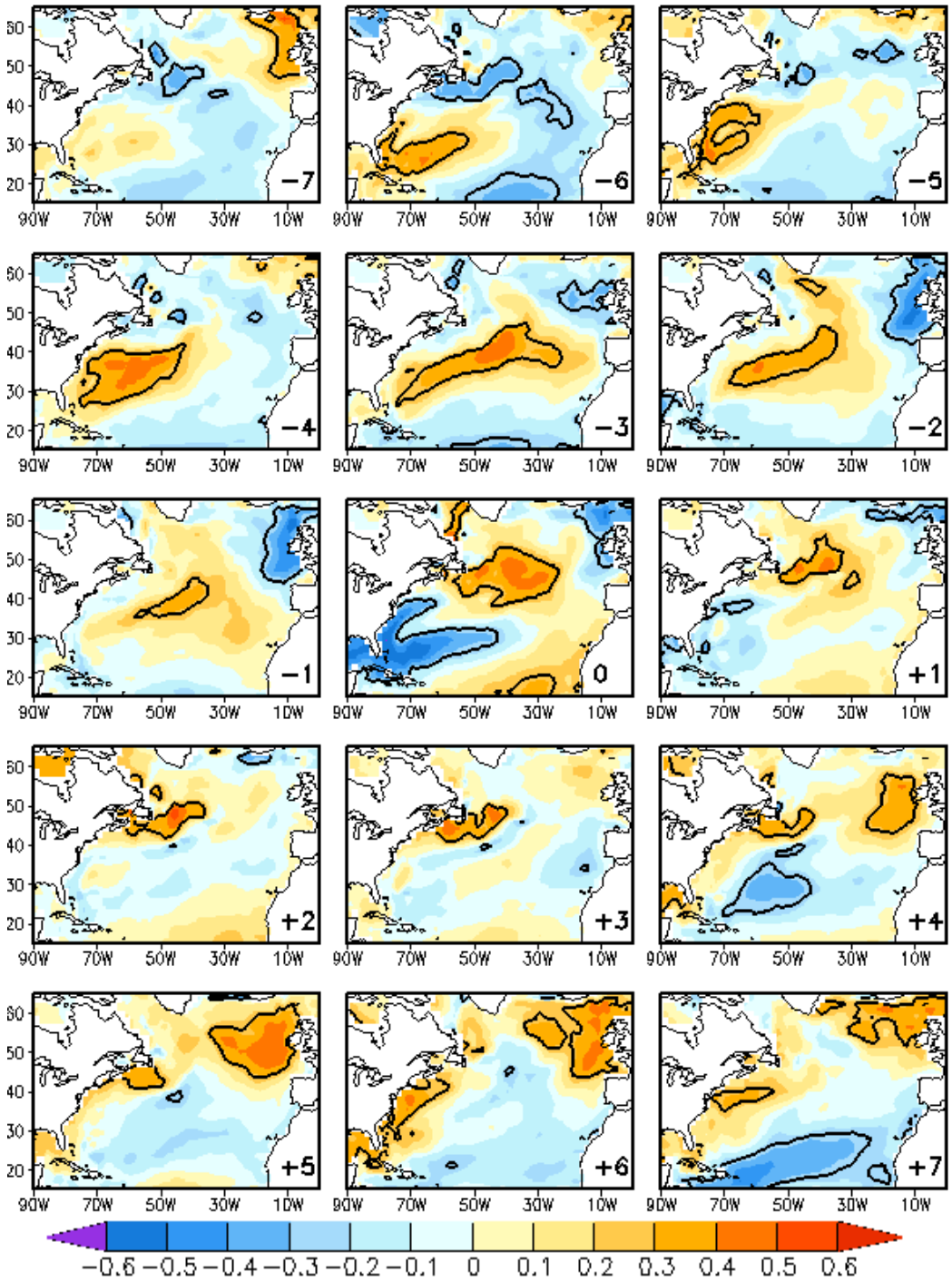

Figure 6.4 Same as Fig. 6.3, but with evolution of SST anomalies from simulation R_NActl: Correlation maps of the observed tripole index Tgs against the R_NActl JFM SST for several time lags (indicated in the bottom right corner of each sub-panel). The Tgs leads for positive lags. Correlation values are indicated with color shading. Thick black contours encircle regions that are statically significant at the 90% level.

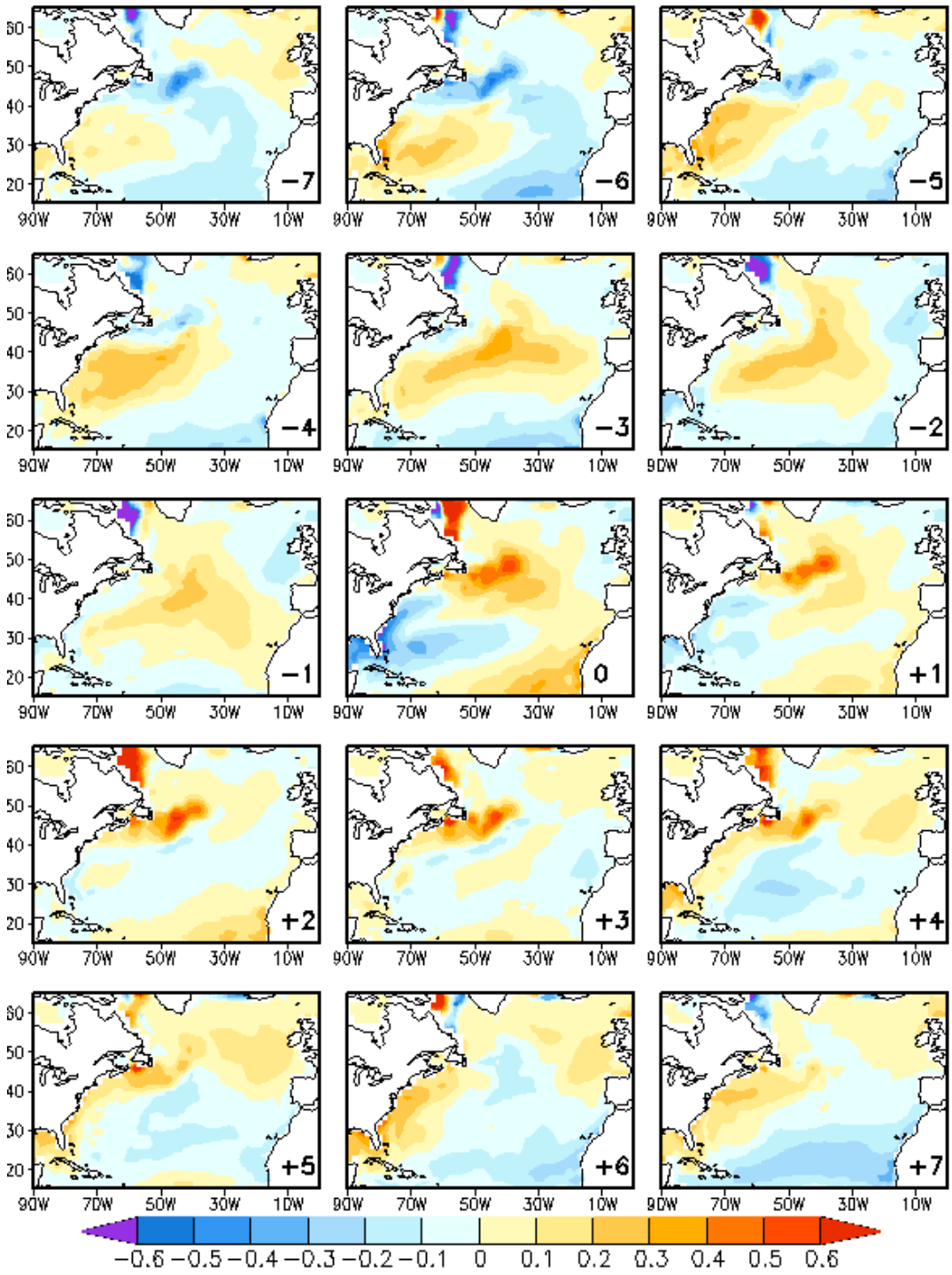

Figure 6.5 Regression maps of the observed tripole index Tgs against the R_NActl JFM SST for several time lags (indicated in the bottom right corner of each sub-panel). The Tgs leads for positive lags. Unit: K per standard deviation of Tgs.

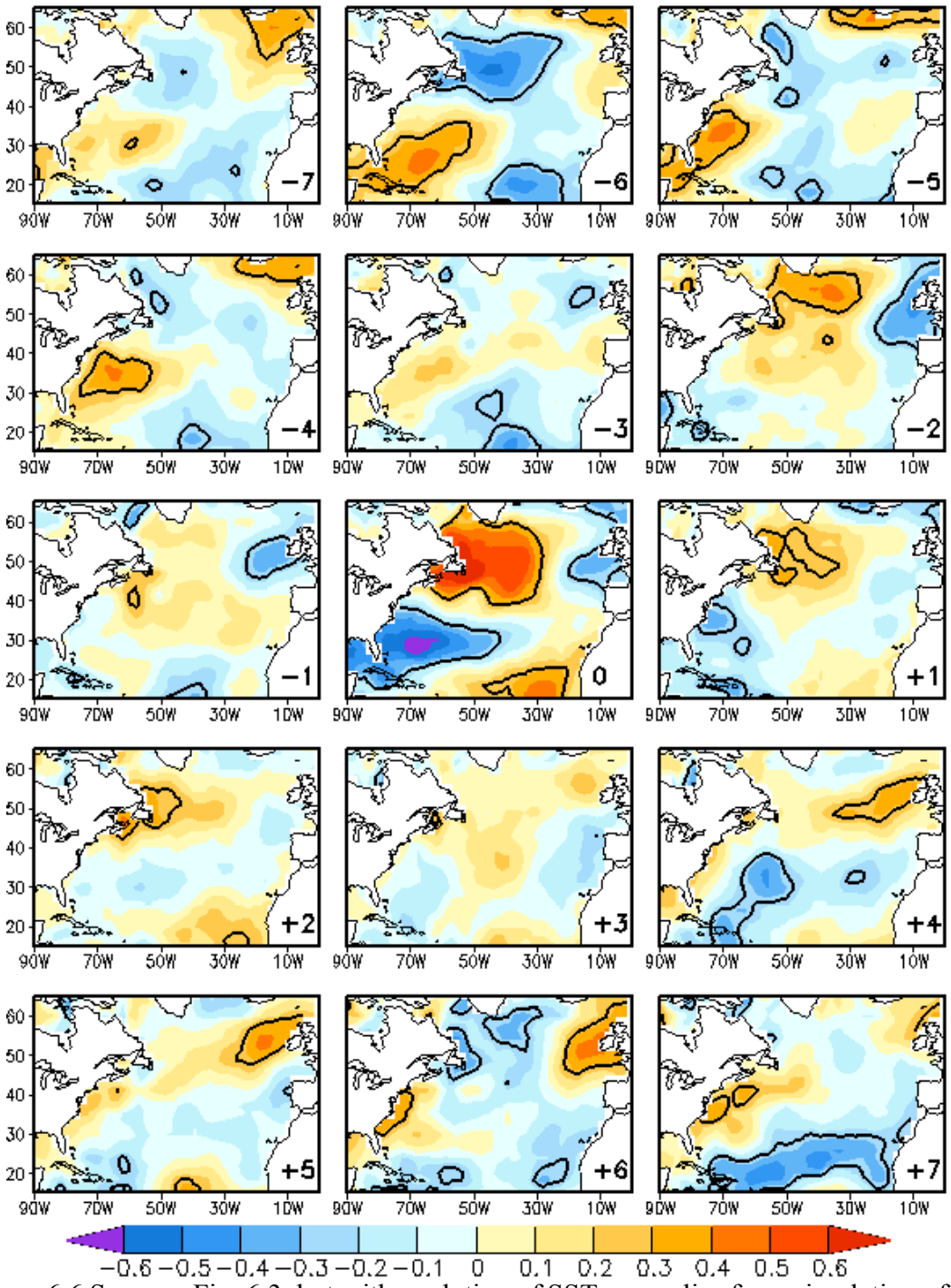

Figure 6.6 Same as Fig. 6.3, but with evolution of SST anomalies from simulation of BB model (chapter 2; local heat flux noise forced): Correlation maps of the observed tripole index Tgs against the BB JFM SST for several time lags (indicated in the bottom right corner of each sub-panel). The index Tgs leads for positive lags. Thick black contours encircle regions that are statically significant at the 90% level.

6.4 The role of atmospheric heat flux noise forcing: result from BB

In chapter section 5.3.1(c), we have shown that the North Atlantic tripole mode, both its time evolution as well as its spatial pattern are reasonably simulated in R_Gctl, R_NActl, R_NAh, and might imply that it is the North Atlantic regional noise heat flux that plays a major role in producing this mode. The noise forced result from a simple model lend further support to this idea.

We use the heat flux noise diagnosed from the NCEP reanalysis (the one used in R_Gctl simulation) to force the interactive ensemble version of BB98 model (chapter 2) and call this simulation BB. The interactive ensemble BB98 model is a zero-dimension (point) coupled model with a slab ocean (50m depth mixed layer). The heat flux noise forcing is totally local and no ocean dynamics are involved, so the result from BB can be used to evaluate the role of atmospheric heat flux noise forcing. Figure 6.6 is correlation maps of observed SST tripole index T_{gs} against BB JFM SST anomalies at lags from -7 to +7. The similarity of patterns between Fig. 6.6 and Fig. 6.4 as well as Fig. 6.3 at lag -6, 0, and +6 are obvious. The 12-14 year period of the tripole variability is clear. However, the propagation seen in Fig. 6.3 and Fig. 6.4 is not seen as clearly in Fig. 6.6. This might imply that the forcing of atmospheric heat flux noise is the fundamental element determining the spatial pattern, the phase switch, as well as the time scale, of the tripole mode. Ocean circulation plays a secondary role in the tripole's major features, in modulating the amplitude of the anomaly. This conclusion seems to contradict the results of Czaja and Marshall (2001, CM01 hereafter), which argues that it is the gyre anomaly driven by SST-induced wind anomaly that controls the oscillation, based on parameter

estimates from a simple theoretical coupled model (Marshall et al 2001, M01 hereafter). The same simple model will be investigated further below.

6.5 The role of ocean gyre circulation

As shown previously, simulation R_NActl can reasonably reproduce the observed evolution of North Atlantic SST tripole mode. In this section, we will use ocean data from simulation R_NActl to investigate the role of ocean circulation on SST tripole mode. The gyre circulation is diagnosed via the geostrophic streamfunction of the vertically integrated transport.

6.5.1. Gyre circulation

The climatological gyre circulation in R_NActl is shown in Figure 6.7(a). It shows a realistic extratropical double-gyre circulation pattern: an anticyclonic subtropical gyre (positive) and a cyclonic subpolar gyre (negative). The subtropical gyre has strength 50 Sv, and the subpolar gyre has strength 20 Sv to the east of Greenland, with an extreme of 50 Sv in the Labrador Sea, which is large compared with ocean analyses.

The leading EOF of geostrophic circulation explains 31% of the total variance and is shown in Figure 6.7(b). The anomalous anticyclonic gyre occupies the subtropics with strength of 6 Sv associated with one standard deviation of the leading PC, and exhibits a core extension to the north with respect to the mean subtropical gyre. The cyclonic gyre anomaly at subpolar latitudes is very weak. This anomalous pattern co-varies with the NAO. This can be seen in Figure 6.7(c), in which the leading PC (red curve) and the observed NAO index (black curve) have similar evolutions with correlation of 0.74.

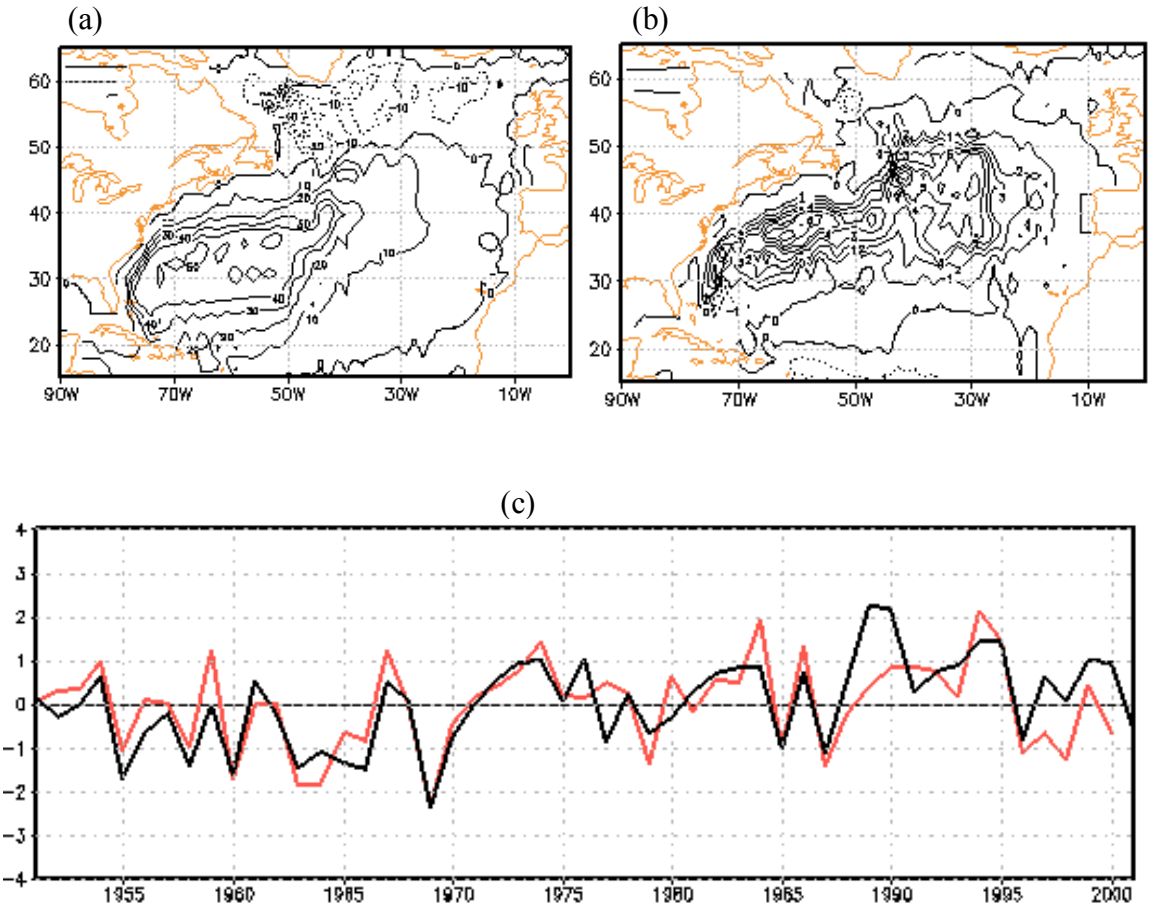

Figure 6.7 (a) Climatological geostrophic streamfunction; (b) Leading EOF of JFM averaged geostrophic streamfunction; (c) Time series of first PC of JFM geostrophic streamfunction (red curve; normalized) and observed NAO index (black curve; ½ amplitude; The JFM NAO index is based on the difference of normalized SLP between Ponta Delgada, Azores and Stykkisholmur/Reykjavik, Iceland; from J. Hurrell's web site http://www.cgd.ucar.edu/cas/jhurrell/indices.data.html#naostatseas). Contour interval in (a) is 10 Sv, in (b) is 1 Sv per standard deviation of first PC. Geostrophic streamfunction data is from simulation R_NActl.

The high correlation between the evolutions of the NAO index and leading PC of the horizontal gyre circulation at zero lag suggests that the major mode of the gyre anomaly is NAO related. Possibly it is the result of ocean instant response to the NAO

windstress forcing. To investigate that possibility, the coherency between changes in the SST tripole index T_{gs} and the horizontal gyre circulation is inspected through lead-lag correlation analysis, with results shown in Figure 6.8. Again, the T_{gs} is from observation and geostrophic streamfunction is from R_NActl , and T_{gs} index leads for positive lags. A significant correlation signature (at 90% level) of a double gyre anomaly pattern is shown at lag of -6, 0, and +6. The pattern resembles the first EOF of the geostrophic streamfunction. At 0 lag, the geostrophic streamfunction anomaly is negative (cyclonic) in the subtropics and positive (anticyclonic) in the subpolar region, with an overall reduction of the heat transport at the subtropical/subpolar gyre boundary. The correlation zero-line exhibits a southwest to northeast tilt, negative to south and positive to north, suggesting negative heat transport across the mean inter-gyre boundary, which has a more zonal orientation (shown in Fig. 6.7(a)). Also, there is evidence of southwestward propagation, especially at positive time lags. At 0 lag, there is a strong positive correlation in the subpolar region. Over time, this positive correlation center propagates southwest. At +3 lag, it reaches the region straddling the climatological subpolar and subtropical gyre. It continuously propagates southwest and reaches the southeast coast of USA at +5 lag, although the feature is not statistically significant at the 90% level based on Student's t- test. A significant positive correlation is shown at +6 lag further to the southwest.

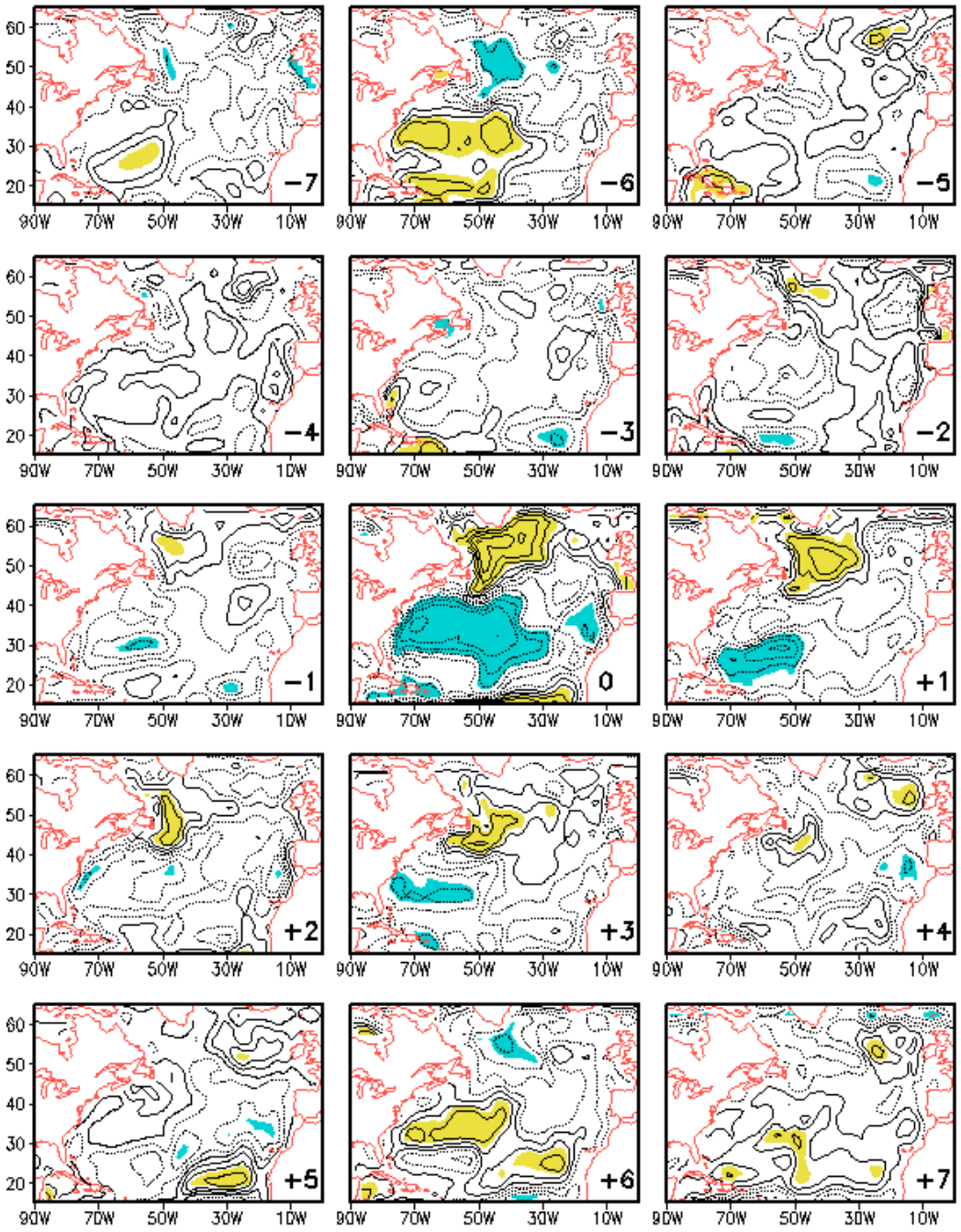

Figure 6.8 Correlation maps of observed Tgs against R_NActl JFM geostrophic streamfunction for several time lags (indicated in the bottom right corner of each sub-panel). The index leads for positive lags. Solid (dashed) contours indicate positive and zero (negative) values, Contour interval is 0.1. shading marks the regions which are statistically significant at 90% level, according to a Student's t- test.

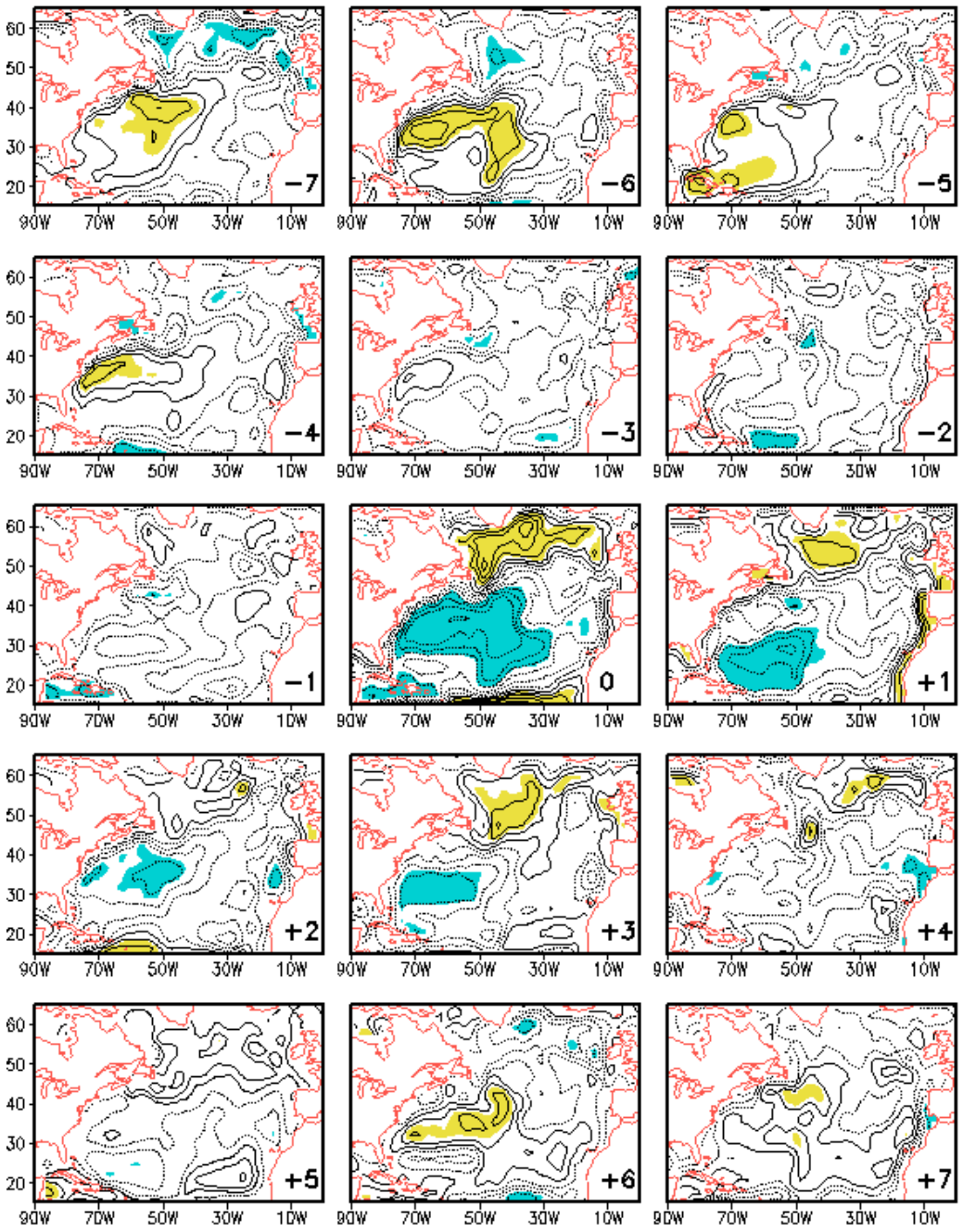

Figure 6.9 As Fig. 6.8 but for geostrophic streamfunction from R_NAm: Correlation maps of observed Tgs against R_NAm JFM geostrophic streamfunction for several time lags (indicated in the bottom right corner of each sub-panel). The index leads for positive lags. Solid (dashed) contours indicate positive and zero (negative) values, Contour interval is 0.1. shading marks the regions which are statistically significant at 90% level, according to a Student's t- test.

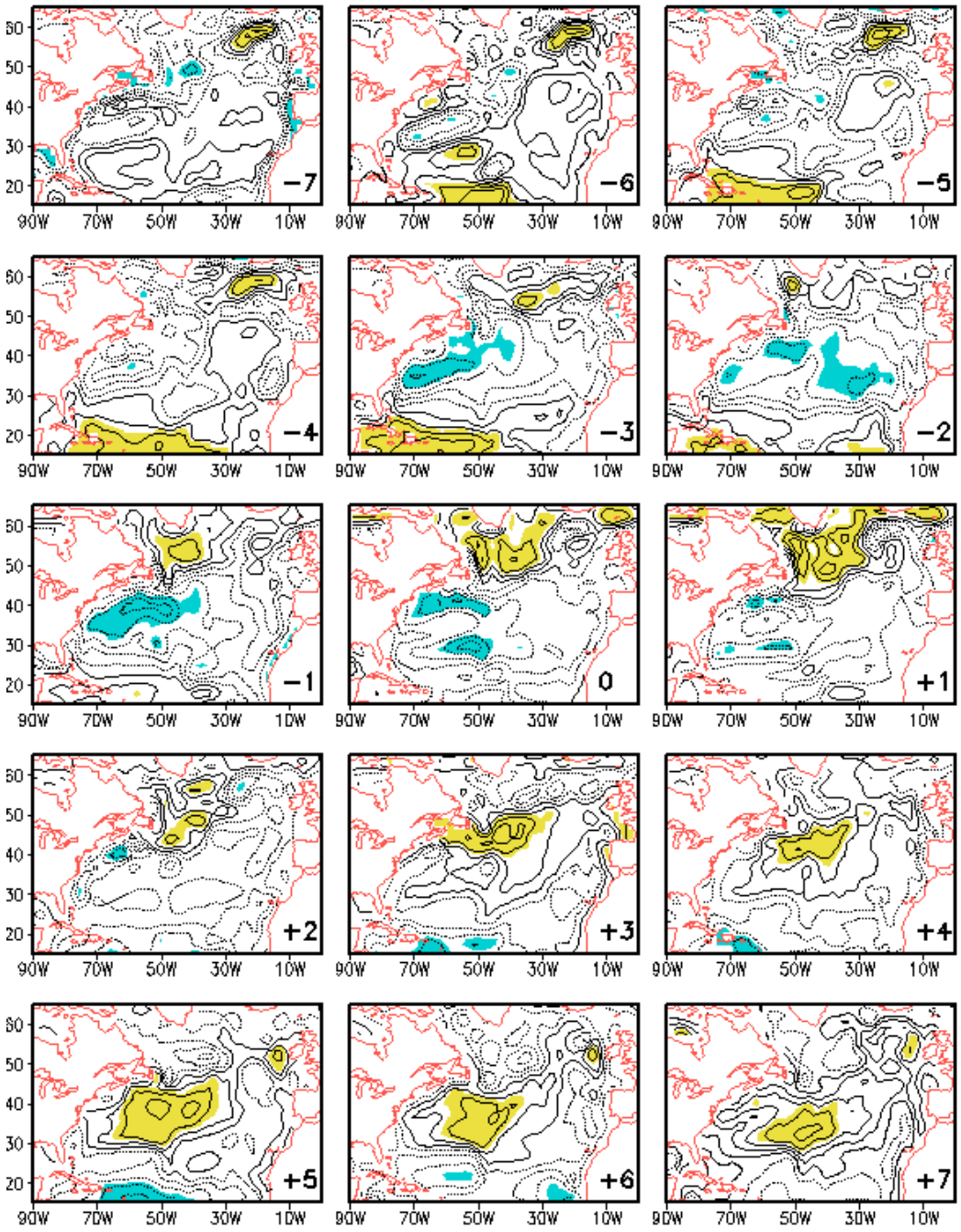

Figure 6.10 As Fig. 6.8 but for geostrophic streamfunction from R_NAh: Correlation maps of observed Tgs against R_NAh JFM geostrophic streamfunction for several time lags (indicated in the bottom right corner of each sub-panel). The index leads for positive lags. Solid (dashed) contours indicate positive and zero (negative) values, Contour interval is 0.1. shading marks the regions which are statistically significant at 90% level, according to a Student's t- test.

It might be possible that the gyre anomaly here is composed of two parts: one is the ocean's instant response to the windstress forcing, the other is the previous signal propagated from the north-east as a Rossby wave. Suppose at year 0, the ocean's instant response to the windstress forcing causes a gyre anomaly, e.g. positive at subpolar and negative at subtropics as in Fig. 6.8 at lag=0. This gyre anomaly propagates southwest-ward due to Rossby wave dynamics. 3 years later (half delay time), the year 0 positive subpolar anomaly signal reaches the subtropical/subpolar gyre boundary region. 6 years later (delay time), it reaches the subtropical region. At the same time, the ocean's instant response to the windstress forcing causes a gyre anomaly which is of opposite sign to year 0, i.e. negative subpolar, positive in the subtropics (same sign as the propagated signal).

From the analysis above, it is hard to say what the role of gyre anomaly plays on SST tripole. The positive correlation at the gyre boundary region at +3 lag (around the time of SST tripole phase switch) increases the heat transport across the gyre boundary, which implies that the gyre anomaly cannot determine the SST tripole phase switch.

Figure 6.9 is the same lead-lag correlation maps as Fig. 6.8, but for geostrophic streamfunction from R_NAm, in which the only atmospheric noise forcing is the windstress. We can see that it is similar to Fig. 6.8, except for the propagating features and the corresponding positive correlation at the gyre boundary region at +3 lag. It seems that the gyre anomaly makes a contribution to the phase switch of the SST tripole. But in fact, the SST tripole is not captured in simulation R_NAm (chapter 5). Fig. 6.9 can be

taken as the ocean's instant response to windstress forcing, so the positive correlation at +3 lag at gyre boundary region in Fig. 6.8 is not seen here.

The southwestward propagation feature of significant correlations for non-zero time-lags is more obvious in Figure 6.10, which is same as Fig. 6.8 but for geostrophic streamfunction from R_NAh. Simulation R_NAh is the one in which the only atmospheric noise forcing is the heat flux; no windstress flux noise is involved. The possible role of windstress in forcing the R_NAh geostrophic streamfunction is only from the atmosphere response to the SST, possibly the SST tripole pattern. If this is the case and if the gyre anomaly here is the ocean's instant response to windstress forcing, then at 0 lag, the feedback from the atmospheric response to the SST tripole has a similar effect on horizontal gyre circulation as the NAO, implying a positive windstress feedback of SST tripole on the NAO. In fact, we will see below that the atmospheric feedback on the SST tripole is negative. Then the gyre anomaly here is possibly the part that propagated from the north-east. Furthermore, it seems that the structures in Fig. 6.8 are a linear combination of those in Fig. 6.9 and Fig. 6.10.

From Fig. 6.10, both the positive and negative correlation at 0 lag propagates southwestward as in R_NActl , but more clearly. For example, at 0 lag, there is a positive correlation in subpolar regions. Over time, this positive correlation center propagates southwest. At +3 lag, it reaches the region straddling the climatological subpolar and subtropical gyre. It continuously propagates southwest and reaches southeast coast of USA at +6 lag. The correlation pattern at +6 lag is close to opposite to the one at 0 lag. The southwestward propagation of the features of the significant correlations here

suggests that the baroclinic Rossby modes might be responsible for the adjustment of the wind-driven circulation to the NAO-related SST tripole-induced windstress anomaly.

6.5.2 Diagnosis of the IGG and coupled behavior by applying a theoretical model

6.5.2.1 Model and damped oscillation theory

To interpret the observed North Atlantic SST tripole evolution, M01 developed a theoretical model, which extends the stochastic climate model of Frankignoul and Hasselmann (1977) by adding a simple representation of anomalous ocean advection and atmosphere-ocean coupling. They also proposed a concept of intergyre gyre (IGG), which is a gyre anomaly "straddling the climatological subtropical and subpolar gyres". The M01 model includes advection by the IGG and the THC. CM01 adapted the model to investigate the role of the IGG on the SST tripole and on the coupled behavior, by simplifying the ocean advection anomaly to IGG only. Here we schematically refer to the dimensional equations B.1 and B.2 in CM01 (here, equation 6.1 and 6.2 respectively):

$$\frac{d\Delta T}{dt} = -\lambda \Delta T - \alpha N + g\psi_g \qquad (6.1)$$

$$\tau = N - f\Delta T \qquad (6.2)$$

Equations 6.1-6.3 (see below) govern the time evolution of the North Atlantic SST tripole index ΔT ($=T_{gs}$), defined as the difference of SST anomalies averaged over a northern and a southern box, $T_N - T_S$) and the zonal wind stress anomaly τ (defined as the difference between anomalous westerlies and trade winds), with N the stochastic (weather noise) component of surface windstress and *f* the feedback of ΔT on the windstress. $g\psi_g$ represents advection of heat by the anomalous gyre circulation (ψ_g,

IGG) from one side of the Gulf Stream to the other, with g the heating rate associated with the anomalous heat transport by the IGG. λ^{-1} denotes a damping timescale for ΔT due to air-sea interactions. αN represents the stochastic turbulent surface heat flux.

According to M01, the coupled behavior of the above model is controlled by a parameter R which measures the magnitude of the heat carried across the gyre boundary by anomalous currents driven by the SST-induced windstress anomaly, relative to the heat lost due to damping of the SST anomalies by air-sea interaction. This depends on both the strength of the feedback of SST on to the NAO (f) and the efficiency of the IGG heat transport mechanism (g), as well as the damping of SST anomalies by air-sea interaction (λ). We will estimate the parameter R below.

In Czaja and Marshall (2001), ψ_g is estimated by invoking time-dependent Sverdrup dynamics, neglecting the stochastic wind forcing N in equation 6.2, and approximating the integral to a midpoint value, giving:

$$\psi_g = \int_{t-t_d}^{t} \tau dt \approx -f\Delta T(t - \frac{t_d}{2}) \qquad (6.3).$$

g is positive, since a positive (anticyclonic) IGG increases heat transport from the south box to north box, leading to a positive ΔT. Assume f is positive as in Czaja and Marshall (2001). Then

$$g\psi_g \propto -\Delta T(t - \frac{t_d}{2}) \qquad (6.3').$$

So the SST-induced gyre anomaly seems to reduce the previous SST anomaly. This is fundamental to the damped decadal oscillation theory (CM01). Two factors are important in the damped decadal oscillation theory. The major role is played by the wind-

driven anomalous ocean circulation, the IGG. The IGG response to the NAO surface windstress forcing has to act as a delayed negative feedback in order to reproduce the low frequency decrease of power seen in the observed SST tripole. The heat transport across the separated Gulf Stream axis by the IGG can compensate the thermal impact of the NAO at the surface at longer time scales. Another factor is the positive feedback of SST tripole on the atmospheric circulation. Once a positive feedback between SST and wind-stress is allowed, the system behaves as a delayed oscillator, with the delay set by the propagation of baroclinic Rossby waves (assumed to be of order 10 years). The ocean-atmosphere coupling introduces enhanced power in the surface temperature spectrum around the delay time-scale, determining a major deviation from the essentially red noise spectrum displayed by the Frankignoul and Hasselmann (1977) model.

For example, suppose the North Atlantic tripole SST is positive in the subpolar region and tropics and negative in the subtropics ($\Delta T > 0$). The atmospheric circulation response to this SST anomaly is a negative NAO like anomaly (positive feedback): reduced surface westerlies across the middle latitudes, combined with weaker than average trade winds in the tropics. This gives a cyclonic (positive) wind stress curl anomaly over the subtropics, while an anticyclonic surface circulation anomaly develops over the subpolar region. The vorticity source associated with the NAO anomaly drives a Sverdrup response of the barotropic wind driven circulation some time later, leading to a negative IGG. This negative IGG produces a reduced meridional heat transport across the subtropical/subpolar gyre boundary, which in turn leads to the cooling (warming) of the subpolar (subtropical) basin. The IGG acts to reduce, with some delay, the anomalous

SST gradient across the climatological gyre boundary. The consequent sign reversal in the North Atlantic SST tripole forces the NAO to enter into a positive phase, through a positive NAO/SST feedback. Once the NAO has stepped into a positive phase, the previously described stages of the oscillation repeat with reversed sign, and the oscillation completes its cycle. Remember that the IGG discussed here is the gyre anomaly driven by the SST-induced wind anomaly (NAO here is the atmospheric feedback to SST).

6.5.2.2 Application of the model

Unlike CM01, where ψ_g, the IGG driven by SST-induced wind anomaly, is estimated based on scale analysis and assumptions, ψ_g here can be determined from simulation data. We define ψ_g as the geostrophic streamfunction anomaly area-averaged inside the core of the IGG (the region between north box and south box, approximately over region between 35-45°N, 60-40°W). To get ψ_g, we use the geostrophic streamfunction data from simulation R_Nah, since in that case the windstress is only the atmospheric response to the SST. The result shows that the correlation between ψ_g and ΔT is largest when ψ_g leads ΔT by 3 years ($t_d/2$), but is positive (0.40), implying a negative feedback of SST on atmospheric circulation ($f < 0$) based on Eq. 6.3. We will see later that f is negative.

Substituting for αN by βH, where β is a coefficient and H is the difference of the surface weather noise heat flux averaged over the northern and southern boxes, Eq. 6.1 becomes:

$$\frac{d\Delta T}{dt} = -\lambda \Delta T + \beta H + g\psi_g \qquad (6.1'),$$

where positive H is downward in the northern box relative to the southern box. Parameters λ, β and g can be estimated by applying the multiple regression least squares method since the time series $\frac{d\Delta T}{dt}$, ΔT, H and ψ_g are known from simulation R_NAh.

As in M01 and CM01, the parameter g must be positive since positive (negative) ψ_g represents anticyclonic (cyclonic) IGG, which means the heat transport by the positive (negative) IGG is positive (negative), i.e. northward (southward). So term $g\psi_g$ in Eq. 6.1' is proportional to ΔT at a previous time. The positive lag correlation found above implies that the role of term $g\psi_g$ is to increase, with 3 years delay, the anomalous SST gradient ΔT across the climatological gyre boundary. This contradicts CM01's result, possibly due to the opposite sign of f.

Following CM01, scaling equations 6.1' and 6.2 by the system relevant scales for time (t_d, related to the propagation of baroclinic Rossby modes near the IGG latitude), IGG strength (Ψ_G), weather noise surface heat flux (Θ), SST anomaly (Y) and zonal windstress (τ_{wind}), a new set of equations is obtained which is formally identical to the previous ones except that now non-dimensional forms of λ, β, g and f parameters appear, defined as $\lambda^* = \lambda t_d$, $\beta^* = \beta t_d \Theta \mathrm{Y}^{-1}$, $g^* = g t_d \Psi_g \mathrm{Y}^{-1}$ and $f^* = f \mathrm{Y} \tau_{wind}{}^{-1}$.

By estimating the efficiency of the IGG heat transport (g^*), the strength of the feedback of SST on the atmospheric circulation (f^*), and the damping of SST anomalies

by air-sea interaction (λ^*), a parameter $R = f^* g^* / \lambda^*$ can be determined. This parameter R determines whether the simple model is a highly damped model (R close to zero), damped oscillatory model ($R < 1$ and close to 1), or a weather noise forced oscillatory model ($R \geq 1$) in the region where $f^* > 0$, $g^* > 0$ and $\lambda^* > 0$ as discussed in Mashall et al. (2001).

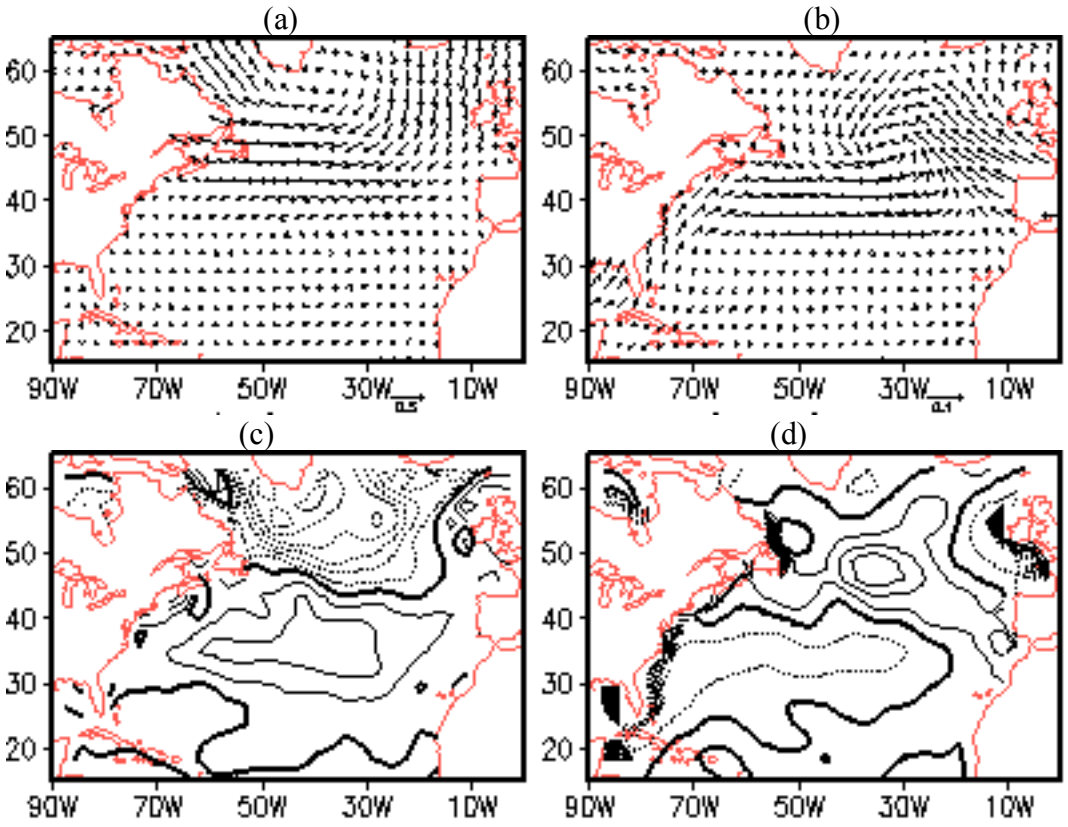

Figure 6.11 Zero lag regressions of (a) Observed windstress, (b) Feedback windstress (10 members ensemble mean from R_10AGCM), (c) Observed windstress curl, (d) Feedback windstress curl (10 members ensemble mean from R_10AGCM), with observed SST tripole index Tgs. Unit scale of the vector for (a) is 0.05 N/m^2, and (b) is 0.01 N/m^2. Contour intervals are (c) $10^{-8} N/m^3$, (d) $0.5*10^{-8}$ N/m^3, respectively, corresponding to one standard deviation of Tgs.

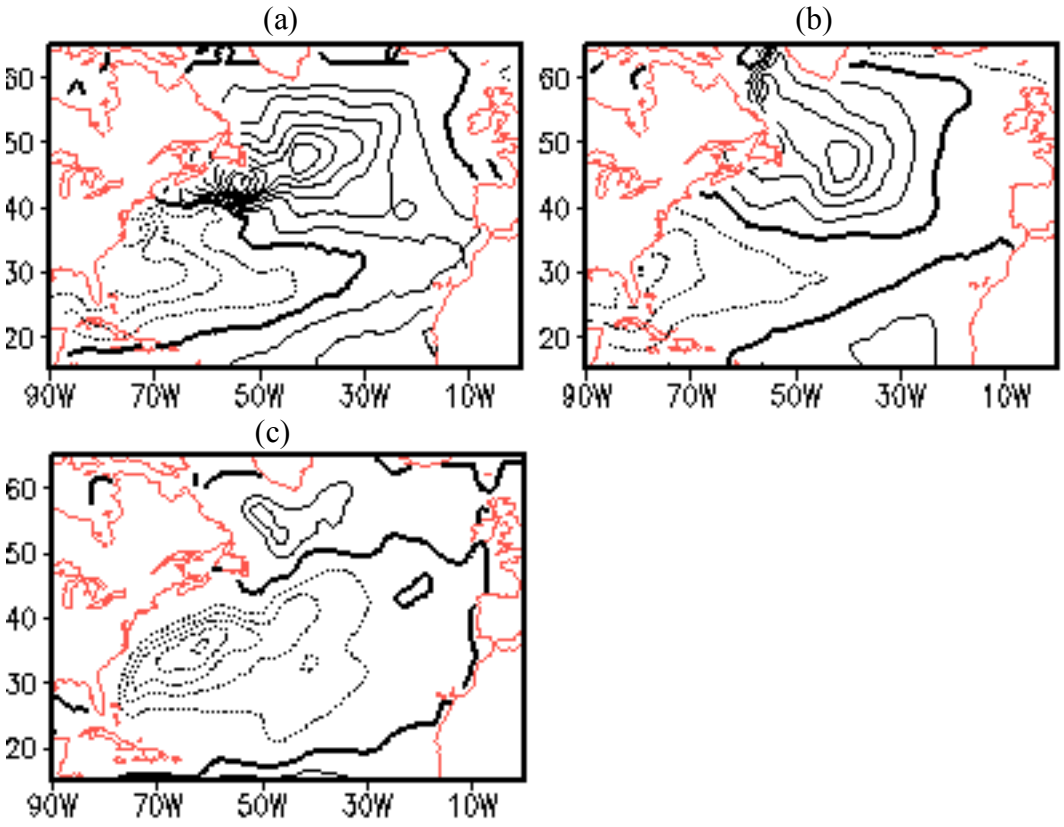

Figure 6.12 Zero lag regressions of (a) Observed SST, (b) Heat flux noise, (c) Geostrophic streamfunction from R_NActl, with observed SST tripole index Tgs. Contour intervals are (a) 0.1K, (b) $10\mathrm{W/m}^2$, (c) 1.0Sv, respectively, corresponding to one standard deviation of Tgs.

To get the scale factors, we project corresponding fields on to the observed T_{gs}. The results are shown in Figure 6.11(a) for windstress (τ_{wind}), in Fig 6.12 for SST anomaly (Y; panel (a)), stochastic surface heat flux (Θ; panel (b)), and IGG strength (Ψ_G; panel (c)), respectively. Corresponding to one standard deviation of ΔT, $\tau_{wind} = 0.03\ \mathrm{Nm}^{-2}$, $\mathrm{Y} = 1^{o}K$, $\Theta = 60\,\mathrm{wm}^{-2}$, and $\Psi_G = 5$ Sv. The temporal scale factor, $t_d = 6$ years, reflects the zonal propagation timescale detected for gyre circulation anomalies around the IGG latitude (Fig. 6.10).

Following Bellucci et al. (2008), the estimate of the parameters contributing to the amplitude of the R factor is performed by applying a linear multiple regression approach.

Eq. 6.1' is a linear model with one predictand $\frac{d\Delta T}{dt}$ and three predictors ΔT, H and ψ_g. Since there is a high correlation between ΔT and H (0.72), we will drop H term when the multiple regression is applied. So parameters λ and g are estimated by fitting a simplified version of Eq. 6.1' (i.e., after removing the noise forcing term: $\frac{d\Delta T}{dt} = -\lambda \Delta T + g\psi_g$) into a linear model:

$$y = \beta_0 + \beta_1 \Delta T + \beta_2 \psi_g \qquad (6.4),$$

with y the predicted value for $\frac{d\Delta T}{dt}$, and β_1 and β_2 the estimates for $-\lambda$ and g, respectively. The corresponding dimensional estimates for the gyre efficiency and SST dipole damping rate are $\lambda = 0.636 \approx 1/(1.6 yr)$ and $g = 0.545^o K S v^{-1} yr^{-1}$ yielding the non-dimensional value $\lambda^* = \lambda t_d \approx 3.82$ and $g^* = g t_d \Psi_G \Upsilon^{-1} \approx 16.34$.

The feedback of the SST tripole windstress f is estimated by projecting the 10-members ensemble mean windsress from R_10AGCM onto T_{gs} (ΔT). The result is shown in Figure 6.11(b). R_10AGCM is an AMIP-like simulation, in which each AGCM (10 members) is forced by the same observed SST, but with slightly different initial condition. Averaging over an ensemble of AMIP simulations allows filtering out the atmospheric weather noise and leaving the atmospheric response forced by the SST, in the limit of large ensemble members. From Fig. 6.11b, there is a negative feedback of the SST tripole on the atmospheric circulation, i.e. a positive ΔT corresponding to a

feedback of positive NAO, but the observed atmosphere is in a negative NAO configuration (Fig. 6.11(a)). From Fig. 6.11(b), we estimate $f = -0.008 Nm^{-2}K^{-1}$, yielding $f^* = -f\Upsilon\tau_{wind}^{-1} \approx -0.267$. Then we get $R = f^* g^* / \lambda^* \approx -1.14$. This value of R is outside of the regime discussed in Marshall et al. (2001), but the model is still applicable, as long as the noise heating term is kept. The negative value of f results from the positive correlation between ψ_g and earlier ΔT, which can be seen in Fig. 10 at +3 lag. This suggests that the "stochastic forcing by NAO variability can 'ring' the system exciting oscillatory modes rather than be resisted by strong damping" (Marshall et al. 2001).

There is an overall consistency between the scale factors diagnosed in this research and the estimates provided by M01 and CM01 (Table 6.1). The time delay t_d in this research (6 years) is between those given in M01 (4 years) and CM01 (10 years). Ψ_G and τ_{wind} are 10 Sv and 0.05 Nm^{-2} in M01 and CM01, but are 5 Sv and 0.03 Nm^{-2} in this research. Remember that Ψ_G is supposed to be induced by τ_{wind}, 5 Sv of Ψ_G corresponding to 0.03 Nm^{-2} of τ_{wind} is consistent with 10 Sv of Ψ_G corresponding to 0.05 Nm^{-2} of τ_{wind}. Table 6.2 is the parameter values from this study and the estimates provided by M01 and CM01 (where available). Although a different estimation method is applied, our estimated values of parameters agree with M01's very well, except for negative f in our case instead of positive f in M01. Given $t_d = 6yr$ instead of $t_d = 4yr$ in M01 will lead to $\lambda^* \approx 3.75$ and $g^* \approx 15$, respectively, which is close to ours $\lambda^* \approx 3.82$ and $g^* \approx 16.34$. The major difference between M01 and CM01 is the damping time.

Table 6.1 Scale factors in this research (COLA), Marshall et al. 2001 (M01), Czaja and Marshall 2001 (CM01), and Bellucci et al. 2008 (B08).

	Y (K)	τ_{wind} (NM^{-2})	Ψ_G (SV)	t_d (YR)
COLA	1	0.03	5	6
M01	1	0.05	10	4
CM01	1	0.05	10	10
B08	1	0.07	5	3

Table 6.2 Estimated parameters in this research (COLA), Marshall et al. 2001 (M01), Czaja and Marshall 2001 (CM01), and Bellucci et al. 2008 (B08), based on Eqs 6.1 and 6.2 (Czaja and Marahsll 2001).

	COLA	M01	CM01	B08
λ	$1/(1.6yr)$	$1/(1.6yr)$	$1/(1yr)$	$1/(2.3yr)$
g	$0.545^{o}KSv^{-1}yr^{-1}$	NA	NA	$0.025^{o}KSv^{-1}yr$
f	$-0.008Nm^{-2}K^{-1}$	NA	$0.015Nm^{-2}K^{-1}$	$0.029Nm^{-2}K^{-1}$
λ^{*}	3.82	2.5	7	1.3
g^{*}	16.34	10	8	0.38
f^{*}	-0.27	0.4	0.3	0.41
$R = f^{*}g^{*}/\lambda^{*}$	-1.14	1.6	0.4	0.1

6.6 Summary and discussion

In this chapter, the possible mechanism of observed North Atlantic SST tripole (or SST gradient across the mean gyre boundary) was investigated, especially for the role of the horizontal gyre circulation, based on geostrophic streamfunction data extracted from our simulations forced by the observed atmospheric noise fluxes. Our analysis reveals that the SST tripole has about a 12 years period and the noise-forcing can reasonably reproduce its period, spatial pattern and variance, possibly because the heat flux noise that we diagnosed by subtracting the COLA AGCM feedback has a similar period. Based on our analysis, it is argued that the SST tripole is mainly forced by atmospheric heat flux noise locally. The gyre circulation plays a secondary role: the anomalous gyre circulation transfers mean thermal features across the inter-gyre boundary, and the mean gyre advection transfer SST anomalies along the inter-gyre boundary.

Significant lead-lag correlations between the SST tripole and the gyre circulation anomalies suggest that the gyre circulation might composed of two parts, one is the oceanic simultaneous response to the atmospheric windstress noise forcing, and the other is driven by the SST-induced windstress anomaly. The former acts as a negative feedback to reduce the observed SST gradient across the mean gyre boundary, as in CM01, but is not a dominant factor on SST tripole mode. The latter (let us call it SST-induced IGG) has southwestward propagation features with propagation speed comparable to the first Rossby wave mode. There is a positive correlation between the SST-induced IGG and the previous SST tripole, corresponding to a negative atmospheric wind feedback on the SST

tripole, suggesting that the SST-induced IGG acts to increase, with some delay, the anomalous SST gradient across the mean gyre boundary. This is conflict to CM01, in which a positive atmospheric feedback to SST forcing is assumed.

Actually, the atmospheric NAO feedback to SST forcing is strongly model dependent. Result from a CAM simulation produces a positive atmospheric windstress anomaly response to the SST tripole, based on the ensemble mean of 5-members of CAM3.0 forced by observed SST (Figure 6.13). These simulations differ from our R_10AGCM in that, in addition to the observed SST forcing, the green-house-gas forcing is also included. CM01 shows that there are two essential processes governing the SST tripole oscillation: 1) a positive feedback of atmosphere wind anomaly to SST, and 2) a delayed negative feedback between ocean gyre circulation and the anomalous SST gradient across the mean subtropical/subpolar gyre boundary.

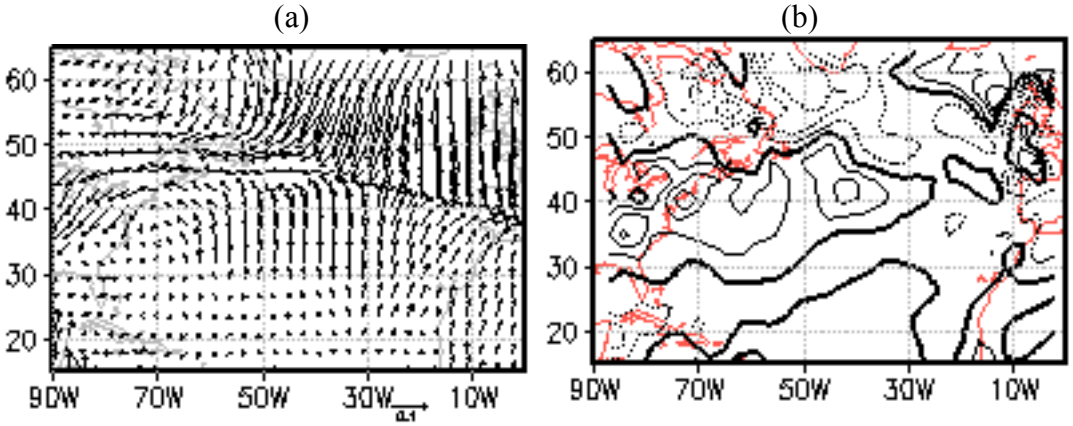

Figure 6.13 Zero lag regressions of (a) Feedback windstress, Feedback windstress curl, with observed SST tripole index Tgs. Unit scale of the vector for (a) is 0.01 N/m^2. Contour intervals for (b) $0.5*10^{-8}$ N/m^3, corresponding to one standard deviation of Tgs. Feedback here is defined as ensemble mean of 5-members of CAM3 simulation forced by observed SST and greenhouse gases.

To further investigate the role of SST-induced IGG on SST evolution, a theoretical model of M01 and CM01 was applied. According to M01, coupled behavior of the model is controlled by a parameter R which measures the magnitude of the heat carried across the gyre boundary by anomalous currents driven by SST-induced windstress anomalies, which depends on both the strength of the feedback of SST onto the atmosphere and the efficiency of the IGG heat transport mechanism, relative to the heat lost due to damping of SST anomalies by air-sea interaction. Diagnosis of our results with respect to the theoretical model of M01 and CM01 shows that, although a different estimation method is applied, our estimated values of parameters agree with M01's very well, except for a negative f (feedback of atmospheric wind anomaly to SST) in our case instead of positive f in M01. Given delay time $t_d = 6yr$ instead of $t_d = 4yr$ in M01 will lead to damping rate $\lambda^* \approx 3.75$ and $g^* \approx 15$, respectively, which is close to ours $\lambda^* \approx 3.82$ and $g^* \approx 16.34$. The coupled parameter is $R = -1.14$ and $R = 1.6$ given $f^* = -0.27$ here and $f^* = 0.4$ in M01, respectively. Our value of R is outside of the regime discussed by M01 and CM01 due to the negative feedback. Nevertheless, from the diagnosis by simple model of M01 and CM01, the evolution of ΔT is heat flux noise forced. Our diagnosis is very different from Bellucci et al. (2008), in which a very small g^* is estimated (0.38) based on a CGCM simulation (SINTEX-G 20C3M experiment).

Certainly, not only the gyre circulation plays a role in mechanism of the SST tripole, but also the thermohaline circulation plays a role, although this was not investigated here.

Chapter 7 Summary

In this study, the role of the weather noise forcing and the coupled feedbacks in low frequency variability of the climate system in North Atlantic is investigated. This is done by applying and generalizing the simple but profound theoretical studies of Hasselmann (1976), Franignoul et al. (1997), and Barsugli and Battisti (1998), to the framework of a state-of-the-art general circulation model of the coupled ocean-atmosphere-land system by using the interactive ensemble technique. In our control and mechanistic experiments, the interactive ensemble coupled GCM is forced by the observed weather noise surface fluxes. The weather noise is determined by removing the atmospheric response forced by the observed surface evolution from the total surface fluxes. The forced response is determined from ensemble simulations (AGCM/land only) forced by the observed SST. Because the interactive ensemble technique is applied, the interactive ensemble coupled GCM will filter out the weather noise forcing of the surface (if given the infinite number of ensemble members), leaving only the coupled feedbacks to produce variability. Noise forced simulations are performed by adding the weather noise fluxes to the fluxes produced by the atmospheric ensemble in the interactive ensemble coupled model.

In the framework of the simple ocean-atmosphere coupled model of BB98, we have shown that the exact ocean temperature of a control case produced by a specific

realization of the weather noise heat flux can be reproduced when forcing the interactive ensemble version with a heat flux diagnosed as the total heat flux minus the SST forced flux. That is, the specific realization of the noise heat flux that forced the control case can be recovered from the "observable" (or analyzable) quantities: the SST evolution and the total heat flux using the intuitive definition of the weather noise. This result is generalizable to the case of an AGCM coupled to a mixed layer ocean, and suggests a null hypothesis for climate variability, that all surface climate variability is forced by atmospheric weather noise. The situations in which the null hypothesis fails are when the surface climate variability is not forced by atmospheric weather noise, due to coupled ocean-atmosphere dynamical feedbacks, or internal variability of the ocean ("ocean weather noise"). Then, using the tools developed in our investigations, observational data and model simulations can be combined to determine the underlying mechanisms for observed climate variability. Perfect data and perfect models will provide an exact diagnosis ("truth"). However, in the real situation of imperfect data and imperfect models, it is necessary to thoroughly analyze and understand the methods and results in order not to be misled.

Our study includes two groups of experiments: 1) perfect-observation/perfect-model, in which the results from a free evolution of a coupled GCM run (CTL), including the surface fluxes and the SST, are taken as the observation dataset; and 2) reanalysis-observation, in which the NCEP/NCAR reanalysis atmosphere data and the Reynolds SST are taken as the observation dataset. The AGCM ensemble diagnosis for both the synthetic and actual observation data gives the result that weather noise is the main

component of atmospheric variability in mid- and high latitudes. In the tropics, the main component of atmospheric variability comes from the atmosphere response to the underlying SST.

The first group of simulations (using synthetic observations from a control simluation) is mainly used to test our method and the null hypothesis *in our CGCM* that SST variability is forced by atmospheric weather noise. If the null hypothesis is satisfied, the control simulation SST variability can be reproduced by the globally weather noise forced simulation. Differences between the control simulation evolution and the global-noise-forced simulation can occur for two possible reasons: 1) error from various approximations made in applying the method, and 2) intrinsic variability of the interactive ensemble not due to the weather noise forcing, including intrinsic atmosphere-ocean coupled variability and oceanic internal chaotic variability, the oceanic weather noise. Potential sources of error from various approximations include the finite model ensemble sizes, the use of monthly mean rather than instantaneous forcing in calculating the atmospheric feedbacks to the control SST and the response to the weather noise, and incomplete implementation of the procedure over land and sea ice.

Comparison of the results from the noise-forced experiments with the synthetic observations show that most of control's SST variability can be reproduced by the interactive ensemble with the control's weather noise flux forcing. This includes the control's low frequency SST patterns in the North Atlantic and their corresponding time evolution. However the control patterns are different from those found in observations. Because of this deficiency of the COLA CGCM in simulating the real climate, we did not

further investigate the mechanisms of the model's intrinsic low frequency SST variability, such as the role of ocean circulation, or the roles of the different noise fluxes noise (heat flux, windstress flux, and salinity) forces.

The results from the second group of simulations, using the NCEP reanalysis of actual observations also suggest that the observed SST variability is mostly atmospheric weather noise forced. JJA SST variability can be better reproduced by noise forcing than JFM's. The regional atmospheric noise forcing, especially the heat flux noise forcing, is the main source of the low frequency SST variability in North Atlantic, but not the complete story. Local oceanic processes such as gyre and THC may modulate the low frequency SST variability. Since the simulated THC variability has obvious deficiencies apparently connected with biases in the low latitude reanalysis surface fluxes, the THC related mechanism of North Atlantic low frequency SST variability is not investigated.

Differences between the observed evolution and the global-noise-forced simulation can occur for several possible reasons: In addition to the two discussed with regard to the synthetic observation case (1) error from various approximations made in applying the method, and 2) violation of the null hypothesis), there are other potential sources of error in the noise estimate based on the reanalysis. These include error in the noise estimates due to unrealistic feedbacks calculated by our atmospheric model and the errors in the reanalysis. Our analysis shows that there is a large jump around 1976 in NCEP heat flux at equatorial Pacific which is probably spurious, and which has a negative impact on our results. The accuracy of the reanalysis depends to a large extent on the realism of the NCEP atmospheric GCM as well as the accuracy and time-space

coverage of the observations; The atmospheric model response to the observed SST forcing (the feedbacks), which includes an implicit response to the external forcing, is model dependent; Our SST forcing in the feedback ensemble is limited to be between 40°S to 65°N.

The mechanism of observed North Atlantic SST tripole (or SST gradient across the mean gyre boundary) was investigated, especially for the role of the horizontal gyre circulation, based on geostrophic streamfunction data extracted from the simulations forced by the observed atmospheric noise fluxes. CM01 shows that there are two essential processes governing the SST tripole oscillation: 1) the feedback of atmosphere wind anomaly to SST through the surface heat flux, and 2) a delayed feedback between ocean gyre circulation and the anomalous SST gradient across the mean subtropical/subpolar gyre boundary. In their analysis, the atmospheric feedback was positive and the delayed gyre feedback was negative. Our analysis reveals that the noise-forcing can reasonably reproduce the period, spatial pattern and variance of the observed SST tripole. Based on our analysis, it is argued that the SST tripole is mainly forced by atmospheric heat flux noise locally. The gyre circulation plays a secondary role: the anomalous gyre circulation advects mean thermal features across the inter-gyre boundary, and the mean gyre advection carries SST anomalies along the inter-gyre boundary.

Significant lead-lag correlations between SST tripole and gyre circulation anomalies suggest that the gyre circulation might be composed of two parts. One is the ocean's instantaneous response to the atmospheric windstress flux noise forcing. The other is driven by SST-induced windstress anomaly. The former acts as a negative

feedback to reduce the observed SST gradient across the mean gyre boundary, as in CM01, but is not a dominant factor on the tripole mode SST. The latter (let us call it SST-induced IGG) has southwestward propagation features with propagation speed comparable to the first Rossby wave mode. There is a positive correlation between the SST-induced IGG and the previous SST tripole, corresponding to a negative atmospheric wind feedback on the SST tripole. This suggests that the SST-induced IGG acts to increase, with some delay, the anomalous SST gradient across the mean gyre boundary. This contradicts CM01, in which a positive atmospheric feedback to SST forcing is assumed. The atmospheric feedback to SST forcing is model dependent. Results from an ensemble of CAM3 simulations force by observed SST produces a positive atmospheric windstress response to the SST tripole.

To further investigate the role of SST-induced IGG on SST evolution, parameters were estimated for the theoretical model of M01 and CM01. According to M01, the coupled behavior of the model is controlled by a parameter R which measures the magnitude of the heat carried across the gyre boundary by anomalous currents driven by the SST-induced windstress anomaly, which depends on both the strength of the feedback of SST on to the atmosphere and the efficiency of the IGG heat transport mechanism, relative to the heat lost due to damping of SST anomalies by air-sea interaction. Although a different estimation method is applied, our estimated values of parameters are consistent with M01's, except that we find a *negative* feedback of atmospheric wind anomaly to the SST. The regime that is found using the COLA model for diagnosis is then different from the damped delayed oscillator regime inferred by M01 and CM01. In

their regime, the time scale of the oscillation results from the competition between the simultaneous positive feedback and the delayed negative feedback, while the oscillation is stimulated by the noise forcing. In our case, all of atmospheric feedbacks are negative, but the delayed ocean circulation provides a positive feedback. It is not clear if this mechanism can lead to a preferred period or what the implications of this mechanism would be for predictability of the tripole mode.

BIBLIOGRAPHY

BIBLIOGRAPHY

Alexander, M.A and C. Deser, 1995: A mechanism for the recurrence of wintertime SST anomalies. *J. Phys. Oceanogr.* , **25**, 122-137.

Barnston, A.G. and R.E. Livezey, 1987: Classification, seasonality and persistence of low-frequency atmospheric circulation patterns. *Mon. Wea. Rev.* , **115**, 1083-1126.

Barsugli, J.J. and D.S. Battisti, 1998: The Basic Effects of Atmosphere-Ocean Thermal Coupling on Midlatitude Variability. *J. Atmos. Sci.* , **55**, 477-93.

Bellucci, A., S. Gualdi, E. Scoccimarro, and A. Navarra, 2008: NAO-Ocean Circulation Interactions in a Coupled General Circulation Model. *Clim. Dyn*. doi: 10.1007/500382-008-0408-04.

Bhatt, U. S., M. A. Alexander, D. S. Battisti, D. D. Houghton and L. M. Keller, 1998: Atmosphere–Ocean Interaction in the North Atlantic: Near-Surface Climate Variability. *J. Climate*, **11**, 1615-1632.

Bladé, I., 1997: The influence of midlatitude ocean-atmosphere coupling on the low-frequency variability of a GCM. Part I: No tropical forcing. *J. Climate*, **10**, 2087-2106.

Blanke, B. J., J. D. Neelin, and D. Gutzler, 1997: Estimating the effect of stochastic wind stress forcing on ENSO irregularity. *J. Climate*, **10**, 1473-1486.

Bretherton, C. S. and D. S. Battisti, 2000: An interpretation of the results from atmospheric general circulation models forced by the time history of the observed sea surface temperature distribution. *Geophys. Res. Lett.*, **27**, p. 767-770.

Boer, G. J., 2004: Long time-scale potential predictability in an ensemble of coupled climate models. *Climate Dyn*., **23**, 29-44.

Briegleb, B. P., 1992: Delta-Eddington approximation for solar radiation in the NCAR Community Climate Model. *J. Geophys. Res.*, **97**, 7603-7612.

Cane, M. A. and E. S. Sarachik, 1977: Forced baroclinic ocean motions: II. The linear equatorial bounded case. *J. Mar. Res*., **35**, 395-432.

Cayan, D.R., 1992a: Latent and sensible heat flux anomalies over the northern oceans: the connection to Monthly Atmospheric Circulation. *J. Climate*, **5**, 354-369.

Cayan, D.R., 1992b: Latent and sensible heat flux anomalies over the northern oceans: Driving the sea surface temperature. *J. Phys. Oceanogr.* , **22**, 859-881.

Cessi, P., 2000: Thermal feedback on wind stress as a contributing cause of climate variability. *J. Climate*, **13**, 232-244.

Czaja, A., P. V. D. Vaart, and J. Marshall, 2002: A Diagnostic study of the role of remote forcing in tropical Atlantic variability. *J. Climate*, **15**, 3280-3290.

Czaja, A., and J. Marshall, 2001: Observations of atmosphere-ocean coupling in the North Atlantic. *Q. J. R. Meteorol. Soc.*, **127**, 1893-1916.

Delworth, T. L., 1996: North Atlantic variability in a coupled ocean-atmosphere model. *J. Climate*, **9**, 2356-2375.

Delworth, T. L., S. Manabe, and R. J. Stouffer, 1993: Interdecadal variations of the thermohaline circulation in a coupled ocean-atmosphere model. *J. Climate*, **6**, 1993-2011.

Deser, C. and M. L. Blackmon, 1993: Surface climate variations over the North Atlantic Ocean during winter: 1900-1989. *J. Climate*, **6**, 1743-1753.

DeWitt, D. G., 1996: The effect of the cumulus convection scheme on the climate of the COLA general circulation model. *COLA Rep.* **27**, 58 pp. [Available from COLA, 4041 Powder Mill Rd., Suite 302, Calverton, MD 20705.]

DeWitt, D. G., and E. K. Schneider, 1996: The Earth radiation budget as simulated by the COLA GCM. *COLA Rep*. **35**, 39pp. [Available from COLA, 4041 Powder Mill Rd., Suite 302, Calverton, MD 20705.]

Dickson, R.R., J. Meincke, S.-A. Malmberg, and A.J. Lee, 1988: The "Great Salinity Anomaly" in the northern North Atlantic 1968-1982. *Prog. Oceanogr.*, **20**, 103-151.

Ferreira, D., C. Frankignoul, and J. Marshall, 2001: Coupled ocean-atmosphere dynamics in a simple midlatitude climate model. *J. Climate*, **14**, 3704-3723.

Frankignoul, C., 1999: A cautionary note on the use of statistical atmospheric models in the middle latitudes: Comments on "Decadal Variability in the North Pacific as Simulated by a Hybrid Coupled Model." *J. Climate*, **12**, 1871-1872.

Frankignoul, C., P. Müller, and E. Zorita, 1997: A simple model of the decadal response of the ocean to stochastic wind forcing. *J. Phys. Oceanogr.*, **27**, 1533-1546.

Gent, P. R., and J. C. McWilliams, 1990: Isopycnal mixing is ocean circulation models. *J. Phys. Oceanogr.* , **25,** 150-155.

Goodman, J. and J. Marshall, 1999: A model of decadal middle-latitude atmosphere-ocean coupled modes. *J. Climate*, **12**, 621-641.

Griffies, S. M. and E. Tziperman, 1995: A linear thermohaline oscillator driven by stochastic atmospheric forcing. *J. Climate*, **8**, 2440-2453.

Grötzner, A., M. Latif, and T. P. Barnett, 1998: A decadal climate cycle in the North Atlantic Ocean as simulated by the ECHO coupled GCM. *J. Climate*, **11**, 831-847.

Gu, D., S. G. H. Philander, 1997: Interdecadal climate fluctuations that depend on exchange between the tropics and extratropics. *Science*, **275**, 805-807

Hakkinen, S., 1999: Variability of the simulated meridional heat transport in the North Atlantic for the period 1951-1993. *J. Geophys. Res.*, **104**, 10991-11007.

Harshvardhan, R. Davies, D. A. Randall and T. G. Corsetti, 1987: A fast radiation parameterization for atmospheric circulation models. *J. Geophys. Res.*, **92(D1)**, 1009-1016.

Hasselmann, K., 1976: Stochastic climate models. Part I: Theory. *Tellus*, **28**, 473-485.

Hayes, S. P., M. J. Mcphaden and J. M. Wallace, 1989: The influence of sea-surface temperature on surface wind in the Eastern Equatorial Pacific: weekly to monthly variability. *J. Climate*, **2**, 1500-1506.

Hoerling, M. P., J. W. Hurrell, and T. Xu, 2001: Tropical origins for recent North Atlantic climate change. *Science*, **292**, 90-92.

Holland, M. M., C. M. Bitz, M. Eby, and A. J. Weaver, 2001: The role of ice-ocean interactions in the variability of the North Atlantic thermohaline circulation. *J. Climate*, **14**, 656-675.

Huang, B., P. S. Schopf, and J. Shukla, 2003: Coupled ocean-atmosphere variability in the tropical Atlantic Ocean. *COLA Technical Report* 135, 57pp.

Hurrell, J.W., 1995: Decadal trends in the North Atlantic Oscillation: regional temperatures and precipitation. *Science*, 269, 676-679.

Jin, F.-F., 1997: A theory of interdecadal climate variability of the North Pacific ocean-atmosphere system. *J. Climate*, **10**, 1821-1835.

Jochum, M., and R. Murtugudde, 2004, Internal variability of the tropical Pacific ocean, *Geophys. Res. Lett.*, 31, L14309, doi: 10.1029/2004GL020488.

Jochum, M., and R. Murtugudde, 2005, Internal Variability of India Ocean SST, *J. climate*, 18, 3726-3737.

Jones, P.D., T. Jonsson, and D. Wheeler, 1997: Extension to the North Atlantic Oscillation using early instrumental pressure observations from Gibraltar and SW Iceland. Int. *J. Climate*, **17**, 1433-1450.

Kalnay, E., M. Kanamitsu, R. Kistler, W Collins, D. Deaven, I. Gandin, M. Iredell, S. Saha, G. White, J. Woollen, Y. Zhu, M. Chelliah, W. Ebisuzaki, W. Higgins, J. Janowiak, K.C. Mo, C. Ropelewski, J. Wang,A. Leetmaa, R. Reynolds, R. Jenne and D. Joseph, 1996:The NCEP/NCAR 40-year Reanalysis Project. *Bull. Am. Met. Soc.*, **77**, 437-471.

Kiehl, J. T., J. J. Hack, G. A. Bonin, B. A. Boville, D. L. Williamson, and P. J. Rasch, 1998: The National Center for Atmospheric Research Community Climate Model: CCM3. *J. Climate,* **11,** 1131–1149.

Kiehl, J. T., J. J. Hack and B. P. Briegleb, 1994: The simulated Earth radiation budget of the National Center for Atmospheric Research community climate model CCM2 and comparisons with the Earth Radiation Budget Experiment (ERBE). *J. Geophys. Res.*, **99**, 20815-20827.

Kirtman B. P., B. Huang, Z. Zhu, and E. K. Schneider, 1997: Multiseasonal prediction with a coupled tropical ocean global atmosphere system. *Mon. Wea. Rev.*, **125**, 789–808.

Kirtman, B. P., 1997: Oceanic Rossby wave dynamics and the ENSO period in a coupled model. *J. Climate*, **10**, 1690-1704.

Kirtman, B. P. and P. S. Schopf, 1998: Decadal Variability in ENSO Predictability and Prediction. *J. Climate*, **11**, 2804–2822.

Kirtman, B. P., and J. Shukla, 2002: Interactive coupled ensemble: A new coupling strategy for CGCMs. *Geophys. Res. Lett.*, **29**, 17-20.

Kirtman, B. P., Y. Fan and E. K. Schneider, 2002: The COLA global coupled and anomaly coupled ocean-atmosphere GCM. *J. Climate*, **15**, 2301-2320.

Kirtman, B. P., K. Pegion, and S. Kinter, 2005: Internal atmospheric dynamics and climate variability. *J. Atmos. Sci.*, **62**, 2220-2233.

Kushnir, Y., 1994: Interdecadal variations in North Atlantic sea surface temperature and associated atmospheric circulation. *J. Climate*, **7**, 141-157.

Kleeman, R. and A. M. Moore, 1997: A theory for the limitation of ENSO predictability due to stochastic atmospheric transients. *J. Atmos. Sci.*, **54**, 753-767.

Kushnir, Y., W. A. Robinson, I. Blade, N. M. J. Hall, S. Peng, and R. Sutton, 2002: Atmospheric GCM response to extratropical SST anomalies: synthesis and evaluation. *J. Climate*, **15**, 2233-2256.

Large, W. G., J. C. McWilliams, and S. C. Doney, 1994: Oceanic vertical mixing: A review and a model with a nonlocal boundary layer parameterization. *Rev. of Geophys.*, **32,** 363-403.

Latif, M. and T. P. Barnett, 1994: Causes of decadal climate variability in the North Pacific/North American sector. *Science*, **266**, 634-637.

Latif, M. and T. P. Barnett, 1996: Decadal climate variability over the North Pacific and North America: Dynamics and predictability. *J. Climate*, **9**, 2407-2423.

Latif, M., 1998: Dynamics of interdecadal variability in coupled ocean-atmosphere models. *J. Climate*, **11**, 602-624.

Lean, J., J.Beer and R.Bradley, 1995: Reconstruction of solar irradiance since 1600: Implications For climate change. *Geophys. Res. Lett.*, **22**,3195-3198.

Levitus S., J. Antonov, and T. Boyer, 1994: Interannual variability of temperature at a depth of 125 m in the North Atlantic Ocean. *Science*, **266**, 96-99.

Li L. Z.X., 2006: Atmospheric GCM response to an idealized anomaly of the Mediterranean sea surface temperature: *Climate Dyn.*, (in press).

Marshall, J., H. Johnson, and J. Goodman, 2001: A study of the interaction of the North Atlantic Oscillation with the ocean circulation. *J. Climate*, **14**, 1399-1421.

Mellor, G. L., and T. Yamada, 1982: Development of a turbulence closure model for geophysical fluid processes. *Rev. Geophys. Space Phys.*, **20**, 851-875.

Mehta, V. M., M. J. Suarez, J. V. Manganello, and T. L. Delworth, 2000: Oceanic influence on the North Atlantic Oscillation and associated Northern Hemisphere climate variations: 1959-1993. *Geophys. Res. Lett.*, **27**, 121-124.

Miyakoda, K., and J. Sirutis, 1977: Comparative integrations of global spectral models with various parameterized processes of subgrid scale vertical transports. *Beitr. Phys. Atmos.,* **50,** 445–480.

Molinari, R.L., D.A. Mayer, J.F. Festa, and H.F. Bezdek, 1997: Multi-year variability in the near-surface temperature structure of the midlatitude western North Atlantic Ocean. *J. Geophys. Res.,* **102**, 3267-3278.

Moorthi, S., and M. J. Suarez, 1992: Relaxed Arakawa-Schubert: A parameterization of moist convection for general circulation models. *Mon. Wea. Rev.*, **120**, 978-1002.

Pacanowski, R. C., and S. M. Griffies, 1998: MOM 3.0 Manual, NOAA/Geophysical Fluid Dynamics Laboratory, Princeton, USA 08542.

Palmer, T. N. and Z. Sun, 1985: A modelling and observational study of the relationship between sea surface temperature in the north-west Atlantic and the atmospheric general circulation. *Quart. J. Roy. Meteor. Soc.*, **111**, 947-976.

Peng, S., L. A. Mysak, H. Ritchie, J. Derome, and B. Dugas, 1995: The differences between early and midwinter atmospheric responses to sea surface temperature anomalies in the northwest Atlantic. *J. Climate*, **8**, 137-157.

Rayner, N. A., D. E. Parker, E. B. Horton, C. K. Folland, L. V. Alexander, D. P. Rowell, E. C. Kent, and A. Kaplan, 2003: Global analyses of sea surface temperature, sea ice, and night marine air temperature since the late nineteenth century. *J. Geophys. Res.,* **108**, 4407.

Redi, M. H., 1982: Oceanic isopycnal mixing by coordinate rotation, *J. of Phys. Oceanogr*., **12**, 1155-1158.

Robertson, A. W., C. R. Mechoso, and Y.-J. Kim, 2000: The influence of Atlantic sea surface temperature anomalies on the North Atlantic Oscillation. *J. Climate*, **13**, 122-138.

Robock. A., and J. Mao,1992: Winter warming from large volcanic eruptions*, Geophys. Res. Lett.,* **12,** 2405-2408

Rodwell, M. J., D. P. Rowell, and C. K. Folland, 1999: Oceanic forcing of the wintertime North Atlantic Oscillation and European climate. *Nature*, **398**, 320-324.

Rogers, J.C., 1984: The Association between the North Atlantic Oscillation and the Southern Oscillation in the Northern Hemisphere. *Mon. Wea. Rev.,* **112**, 1999-2015.

Rogers, J.C., 1990: Patterns of low-frequency monthly sealevel pressure variability (1899-1986) and associated wave cyclone frequencies. *J. Climate*, **3**, 1364-1379.

Sarachik, E. S., M. Winton, and F. L. Yin, 1996: Mechanisms for decadal-to-centennial climate variability. Decadal Climate Variability: Dynamics and Predictability (D. L. T. Anderson and J. Willebrand, eds.). NATO ASI Series, **44**, 158-210.

Saravanan, R. and J. C. McWilliams, 1998: Advective ocean-atmosphere interaction: An analytical stochastic model with implications for decadal variability. *J. Climate*, **11**, 165-188.

Schneider, E. K., B. Huang and J. Shukla, 1995: Ocean wave dynamics and El Nino. *J. Atmos. Sci.*, **8**, 2415-2439.

Schneider, E. K., 2002: Understanding differences between the equatorial Pacific as simulated by two coupled GCMs. *J. Climate*, **15**, 449-469.

Schneider, E. K., L. Bengtsson, and Z.-Z. Hu, 2003: Forcing of Northern Hemisphere climate trends. *J. Atmos. Sci.*, **60**, 1504-1521.

Schneider, E. K., M. Fan, B. P. Kirtman, and P. A. Dirmeyer, 2006: Potential effects of Amazon Deforestation on tropical climate. *COLA Tech. Rep.* **226**, 41pp.

Schneider, E. K. and M. Fan, 2007: Weather noise forcing of surface climate variability. *J. Atmos. Sci*., **64**, 3265-3280.

Seager, R., Y. Kushnir, M. Visberk, N. Naik, J. Miller, G. Krahmann, and H. Cullen, 2000: Causes of Atlantic Ocean climate variability between 1958 and 1998. *J. Climate*, **13**,2845-2862.

Shindell, D. T., R. L. Mille, G, Schmidt, and L. Pandolfo: Simulation of recent northern winter climate trends by greenhouse-gas forcing, *Nature*, **399**, 452-455, 1999.

Smagorinsky, J., 1963: General circulation experiments with the primitive equations: I. The basic experiment. *Mon. Wea. Rev.,* **91,** 99-164.

Smith, T. M., R. W. Reynolds, R. E. Livezey, and D. C. Stokes, 1996: Reconstruction of historical sea surface temperature using empirical orthogonal functions. *J. Climate,* **9,** 1403–1420.

Solomon, A., McCreary, J. P., Kleeman, R., and Klinger, B. A., 2003: Interannual and decadal variability in an intermediate coupled model of the Pacific region. *J. Climate*, **16**, 383–405.

Suarez, M. J., and P. S. Schopf, 1988: A delayed action oscillator for ENSO. *J. Atmos. Sci.*, **45**, 3283-3287.

Timmerman, A., M. Latif, R. Voss, and A. Grötzner, 1998: Northern hemispheric interdecadal variability: A coupled air-sea mode. *J. Climate*, **11**, 1906-1931.

Trenberth, K. E., W. G. Large, and J. G. Olson, 1990: The mean annual cycle in global ocean wind stress. *J. Phys. Oceanogr. ,* **20,** 1742–1760.

Woodruff, S. D., R. J. Slutz, R. L. Jenne, and P. M. Steurer, 1987: A comprehensive ocean-atmosphere dataset. *Bull. Amer. Meteor. Soc*., **68**, 1239-1250.

Wu, Z., E. K. Schneider, and B. P. Kirtman, 2004: Causes of low frequency North Atlantic SST variability in a coupled GCM. *Geophys. Res. Lett.* , **31**, L09210.

Wu, L., Z. Liu, R. Gallimore, R. Jacob, D. Lee, and Y. Zhong, 2003: Pacific decadal variability: The tropical Pacific mode and the North Pacific mode. *J. Climate*, **16**, 1101-1120.

Wu, L., Z. Liu, 2005: North Atlantic decadal variability: air-sea coupling, oceanic memory, and potential northern hemisphere resonance. *J. Climate*, **18,** 331-349.

Xue, Y., P. J. Sellers, J. L. kinter, and Shukla, 1991: A Simplified biosphere model for global climate studies, *J. Climate*, **4**, 345-364.

Yeh, S.-W., and B. P. Kirtman, 2004: The impact of internal atmospheric dynamics for the North Pacific SST variability, *Climate. Dyn*. doi:10.1007/s00382-004-0399-8.

Zebiak, S. E., and M. A. Cane, 1987: A model of El Niño and Southern Oscillation. *Mon. Wea. Rev.*, **115**, 2262-2278.

Zebiak, S. E., 1989: On the 30-60 day oscillation and the prediction of El Nino. *J. Climate*, **2**, 1381-1387.

Zhu, Z., and E. K. Schneider, 1995: Experimental multi-season ENSO predictions with an anomaly coupled general circulation model. *COLA Tech. Rep.* **10**, 18 pp.

Zorita, E. and C. Frankignoul, 1997: Modes of North Atlantic decadal variability in the ECHAM/LSG coupled ocean-atmosphere general circulation model. *J. Climate*, **10**, 183-200.

Website:
http://www.clivar.org/publications/other_pubs/iplan/iip/pd1.htm

http://www.cgd.ucar.edu/cas/jhurrell/indices.data.html#naostatseas

CURRICULUM VITAE

Meizhu Fan graduated from Ocean University of Qingdao (China) in 1989 with Bachelor of Science in Atmosphere Dynamics. She received her Master of Science degree in Climatology under Professor Tao Shiyan from Chinese Academy of Meteorological Science in 1992. She worked for 8 ½ years as a research scientist at (Chinese) National Satellite Meteorological Center. She came to USA with her family at the end of 2000. She received her Master of Science degree in Computer Science from University of Northern Virginia in 2003, and then came to the Climate Dynamics PhD Program at George Mason University under Professor Edwin K. Schneider.